SPECTROELECTROCHEMICAL STUDIES ON PORPHYRINS AND RELATED TETRA-AZAMACROCYCLES

MURRAY R. LOW

Ph.D. Thesis
University of Edinburgh
1987

To the folk I ken,

and wha' ken me .

DECLARATION

Except where specific reference is made to other sources, the work presented in this thesis is the original work of the author. It has not been submitted, in whole or in part, for any other degree. Certain of the results presented have already been published.

(Murray Low)

ABSTRACT

Metalloporphyrins and related tetra-azamacrocyclic complexes fulfil a wide range of bioactive roles. They are employed extensively in electron-transfer catalytic cycles and as such they can exist in a variety of oxidation states. The work presented in this thesis is devoted to a study of the redox properties of series of model transition-metal porphyrin and porphyrin-like complexes.

Detailed voltammetric studies have uniquely enabled us to evaluate the importance of back-bonding from the metal to the chelating ligand. In addition, in situ spectro-electrochemical techniques, incorporating both electronic absorption spectroscopy and ESR spectroscopy, have allowed us to unambiguously assign the electron-transfer step occurring as a metal-based or macrocycle-based redox couple. A rationalisation of the electronic spectral properties of the electrode products is presented. A re-examination of the electrochemistry of some iron and ruthenium porphyrins leads us to disagree, to a significant extent, with previous reports. We also discuss in detail the redox properties of a series of metallochlorins and utilise the results to explain the spectroelectrochemical behaviour of bonellin, a most remarkable naturally occurring macro-cycle.

CONTENTS

LIST OF FIGURES

CHAPTER 3

CHAPTER 4

LIST OF TABLES

Extinction coefficient values are quoted in $dm^3\ mol^{-1}\ cm^{-1}$ throughout this thesis.

CHAPTER 1 : INTRODUCTORY REMARKS

Inorganic complexes which incorporate soft ligands are a common occurrence in many biological systems.[1] These ligands are often tetra-aza macrocycles, and the most abundant pigments by far are those based on the porphin moiety (1).

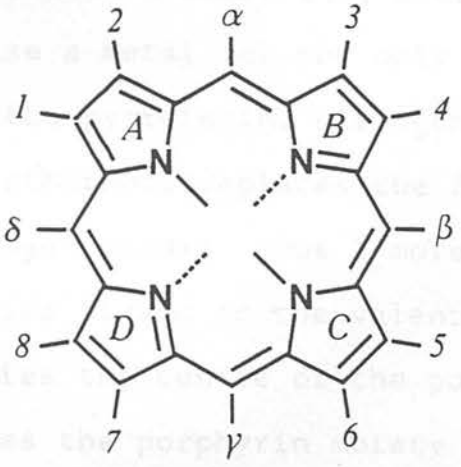

(1)

Porphyrins are formally derived from porphin by substitution of some or all of the peripheral positions with various side chains. In the classical system of nomenclature the peripheral positions are numbered from 1 to 8 and the 'interpyrrolic' methine positions, usually termed meso, are designated α, β, γ and δ . The rings are usually lettered A, B, C and D.

As a direct consequence of their natural importance, research into the chemical and physical properties of porphyrins has been prolific for over one hundred years. Many excellent reviews[2-7] covering most aspects of porphyrin chemistry have

been written throughout this time. From the broad base of knowledge thus available it soon became apparent the porphin chromophore had the ability to complex a wide range of metal centres, in a variety of oxidation states. Metalloporphyrins are porphin derivatives in which at least one of the lone electron pairs residing on the central nitrogen atoms of porphin is shared with a metal ion, acting as a Lewis acid. In the normal case a metal ion not only coordinates to the 2 lone pairs on the pyrrolenine nitrogen atoms of a free-base porphyrin but furthermore replaces the 2 hydrogen atoms on the pyrrole nitrogen atoms; thus 2 more lone pairs are donated from the porphinato ligand to the valence shell of the metal ion, which occupies the centre of the porphyrin hole. (In more unusual cases the porphyrin moiety can act as a bi-, tri-, or hexadentate ligand[8]). Naturally occurring metalloporphyrins include complexes of main group metals (e.g. Mg(II), Al(III), Sn(IV)) but more commonly, transition metals. Nickel porphyrins have been extracted from oil shales, crude petroleum oils, bituminous sands and asphaltic materials[9,10]. Fe(II), Fe(III), Co(II), Cu(II), and Zn(II) are all incorporated into porphyrins by chromatophore preparations from purple bacteria as well as preparations from liver mitochondria.[11]

The porphyrin macrocycle is also capable of undergoing a remarkable range of organic chemistry <u>in vivo</u> . Vinylation, alkylation, hydrogenation and exo-ring formation can all occur at the basic porphyrin skeleton. Also electrophilic sub-

stitution reactions can occur at the unsubstituted positions e.g. nitration, halogenation, sulphonation, formylation and acylation. This, with the great diversity of metals available gives rise to a wide variety of complexes. Some examples are shown in Figure 1.

Figure 1.1 Typical naturally-occurring porphinato complexes

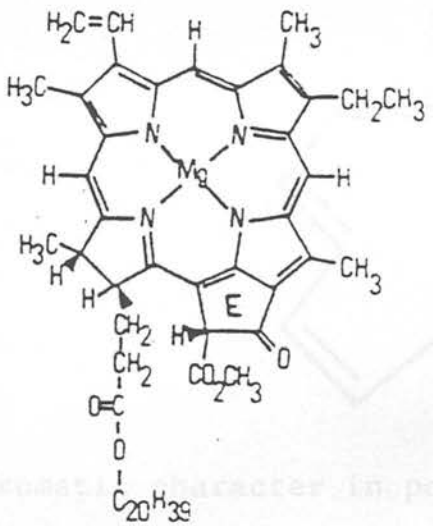

Chlorophyll a

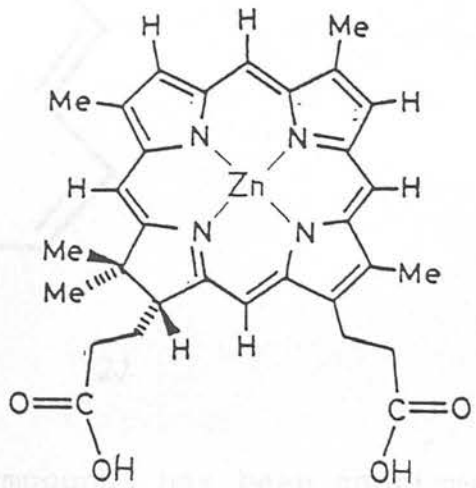

Zinc Bonelliate

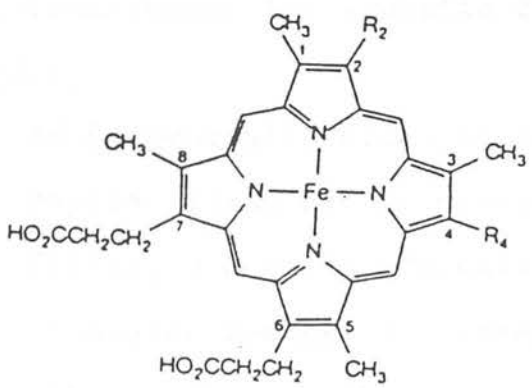

Protohaem	$R_2, R_4 = -CH=CH_2$ = Protoporphyrin IX
Synonyms	Fe(II), haem; Fe(III), haematin
Mesohaem	$R_2, R_4 = CH_2CH_3$
Deuterohaem	$R_2, R_4 = H$
Pyrrohaem	$R_2, R_4 = C_2H_5$, H for $CH_2CH_2CO_2H$ at 6
Haem a_2	$R_2 = -CH=CH_2$, $R_4 = -CHOHCH_3$
Haem C	$R_2, R_4 = -CHCH_3$ | S—

The Haems

For all the variance however, a common factor relates all porphinato complexes. Every single biologically relevant porphyrin has the same essential electronic 'core'. This consists of an intact conjugative pathway containing 18 atoms and 18 π electrons (2) and as such conforms with Huckel's 4n + 2 rule for aromaticity.

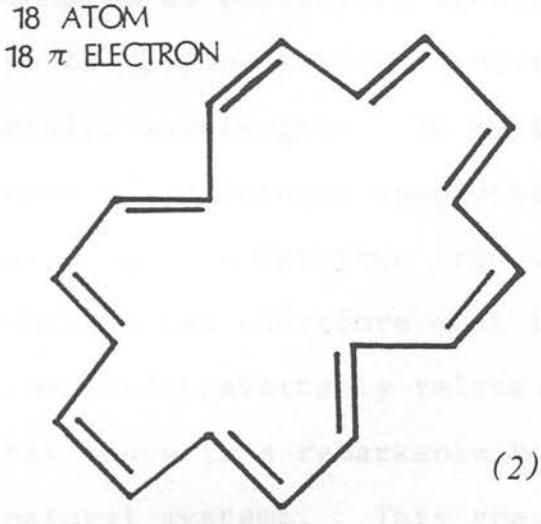

(2)

Aromatic character in porphyrin compounds has been confirmed by measurements of their heats of combustion[12]. Also, X-ray investigations[13] of both metal-free and metalloporphyrins have shown the basic planarity of the nucleus; an essential requirement for aromatic character.

As is generally accepted for aromatic systems then, the porphyrin ligand can be viewed as having a series of independent, filled, π bonding orbitals each containing two electrons and, at higher energy, a corresponding series of unfilled π^* anti-bonding orbitals. In the frontier orbital region of this quantised array of occupied and unoccupied levels specific transitions can occur at discrete excitation energies. These intraligand $\pi - \pi^*$ transitions invariably fall in the visible

/U.V. region of the electromagnetic spectrum, and have very considerable extinction coefficients ($\epsilon \sim 10^5$ $M^{-1}_{cm}{}^{-1}$) being both spin and orbitally allowed. The exact position of these absorption bands will obviously depend on the size of the HOMO (highest occupied molecular orbital)/LUMO (lowest unoccupied molecular orbital) energy gap. Porphyrins are extensively employed as photolytic agents in nature[14] and as such require to respond to their environment by absorbing light of a specific wavelength. To meet this biological need, the colours of porphinato complexes vary throughout the visible region of the spectrum from violet through to red. The HOMO/LUMO gap therefore must be carefully 'tuned' and this must be incontravertably related to the earlier observation that there is a remarkable breadth of porphyrin structure in natural systems. This thesis is dedicated to the study of the electronic effects both the central metal and ring-substitution patterns have in affecting the HOMO/LUMO gap and thus the absorption of light in metalloporphyrins.

Spectroelectrochemical techniques proved to be ideally suited to this purpose as over the past twenty years or so it has become evident that the photolytic activity in these chromophores is invariably accompanied by a reversible change in the redox state of the chromophore, as part of an extensive in vivo electron-transfer chain mechanism[15]. It has been widely noted that an electron or electrons can be added or

removed from metalloporphyrins. A considerable number of studies[16, 17, 18] have reported the chemical reduction and oxidation of various biologically important porphyrins. As a natural extension to this work metalloporphyrins have also been the subject of electrochemical studies in both protic and aprotic media,[19,20] where the reversibility of each redox step was found to be highly dependent on the environment employed. Generally it has been noted free-base porphyrin-type chromophores undergo two one-electron oxidations to give a π cation radical and a π dication and 2 one-electron reductions to give a π anion radical and a π dianion. In suitably dry media it has been reported[21] the porphyrin free base undergoes up to 4 successive one-electron reductions. This pattern of reduction for these pigments indicates that the porphyrin ring has at least two low-lying π^* acceptor orbitals and as such one might expect the porphyrin macrocycle, when complexed, to stabilise low oxidation states of the central metal through π back-bonding. The significance of this however must be tempered by the experimental observation that high oxidation state metal centres can also form very stable porphyrin complexes. In these cases the σ electron-density contribution from the square-plane of the N-donor atoms must be predominant over any π contribution to the bonding. The extent and importance of $d\pi - \pi^*$ back-bonding, previous to this work, have largely been dismissed as negligible.

An extra dimension to the electrochemical behaviour of these ligands appears when they are incorporated in a metal complex. Two distinct electron-transfer sites now exist, the metal centre and the chelating macrocycle. Electron transfer almost invariably takes place on the ligand for main-group metallo-porphyrins. However for transition metal complexes, both oxidation and reduction can result in electron-transfer being either metal-based or ligand-based. For example a one electron oxidation can result in either a porphyrin π -cation radical or the central metal in a higher oxidation state:-

$$(M(II)P) \xrightarrow{-e^-} (M(II)P^{\bullet})^{+}$$

or

$$(M(II)P) \xrightarrow{-e^-} (M(III)P)^{+}$$

P = porphyrin macrocycle.

Similarly a one-electron reduction results in either a porphyrin π -anion radical or the central metal in a lower oxidation state:-

$$(M(II)P) \xrightarrow{+e^-} (M(II)P^{\bullet})^{-}$$

or

$$(M(II)P) \xrightarrow{+e^-} (M(I)P)^{-}$$

Importantly, it must be recognised these absolute assignments are only approximations to the actual situation as, by definition,

we are concerned here with a molecular orbital array, and as such the frontier orbitals will have both ligand and metal character. The amount each contributes is of course dependent on the symmetry of the complex and the subsequent mixing interaction between the metal orbitals and the porphinato π / π^* array (i.e. the covalency of the metal-ligand co-ordinate bond). It is acceptable in the real chemical sense to talk of localisation of the electron-transfer site however, as expansive M.O. calculations[22] have shown that orbital mixing is only ever minimal (with a few rare exceptions).

Confident assignment of the electron-transfer site however has generally been lacking in the literature. The first-row transition metal complexes in particular have been the subject of numerous electrochemical studies directed to this problem but these have largely suffered from one or more of the following drawbacks-

a) Impure samples
b) Lack of uniformity in the media employed, making internal comparisons difficult
c) Solvent coordination to complex
d) Unrecognised involvement of trace impurities in redox mechanism
e) Rapid decomposition of electrogenerated species and consequently insufficient independent spectral characterisation of electrode products.

By combining strict electrochemical methodology with thermally controlled in situ spectroscopic characterisation of the electrode products, the present work attempts to study various transition metalloporphyrins in oxidation states other than their ground state and unambiguously assign their electronic structure.

Combining electrochemistry with electronic spectroscopy is particularly appealing for the highly coloured metalloporphyrins. Both techniques give an independent means of measuring the frontier orbital gap as shown below in Figure 2.

Figure 1.2 Mapping the Electronic Frontier Orbitals

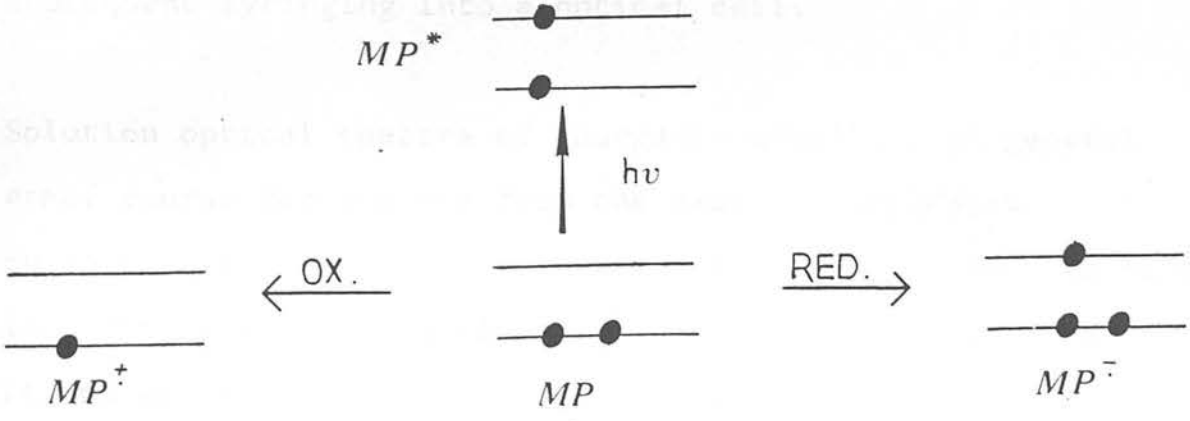

It is clear the energy of the 'vertical' promotion of an electron from the HOMO to the LUMO by the absorption of a photon ($h\upsilon$) is reflected in the E° values for the first one electron oxidation and reduction steps i.e. $h\upsilon = E^\circ_{1st\ ox} - E^\circ_{1st\ red}$. Straightforward voltammetric experiments will therefore

give a measure, if only relative, of the energy of both the HOMO and the LUMO within a series of related metalloporphyrins.

Electronic spectral characterisation for these same metalloporphyrins, in all their available oxidation states, has also been uniquely achieved. This was made possible using an optically transparent electrochemical cell, mounted directly in the spectrophotometer beam. In situ techniques such as this have the great advantage that the course of the electrode reaction can be continuously monitored and reversibility easily checked. Also many of the electrogenerated species were extremely unstable when the applied potential was removed, quickly relaxing back to the starting material. This then precluded normal bulk electrogeneration methods with subsequent syringing into a optical cell.

Solution optical spectra of inorganic complexes in general are of course far removed from the exact structurally characterising nature of say nmr spectroscopy. This is particularly true for metalloporphyrin complexes as many transitions are by their very nature broad and unstructured and often overlapping. However, qualitative and to a lesser extent quantitative comparative absorption spectroscopy has proved particularly worthwhile in this work in elucidating the electronic structure of the electrode products.

The development of a novel cell design also allowed for electro-

generation within the cavity of an electron spin resonance (esr) spectrometer. This proved invaluable for the characterisation of paramagnetic species, generally the π mono-cation and mono- anion radicals. The cell design also, uniquely and importantly, allowed in situ esr monitoring of subsequent redox reactions of these primary electrode products.

Complementary studies on several porphyrin structural analogues are also included. These related species fall into two main categories. The first consists of the biologically relevant complexes based on the chlorin (3) and bacteriochlorin (4) macrocycles.

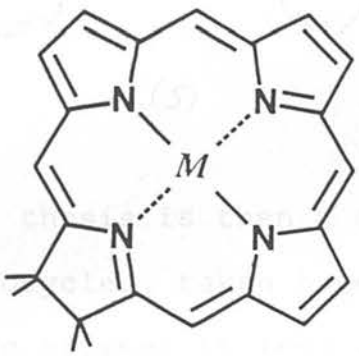

(3)

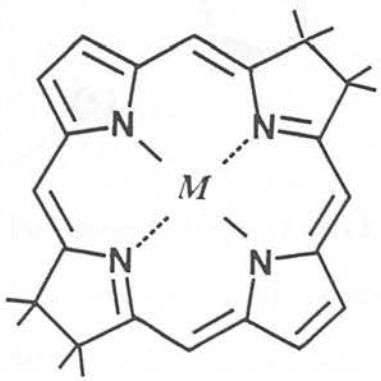

(4)

Chlorins are 7, 8-dihydroporphyrins in which the saturation is traditionally shown in ring D. Bacteriochlorins are tetrahydroporphyrins where opposite subunits are reduced. Both macrocycles have the same conjugative pathway as porphyrins, though less resonance forms can be written for them. These chromophores are especially important in chlorophyll and bacteriochlorophyll biochemistry.[23]

The second category consists of macrocycles with extended conjugative pathways; the phthalocyanines (5) and the tetrabenzoporphyrins (6). These bulky, more insoluble pigments have no natural occurrence but generate a great deal of chemical interest through their varied industrial applications.[24, 25]

(5)

(6)

This thesis is then a study of metallo-complexes of all these macrocycles, taken together as a series of related compounds, in an attempt to lend insight into the subtle variance of electronic properties exhibited by tetra-aza macrocycles.

REFERENCES : CHAPTER 1

1. R.W. Hay "Bio-inorganic Chemistry", Wiley, Chichester, West Sussex (1984).
2. "The Chemical and Physical Behaviour of Porphyrin Compounds and Related Structures", Ann. N.Y. Acad. Sci. 1973, 206, 1.
3. R. Willstatter and A. Stoll, "Investigations on Chlorophyll", Science Press, Lancaster, Ohio (1928).
4. R. Lemberg and J.W. Legge, "Haematin Compounds and Bile Pigments", Interscience, New York (1949).
5. "The Porphyrins", Ed. D. Dolphin, Academic Press, New York, (1980).
6. J.E. Falk, 'Porphyrins and Metalloporphyrins', Elsevier, Amsterdam (1964).
7. A. Treibs, 'Das Leben und Wirken von Hans Fischer', Hans Fischer Gesellschaft e.V., Munchen (1971).
8. J.W. Buchler, "Porphyrins and Metalloporphyrins" Ed. K.M. Smith, Elsevier, Amsterdam (1975), Chapter 5.
9. A. Treibs, Ann. Chem 1935, 517, 172.
10. G. Hodgson, Ann. N.Y. Acad. Sci. 1973, 206, 670.
11. O.T.G. Jones, in ref. 2 above.
12. (a) A. Stern and G. Klebs, Ann. Chem. 1932, 500, 91.
    (b) A. Stern and G. Klebs, Ann. Chem. 1933, 505, 295.
13. J.L. Hoard in ref. 8, Chapter 8.
14. H. Scheer, W.A. Svec, B.T. Cope, M.H. Studier, R.G. Scott

and J.J. Katz, J. Am. Chem. Soc., 1974, 96, 3714.

15. R.E. Dickerson and I. Geis, "The Structure and Action of Proteins", Harper and Row (1969).
16. P. George, Biochem. J. 1953, 54, 267.
17. J.D. McElroy, G. Feher and D. Mauzerall, Biochim. Biophys. Acta. 1972, 267, 363.
18. D. Dolphin and R.H. Felton, Acc. Chem. Res., 1974, 7, 26.
19. R.H. Felton and H. Linschitz , J. Am. Chem. Soc. 1966, 88, 1113.
20. K.M. Kadish and J. Jordan Anal. Lett., 1970, 3, 113.
21. D.W. Clack and N.S. Hush, J. Am. Chem. Soc. 1965, 87, 4238.
22. M. Gouterman, J. Chem. Phys. 1959, 30, 1139.
23. D.C. Borg, J. Fajer, R.H. Felton and D. Dolphin, Proc. Nat. Acad. Sci., 1970, 67, 813.
24. J. Martinsen, L.J. Pace, T.E. Philips, B.M. Hoffman and J.A. Ibers, J. Am. Chem. Soc., 1982, 104, 83.

CHAPTER 2 : AN ELECTROCHEMICAL STUDY OF METALLOPORPHYRINS

2.1 INTRODUCTION

There have been many previous reports in the literature on the electronic and redox properties of the porphin ring in both protic and aprotic media[1-12]. The common macrocycles $\alpha, \beta, \gamma, \delta$, - tetraphenylporphyrin (TPP) (1) and 1, 2, ... 7, 8-octaethylporphyrin (OEP) (2) have been the favoured models for both optical and electrochemical study.

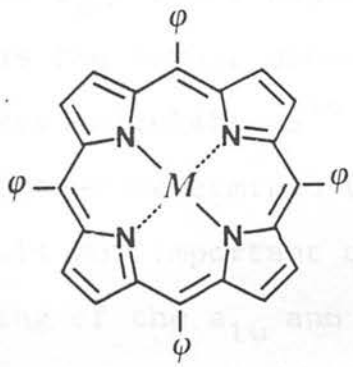

(1)

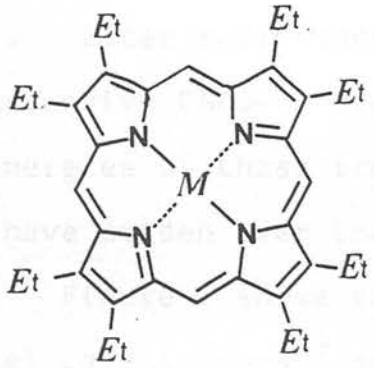

(2)

Porphin itself has not been so extensively studied as these synthetic derivatives because it has only been made in low yield preparations and only recently have the best conditions for synthesis been determined[13]. Molecular orbital calculations on both OEP and TPP have shown them to be electronically representative of the parent porphin[14].

Optical absorption spectroscopy and electrochemistry are fundamentally concerned with the energy gap between the frontier orbitals. It is essential therefore to appreciate the nature of the symmetry of these orbitals when interpreting both optical and redox data.

An early Huckel model by Longuet-Higgens et al[15] envisaged the porphyrin ring as an 18 membered cyclic polyene, having 18 π electrons. These calculations showed 2 π orbitals very close in energy as the highest filled orbitals of symmetry a_{1u} and a_{2u}, and a degenerate pair of π^* orbitals of symmetry e_g as the lowest unoccupied orbital. Later refinements to these calculations[16,17] and more extensive CNDO-CI studies[18] have better determined the relative energies of these frontier orbitals but important disagreements have arisen over the ordering of the a_{1u} and a_{2u} orbitals. Figure 1 shows the M.O. Array arising from both the Huckel calculations[19] and a subsequent SCF study[18]. As will be shown in Chapter 3 the relative order of the a_{2u} and a_{1u} orbitals can invert in certain cases and thus both sets of calculations have their merits. It is generally found however that the a_{2u} orbital is higher in energy than a_{1u} for most metalloporphyrins. As the calculated energy gap between these frontier orbitals lies in the visible region it is the π/π^* transitions ($1a_{1u} - 4e_g$) and ($3a_{2u} - 4e_g$) which give these chromophores their strong colouring. Typical metalloporphyrin optical

Figure 2.1 M.O. Array of the porhinato moiety

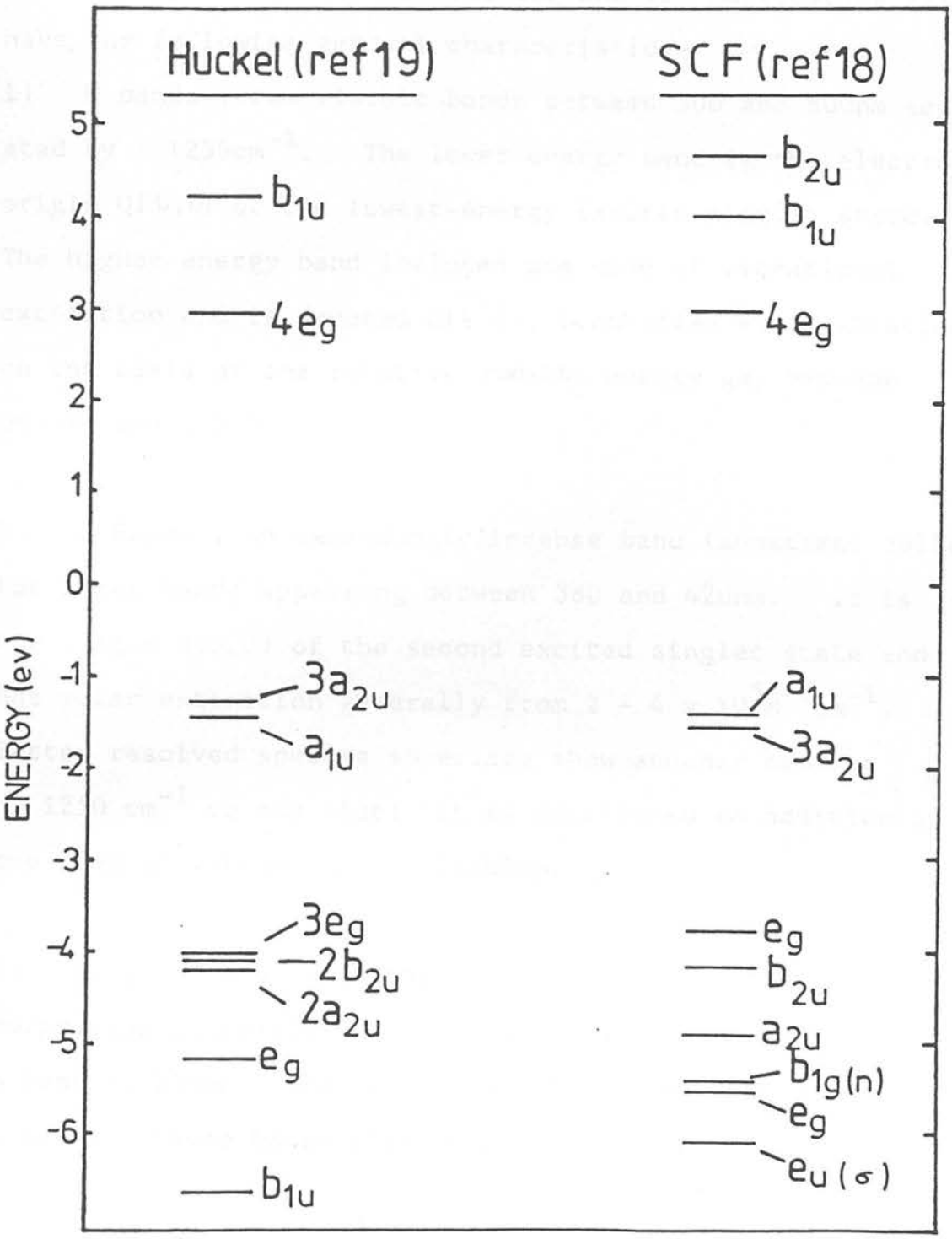

absorption spectra are shown in Figure 2.

Metalloporphyrins based on the OEP and TPP macrocycles all have the following general characeristics-

1) Q bands : two visible bands between 500 and 600nm separated by $1250cm^{-1}$. The lower energy band is the electronic origin Q(0,0) of the lowest-energy excited singlet state. The higher energy band includes one mode of vibrational excitation and is denoted Q(1,0), identified as a vibration on the basis of the relative constant energy gap between Q(1,0) and Q(0,0).

2) B Bands : An exceedingly intense band (sometimes called the Soret band) appearing between 380 and 420nm. It is the origin B(0,0) of the second excited singlet state and has molar extinction generally from $2 - 4 \times 10^5 M^{-1} cm^{-1}$. Better resolved spectra sometimes show another band at $\sim 1250\ cm^{-1}$ to the blue; it is attributed to addition of one mode of vibrational excitation.

3) N, L, M bands - To the blue of the Soret band; metalloporphyrins generally show a weaker N band at ~ 325nm and an M band at 215nm. Between these they often show a weaker L band. These bands will be mentioned only in passing.

All the above bands are π / π^* in origin. The classification

Figure 2.2 Electronic absorption spectra of Co(II)TPP and Zn(II)OEP

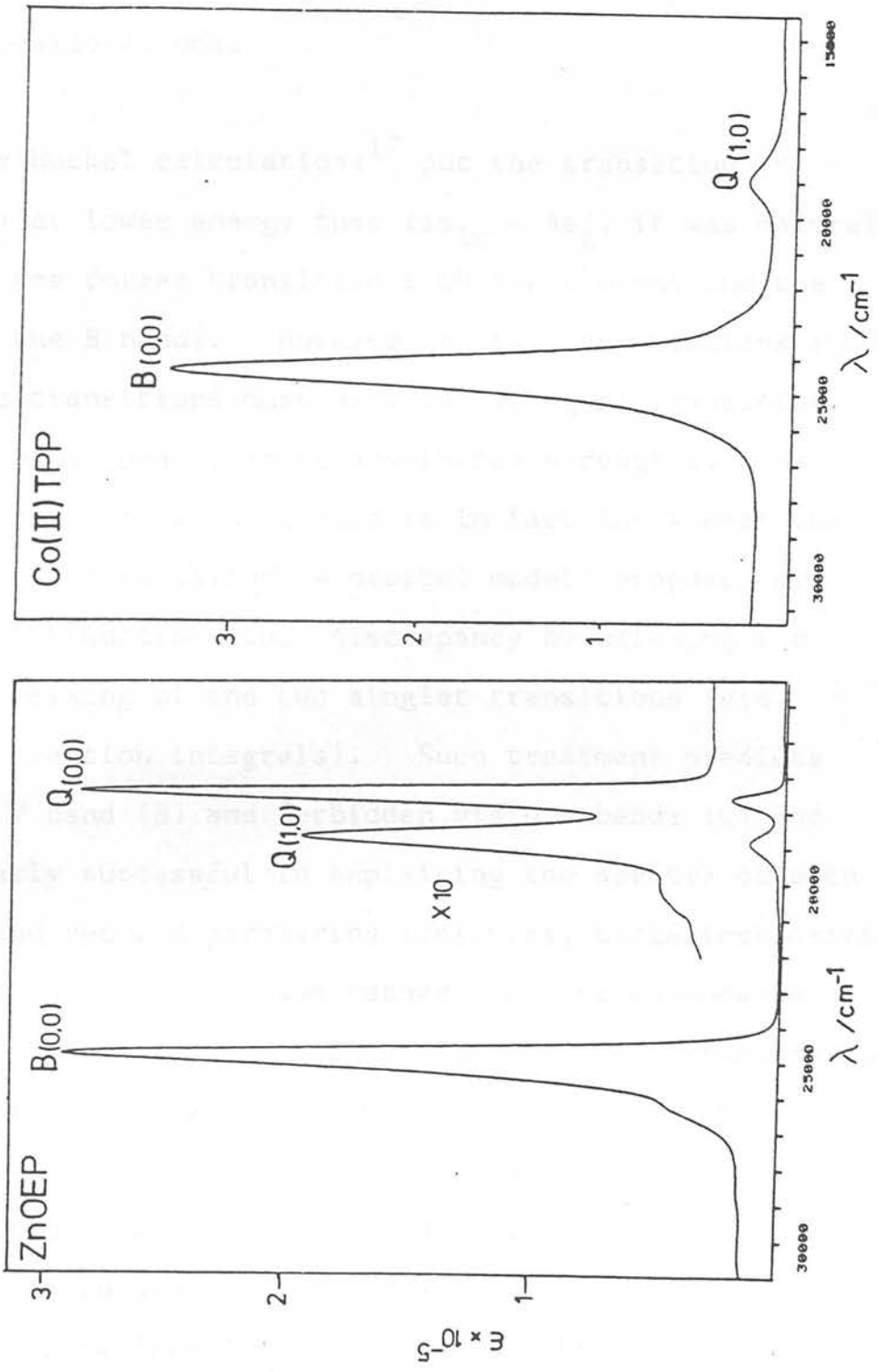

of these bands comes from the pioneering study of Platt[20] where B is termed as a strongly allowed excited state and Q as a quasi-allowed one.

As the early Huckel calculations[17] put the transition ($3a_{2u} - 4e_g$) at lower energy than ($1a_{1u} - 4e_g$) it was natural to identify the former transition with the Q bands and the latter with the B bands. However the same calculations show that the two transitions must have nearly equal transition dipoles and hence nearly equal absorption strengths. As is clear from Figure 2 the Q band is in fact far weaker than the B band. The so called '4 orbital model' proposed by Gouterman[16] rationalised this discrepancy by allowing for considerable mixing of the two singlet transitions (via electron interaction integrals). Such treatment predicts an allowed UV band (B) and forbidden visible bands (Q) and is particularly successful in explaining the spectra of both porphyrins and reduced porphyrins (chlorins, bacteriochlorins, etc.) This early theory gave rather poor correspondence between bond-order and bond length but later Pariser-Parr-Pople (PPP) calculations[17] refined it to such an extent the 4 orbital model is widely accepted as the best method for explaining porphyrin optical data. However the essence of PPP computer calculations is to separate the loosely bound π electrons from the remaining 'core' and to treat electron interaction among the π electrons explicitly. This treatment then

precludes any effect the central substituent may have on the frontier orbitals and thus on the energy of the π / π^* transitions. In fact, the nature of the central metal has been found to have such a significant effect it has been necessary to separate porphyrin spectra into 'regular' and 'irregular' categories.[14] A regular porphyrin is one whose optical absorption and emission spectra are determined essentially by the π electrons of the porphyrin ring with only minor perturbation from the electrons of the central substituent (Groups I - V, Valence I - V respectively). Irregular porphyrins are those where the nature of the optical absorption and emission spectra are greatly affected by the central metal. They can in turn be sub-divided into two classes of unusual absorption types, namely hypso and hyper, which are defined below.

a) Hypso absorption spectra are like normal absorption spectra but are blue-shifted. Such spectra are shown by transition metal porphyrins of Groups VIII and IB with electron configuration d^n where n = 6-9.

b) Hyper absorption spectra show prominent extra absorption bands in addition to the Q, B and N bands in the region $\lambda > 320$nm.

Therefore for irregular porphyrins there would seem to be extensive interaction between the π electrons of the ring

and the electrons of the central atom and interpretation of these experimental observations must go beyond the π electron methods described earlier. Iterative extended Huckel (IEH) models[21], in which valence electrons of the porphyrin ring, the central metal and any axial ligands are included, have recently proved popular for this purpose. However although successful in predicting transitions which might occur, the method is unreliable when predicting the exact energy of that transition. As IEH calculations cannot accurately predict transition energies, IEH theory cannot quantitatively explain observations such as why the Q(0,0) absorption band systematically moves to the blue through the series $Fe(OEP)py_2$, $Ru(OEP)py_2$ and $Os(OEP)py_2$[22]. Antipas et al[22] have tentatively assigned this phenomena, and hypso absorption spectra in general, as arising from mixing of the empty $e_g(\pi^*)$ orbitals of the ring with the filled d π orbitals of the metal. This is more familiarly described as metal to ligand d π - π^* back bonding, a common occurrence in inorganic chemistry, especially for organo-metallic complexes where the ligand possesses both Lewis base properties and π acid properties, as is the expected case for the porphinato moiety.

There is an independent means of testing this assignment. As has previously been shown the electrochemical values of $E_{\frac{1}{2}}$(1st ox) and $E_{\frac{1}{2}}$(1st red) allow an alternative method for measuring the frontier orbital gap. Thus the behaviour noted

optically should be mirrored in electrochemical studies of the same metalloporphyrins. Despite the plethora of reports on the redox properties of metalloporphyrins in the literature[23] no evidence for $d\pi - \pi^*$ back-bonding in these complexes has been noted. Although this particular problem has not been specifically tackled previous to recent work in our laboratory[24], what is most disappointing is that existing electrochemical data for metalloporphyrins and the interpretation of the results to date, unanimously dismiss the back donation of electron density from the metal to the porphyrin ring as insignificant.

Electrochemical studies of metalloporphyrins started at around the same time as the spectroscopic work detailed above, both techniques flourishing as the excitement of porphyrin chemistry and the awareness of their biological role grew in the early 1960's. The first important redox work was by Closs and Closs[25] who demonstrated ZnTPP could be reduced to both an anion radical and dianion, the final oxidation state depending on the reducing strength of the chemical agent involved. The stepwise addition of two electrons into the π orbital manifold of other polynuclear aromatic hydrocarbons had been looked at previously[26], but these initial products were viewed as being only transient intermediates towards subsequently hydrogenated products thus-

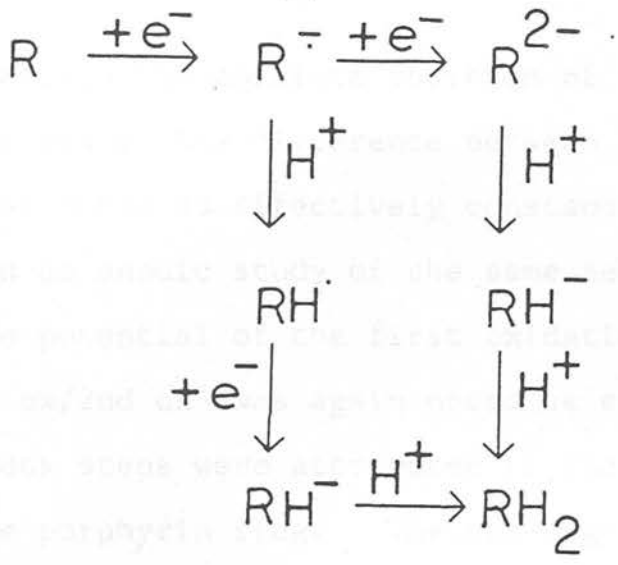

Closs and Closs's achievement was to highlight the degree of stability both the anion radical and dianion of a metalloporphyrin possessed in reasonably aprotic media.

Subsequent cathodic electrochemical investigations by Felton[1] and Hush[2] showed metalloporphyrins, and close structural analogues, could be reduced in four successive one-electron steps. Later, porphyrin redox chemistry was extended into the anodic region, when Stanienda and Biebl[3] showed the porphyrin macrocycle was also capable of losing two electrons stepwise to an external electrode. The products were assigned as a π cation radical and a π dication. Thus the porphinato moiety was quickly shown to have the ability to exist in a rich variety of oxidation states.

Much of the characterisation of these products was based on the worthwhile, but non-rigorous, internal comparison of $E_{\frac{1}{2}}$ values within a series of related metalloporphyrins. Thus for Felton's polarographic study of MTPP (M = Co, Ni, Cu, Zn)[1]

in DMSO, although the absolute position of the first reduction varied considerably the difference between first and second reduction was noted as effectively constant (-0.40V). Similarly in an anodic study of the same series[4], in butyronitrile, the potential of the first oxidation varied widely but ΔE(1st ox/2nd ox) was again noted as constant and as such all redox steps were attributed to changes in oxidation state of the porphyrin ring. The non-rigorous methodology employed is however highlighted in this particular case as the first oxidation of Co(II)TPP is presently attributed not to a $P/P^{+\cdot}$ couple but rather a Co(II)/(III) oxidation.

The variance in the absolute values of both the $MP/MP^{+\cdot}$ and $MP/MP^{-\cdot}$ couples with central metal substituent engendered a great deal of discussion. Various correlations relating ring reduction potential to electronegativity of the central metal and ring oxidation potentials to the second and third ionisation potential of the central metal had varying success[1-5]. An important landmark paper which appeared in 1973 by Fuhrhop et al[27] appeared to explain the redox behaviour of metalloporphyrins satisfactorily. This was the first work which combined cathodic (in DMSO) and anodic (in Butyronitrile) studies on a series of metalloporphyrins, namely twenty-five metallo-octaethylporphyrins. It was also the first to compare the electrochemical behaviour of regular and irregular metalloporphyrins. They observed that in the absence of redox

active metal centres the separation between the first oxidation and the first reduction was constant at 2.25 ± 0.15V. The previously observed trends in $\Delta E_{\frac{1}{2}}$(1st red/2nd red) and $\Delta E_{\frac{1}{2}}$ (1st ox/2nd ox) were noted and quantified as 0.20 ± 0.05V and 0.42 ± 0.05V respectively. The value of 2.25V for ΔE (1st ox/1st red) was particularly gratifying as it agreed closely with the Huckel calculations, mentioned earlier, which predicted the transition energy of the Q band to be approximately $16000cm^{-1}$ or 2.0eV[14]. Departures from this value were used to identify intervening metal-based redox processes. The apparent consistencies within the electrochemical data for the MOEP series led Fuhrhop to propose that the effect of the central metal on the porphyrin ring was purely inductive. He envisaged that the more electron-donating the metal the more difficult it would be to reduce the porphyrin ring and the easier it would be to oxidise. This then would explain the variance in absolute $E_{\frac{1}{2}}$ values and account for the constant $\Delta E_{\frac{1}{2}}$ (1st ox/1st red). Moreover this inductive term would not appear when considering the differences $\Delta E_{\frac{1}{2}}$ (1st ox/2nd ox) and $\Delta E_{\frac{1}{2}}$ (1st red/2nd red) and these values should consequently be constant throughout the series, as was found. The inductive model of Fuhrhop is displayed graphically in Figure 3. When $E_{\frac{1}{2}}$ (1st ox) and $E_{\frac{1}{2}}$ (1st red) were plotted against central metal electronegativity they gave linear, parallel lines. This correlation was limited to a small subset of divalent metals for which

Figure 2.3 Summary of Fuhrhop's Inductive Model for the Electrochemical Behaviour of Metalloporphyrins

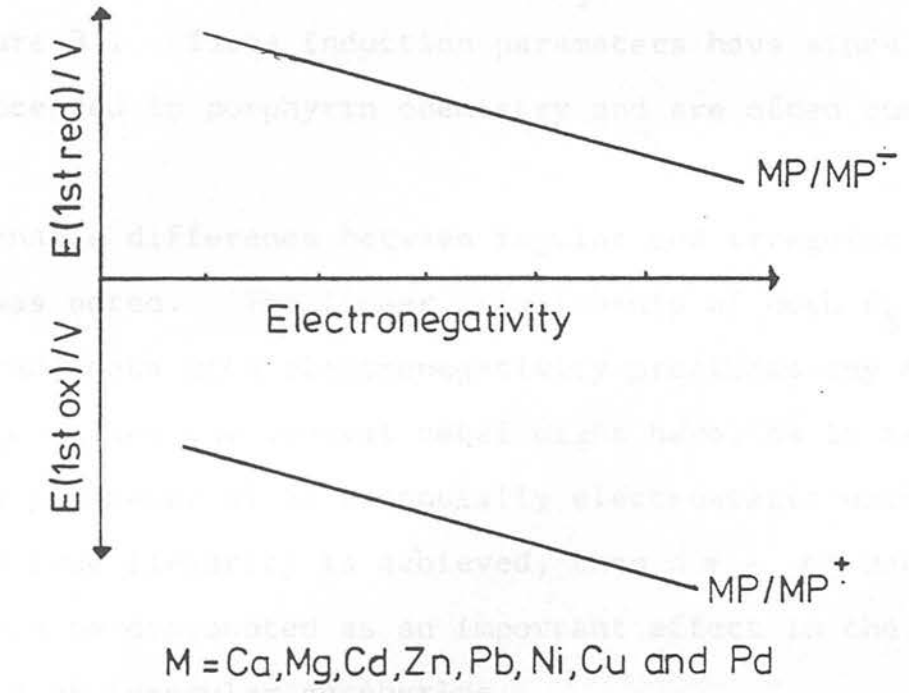

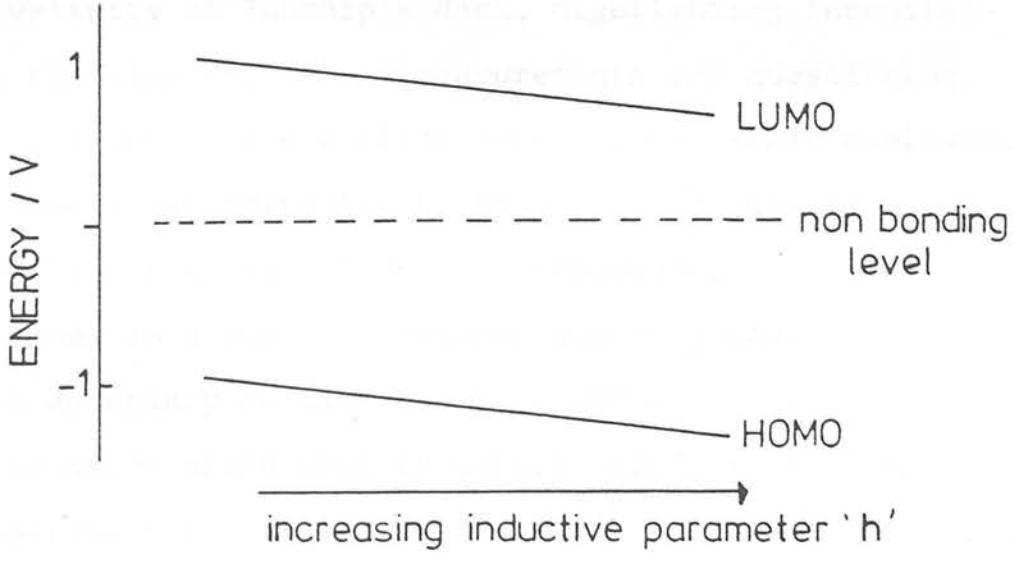

suitable electronegativity values could be found. Satisfied with the linearity of the $E_{\frac{1}{2}}$ electronegativity plots, the authors then defined a metal induction parameter, h, for all the metal centres such that a linear $E_{\frac{1}{2}}/h$ graph was obtained (see Figure 3). These induction parameters have since been widely accepted in porphyrin chemistry and are often quoted.

No discernable difference between regular and irregular porphyrins was noted. The linear relationship of both $E_{\frac{1}{2}}$ (ox) and $E_{\frac{1}{2}}$ (red) data with electronegativity precludes any π back-bonding qualities the central metal might have, as it is an inductive parameter of an essentially electrostatic nature. If indeed true linearity is achieved, then $d\pi - \pi^*$ back bonding can be discounted as an important effect in the optical properties of irregular porphyrins.

Recent work in our laboratory[24, 28, 29] has however cast doubt over the validity of Fuhrhop's data, highlighting inconsistencies in the electrochemical measurements and questioning the appropriateness of the electronegativity values employed. These studies arose primarily to allow measurement of $E_{\frac{1}{2}}$ values of first row transition metalloporphyrins and metallophthalocyanines in a strictly non-coordinating medium. This was deemed necessary as subsequent to Fuhmop's work reports in the literature noted that E° values were strongly dependent on the experimental environment employed. The unlikely medium

chosen was methylnaphthalene, heated to 150°C to facilitate solubility of the pigments. Unfortunately the available electrochemical solvent range of methylnaphthalene allowed only the study of the cathodic redox properties of these pigments. Still, even within the limits imposed by the medium it was confidently concluded that only a loose quantitative association between reduction potentials and electronegativity could be drawn (i.e. the more electronegative the metal the less negative the ligand reduction potential). However although critical of a direct correlation of E° values with any single inductive parameter, the order of reduction potentials gave rise to the conclusion that the metal exerted predominantly a polarising electrostatic effect and π back-bonding contributions to the bonding were unnecessary in explaining the data.

It would appear then the complementary relationship between electrochemical and optical data has broken down. Redox data has thus far been unable to validate the importance of $d\pi - \pi^*$ back-bonding which spectroscopists have assumed responsible for the blue-shifted nature of hypso-porphyrins.

In this work we re-examine the electrochemistry of a logical series of metalloporphyrins to reassess the relative importance of the σ and π contributions in the bonding of such complexes. The $3d^{6-10}$ first row transition metal complexes

of OEP and TPP were studied. In the event, redox processes occurring at the metal centre for the Fe(II) and Co(II) porphyrins severely limited suitable interpretation of the data for those particular complexes. Aware that $d\pi - \pi^*$ back-bonding would be greater for the second and third row transition metals it was proposed also to study an isovalent triad of metalloporphyrin complexes. As noted previously, optical studies on Fe(II), Ru(II) and Os(II) porphyrins show the Q(0,0) band moves systematically to the blue on going from first row through to third row transition metal[22]. Here it was decided to concentrate not on the d^6 triad as again probable metal-centered redox processes would prevent clear interpretation, but rather on the d^8 triad, Ni(II), Pd(II), and Pt(II). It was hoped these metalloporphyrins would exhibit only ligand-based redox processes allowing direct comparison of $E_{\frac{1}{2}}$ values down the group.

Our chosen experimental medium was limited by a number of considerations. Previous studies[30-32] have shown solvent interaction with metalloporphyrins grossly distorted redox trends and thus a non-coordinating solvent was essential. Also as the effects we hoped to measure were expected to be comparatively small we were intent on studying both the anodic and cathodic redox properties in a uniform medium for the first time. The chosen solvent therefore required to have a potential range of ± 2.5 volts vs Ag/AgCl reference. CH_2Cl_2 met both the above criteria. The unfavourably low

dielectric constant of CH_2Cl_2 (9.08) for electrochemical purposes was overcome by employing a large excess of inert electrolyte, tetrabutylammonium tetrafluoroborate ($TBABF_4$). $TBABF_4$, importantly, is considered to be non-coordinating. Given our interest in determining accurately the relative reduction potential values of the various derivatives, conventional electrochemical measurements on individual compounds in isolation was felt to be inadequate. A scheme of cross-referenced experiments was devised, where in each case two or more compounds were studied simultaneously in the same solution.

By such rigorous methodology it was hoped to solve the existing compelling contradictions in the literature.

2.2 RESULTS

The electrode potentials measured for all the metalloporphyrins studied, including those for the free bases H_2OEP and H_2TPP are listed in Table 1 (anodic values) and Table 2 (cathodic values). Spectroelectrochemical characterisation of the electrode products and subsequent assignment of the redox-couple involved will be discussed in Chapter 3. We are concerned in this chapter primarily with the macrocycle-based electron-transfer steps $MP^{o/+\cdot}$ ($E_{\frac{1}{2}}$ (1st ox)), $MP^{+\cdot/2+}$ ($E_{\frac{1}{2}}$ (2nd ox)), $MP^{0/-}$ ($E_{\frac{1}{2}}$(1st red)) and $MP^{-/2-}$ ($E_{\frac{1}{2}}$(2nd red)), where the oxidation state of the metal centre stays constant throughout. All of the metallo-

Table 2.1 Anodic Redox Potentials for MOEP and MTPP in CH_2Cl_2/0.5M $TBABF_4$ at 20°C

	$E_{1/2}(M^{II/III})$/V*	$E_{1/2}$(1st ox)/V	$E_{1/2}$(2nd ox)/V	ΔE(1st ox/2nd ox)
H_2TPP	-	0.76	1.00	0.23
ZnTPP	-	0.60	0.86	0.26
CuTPP	-	0.70	0.99	0.29
NiTPP	-	0.77	1.01	0.24
CoTPP	0.41	0.83	1.02	0.19
FeTPPCl	-0.59	0.87	1.16	0.29
PdTPP	-	0.84	1.27	0.43
AgTPP	0.32	0.88	1.19	0.21
PtTPP	0.82	1.31	1.54	0.23
H_2OEP	-	0.66	1.16	0.50
ZnOEP	-	0.44	0.74	0.30
CuOEP	-	0.51	0.93	0.42
NiOEP	-	0.56	1.08	0.52
CoOEP	0.43	0.64	0.92	0.28
FeOEPCl	-0.63	0.70	1.12	0.42
PdOEP	-	0.63	1.31	0.68
AgOEP	0.30	0.68	0.96	0.28
PtOEP	-	0.68	1.40	0.72

* Volts vs Ag/AgCl reference electrode.

Table 2.2 Cathodic Redox Potentials for MOEP and MTPP in CH_2Cl_2/0.5M $TBABF_4$ at 20°C

	$E_{1/2}(M^{II/I})$/V*	$E_{1/2}$(1st red)/V	$E_{1/2}$(2nd red)/V	ΔE(1st red /2nd red)
H_2TPP	-	-1.41	-1.77	0.36
ZnTPP	-	-1.57	-1.94	0.37
CuTPP	-	-1.51	-1.92	0.41
NiTPP	-	-1.49	-2.06	0.57
CoTPP	-1.11	-2.16	-	-
FeTPPCl	-1.32	-1.91	-2.33	0.42
PdTPP	-	-1.54	-1.98	0.45
AgTPP	-1.27	-1.99	-	-
PtTPP	-	-1.56	-2.04	0.48
H_2OEP	-	-1.54	-2.00	0.46
ZnOEP	-	-1.76	-2.22	0.46
CuOEP	-	-1.70	-2.14	0.49
NiOEP	-	-1.68	-2.28	0.60
CoOEP	-1.26	-2.51	-	-
FeOEPCl	-1.44	-2.03	-2.46	0.43
PdOEP	-	-1.75	-2.40	0.65
AgOEP	-1.30	-2.23	-	-
PtOEP	-	-1.78	-2.44	0.66

* Volts vs Ag/AgCl reference electrode

porphyrins studied exhibited two successive macrocycle-based oxidations and all except the cobalt and silver porphyrins exhibited two successive macrocycle-based reductions. Reduction potentials were independent of electrode surface employed whether gold, platinum, or mercury. Oxidation potentials could only be measured at a platinum button electrode as the oxidation of both Au and Hg precede that of the metalloporphyrins.

It is emphasised that a platinum electrode allowed measurement of both reduction and oxidation waves in one voltage scan, and thus precise values for Δ E (1st ox/2nd ox), ΔE(1st red/2nd red) and most importantly and uniquely ΔE (1st ox/1st red) were obtained from one voltammogram. The full a.c. voltammogram for H_2TPP, for example, is shown in Figure 4.

An example of the cross-referenced experiment referred to earlier is shown in Figure 5, from the like of which an exact order of ease of reduction and oxidation for the metalloporphyrins could be obtained. Thus absolute incremental differences between $E_{\frac{1}{2}}$ potentials within each series and between series, could be evaluated accurately.

We were strongly reassured of the non-coordinating nature of the $CH_2Cl_2/TBABF_4$ medium by the striking similarity of the present cathodic data with the previous methylnaphthalene

Figure 2.4 A.c. voltammogram of H_2TPP

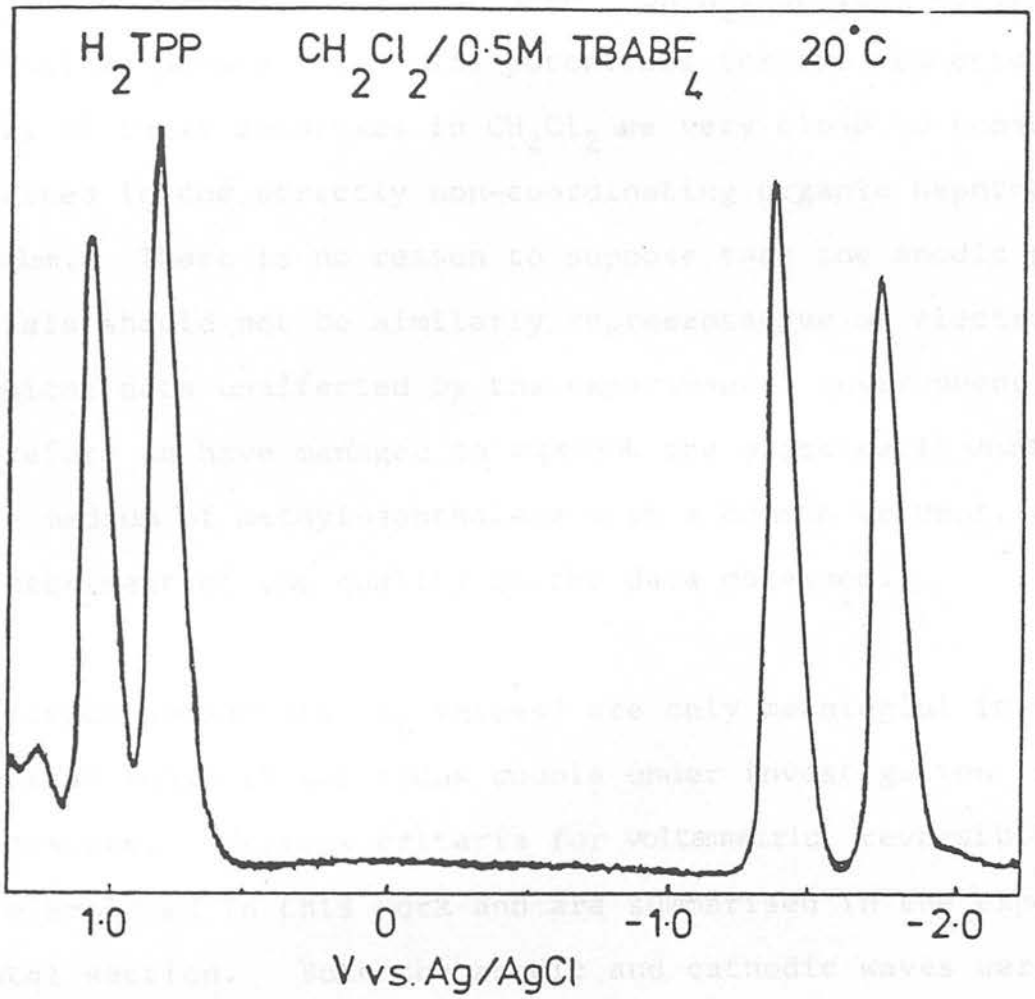

Figure 2.5 A.c. voltammogram of ZnTPP and ZnOEP in CH_2Cl_2/0.5M $TBABF_4$ at 20°C

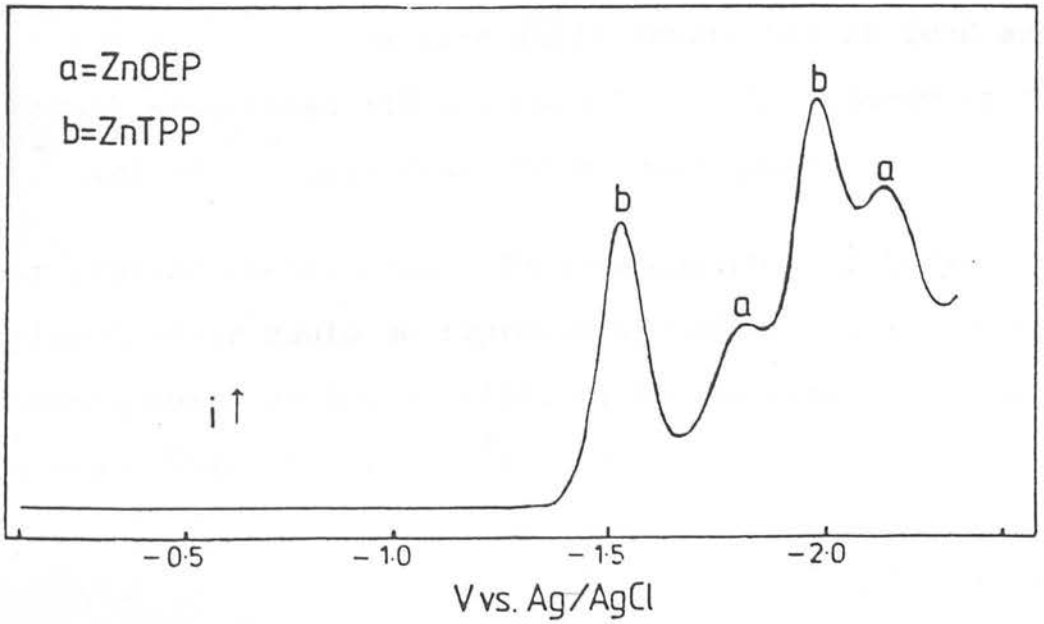

studies by Campbell[28] and McQueen[24] on H_2, Zn(II), Cu(II) and Ni(II) porphyrins. The potentials for the reduction waves of these complexes in CH_2Cl_2 are very close to those obtained in the strictly non-coordinating organic naphthalene medium. There is no reason to suppose that the anodic potentials should not be similarly representative of electrochemical data unaffected by the experimental environment. Therefore we have managed to supplant the practically unmalleable medium of methylnaphthalene with a common solvent, to no detriment of the quality of the data obtained.

Electrode potentials ($E_{\frac{1}{2}}$ values) are only meaningful in a chemical sense if the redox couple under investigation is reversible. Various criteria for voltammetric reversibility were employed in this work and are summarised in the experimental section. Both the anodic and cathodic waves were all shown to be diffusion-controlled reversible one-electron transfers by analysis of the a.c. polarographic and cyclic voltammetric behaviour. It was generally found the $MP^{0/+\cdot}$ and $MP^{0/-\cdot}$ couples were fully reversible at 20°C and at normal sweep rates (10 - 100mVs^{-1}). The subsequent couples $MP^{+/2+\cdot}$ and $MP^{-/2-\cdot}$ were found to be only quasi-reversible under similar conditions. The reversibility of these redox couples however could be improved by cooling the solution down to temperatures as low as -70°C or by scanning at unusually fast scan rates (1 - 10 Vs^{-1}). Specific experimental con-

ditions for reversibility of each wave to be achieved are noted in Chapter 3.

Figure 6 shows a cyclic voltammogram sweep rate dependence experiment for the first oxidation of PdTPP where the height of the wave is linearly related to the square root of the sweep rate employed. Figure 7 shows the dependence of a.c. peak height on the frequency of the a.c. pulse employed, for the oxidations of ZnTPP. A plot of peak height against the square root of the a.c. frequency is linear for a fully reversible wave.

All measured $E_{\frac{1}{2}}$ values were found to be completely independent of solution temperature (+20°C to - 70°C) and concentration of complex (1.5×10^{-5} to 4.0×10^{-3}M).

The metal complexes of both porphinato ligands, OEP and TPP, exhibit similar electrochemical properties. Generally the MOEP series is harder to reduce and easier to oxidise than the corresponding MTPP complexes. This is consistent with the electron-donating nature of the ethyl substituents of OEP pushing electron density into the ring. The meso-phenyl substituents of TPP play no such inductive role, being almost perpendicular to the plane of the ring[33] and thus to a great extent unable to participate in the π conjugative pathway.

Figure 2.6 C.V. scan rate dependence experiment on the $Pd(II)TPP/Pd(II)TPP^{+}$ redox couple

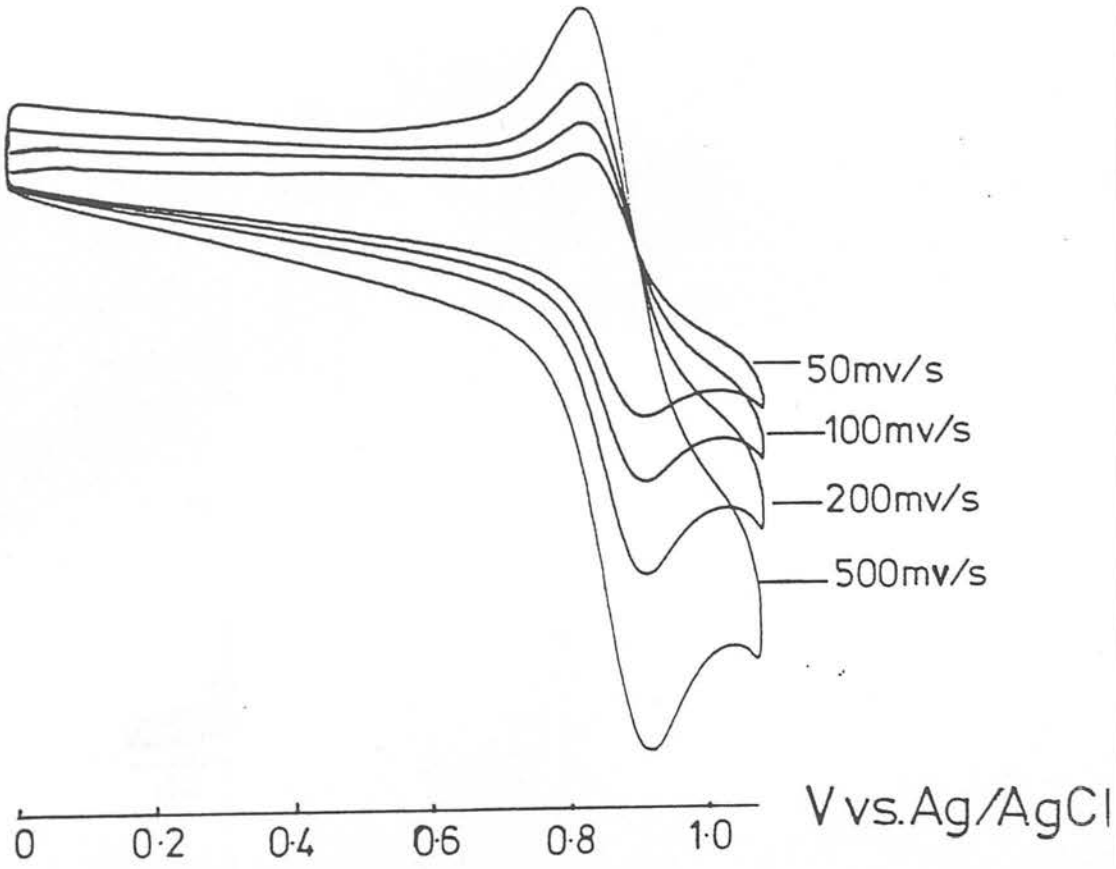

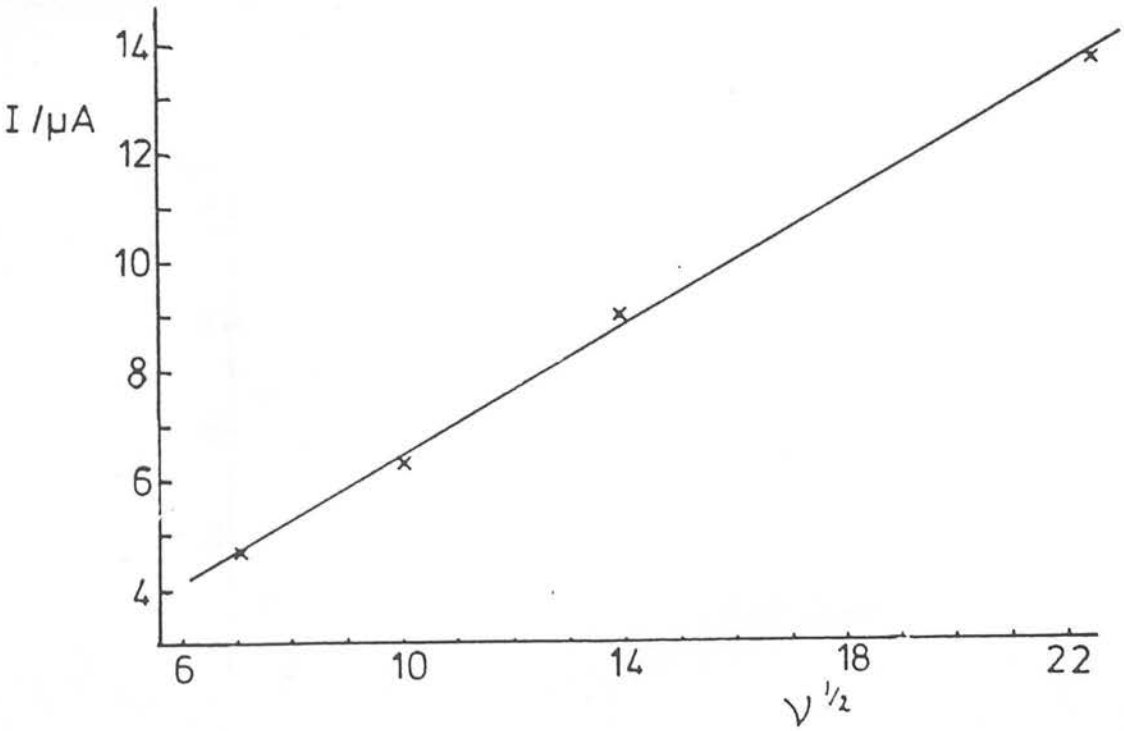

Figure 2.7 A.c. frequency dependence experiment on the anodic waves of ZnTPP

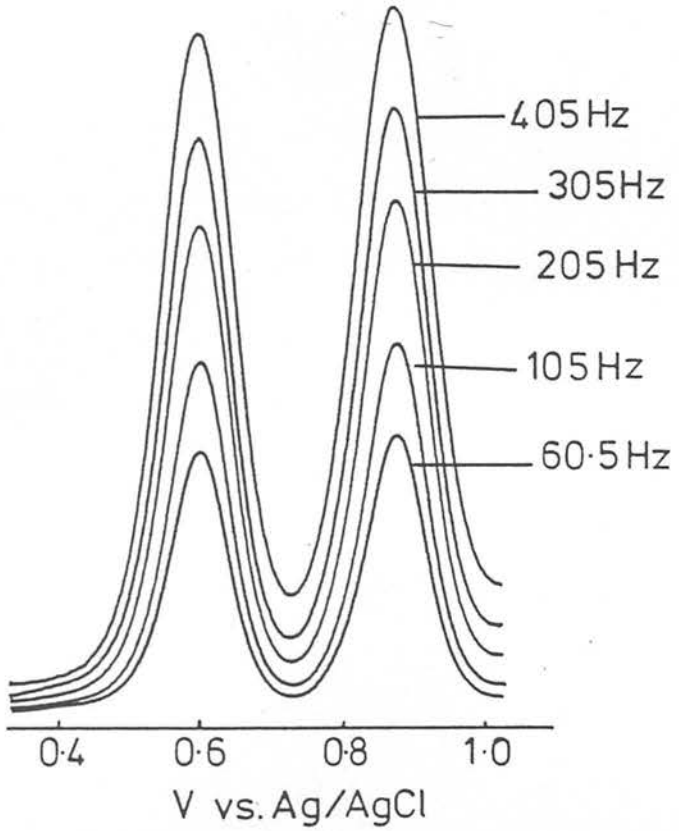

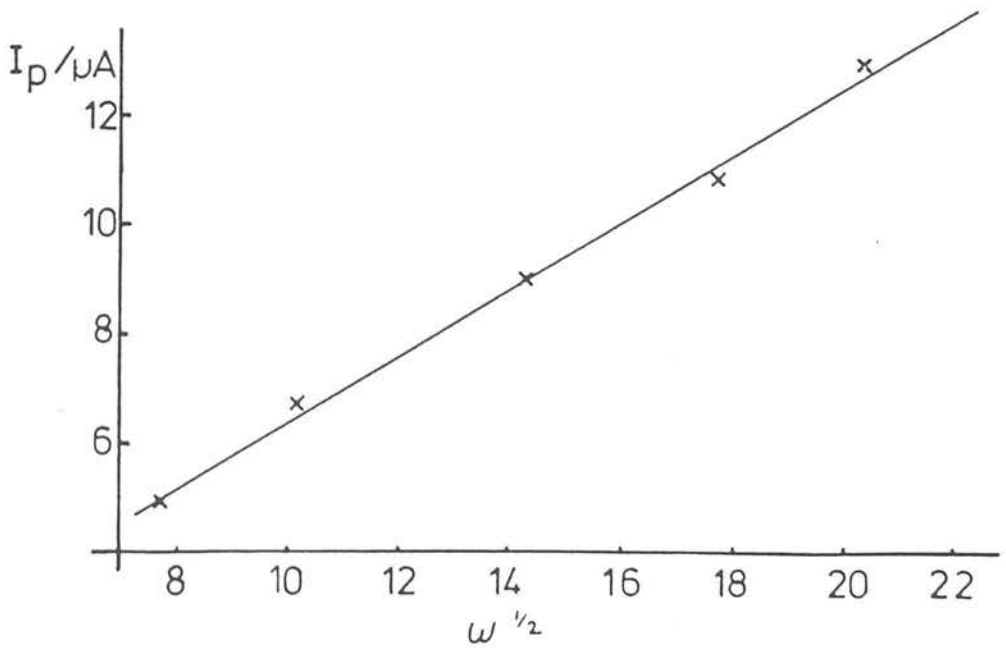

(w = frequency of a.c. pulse)

As has been noted in previous electrochemical studies the absolute values of $E_{\frac{1}{2}}$ (1st red) and $E_{\frac{1}{2}}$ (1st ox) vary considerably with metal centre, and similar trends of ease of oxidation and ease of reduction are found for both series of metalloporphyrins. The order of ease of primary oxidation for the divalent metal centre complexes, is found to be -

$$Zn(II) < Cu(II) < Ni(II) < Pd(II) < Pt(II)^*$$

(*OEP figure only).

This order is repeated for the second oxidation wave. We were most interested in testing our data against the parameters set down by Fuhrhop's inductive model[27], to check upon the validity it truly holds for metalloporphyrins. As previously outlined Fuhrhop chose electronegativity as a measure of the inductive power of the central metal. The two most common sets of electronegativity values are the Pauling scale and the Allred-Rochow scale[34]. Fuhrhop however used neither of these scales but numbers obtained from a dated paper by Gordy and Thomas[35]. These values were chosen essentially on a random combination of bond energies, ionisation energies and force constant calculations. This has been discussed at length by McQueen[24] who dismissed the appropriateness of this rather contrived scale. It was subsequently found Pauling's electronegativity values fit Fuhrhop's data to within the same degree of error as the Gordy/Thomas figures. The Allred-Rochow scale gave no meaningful correlation with the

electrochemical data. We chose therefore to adopt the Pauling electronegativity scale (X) as the inductive parameter to evaluate our data against.

Figure 8 shows the anodic redox data for the MOEP and MTPP series plotted against the Pauling electronegativity value of the central metal. The $MOEP^{0/+\cdot}$ and $MTPP^{0/+\cdot}$ redox couples give straight line plots which, in addition, are parallel. The parallel behaviour of both porphyrin rings shows the two macrocycles are affected to the same degree by the central metal electronegativity. The linear relationship is of course as predicted by Fuhrhop.

Approximate linearity is also obtained for the second oxidation $E_{\frac{1}{2}}$ values.(Fig. 8). Importantly, however, these lines are <u>not</u> parallel to either each other or to the behaviour of the first oxidations. The gradients of both the $MTPP^{+/2+\cdot}$ and $MOEP^{+/2+\cdot}$ lines are much greater than that observed for $MTPP^{0/+\cdot}$ and $MOEP^{0/+\cdot}$. The $MOEP^{+/2+\cdot}$ plot, in particular, diverges quite dramatically from the corresponding first oxidation line. This observation can be more clearly stated as, the greater the value of the central metal electronegativity, the greater is the resulting value of ΔE(1st ox/2nd ox). This is a new observation and contrasts with the previous widespread acceptance that these macrocycles display a constant energy gap between the two successive one electron oxid-

Figure 2.8 Anodic redox potentials for the MOEP and MTPP series plotted versus electronegativity of the central metal

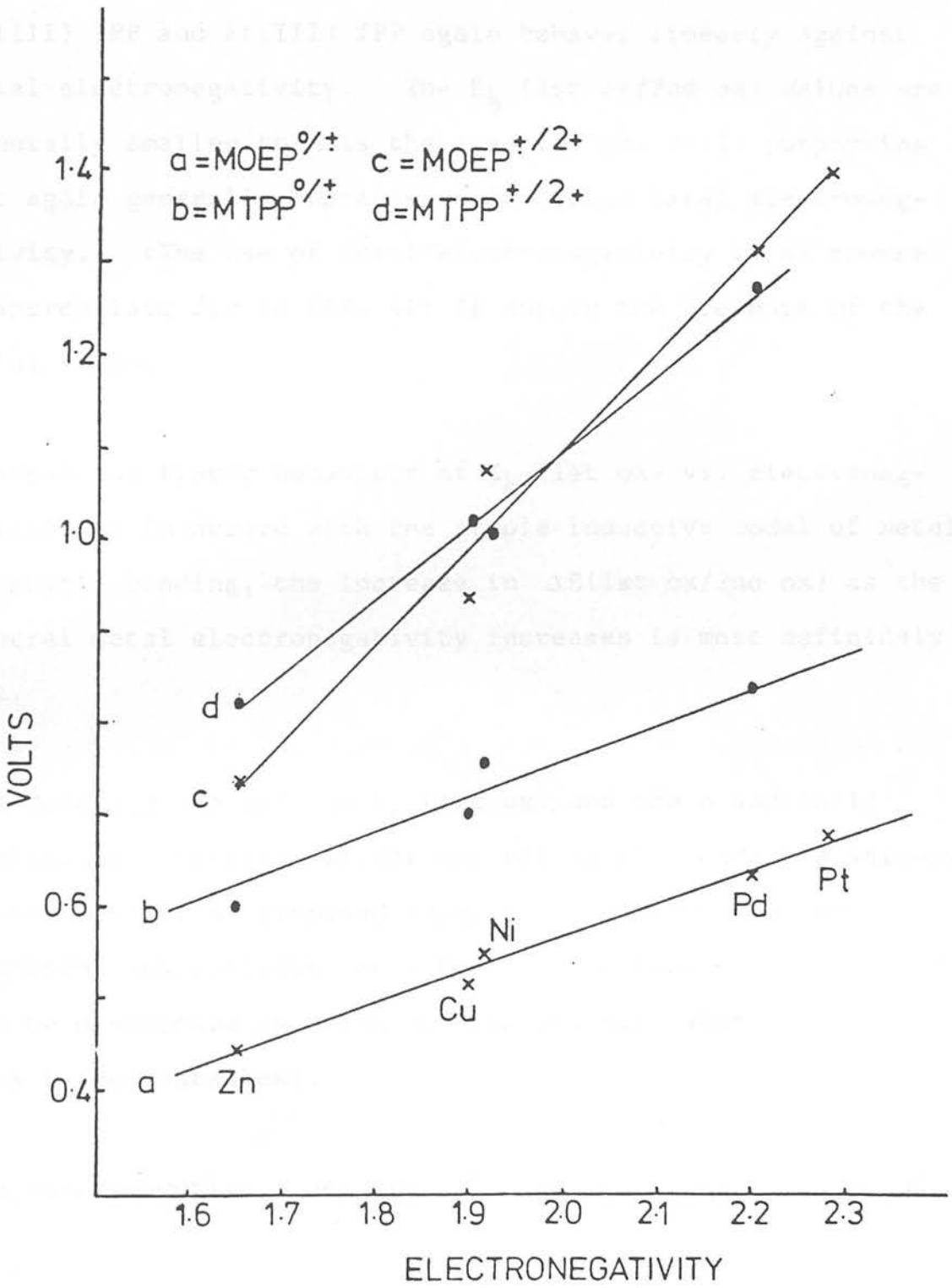

ations, independent of central metal.

This behaviour is repeated for the metalloporphyrins with metal valence (III). The first ring oxidation of Co(III) TPP, Ag(III) TPP and Pt(III) TPP again behaves linearly against metal electronegativity. The $E_{\frac{1}{2}}$ (1st ox/2nd ox) values are generally smaller than is the case for the M(II) porphyrins but again generally increase on increased metal electronegativity. (The use of metal electronegativity is of course inappropriate for Fe(III) TPP Cl due to the presence of the axial ligand).

Whereas the linear behaviour of $E_{\frac{1}{2}}$ (1st ox) vs. electronegativity is in accord with the simple inductive model of metalloporphyrin bonding, the increase in ΔE(1st ox/2nd ox) as the central metal electronegativity increases is most definitely not.

The relationship between $E_{\frac{1}{2}}$ (1st ox) and the n and (n+1) ionisation potentials of the central metal (where n = valency of the metal), as proposed separately by Stanienda[3] and Manassen[4] respectively, were found to be less satisfying and can be discounted as being non-informative, when applied to this larger data-base.

The pure inductive model predicts that the order of ease of

reduction of the macrocycle should be exactly the opposite to the order of ease of oxidation. This holds true for the first row transition metal porphyrins but breaks down for the palladium and platinum complexes. The full order for ease of primary reduction is-

$$Ni(II) < Cu(II) < Pd(II) < Pt(II) < Zn(II)$$

Moreover this order changes dramatically for the second reduction step, where the d^8 triad are all harder to reduce than the corresponding Zinc porphyrins-

$$Cu(II) < Zn(II) < Ni(II) < Pd(II) < Pt(II)$$

This change in order of ease of reduction between the two successive one-electron reductions is reflected in the increase of E(1st red/2nd red) through the series-

$$Zn(II) < Cu(II) < Ni(II) < Pd(II) < Pt(II)$$

These results are again in direct contrast to those expected from a purely inductive interaction between metal ion and macrocycle. This irregular cathodic behaviour is reflected in Figure 9 where $E_{\frac{1}{2}}$ (1st red) and $E_{\frac{1}{2}}$ (2nd red) of both porphyrin series are plotted against Pauling's electronegativity values of the central metal. Both sets of redox couples clearly do not vary linearly with X. The solid black lines in Figure 9 represent the gradient of line expected from the anodic data, if indeed $E_{\frac{1}{2}}$ (1st red) behaves as Fuhrhop predicted,

Figure 2.9 Cathodic redox potentials for the MOEP and MTPP series plotted versus electronegativity of the central metal

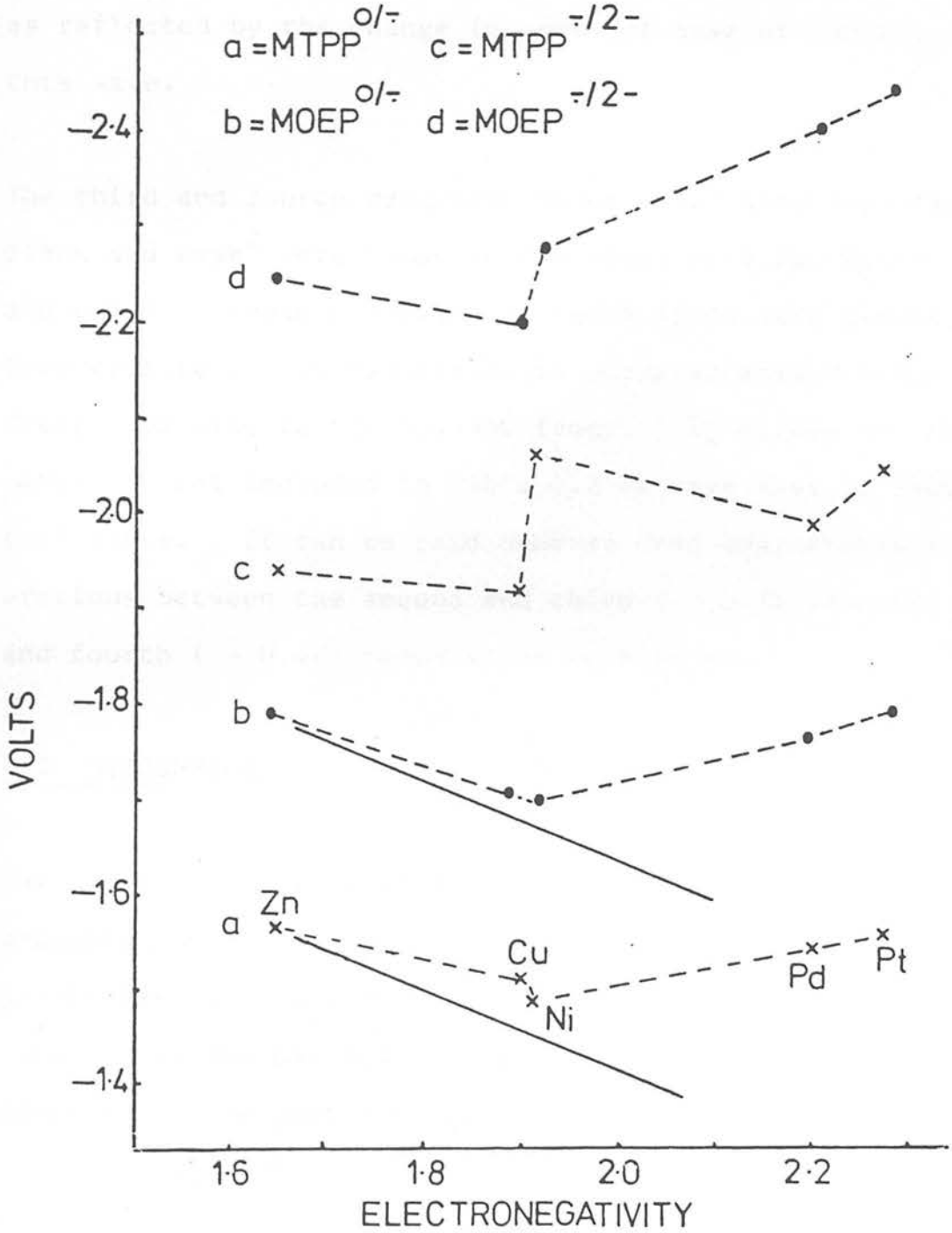

i.e. parallel behaviour to that observed for $E_{\frac{1}{2}}$ (1st ox) vs. X (see Figure 3). Clearly then, all the transition metal complexes of OEP and TPP are more difficult to reduce than expected, particularly the palladium and platinum porphyrins. This trend is even more apparent for the second reduction, as reflected by the change in order of ease of reduction at this wave.

The third and fourth reduction waves which were reported by Clack and Hush[2] were noted in the study only for H_2TPP, ZnTPP and CuTPP. These one-electron redox steps were generally irreversible and voltammetrically uncharacterisable due to their proximity to the solvent front. $E_{\frac{1}{2}}$ values for these waves are not included in Table 2.2 as they have no real chemical sense. It can be said however that characteristic separations between the second and third (- 0.7V) and the third and fourth (- 0.4V) redox steps were noted.

2.3 DISCUSSION

There are broad areas of disagreement between the results presented here and previous studies into the electrochemical properties of metalloporphyrins. The consistent values of ΔE(1st ox/2nd ox) and ΔE(1st red/2nd red) which have been proposed in the past are not observed here. ΔE (1st ox/2nd ox) varies widely from 0.19V for Co(III) TPP to 0.72V

for Pt(II) OEP. The literature value[27] of 0.29 ± 0.05V clearly then is not widely applicable. Nor indeed is the 0.42 ± 0.05V previously quoted[27] for ΔE(1st red/2nd red) as the d^8 metalloporphyrins exhibit far larger differences between the two ring reductions (e.g. PdOEP : 0.65V; NiTPP : 0.57V)

The most important observation from these results however, is that the order of ease of reduction is shown quite conclusively not to be solely dependent on the electronegativity of the central metal. Indeed the order of ease of reduction cannot be explained at all by any purely inductive parameter. This is most apparent when considering the cathodic data for the palladium and platinum porphyrins. Figure 9 clearly shows that although Pd and Pt have larger Pauling electronegativity values, the porphyrin complexes of these metals are harder to reduce than the corresponding nickel and copper porphyrins.

The absolute $E_{\frac{1}{2}}$ (1st ox) values for all the metalloporphyrins do however behave as predicted by the inductive model, varying linearly vs. electronegativity (Figure 8). Thus the energy of the HOMO of the metalloporphyrins would seem to be dominated by the polarising effect of the metal whereas the energy of the LUMO is not. Any rationalisation of this phenomenon must therefore explain why the energy of the LUMO is higher than expected, while the relative energy of the HOMO is app-

arently unaffected.

An early study of the optical absorption properties of metalloporphyrins in the vapour phase by Gouterman et al.[36] showed the wavelength of the Q(0,0) band increased along the series Fe(II) < Co(II) < Ni(II) < Cu(II) < Zn(II). Solution studies here, in the identical medium to that used for the electrochemical measurements, showed a similar trend. The results for the relevant porphyrins are listed in Table 3. The energy of the Q(0,0) band is seen to increase through the series-

$$Zn(II) < Cu(II) < Ni(II) < Co(II) < Pd(II) < Pt(II)$$

i.e. the energy of the band decreases as one moves along a transition series and increases down a triad. This behaviour is, for the first time, also reflected in the electrochemical data. We note the value of ΔE(1st ox/1st red), the electrochemical measure of the HOMO/LUMO gap, increases along the series Zn(II) < Cu(II) < Ni(II) and Ni(II) < Pd(II) < Pt(II). (For both the cobalt and iron porphyrins the occurrence of metal-based redox processes precludes direct comparison between the optical and electrochemical data). Table 4 compares the redox value of ΔE(1st/1st red) to the energy of the Q(0,0) band. For NiOEP, CuOEP and ZnOEP this comparison has remarkable success, both modes of measurement giving virtually coincidental figures. NiTPP, CuTPP and ZnTPP do not display such a good fit in absolute terms but the internal differences

Table 2.3 Spectroscopic measurement of the Frontier Orbital Gap : Q band energies in CH_2Cl_2/0.5M $TBABF_4$ at 20°C.

	Q(0,0)/nm	Q(0,0)/cm^{-1}	Q(0,0)/eV
ZnOEP	568	17,600	2.18
CuOEP	560	17,850	2.21
NiOEP	551	18,150	2.25
PdOEP	545	18,350	2.27
PtOEP	534	18,700	2.31
ZnTPP	592	16,900	2.10
CuTPP	581	17,200	2.13
NiTPP	562*	17,800	2.21
PdTPP	555	18,000	2.23
PtTPP	537	18,600	2.30

*estimated from the position of the Q(1,0) band.

Table 2.4 Comparison of the energy of the Frontier Orbital Gap as measured spectroscopically and electrochemically

	Q(0,0)/eV	ΔE(1st ox-1st red)/V
ZnOEP	2.18	2.20
CuOEP	2.21	2.21
NiOEP	2.25	2.24
PdOEP	2.27	2.38
PtOEP	2.31	2.46
ZnTPP	2.10	2.17
CuTPP	2.13	2.21
NiTPP	2.21	2.26
PdTPP	2.23	2.38
PtTPP	2.30	2.38*

* This value is the difference between the $Pt(II)TPP^{0/-\cdot}$ and the Pt(II)/III couple and as such is a minimum value i.e. the theoretical $Pt(II)TPP^{0/+\cdot}$ couple must be at a more positive potential.

are relatively constant for each technique. For the Pd(II) and Pt(II) porphyrins, although both techniques show the HOMO/LUMO gap to increase down the d^8 triad, the correlation between the two sets of numbers is quantitatively less satisfying than for the first row. This is, in fact, less surprising than the Cu(II), Ni(II) and Zn(II) data giving such a good fit. When considering the contrasting processes of the electrochemical and optical absorption events (see Fig. 1.2), one must note an intrinsic difference between the two techniques. The photon absorption event involves the ground state and the immediate excited state (Franck-Condon excited state) in which the electronically excited molecule retains its ground state geometry (and is thus vibrationally excited). Electrode potentials on the other hand have thermodynamic significance and refer on all occasions to the thermally equilibrated molecules. Enthalpy and particularly entropy terms, related to $E_{\frac{1}{2}}$ data by the common Gibbs-Helmholtz equation, will subtly render $h\nu$ and ΔE(1st ox/1st red) inequal. It is interesting that such inequalities only manifest when considering the 2nd and 3rd row transition metals.

The electrochemical results then allow us to rationalise the increase of the frontier orbital gap in 'hypso' porphyrins as an increase in the energy of the LUMO e_g pair rather than a decrease in the energy of the HOMO. This information is of course not available from optical absorption data alone. Further, the redox chemistry supports the idea that donation of electron density from the central metal back to the porphyrin macrocycle is an important consideration in the bonding of

metalloporphyrins. This can arise through $d\pi - \pi^*$ back bonding which will occur if the empty e_g (π^*) orbitals of the ring mix with the filled d(π) orbitals of the metal. This interaction is displayed in Figure 10.

The size of this effect will depend largely on the degree of mixing of the π^* and metal d-orbitals. The extent of this mixing will in turn depend on two factors - the overlap of macrocycle e_g π^* and metal $d\pi$ orbitals and the energy separation, (Fig. 10), between the two. For the first row transition metals, as their ionic size is relatively constant, the term Δ will be the determining factor for mixing. Δ will increase along the $3d^6$-d^{10} series. Thus Δ will be at a maximum for Zn(II) and indeed the degree of mixing must be negligible for zinc porphyrins as they are considered optically as regular and not 'hypso'.

For the d^8 triad, the determining factor will be the overlap of the orbitals as both Pd(II) and Pt(II) have much larger ionic radii than Ni(II). Thus the 4d and 5d orbitals will overlap to a greater extent than the 3d orbitals, resulting in greater mixing with the e_g (π^*) of the macrocycle.

A greater degree of mixing of these orbitals will result in a greater rise in the energy i.e. destabilisation of the e_g (π^*) degenerate pair and thus the greater the energy

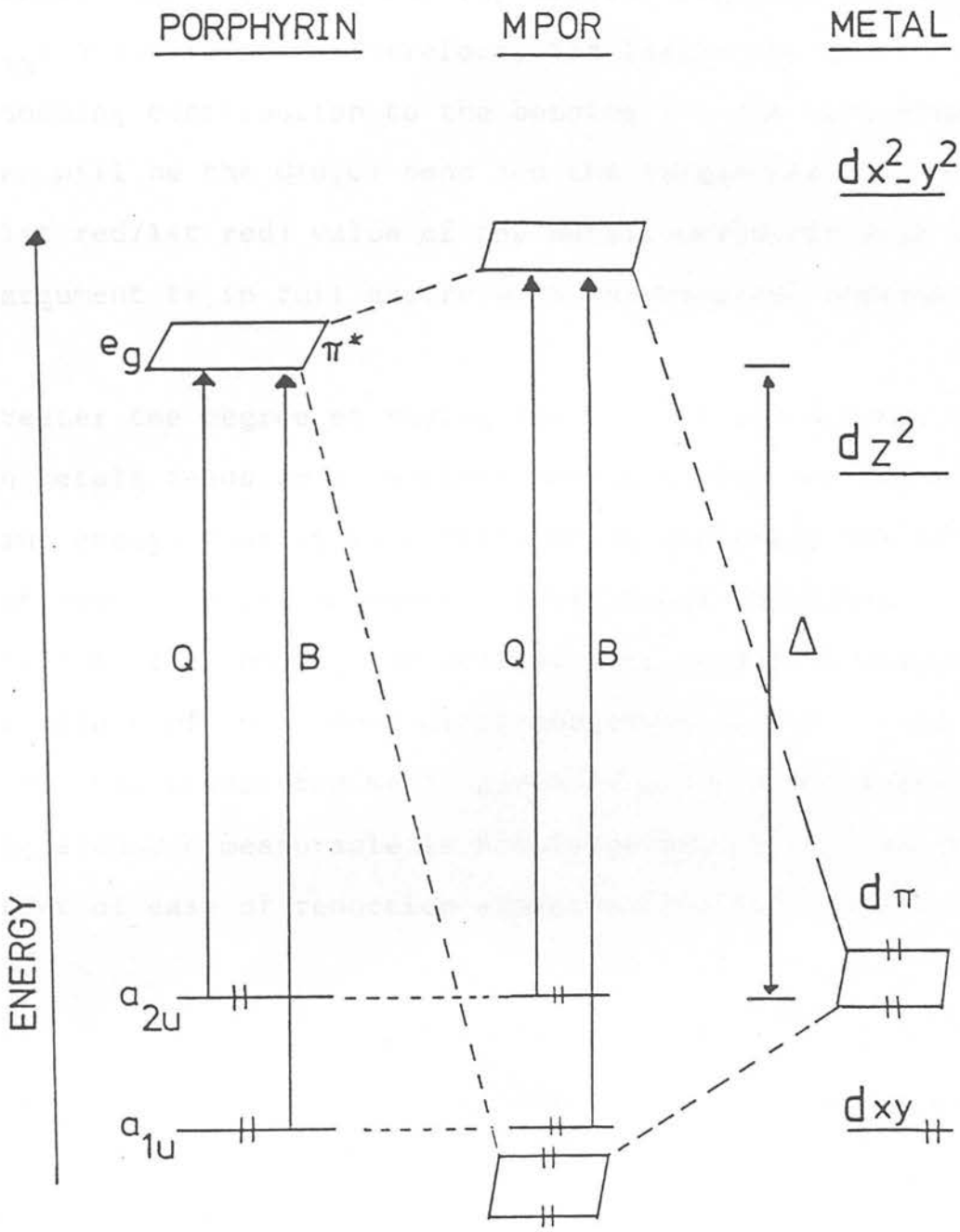

Figure 2.10 Schematic illustration of hypsoporphyrins indicating mixing of e_g (π^*) and d(π) orbitals

gap between e_g (π^*) and the top filled ring orbitals a_{2u}(π) and a_{1u}(π) will be. Therefore, the larger the $d\pi - \pi^*$ back-bonding contribution to the bonding is, the more blue-shifted will be the Q(0,0) bond and the larger the ΔE(1st red/1st red) value of the metalloporphyrin will be. This argument is in full accord with experimental observation.

The greater the degree of mixing for the 2nd and 3rd row transition metals leads to a π contribution to the bonding significant enough that it is sufficient to determine the relative ease of reduction of the macrocycle in these complexes. This is not withstanding the accompanying increased electrostatic effect of these more electronegative metals. For the first row transition metal porphyrins $d\pi - \pi^*$ back-bonding although measurable is not large enough to invert the order of ease of reduction expected from the inductive model.+

+ This is not always the case for 1st row transition metal tetraazamacrocyclic complexes. In Chapter 5 we note that NiPc is actually harder to reduce than CuPc. This is the reverse of the order found for Ni(II) and Cu(II) porphyrins and we attribute this to the greater degree of $4e_g$ (π^*)/$d\pi$ mixing in phthalocyanines due to the smaller cavity size of the Pc ring.

The value of ΔE(1st ox/1st red) has been noted then to increase as the electronegativity of the central metal increases. This is best shown graphically (Figure 11) where the first reduction and first oxidation of the d^8 MOEP and MTPP series are plotted against X. The cathodic behaviour obviously differs from that predicted by Fuhrhop's electrostatic model (Figure 3). The two lines for $E_{\frac{1}{2}}$ (1st ox) and $E_{\frac{1}{2}}$ (1st red) clearly <u>diverge</u> rather than following parallel tracks. (The linearity displayed by $E_{\frac{1}{2}}$ (1st red) must in fact be coincidental as it reflects the sum of the electrostatic and π bonding effects).

The inductive model also predicts constant values for ΔE(1st ox/2nd ox) and ΔE(1st red/2nd red) as they are viewed as merely a reflection of the electron repulsion and spin exchange energies encountered on each redox step. However no consistency for either of these electrochemical differences was noted here. It was found, in the non-coordinating medium employed in this work <u>both</u> ΔE (1st ox/2nd ox) and ΔE(1st red/2nd red) increase as the central metal electronegativity increases (Figs. 8 and 9) for a given metal oxidation state. (This is generally true for all the metalloporphyrins studied with only one exception, Ni(II) TPP, where ΔE(1st red/2nd red) is anomalously high. This observation remains unexplained).

Figure 2.11 Cathodic and Anodic redox potentials of the d^8 MOEP and MTPP complexes plotted versus central metal electronegativity

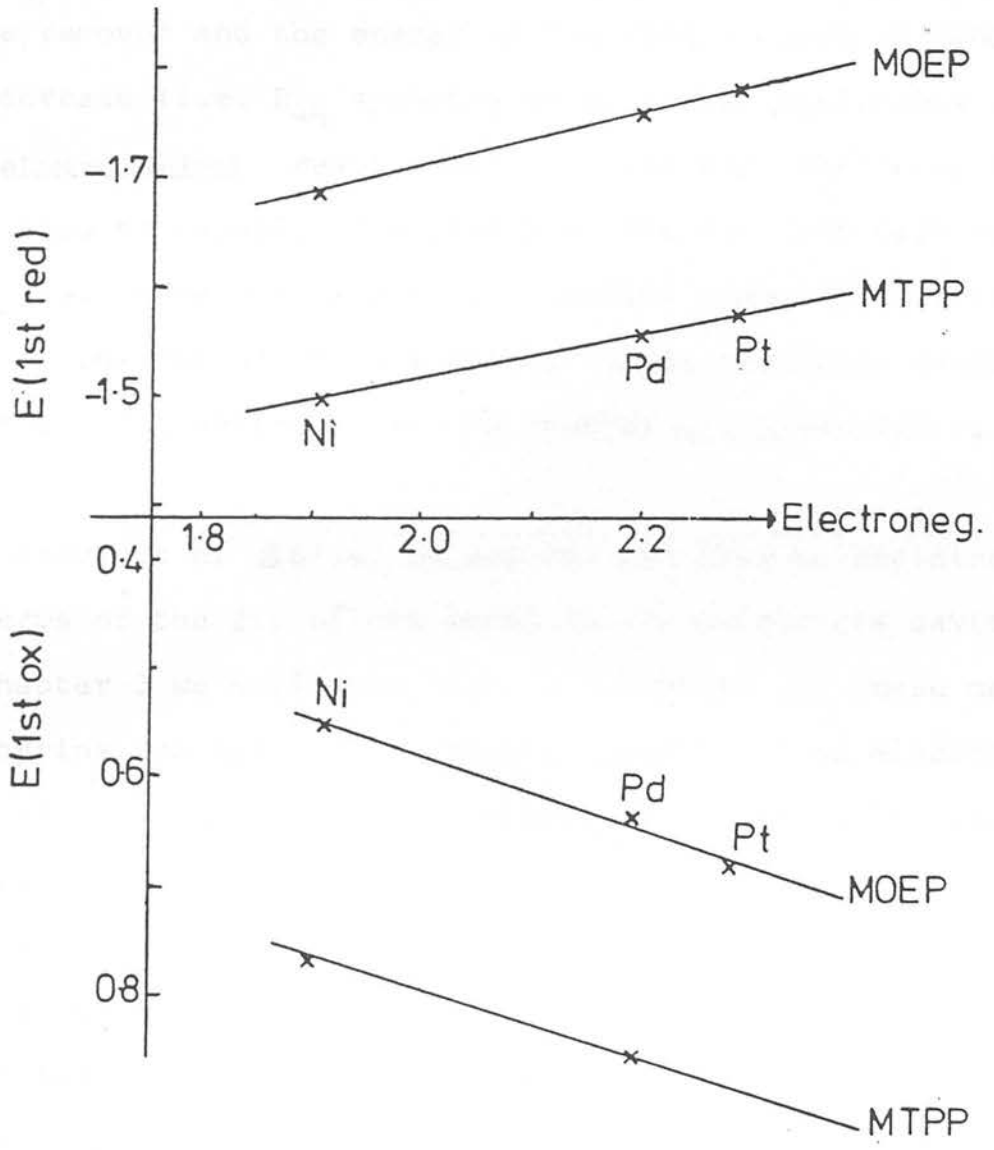

The trend observed for ΔE(1st red/2nd red) strongly suggests that there is a degree of π back bonding present in the metalloporphyrin monoanion radicals as well as the neutral complexes. The spectroelectrochemical characterisation of these species (see Chapter 3) shows that the addition of one electron into the e_g (π^*) orbital causes the degeneracy of this orbital to be removed and the energy of the singly occupied orbital to decrease (i.e. D_{4h} symmetry is no longer applicable). The electrochemical results point to the fact that this orbital must also be capable of mixing with the dπ orbitals of the metal and therefore have an appropriate symmetry to allow this. The extent of this mixing has an identical qualitative order to that observed for the neutral metalloporphyrins.

The behaviour of ΔE(1st ox/2nd ox) can also be explained in terms of the fit of the metal in the macrocycle cavity. In Chapter 3 we will show that oxidation of all these metalloporphyrins (except ZnOEP) involves removal of an electron from an a_{2u} orbital. This orbital has considerable electron density at the pyrrolic nitrogens and electron donation to the metal centre will thus be less for the porphyrin anion radical than for the oxidised ring. This will then result in an amplification of the electrostatic polarisability of the ring by the metal. This is reflected in Figure 8 where the gradient of the $MP^{+\bullet}/MP^{2+}$ couple is far larger than the $MP/MP^{+\bullet}$ couple. This rationalisation receives support from

two areas. Firstly we note that ΔE (1st ox/2nd ox) is smaller when the metal centre has been oxidised in a previous anodic redox step i.e. for (M(III) porphyrin)$^{+}$. Oxidation of the metal will result in a smaller ionic radius for the central ion and thus the inductive effect on the ring will not be as great as for the divalent metals.

Also the trend indicated (increase of ΔE(1st ox/2nd ox) with increased metal electronegativity) is noted to be more pronounced for the MOEP series than the MTPP series (Figure 8). X-ray[37, 38] and thermodynamic[39] studies have shown the better 'fit' of the metal within the OEP macrocycle over the TPP macrocycle. The N-M bonds are shorter and stronger in the MOEP series. This must also be true for the metalloporphyrin cation radicals as there is a greater relative increase in the inductive effect of the metal for the OEP macrocycle than the TPP macrocycle for the redox couple $MP^{+/2+}$.

The redox values ΔE(1st ox/1st red), ΔE(1st ox/2nd ox) and ΔE(1st red/2nd red) then <u>all</u> vary depending on the metal centre. The use of these numbers in predicting whether a redox couple is macrocycle or metal-based should then be done cautiously, with the observed trends in mind.

Fuhrhop's electrostatic model should still be applicable for regular prophyrins i.e. those which cannot contribute to

bonding within the complex. In accordance with this MgOEP was found to display similar values of all 3 ΔE values as ZnOEP-

	$E_{\frac{1}{2}}$(1st ox)/V	$E_{\frac{1}{2}}$(2nd ox)/V	ΔE(1st ox/2nd ox)
MgOEP	0.30	0.59	0.29
ZnOEP	0.44	0.74	0.30

	$E_{\frac{1}{2}}$(1st red)/V	$E_{\frac{1}{2}}$(2nd red)/V	ΔE(1st red/2nd red)
MgOEP	-1.90	-2.36	0.46
ZnOEP	-1.76	-2.24	0.46

ΔE(1st ox/1st red) = 2.20V in both cases.

However a further definite limitation of the inductive model is apparent for the porphyrin complexes of the heavier regular metals, which do not fit fully into the plane of the ring. CdOEP, for instance, exhibits a ΔE(1st ox/1st red) value much smaller than that displayed by ZnOEP-

	$E_{\frac{1}{2}}$(1st ox)/V	$E_{\frac{1}{2}}$(1st red)/V	ΔE(1st ox/1st red)
CdOEP	0.37	-1.63	2.00

This observation is most likely due to Cd(II) being too large to occupy the centre of the porphyrin ring, rather assuming a domed structure. The metal/macrocycle overlap will then

be far less efficient and thus not directly analogous to the D_{4h} metalloporphyrins. More extensive work is required on regular metalloporphyrins of the heavier transition metals to quantify the energetic effect on the frontier orbitals that lowering the symmetry of the complex obviously has.

2.4 Conclusion

The present electrochemical study of metalloporphyrins in a non-coordinating aprotic medium has allowed new insight into the redox properties of these biologically important pigments. The previously accepted electrostatic model of metal-macrocycle interactions, where the central metal raises or lowers the energies of the HOMO and the LUMO of the complex equally in direction and magnitude, clearly fails to explain the data presented here. Instead more refined considerations of the bonding in these complexes is required to explain both the cathodic and anodic behaviour of metalloporphyrins.

The parallel behaviour of $E_{\frac{1}{2}}$(1st red) and $E_{\frac{1}{2}}$(1st ox) with electronegativity of the central metal as proposed by Fuhrhop[27] (see Fig. 3) is clearly not appropriate for these complexes especially for the heavier transitions metal porphyrins.

Spectroscopists, in their identification of the 'hypso' behaviour of metalloporphyrins with metal ions containing between 6 and 9 d electrons, had shown that there must be some

other bonding contribution affecting the size of the HOMO/LUMO gap. Electrochemistry allows us not just to measure the HOMO/LUMO gap but to study the relative energies of both the frontier orbitals separately. From analysis of both $E_{\frac{1}{2}}$ (1st ox) and $E_{\frac{1}{2}}$ (1st red) it is clear that hypso behaviour arises because the energy of the LUMO is higher than would be expected from the inductive model. We attribute this to back-bonding of electron density from the metal to the ligand through $d\pi - \pi^*$ back-bonding which consequently raises the energy of the e_g doubly-degenerate π^* orbital. For the d^8 triad this results in ΔE(1st ox/1st red) increasing to such an extent a plot of $E_{\frac{1}{2}}$ (1st red) and $E_{\frac{1}{2}}$ (1st ox) against X, results in diverging, rather than parallel, lines (Figure 11).

Thus the confidence which Fuhrhop placed on the relationship between ΔE(1st ox/1st red) and electronegativity is misplaced. The accuracy of his derived induction parameters for various metal centres must also therefore be questionable and careful consideration should be given to their further usefulness in porphyrin chemistry.

The kind of manipulation of redox data shown here should be applicable for a wide range of coordination complexes. This work highlights the role of electrochemistry as an investigative technique into the bonding of such complexes.

2.5 Experimental

H_2TPP was synthesised using the single step preparation of Adler et al.[40] and purified by the method of Smith[41]. H_2OEP was prepared as in the 8 step synthesis of Whitlock[42]. MTPP and MOEP complexes were prepared by standard literature preparations[43] and purity of each checked by CHN analysis and optical absorption spectroscopy. All were also electrochemically clean. Fe(II)TPP and Fe(II) OEP were unstable in our hands and the iron complexes were prepared as the ferric chloride porphyrins[44].

Dichloromethane was stored over KOH for 48 hours and distilled from phosphorus pentoxide before use. Tetrabutylammonium fluoroborate ($TBABF_4$) was prepared by the method of Heath et al[45], replacing tetraethylammonium hydroxide by tetrabutyl ammonium hydroxide. Electrolyte concentration was 0.5M in all cases. Optical absorption spectra were measured on a Pye-Unicam SP8-400 spectrophotometer.

Voltammetric experiments were performed in a jacketed-cell. Cell temperature was kept constant (20°C) by means of a methanol-circulating bath (Haake F 3). The well-documented[46] three-electrode configuration was used for all voltammetric measurements consisting of a working electrode (platinum microelectrode, gold or dropping mercury electrode), Ag/AgCl reference electrode,

separated from the bulk solution by a glass frit[47], and a platinum counter electrode. Solutions were purged with argon so as to render them oxygen-free. D.c. and a.c. voltammograms were recorded using a Princeton Applied Research Model 170 with full positive-feedback IR compensation. A.c. measurements employed phase-sensitive detection also. Cyclic voltammograms were recorded using a HI-TEK Potentiostat DT 2101 and Waveform generator PPRI. C.v's were displayed on a Teletronix D11 storage oxilloscope or plotted on a Hewlett-Packard 7045A X-Y Recorder.

Three main types of voltammetric techniques were used in this work, d.c. voltammetry, a.c. voltammetry, and cyclic voltammetry (cv). Typical wave shapes for a reversible one-electron process for all three techniques are shown in Figure 12 and summarised below.

A. D.c. Voltammogram -

For the case of an ideally behaved one-electron process, a classical Nernstian direct current response is observed upon application of a linearly increasing potential, while stirring the solution. As the species under investigation undergoes electron-transfer, the current reaches a maximum plateau value, the diffusion current (id), determined by the rate of diffusion of substrate to the electrode surface. For an ideal reversible system, the midpoint of the wave, termed $E_{\frac{1}{2}}$, is equal to the standard electrode potential E°, as defined by the

Figure 2.12 Typical Voltammetric wave forms

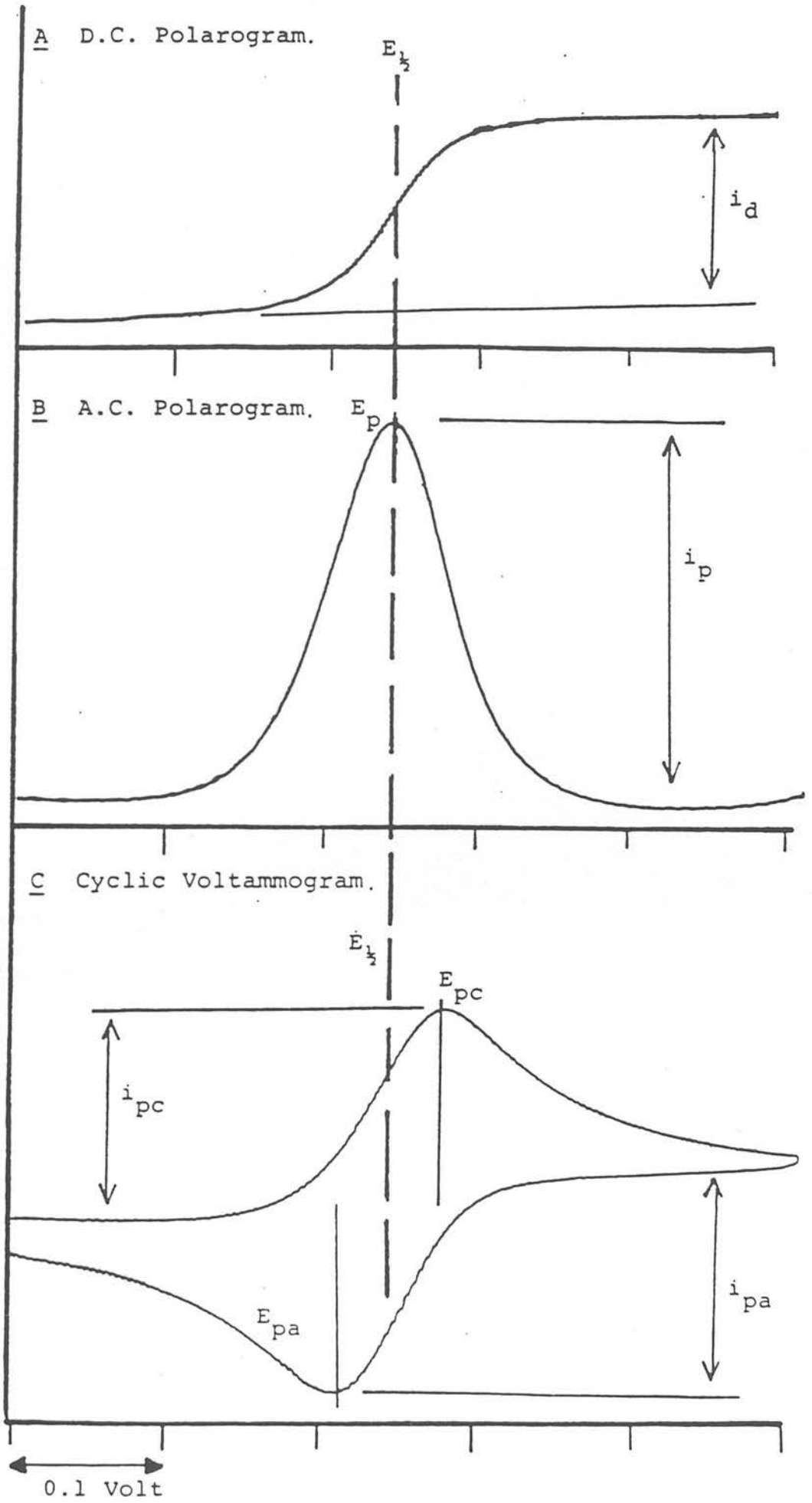

Nernst equation. Typical scan rates are 5-10mVs^{-1}.

B. A.c. voltammogram

In this technique a small sinusoidal alternating potential is superimposed on the d.c. potential. The alternating component of current is then monitored selectively as a function of the d.c. linearly increasing potential. The resulting wave form is a symmetrical peak. For a fully reversible electron-transfer step Ep (Fig 12) corresponds to $E_{\frac{1}{2}}$. Scan rates are typically 5-20mVs^{-1}.

C. Cyclic Voltammogram

The usefulness of cyclic voltammetry over potentiometric and classical polarographic methods is that both the starting material and generated reaction product can be simultaneously investigated in situ verifying the absence of chemical reactions coupled to electron transfer. The technique involves the application of a triangular potential ramp to the cell. Stationary electrodes are used in quiescent solution and fast potential scanning is necessary to minimise the effects of diffusion and convection (10 - 5000 mVs^{-1}). The potential midway between the cathodic and anodic peak potentials (Epc and Epa respectively, Fig 12) is equal to $E_{\frac{1}{2}}$.

All the above techniques give useful information on the

reversibility of an electron-transfer process and the number of electrons (n) passed. Cyclic voltammetry in particular gives much information on the reversibility of each redox step. Common reversibility criteria[48] for each technique at 20°C are listed below-

d.c. voltammetry-

Plot of E vs log $(\frac{(id-i)}{i})$ is linear with slope = $^{59}/_{n}$ mV

a.c. Voltammetry-

Ep = $E_{\frac{1}{2}}$; wave symmetric; width at half height = $^{90}/_{n}$ mV.

Plot of Ip vs $w^{\frac{1}{2}}$ is linear through origin (w = a.c. frequency).

Cyclic voltammetry-

a)

Reversible: $E_{\frac{1}{2}}$ is independent of v (v = sweep rate in mVs^{-1})

$Ep_c - Ep_a = \frac{59}{n}$ mV and is independent of v

$\frac{1}{2}(Ep_c + Ep_a) = E_{\frac{1}{2}}$ independent of concentration

Plot of Ip vs $v^{\frac{1}{2}}$ is linear and through origin

$\frac{ip_c}{ip_a} = 1$, independent of v

Quasi-reversible: Ep shifts with v

$Ep_c - Ep_a$ increases as v increases

$I_p/v^{\frac{1}{2}}$ is independent of v

$\frac{ip_c}{ip_a}$ generally = 1

Partially reversible: Ep increases by $^{30}/_{n}$ mV for a ten-fold increase in v , at low v

$i_p / v^{\frac{1}{2}}$ is independent of v

ip_c/ip_a increases toward 1 as increases.

Irreversible: Ep shifts with v

$ip/v^{\frac{1}{2}}$ is independent of v

No current on reverse scan

REFERENCES : CHAPTER 2

1. R.H. Felton and H. Linschitz, J. Am. Chem. Soc., 1966, 88, 1113.
2. D.W. Clack and N.S. Hush, J. Am. Chem. Soc., 1965, 87, 4238.
3. A. Stanienda and G. Biebl, Z. Phys. Chem. (Frankfurt am Main), 1967, 52, 254.
4. J. Manassen and A. Wolberg, J. Am Chem. Soc., 1970, 92, 2982.
5. R.H. Felton, J. Fajer, D.C. Borg and D. Dolphin, J. Am. Chem. Soc., 1970, 92, 3451.
6. G. Peychal-Heiling and G. Wilson, Anal. Chem., 1971, 43, 545.
7. D.G. Davis and D.J. Orgeron, Anal. Chem., 1966, 38, 179.
8. R.F. Martin and D.G. Davis, Biochemistry, 1968, 7, 3906.
9. K.M. Kadish, D.G. Davis and J-H Fuhrhop, Angew. Chem., 1972, 84, 1072.
10. E.E. Johnson, T. Niem and D. Dolphin, Can. J. Chem., 1978, 56, 1381.
11. (a) K.M. Kadish and M.M. Morrison, Inorg. Chem. 1976, 15, 980.
    (b) K.M. Kadish, L.R. Shive, R.K. Rhodes and L.A. Bottomley, Inorg. Chem. 1981, 20, 1274.
    (c) K.M. Kadish and L.R. Shive, Inorg. Chem. 1982, 21, 3623.

(d) K.M. Kadish and C.H. Shu, J. Am. Chem. Soc. 1983, 105, 1977.

12. D. Chang, T. Malinski, A. Ulman and K.M. Kadish, Inorg. Chem. 1984, 23, 817.

13. F.R. Longo, E.J. Thorne, A.D. Adler and S. Dym, J. Heterocycl. Chem. 1975, 12, 1305.

14. M. Gouterman, "The Porphyrins", Ed. D. Dolphin, Academic Press, New York (1980) Vol. 3, p.1.

15. H.C. Longuet-Higgins, C.W. Rector and J.R. Platt, J. Chem. Phys., 1950, 18, 1174.

16. M. Gouterman, J. Mol. Spectrosc., 1961, 6, 138.

17. (a) M. Gouterman, G.H. Wagniere and L.C. Snyder, J. Mol. Spectrosc. 1963, 11, 108.

(b) C. Weiss, H. Kobayashi and M. Gouterman, J. Mol. Spectrosc. 1965, 16, 415.

18. L.K. Lee, N.H. Sabelli and P.R. LeBreton, J. Phys. Chem. 1982, 86, 3926.

19. R.H. Felton, PhD Thesis, Harvard University, USA, 1964.

20. J.R. Platt, J. Opt. Soc. Am. 1953, 43, 252.

21. A. Antipas, D. Dolphin, M. Gouterman and E.C. Johnson, J. Am. Chem. Soc., 1978, 100, 7705.

22. A. Antipas, J.W. Buchler, M. Gouterman and P.D. Smith, J. Am. Chem. Soc., 1978, 100, 3015.

23. R.H. Felton, "The Porphyrins", Ed. D. Dolphin, Academic Press, New York, (1980), Vol. 5, p. 53 and references therein.

24. R.C.S. McQueen, PhD Thesis, Edinburgh University, 1983.

25. G.L. Closs and L.E. Closs, J. Am. Chem. Soc. 1963, 85, 818.

26. D. Mauzerall, J. Am. Chem. Soc., 1962, 84, 2437.

27. J.H. Fuhrhop, K.M. Kadish and D.G. Davis, J. Am. Chem. Soc. 1973, 95, 5140.

28. R.H. Campbell, Honours Project Report, Stirling University, 1978.

29. R.H. Campbell, G.A. Heath, G.T. Hefter and R.C.S. McQueen J. Chem. Soc. Chem. Commun., 1983, 1123.

30. A.B.P. Lever and J.P. Wilshire, Can. J. Chem., 1976, 54, 2514.

31. A.B.P. Lever and J.P. Wilshire, Inorg. Chem., 1978, 17, 1145.

32. (a) L.A. Constant and D.G. Davis, Anal. Chem., 1975, 47, 2253.

(b) L.A. Truxillo and D.G. Davis, Anal. Chem., 1975, 47, 2260.

33. C.H. Kirksey, P. Hambright and C.B. Storm, Inorg. Chem., 1969, 8, 2141.

34. F.A. Cotton and G. Wilkinson, "Advanced Inorganic Chemistry", Wiley, USA, 1972, 3rd Edition, p. 115 and references therein.

35. W. Gordy and W.J.D. Thomas, J. Chem. Phys., 1956, 24, 436.

36. (a) L. Edwards, D.H. Dolphin and M. Goutermann, J. Mol.

Spectrosc. 1971, 38, 16.

37. J.L. Hoard and W.R. Schiedt, Proc. Natl. Acad. Sci., USA, 1973, 70, 3919.

38. J.L. Hoard, "Porphyrins and Metalloporphyrins" Ed. K.M. Smith, Elsevier Amsterdam (1975), Chapter 8 and references therein.

39. K. Rohbock, Dissertation, Technische Hochschule Aachen (1972).

40. A.D. Adler, F.R. Longo, J.D. Finarelli, J. Goldmacher, J. Assour and L. Korsakoff, J. Org. Chem., 1967, 32, 476.

41. G.H. Barnett, M.F. Hudson and K.M. Smith, Tetrahedron Lett., 1973, 2887.

42. H.W. Whitlock and R. Hanaver, J. Org. Chem., 1968, 33, 2169.

43. J.H. Fuhrhop and K.M. Smith, Chapter 19 of ref. 38.

44. A.D. Adler, F.R. Longo, F. Kampas and J. Kim, J. Inorg. Nucl. Chem., 1970, 32, 2443.

45. G.A. Heath, G.T. Hefter, T.W. Boyle, C.D. Desjardins and D.W.A. Sharp, J. Fluor, Chem. II., 1978, 399.

46. G.L. Booman and W.B. Holbrook, Anal. Chem. 1965, 37, 795.

47. D.T. Sawyer and J.L. Roberts, "Experimental Electrochemistry for Chemists", Wiley-Interscience, New York, 1974, p. 54.

CHAPTER 3 : SPECTROELECTROCHEMICAL STUDIES ON THE ELECTRODE PRODUCTS OF M(II) TPP AND M(II) OEP

3.1 INTRODUCTION

The chemically important electrons of the porphinato ligand are those belonging to the conjugated π -electron system. These occupy orbitals that transform like the A_{1u}, A_{2u}, B_{1u}, B_{2u} and E_g representations of D_{4h}.[1] As we have noted, the e_g orbitals can mix with the d orbitals (d_{xz}, d_{yz}) of the metal (Chapter 2). This overlap, though significant, is relatively small in overall electron density terms and it is justifiable to describe metalloporphyrins as possessing two somewhat isolated electronic systems, one belonging to the metal and the other to the ligand. Consequently it is possible in almost all cases to assign either a metal or a ligand reaction to a given oxidation or reduction step of a metalloporphyrin. It is to these assignments that this chapter is dedicated. Four possible scenarios exist for the relative ordering of the molecular orbitals of metalloporphyrins. Examples of each of these are depicted in Figure 1 and summarised below.

1) Both the HOMO and the LUMO of the metalloporphyrin are based on the macrocycle.
2) The HOMO is macrocycle based and the LUMO is an orbital

of predominantly metal character.

3) The HOMO is metal based and the LUMO ligand based.

4) Both the HOMO and LUMO are metal based.

Figure 1 also shows all the possible electronic transitions that exist for each of the above cases.

As described earlier, the electronic absorption spectra of metalloporphyrins are dominated by the very strong $\pi - \pi^*$ transitions of the ligand electrons. These completely mask the much weaker d-d transitions of the metal. Charge transfer bands are also predicted[2] to be strongly forbidden and very few have been observed experimentally. The absence of MLCT (metal to ligand charge transfer) and LMCT (ligand to metal charge transfer) bands is particularly unfortunate in that detailed orbital mapping of the d-orbitals is consequently impossible and their energy relative to that of the porphyrin orbitals remains unknown. Molecular orbital calculations[3] to date also fail to predict the energy of the d-orbitals accurately.

Generally, the energies of the d-orbitals will decrease along a transition series and therefore metal-based redox steps are far less likely for the d^8 and d^9 metals than for the metals of electron configuration d^5, d^6 and d^7. Zinc(II) is considered to be redox inert and all redox processes of

Figure 3.1 Schematic illustration of the possible relative energies of the metal d-orbitals and ligand π orbitals for a d^6 metalloporphyrin

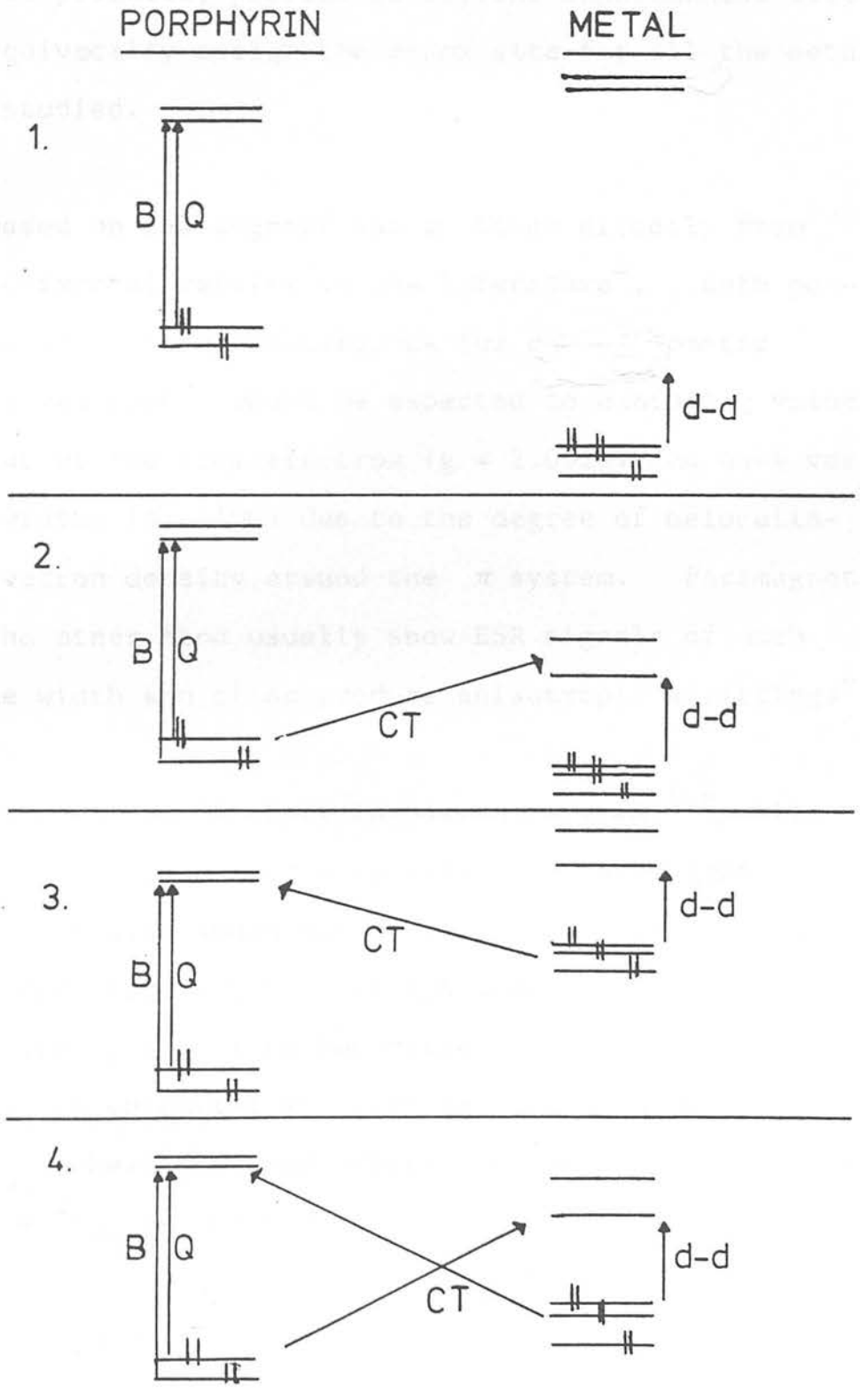

zinc porphyrins will then of course be macrocycle-based.

In this evaluation of redox potentials, coupled with comparative absorption spectroscopy and ESR characterisation of the electrode products, provide sufficient experimental evidence to unequivocally assign the redox site for all the metalloporphyrins studied.

Arguments based on ESR signals can be taken directly from related experimental results in the literature[4]. Both porphyrin anion and cation radicals, as for other aromatic organic free radicals[5], would be expected to exhibit g values close to that of the free electron (g = 2.0023) and have very small line widths (5 - 10G) due to the degree of delocalisation of electron density around the π system. Paramagnetic metals on the other hand usually show ESR signals of much greater line width and often produce anisotropic splittings[6,7].

Previous ESR studies of porphyrin cation radicals[8,9], while producing evidence of electron removal from the organic π-system, have also shown marked differences exist in spin density distribution within these species. The π -cation radicals generally fall into two categories-

a) radicals in which the electron has been removed from the a_{2u} highest occupied orbital of the porphyrin resulting in a $^2A_{2u}$ ground state. (D_{4h} symmetry).

b) those presumed to arise by removal of an electron from an a_{1u} orbital yielding a $^2A_{1u}$ ground state.

These assignments are based on Pariser-Parr-Pople self consistent field molecular orbital (SCF-MO) calculations which predict quite different spin densities for the two ground states[10] (Table 1).

The one electron oxidation products of ZnTPP, MgTPP and CdTPP have been studied extensively[10-16] and characterised as having a $^2A_{2u}$ ground state. Selective isotopic substitution experiments[14] on the cation radicals showed the ESR signal of the unpaired electron was split not only by the four equivalent pyrrolic nigrogens (^{14}N, I = 1) but also by the protons on the phenyl ring. The interaction of the unpaired electron with the phenyl rings was considered surprising as crystallographic data[17] for ZnTPP has shown the phenyl rings to be perpendicular to the plane of the porphyrin ring and assumed therefore to be unable to extend the conjugative π-system. Fajer and Davis[10] postulated the spin delocalisation mechanism to be a $\sigma - \pi$ interaction due to overlap of the ortho-protons of the phenyl ring into the π-cloud of the porphyrin which for a $^2A_{2u}$ state has high spin density at the meso-positions. Kadish[18] has more recently shown that there is considerable electronic interaction between the meso-phenyl substituent and the porphyrin aromatic core by studying the redox properties of compounds of the general formula (M(II) (p-X)TPP) where X can be either electron-donating or electron-withdraw-

Table 3.1 Calculated spin densities for porphyrin cation radicals

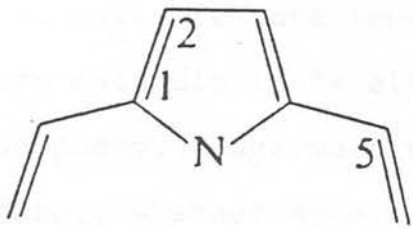

	$^2A_{2u}$	$^2A_{1u}$
C-1	-0.0094	0.0981
C-2	0.0134	0.0262
C-5	0.1932	0.0012
N	0.049	0.000

Table 3.2 Calculated spin densities for porphyrin anion radicals

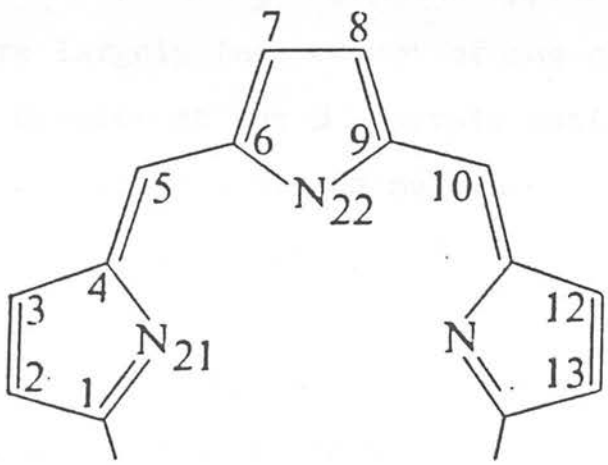

N-21	0.025	C-6	0.038
C-1	0.038	C-7	0.033
C-2	0.032	N-22	0.025
C-5	0.083		

ing. These substituents had a profound effect on the electrode potentials of both the $MP/MP^{+\cdot}$ and $MP/MP^{-\cdot}$ couples, moving them systematically to more anodic (X is electron-withdrawing) or more cathodic (X is electron-donating) potentials. The meso-phenyl rings must therefore have a sizeable electronic effect, whether hyperconjugative or inductive, on the 18 atom/18π electron core of the porphyrin.

The experimental ESR evidence accumulated for these M(II)TPP complexes provides clear support for the $^2A_{2u}$ ground state predicted from M.O. calculations (Table 1). It can be summarised as follows-

1) High spin density is found at the meso-positions from which charge can overlap onto the phenyl substituents.
2) Spin density is observed at the magnetically equivalent nitrogens to yield a_N values of approximately 1.5G, which are largely independent of the central metal.
3) No spin density at the β -pyrrole positions, that is the outer periphery of the molecule.
4) Small spin densities are found on the metal.

In contrast the one electron oxidation products of ZnOEP and MgOEP have been assigned as having an $^2A_{1u}$ ground state[15]. From Table 1, zero electron density at the pyrrolic nitrogens is predicted for this ground state and indeed no nitrogen hyperfine has to date been resolved in $^2A_{1u}$ ESR spectra[19,20] Also much smaller spin densities at the meso-positions are expected, with computer simulations predicting $a_{H(meso)}$ to be as small as 0.3G[14]. The experimentally observed ESR signal

for these species is consequently always an unresolved singlet.

Much less work has been done on the ESR of porphyrin anion radicals, probably due to their inherent instability. It is assumed that the added electron will occupy the lowest vacant $e_g(\pi^*)$ orbital (D_{4h} symmetry) which is doubly degenerate. This will result in a ^2E_g ground state for the anion radical which should then be ESR active. Guzy et al[21] noted that the e_g (π^*) and b_{1u} (π^*) levels lie close together and suggested instead that their orders are reversed and that the b_{1u} orbital is the one filled. Felton and Linshitz[22] pointed out that the degenerate components of the ^2E_g state could be affected by interactions with solvents or cations and by vibronic coupling to yield an averaged spin distribution. Maslov[23], more recently, concluded on the basis of photochemically induced dichroism that the orbital degeneracy in the anion of zinc etioporphyrin (at 77K) is removed to the extent that the population of the higher state is small. SCF-MO calculations by Felton[20] for an averaged spin delocalization, are listed in Table 2. The chemically generated anion radical of ZnTPP has been the subject of a number of studies[12, 22, 24,25]. Examination of the result however reveals large variations in line widths (5 - 26G) and g values. This is probably due to the presence of subsequent reaction products.

Uv/visible data are also extremely useful in assigning metal and/or porphyrin ring reactions. As outlined previously a two-banded visible absorption spectrum is characteristic of all metalloporphyrins. Sometimes, as for Fe(III) TPPCl these may be broadened somewhat by intramolecular charge transfer to axial ligands ('hyper' type spectra), but in these cases the intact π electron system is easily recognised by an intensive Soret band in the uv. M.O. calculations[26] show that removal of an electron from either the a_{2u} or a_{1u} highest occupied orbital will result in a loss of its energy through diminution of the electron-electron repulsion term, mixing the HOMO thoroughly with lower orbitals. This then leads to the participation of many different configurations to the excited state and to broad absorptions. It has been reported previously[16] that porphyrin ring cation radicals show only one band covering the whole visible range up to the near infra-red.

Thus if the electron is removed from the central metals during oxidation, one would expect the π / π^* bands to shift in energy but to retain the two band structure in the visible region. If however the electron is removed from a macrocycle-based orbital the resulting spectrum is expected to be quite different, with diffuse absorption occurring in the visible region.

The same type of arguments can be applied to the reduction

of metalloporphyrins. Again, if the electron-transfer process occurs at the metal and the π aromatic system of the porphyrin remains intact, the two bands in the visible region, though shifted, should be retained.

M.O. calculations[27] predict that for the metalloporphyrin anion radical, the addition of an electron to an unoccupied e_g orbital will lead to new low energy transitions producing relatively intense bands in the near infra-red. Existing experimental evidence supports this theoretical prediction. Closs and Closs[24] report that on treatment of ZnTPP with sodium benzophenone ketyl in THF the salt Na^+ZnTPP^- was formed and this product displayed a broad absorption at 900nm in its electronic absorption spectrum.

Chemically induced oxidations and reductions, in general however often give rise to more than one product and isolation of these products has proved impracticable. Thus, we have chosen to generate these species electrochemically.

Preparative electrolysis is governed by five interdependent variables : current, potential, concentration, temperature and time. If one wishes to prepare a porphyrin macrocycle in any oxidation state different from that of the parent molecule then it has to be oxidised (or reduced) at a potential slightly above (or below) the potential of the corresponding

wave. Fuhrhop[28] cites two main limiting factors in electrochemical synthesis-

1) the relatively low concentrations obtainable with porphyrin solutions
2) the limited lifetime of the electrode products which prevents extended electrolysis time.

We find that both the cathodic and anodic products can be generated at a large Pt electrode, under an inert atmosphere of nitrogen or argon, in a conventional electrochemical cell, providing the solvent is adequately free from H_2O. Concentrations of 1×10^{-5} M to 4×10^{-4} M of the metalloporphyrin prove adequate for these experiments and are easily obtainable in CH_2Cl_2. The number of electrons involved in each electron transfer step was determined precisely by coulometry and the reversibility checked by stirred d.c. voltammetric methods and full regeneration of the initial metalloporphyrin on returning the applied potential to an appropriate value. However on removal of the applied potential the lifetime of the electrode products was extremely limited, all quickly relaxing back to the neutral metalloporphyrin.

The problem of characterising these unstable compounds was overcome by carrying out the electrogeneration directly within the cavity of an ESR spectrometer or in the optical beam of a spectrophotometer and spectroscopically monitoring the course

of the electrolysis, in situ.

For electronic absorption measurements a very thin quartz cell was employed as the reaction vessel. An optically transparent thin layer electrode (O.T.T.L.E.) is used as a working electrode. This is simply a platinum minigrid which combines optical transparency and a large surface area enabling exhaustive electrolysis of the reactant. The cell itself is mounted in a gas-tight poly(tetrafluoroethylene) block as described by Heath and Yellowlees[29]. The temperature of the cell can be controlled by the passage of precooled N_2 gas (see figure 2).

Electrogeneration within an ESR cavity is not a novel idea. Previous cell designs[30,31] have however totally failed to achieve 100% electrolysis due to restrictions imposed by the size of the working electrode and major problems of migration of the substrate to the electrode. Consequently no more than one electron transfer step of a complex could be studied.

An original cell has been designed in this work, which is capable of exhaustively electrolysing the electro-active species and therefore any number of successive electrogenerations can be carried out and an ESR spectrum measured at each step. The cell employs a hollow platinum tube as the working electrode down which an Ag wire reference electrode is passed. The cylindrical geometry of the cell allows a uniform potential to be applied throughout with minimum cell

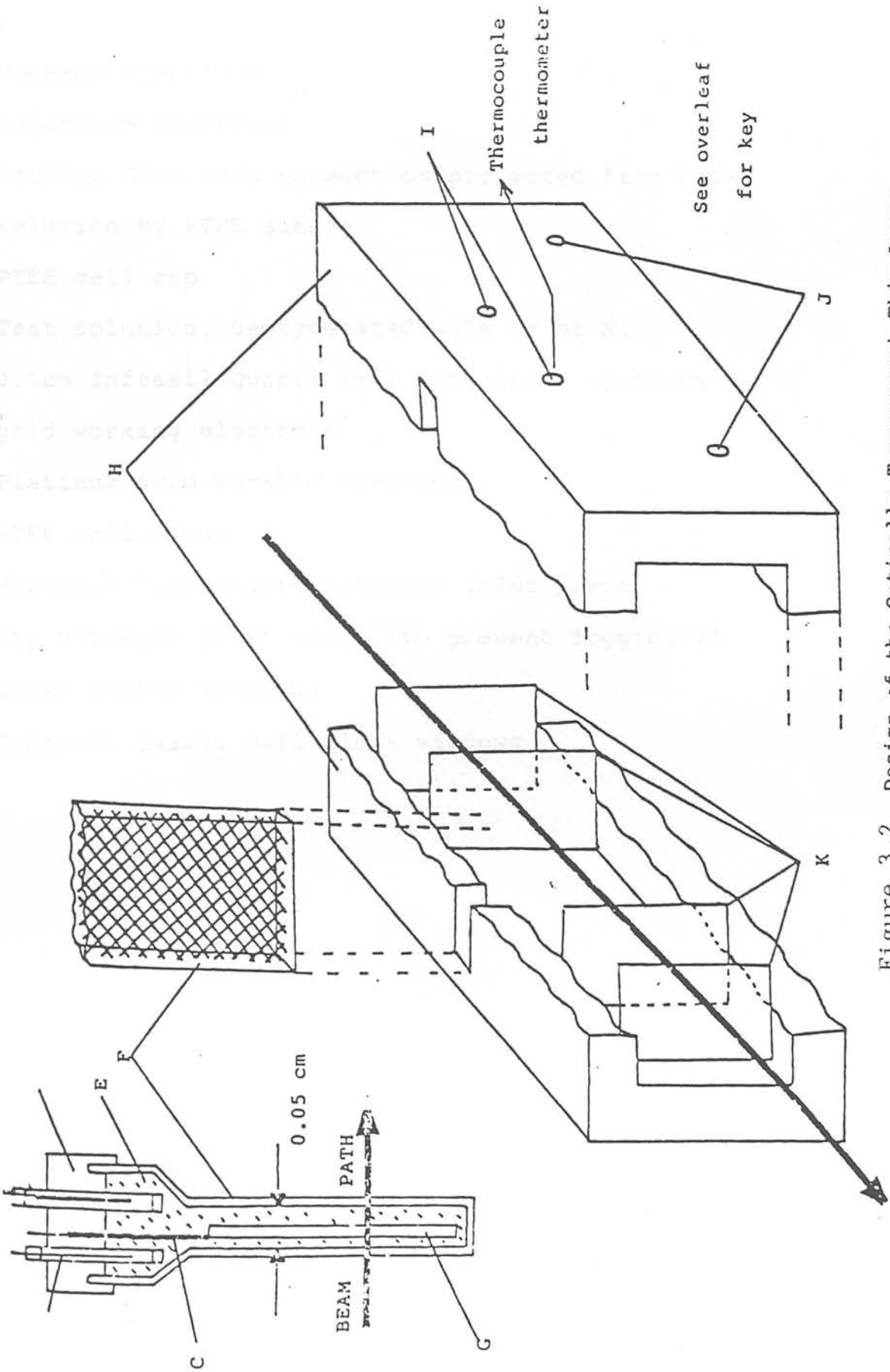

Figure 3.2 Design of the Optically Transparent Thin Layer Electrode

Key to Figure 3.2

A Counter Electrode

B Reference Electrode

C Working Electrode connection protected from bulk solution by PTFE sleeve

D PTFE cell cap

E Test solution, deoxygenated with Ar or N_2

F 0.1cm Infrasil Quartz cell containing platinum grid working electrode

G Platinum grid working electrode

H PTFE cell block

I Variable Temperature nitrogen inlet ports

J Dry nitrogen inlet ports (to prevent fogging of inner quartz windows)

K Infrasil Quartz cell block windows

resistance encountered. The passage of N_2 gas is used to aid migration of the complex to the working electrode. A commercial variable temperature unit allows spectra to be run at temperatures from -150°C to 25°C.

Experimental details are given at the end of the chapter.

In the present work we have succeeded not only in electrogenerating the anion radical and cation radical of all the M(II)TPP and M(II) OEP complexes studied but in the majority of cases the dianion and dication also. By monitoring the potential and current throughout and imposing strict reversibility criteria we can be certain no subsequent reaction of the electrogenerated species is occurring to give unwanted by-products. It was generally found that whereas the metalloporphyrin cation radical was a relatively stable species, the dication was highly electrophilic and prone to reaction with the media. Depressing the temperature of the electrogeneration cell helped to stabilise the dication, suppressing following reactions. The reduced products of the metalloporphyrins proved far more difficult to electrogenerate cleanly. The anion radical and particularly the dianion tended to undergo very facile reaction with trace protons and H_2O in the solvent. However, in carefully dried solvent the <u>total</u> exclusion of O_2 from the cell, and at depressed temperatures (-40 to -70°C), electrochemical and spectroscopic characterisation of these products in CH_2Cl_2 proved possible in the majority of cases.

The further reactions of the dication and dianion with the experimental medium are also briefly discussed.

The free-bases H_2OEP and H_2TPP proved limited in the role of models for the metalloporphyrins due to the limited lifetime of their redox products. However the electrogenerated products of the zinc complexes, ZnTPP and ZnOEP, wnere the redox-inert metal centre ensures all electron-transfer processes are occurring at the macrocycle, can be considered typical of metalloporphyrin cation radicals, dications, anion radicals and dianions. With these finger-print reference spectra it was then possible to assign the electron transfer site for the porphyrins where there was a possibility of change in the formal oxidation state of the central metal.

3.2 THE FREE-BASE PORPHYRINS H_2OEP, H_2TPP AND THEIR ZINC COMPLEXES

Both the free-base porphyrins and zinc porphyrins exhibit two reversible reductions and two reversible oxidations in CH_2Cl_2/0.5M $TBABF_4$. The $E_{\frac{1}{2}}$ values for each redox step are listed below-

	$E_{\frac{1}{2}}$(2nd ox)/V*	$E_{\frac{1}{2}}$(1st ox)	$E_{\frac{1}{2}}$(1st red)	$E_{\frac{1}{2}}$(2nd red)
H_2TPP	1.00	0.76	-1.41	-1.77
ZnTPP	0.82	0.60	-1.57	-1.94
H_2OEP	1.16	0.66	-1.54	-2.00
ZnOEP	0.74	0.44	-1.73	-2.19

* Volts vs Ag/AgCl reference electrode

All waves are diffusion controlled and fully reversible on a voltammetric time scale. Coulometry confirmed all redox couples to be one electron steps. (The redox products of H_2OEP and the oxidation products of H_2TPP were not stable on the extended time scale required for coulometric measurement. However comparative d.c. voltammetry confirmed each step to involve one electron).

The electrostatic effect of zinc as the central substituent (instead of the two protons present for the free bases) is to make the porphyrin moiety easier to oxidise and harder to reduce. This effect is equal in magnitude for both the primary cathodic and anodic redox couples, resulting in a constant value of ΔE(1st ox/1st red) throughout.

Spectroelectrochemical characterisation of the redox products of H_2OEP was not achieved due to the rapid decomposition of $H_2OEP^{+\cdot}$ and $H_2OEP^{-\cdot}$ even at -70°C. H_2OEC (OEC = octaethylchlorin) was detected as a decomposition product of the anion radical

but this was not a quantitative step. The other decomposition products were not identified and will not be referred to again.

On oxidation of H_2TPP at the plateau of the first oxidation wave a green product was generated, which exhibited an isotropic ESR signal, g = 2.0009 and ΔH = 5G. This is similar to that reported by Wolberg and Manassen[32] for $H_2TPP^{+\cdot}$ in benzonitrile. We however attribute the ESR signal to an unknown decomposition product, as H_2TPP cannot be recovered on reduction of this species. In situ uv/visible characterisation of the oxidation confirmed that $H_2TPP^{+\cdot}$ was only a transient species, decomposing to more than one product.

In contrast the cathodic electrochemistry of H_2TPP gives rise to stable primary products. Electrogeneration at the plateau of the first reduction results in a green product which is assigned as the monoanion radical $H_2TPP^{-\cdot}$. This species displays an isotropic ESR signal with g = 2.0015 and ΔH = 12G at 250K. No hyperfine splitting is observed even on cooling to 123K. Figure 3 shows the visible spectral progression on reduction of H_2TPP to $H_2TPP^{-\cdot}$. Unlike the metalloporphyrins, free base porphyrins are characterised by four visible bands in their electronic optical spectrum[33]. This difference arises from the two hydrogens in the centre strongly reducing the conjugated ring symmetry from square to rectangular, that is from D_{4h} to D_{2h}. This results in Q(0,0) splitting into

Figure 3.3 Visible spectrum of H_2TPP^- in CH_2Cl_2/0.5M $TBABF_4$ at -20°C

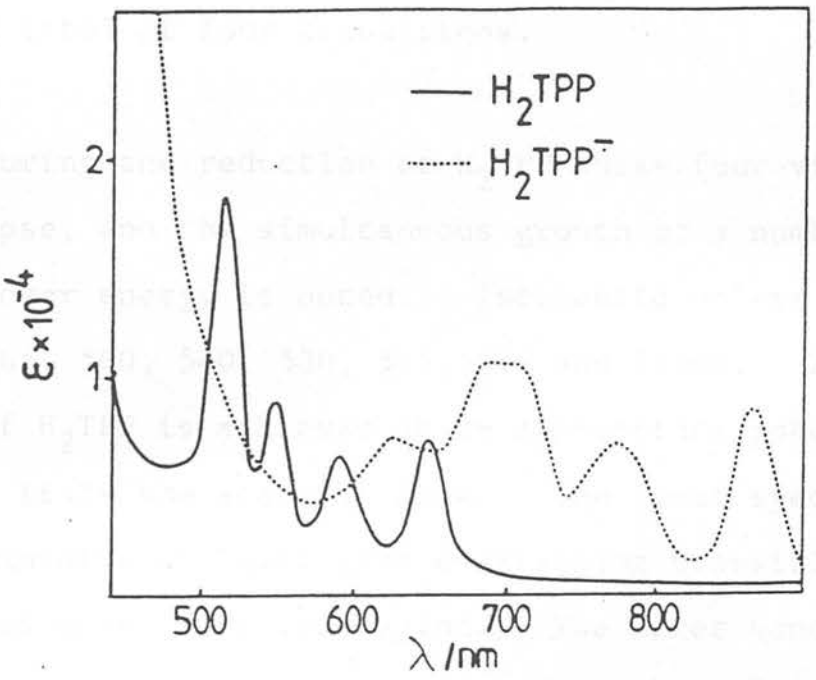

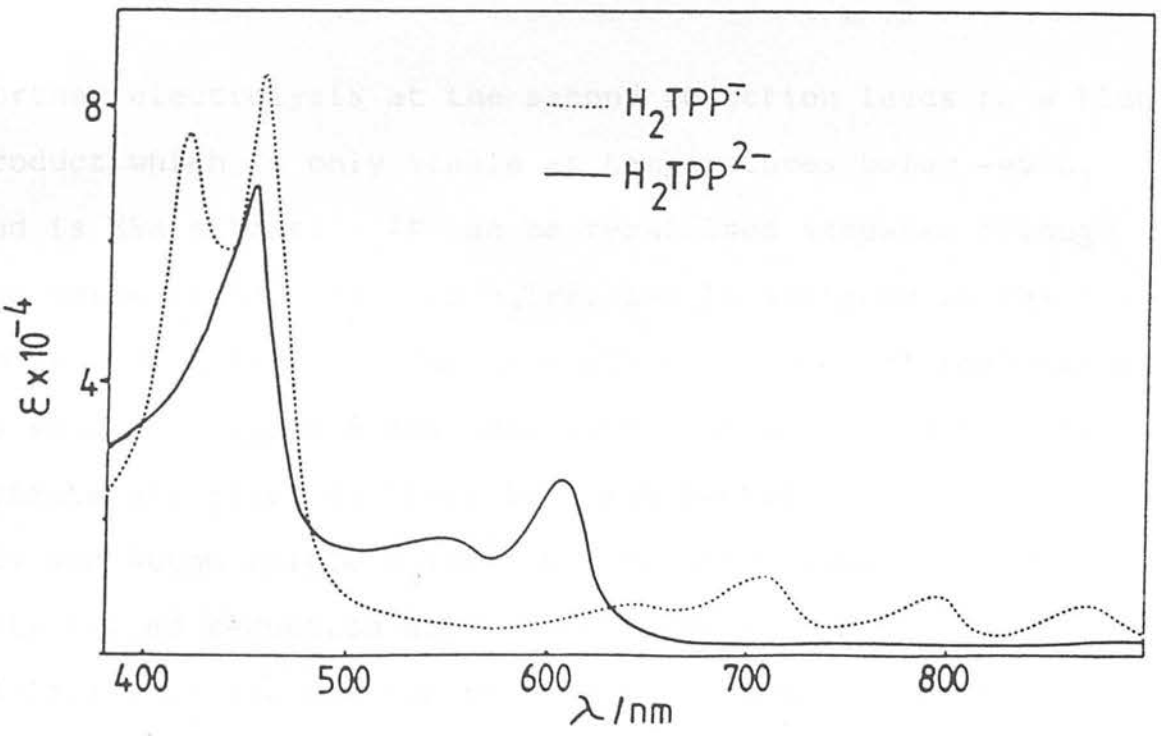

Figure 3.4 Visible spectrum of the π anion radical and π dianion of H_2TPP

two components Qx(0,0) and Qy(0,0) separated by about $3,000cm^{-1}$. Each band has a vibronic overtone resulting in a total of four transitions.

During the reduction of H_2TPP these four visible bands collapse, and the simultaneous growth of a number of bands to lower energy is noted. Isosbestic points are noted at 596, 585, 560, 540, 530, 505, 426 and 415nm. Full regeneration of H_2TPP is achieved at an appropriate potential. Table 3 lists the spectral data. The final spectrum of $H_2TPP^{\cdot-}$ exhibits at least five overlapping transitions in the visible and near infra-red region. The Soret band to higher energy is split into two separate transitions both of much lower intensity than the Soret band of the neutral porphyrin.

Further electrolysis at the second reduction leads to a blue product which is only stable at temperatures below -40°C, and is ESR silent. It can be reoxidised stepwise through the anion radical back to H_2TPP, and is assigned as the π dianion H_2TPP^{2-}. The uv/visible spectrum of the dianion is shown in Figure 4 and peak positions and extinction coefficients are given in Table 3. Isosbestic points at 630, 485 and 400nm relate H_2TPP^{2-} to the anion radical. During this second reduction all the low energy bands of the anion radical collapse and two relatively intense bands grow in the visible region at 595 and 548nm, and a small blue shift

Table 3.3 Spectral data for the reduction products of H_2TPP in CH_2Cl_2/0.5M $TBABF_4$

	Wavelength maxima, nm (extinction coefficient x 10^{-3})
H_2TPP	642(3.9), 587(5.2), 550(8.5) 514(18.4), 418(460)
H_2TPP^-	870(9.5), 768(8.5), 705(15.0), 683(12.5), 626(10.0), 449(82.5), 405(78.0)
H_2TPP^{2-}	600(23.0), 550(19.3), 442(70.1)

Table 3.4 Spectral data for the reduction products of ZnTPP in CH_2Cl_2/0.5M $TBABF_4$

	Wavelength maxima, nm (extinction coefficient x 10^{-3})
ZnTPP	592(9.4), 554(19.6), 420(550)
$ZnTPP^-$	905(10.0), 810(4.2), 750(12.2), 740(13.0), 680(7.0), 550(7.2), 445(182), 420(310)
$ZnTPP^{2-}$	610(20.6), 567(15.1), 422(160)

Table 3.5 Spectral data for the reduction products of ZnOEP in CH_2Cl_2/0.5M $TBABF_4$

	Wavelength maxima, nm (extinction coefficient x 10^{-3})
ZnOEP	568(28.1), 534(19.4), 399(350)
$ZnOEP^-$	872(14.1), 760(9.2), 630(20.1), 440(204), 400(242)
$ZnOEP^{2-}$	590(29.6), 568(20.0), 396(172)

in the Soret transition occurs. Unlike the anion radical the dianion has a single Soret band.

Both ZnTPP and ZnOEP exhibit similar cathodic behaviour to H_2TPP, in CH_2Cl_2. The one-electron reduction of ZnTPP gives rise to the optical spectral changes shown in Figure 5. This is similar in many respects to the visible spectrum reported for the salt Na^+ZnTPP^- by Closs and Closs[24] but far more structural detail is seen here. In addition the uv spectrum was measured and is shown in Figure 6. The spectral changes are grossly similar to those noted for the reduction of H_2TPP, with the growth of bands to lower energies than the visible bands for the neutral porphyrin and a splitting of the Soret band. Isosbestic points are noted at 608, 594, 590, 540, 450 and 420nm, during reduction. The ESR spectrum at -50°C of the one-electron reduction product is completely isotropic and no hyperfine is observed. ($g = 2.0010$, $\Delta H = 14G$).

Again the product of the second reduction is unstable at temperatures above -40°C. The absorption spectrum of the π dianion $ZnTPP^{2-}$ is shown in Figure 7. It is very similar in the visible region to the parent ZnTPP but the Soret band is markedly reduced in intensity (see Table 4).

The electronic absorption properties of $ZnOEP^-$ and $ZnOEP^{2-}$

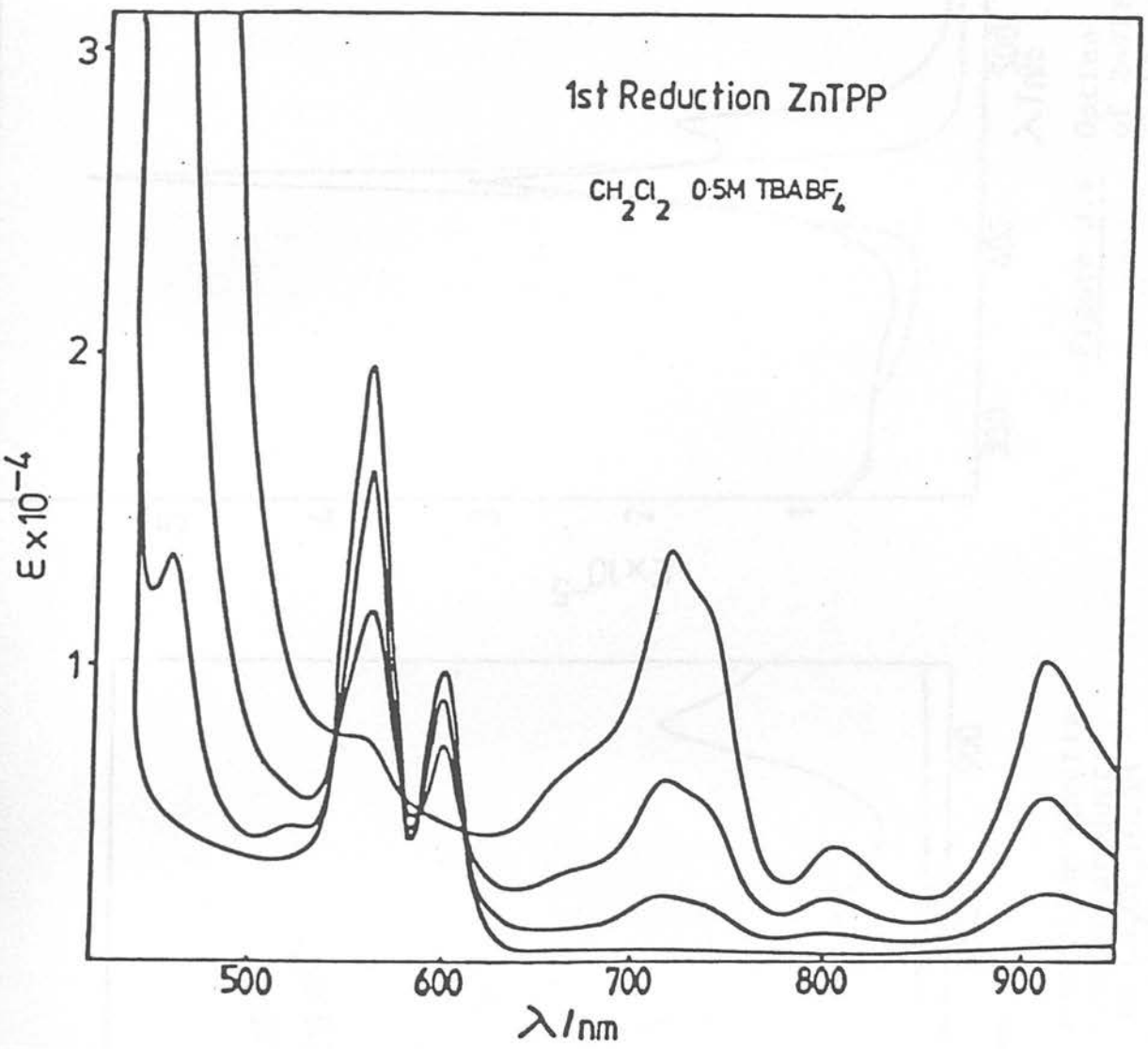

Figure 3.5 Optical progression during the first reduction of ZnTPP (20°C)

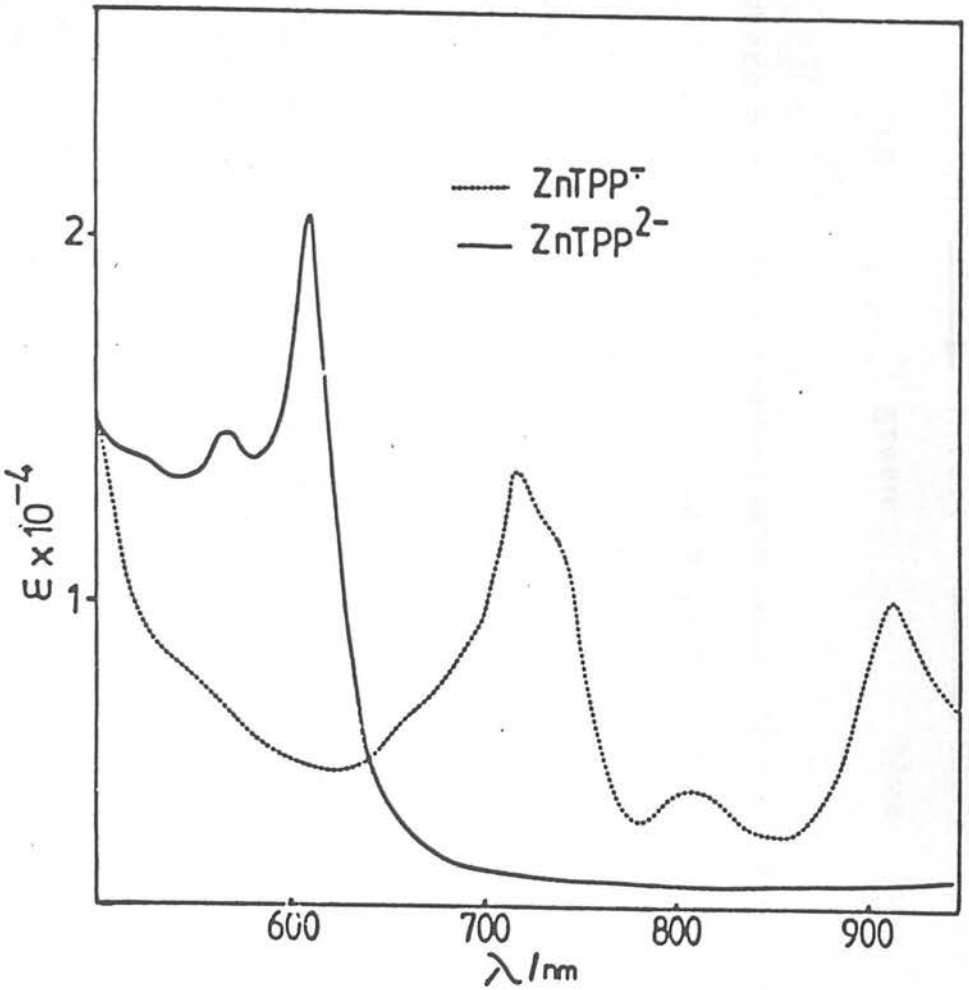

Figure 3.7 Optical absorption spectra of the cathodic products of ZnTPP in CH_2Cl_2/0.5M $TBABF_4$ at -45°C

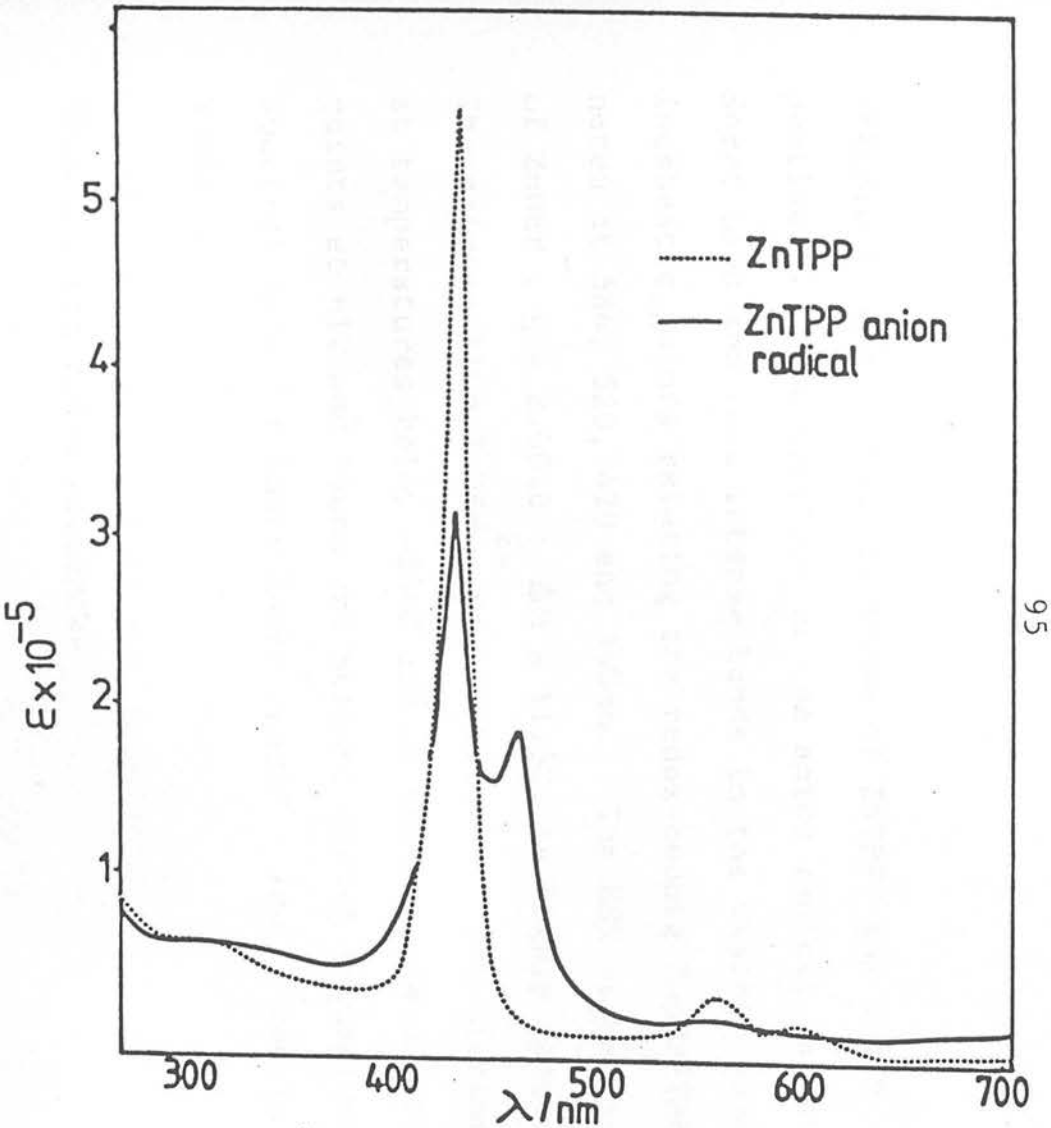

Figure 3.6 Optical absorption spectrum of $ZnTPP^-$ in CH_2Cl_2/0.5M $TBABF_4$ at -45°C

(Figure 8) are similar to those of $ZnTPP^{\cdot-}$ and $ZnTPP^{2-}$ respectively. The spectrum of the anion radical has a split Soret band and less intense bands in the visible/near ir region. Isosbestic points relating the redox-couple $ZnOEP/ZnOEP^{-}$ are noted at 584, 520, 420 and 380nm. The ESR signal (-50°C) of $ZnOEP^{\cdot-}$, g = 2.0016 : ΔH = 11.5G, is highly isotropic. The crimson/blue $ZnOEP^{2-}$ is ESR silent. The dianion is stable at temperatures below -50°C and at these temperatures isosbestic points at 612 and 460nm are present during reduction. Spectral data for $ZnOEP/ZnOEP^{-}/ZnOEP^{2-}$ are listed in Table 5.

Thus for the redox sequence-

$$\underset{\text{red}}{M(Por)} \xrightarrow{+e^-} \underset{\text{green}}{M(Por)^{\cdot-}} \xrightarrow{+e^-} \underset{\text{blue}}{M(Por)^{2-}}$$

where M = H_2 or a redox-inert metal we now have characterising ESR and optical spectral data to recognise porphyrin-based cathodic redox couples, which are common to both model macrocycles.

The importance of studying these porphyrin complexes in non-coordinating media is highlighted by the totally different

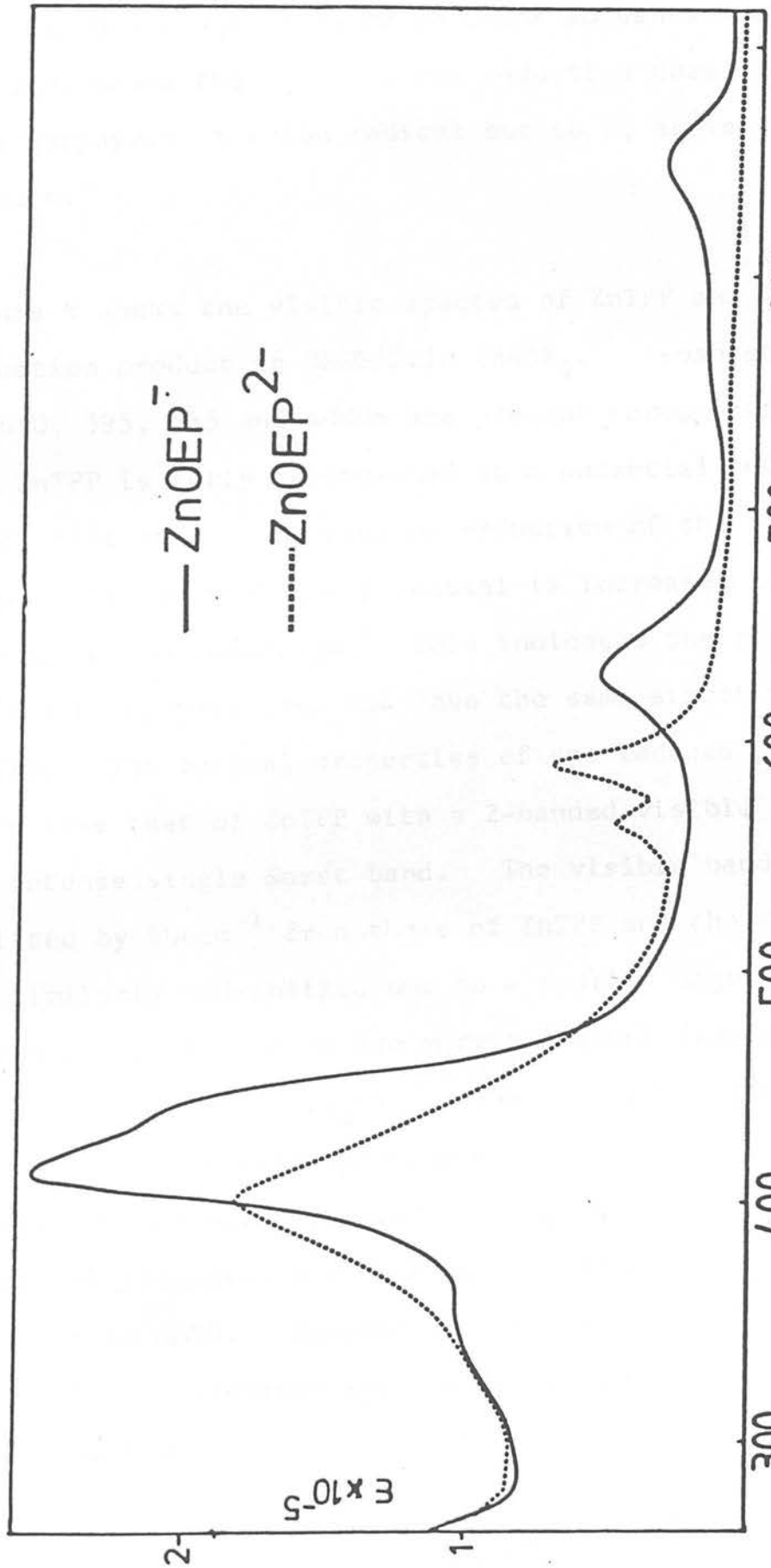

Figure 3.8 Optical Absorption spectra of the cathodic products of ZnOEP

cathodic behaviour of ZnTPP in donor solvents such as DMSO and DMF, where the one electron reduction does not result in a porphyrin π anion radical but to a, as yet, unidentified product.

Figure 9 shows the visible spectra of ZnTPP and its one-electron reduction product in DMSO/0.1M $TBABF_4$. Isosbestic points at 610, 595, 565 and 400nm are present throughout the reduction and ZnTPP is fully regenerated at a potential 200mV anodic of $E_{\frac{1}{2}}$ (1st red). However no reduction of the first cathodic product occurs when the potential is increased to the plateau of the second reduction. This indicates the reduction product of the first wave does not have the same structure as parent ZnTPP. The optical properties of the reduced product are very like that of ZnTPP with a 2-banded visible spectrum and an intense single Soret band. The visible bands are red-shifted by $900cm^{-1}$ from those of ZnTPP and the Soret band is similarly red-shifted but to a smaller degree ($400cm^{-1}$). These spectral changes are very different from those observed during reduction in CH_2Cl_2. The reduced product in DMSO exhibits the typical spectrum of a neutral porphyrin macrocycle with an uninterrupted π conjugation pathway. The spectral progression in DMF at room temperature is analogous to that in DMSO. However when the reduction is carried out at -50°C, a transient species is noted with characteristic peaks in the near ir, of a π anion radical. Coulometry

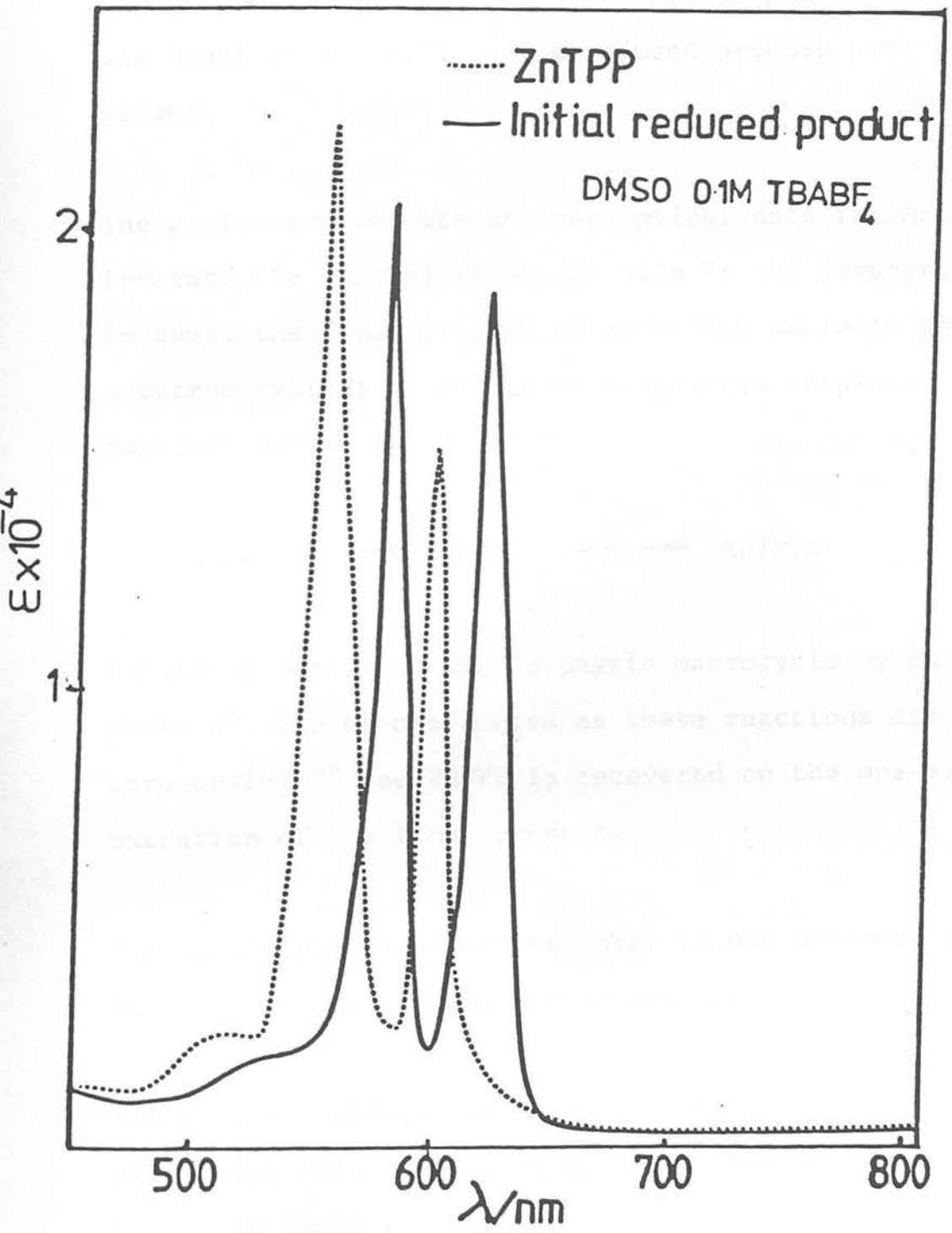

Figure 3.9 The one-electron reduction product of ZnTPP in DMSO (20°C)

over a ten-fold concentration range (1×10^{-5}M - 1×10^{-4}M) showed the number of moles of electrons passed during reduction was equal to 1 ± 0.05. The reduced product however is ESR silent.

The coulometry results and the optical data in DMF at -50°C indicate the initial reduction site is the porphyrin macrocycle. However, the final product of reduction exhibits an optical spectrum typical of a neutral porphinato complex. The reaction scheme -

$$\text{ZnTPP} \xrightarrow{+e^-} \text{ZnTPP}^{\cdot-} \xrightarrow{X^+} \text{ZnTPPX}$$

involving attack at the porphyrin macrocycle by an electrophile X^+, can be discounted as these reactions are generally irreversible[34] and ZnTPP is recovered on the one-electron oxidation of the final product.

The remarkable behaviour of ZnTPP is not observed for any of the other metalloporphyrins studied.

Voltammetric studies of ZnTPP in DMSO and DMF show the value of $E_{\frac{1}{2}}$ (1st red) to move to more cathodic potentials than displayed in CH_2Cl_2-

	$E_{\frac{1}{2}}$ (1st red)/V*
CH_2Cl_2	-1.57
DMF	-1.69
DMSO	-1.73

* Volts vs Ag/AgCl fully corrected for liquid junction potentials.

These results are in good agreement with a similar study by Heath et al on ZnOEP[35]. The values of $E_{\frac{1}{2}}$ (1st red) for the other metalloporphyrins were less dependent on the experimental media.

It has long been known that zinc porphyrins are more prone to axial ligation than other first-row transition metal porphyrins[36-39]. Spectroscopic studies of the equilibrium coordination of nitrogenous bases to metalloporphyrins have yielded formation constants, β_1, of typically 10^4 for zinc, 10^2 for nickel and 10^{-1} for copper[37]. X-ray data show that zinc porphyrins crystallised from coordinating media retain an axial ligand and that the zinc ion is displaced from the plane of the macrocycle towards the axial ligand, adopting a distorted square-pyramidal structure[38]. Optical absorption studies have shown that ZnTPP is monoligated in the presence of nitrogenous bases[39]. These results are obvious, as the spherically symmetrical d^{10} Zn(II) ion will prefer an octahedral, tetrahedral or similar three-dimensional environment to the

square planar geometry offered by the porphyrin macrocycle. The first reduction of ZnTPP in coordinating solvents is thus better described as the following redox couple-

$$ZnTPP\ (solvent)_n \xrightarrow{+e^-} (ZnTPP\ (solvent)_n)^-$$

where n = 1,2

The number of solvent molecules coordinated (n), need not be the same for both halves of the redox couple and more detailed electrochemical study is required to determine this.

The absorption bands for ZnTPP move to the red on reduction in DMSO. This is indicative that the energy gap between the highest-occupied π orbitals (a_{1u} and a_{2u}) and the lowest unoccupied π^* orbital (e_g degenerate pair) is smaller. The absorption spectrum also shows that although the porphyrin ring is the site of initial reduction the electron must reside elsewhere in the thermally-equilibrated reduction product. We propose the following reaction scheme-

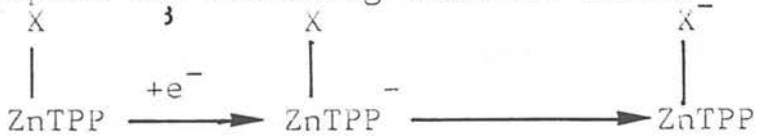

where the axially ligated group X is a solvent molecule or some unidentified impurity in the solvent. The lack of an ESR signal (although exactly one mole of electron is added) suggests a degree of aggregation of the reduced species or perhaps even a dimeric structure with ZnTPP moieties connected

via a reduced bridging group(s). The reduced product remains unidentified, but is included as an example of what can occur to porphyrin π anions in coordinating media.

Anodic Behaviour of Zinc Porphyrins

The one-electron oxidation of ZnOEP gives rise to a stable green cation radical which exhibits a singlet ESR spectrum at 250K. No hyperfine splitting is observed, even at 77K. The measured g factor of 2.0119 (ΔH = 5G) is markedly higher than that reported by Mauzerall[40] under similar conditions but with a perchlorate electrolyte. Also, no evidence of aggregation of the π-cation radical $ZnOEP^{+\cdot}$, as has been reported previously elsewhere[41], was noted in the present study. Felton et al[41] observed that the ESR signal of both $MgOEP^{+\cdot}X^{-}$ and $ZnOEP^{+\cdot}X^{-}$ ($X = Br^{-}, ClO_4^{-}$) decayed to zero at temperatures below -50°C. They attributed this to the cation radicals dimerising at low temperature e.g.$(ZnOEP^{+\cdot}Br^{-})_2$, the ground states of which are predicted to be singlets. No such phenomenon was observed here, the ESR signal remaining temperature independent (77 - 300K).

Fuhrhop et al.[42] envisaged the bonding of the proposed dimers to be a π-π ' interaction between two face-to-face porphyrin rings, and as such is an extreme form of the π - π type complex first described by Hausser and Murrell[43]. As two identical

radicals approach one another to the point that the electronic wave functions interact strongly, the doublet states will split into singlet and triplet states. The resulting dimer will have a singlet ground state only if the electron-pairing results in sufficient concentration of electrons in the bonding region to overcome the inherently lower energy of the triplet state. The so-called π- π' bond then is based on multicentre overlap and pairing of the previously half-filled π orbitals of the cation radicals in a face-to-face dimer. Such dimerisation has also been noted for zinc haematoporphyrin[44] and a β-ketoester of ZnOEP[45] cation radicals, but to date only Mg and Zn porphyrin radicals are known to dimerise. The non-dimerisation of $ZnOEP^{+\cdot}$ (or any of the other metalloporphyrin π cation radicals studied) in $CH_2Cl_2/TBABF_4$ strongly suggests the non-innocent participation of the counter-ion in the aggregation process. We have already noted the willingness of zinc to accept a ligand in a fifth axial site in coordinating media and to assume a capped configuration. In the presence of ClO_4^- and Br^- then we would expect zinc to be removed from the plane of the ring towards the axial ligand. This would facilitate the dimerisation of the porphyrin rings reducing metal-metal repulsion by increasing the distance between the zinc atoms. This effect is absent, or greatly reduced, with BF_4^- as the non-coordinating counter ion. The absence of this 'doming' effect must therefore be sufficient to hinder the mutual approach of the

cation radicals, preventing formation of the π- π ' bond. This argument can be extended to MgOEP as it too will be prone to axial ligation, having a spherically symmetrical central metal ion.

Further oxidation of the green π cation radical $ZnOEP^{+\cdot}$ at the second oxidation, gives rise to an ESR silent brown product assigned as the π dication $ZnOEP^{2+}$, which is stable only at temperatures below -40°C.

The optical changes which occur during the first oxidation are shown in Figure 10. Isosbestic points are noted at 575, 548, 510 and 416nm. The Soret band reduces considerably in intensity, broadens, and shifts slightly to the blue. The collapse of the visible bands is accompanied by the growth of three new relatively intense overlapping bands in the visible region. In addition to the relatively well resolved visible peaks, 2 unresolved shoulders are apparent at 480nm and 454nm. During the second oxidation absorption in this area of the spectrum increases (Figure 11). Other spectral changes involve a decrease in intensity and a further blue shift of the Soret transition and diffuse absorption appearing between 900 - 700nm. Isosbestic points are present at 690, 508 and 424nm during the second oxidation and ZnOEP is fully recoverable via the cation radical on reversing the potential stepwise back to the rest potential. The full absorption spectra

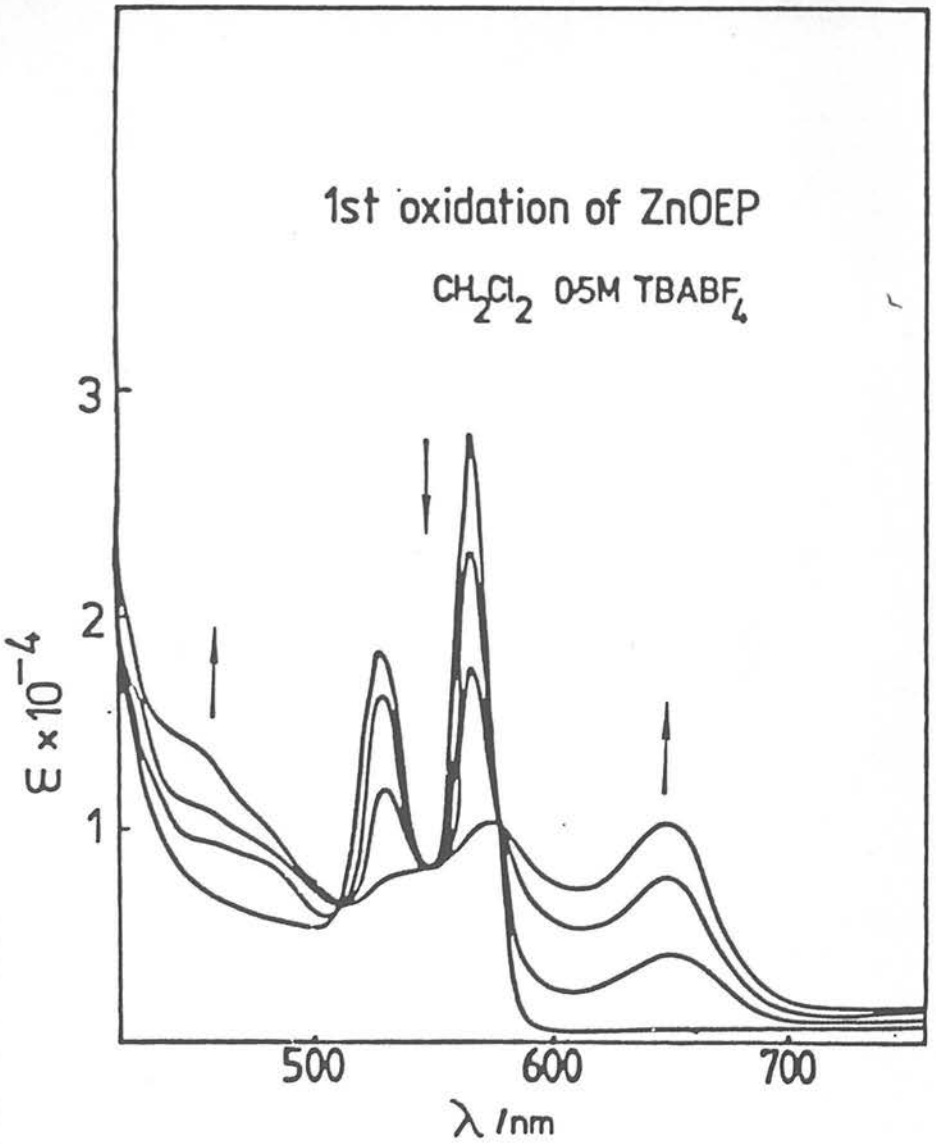

Figure 3.10 Optical progression during the first oxidation of ZnOEP

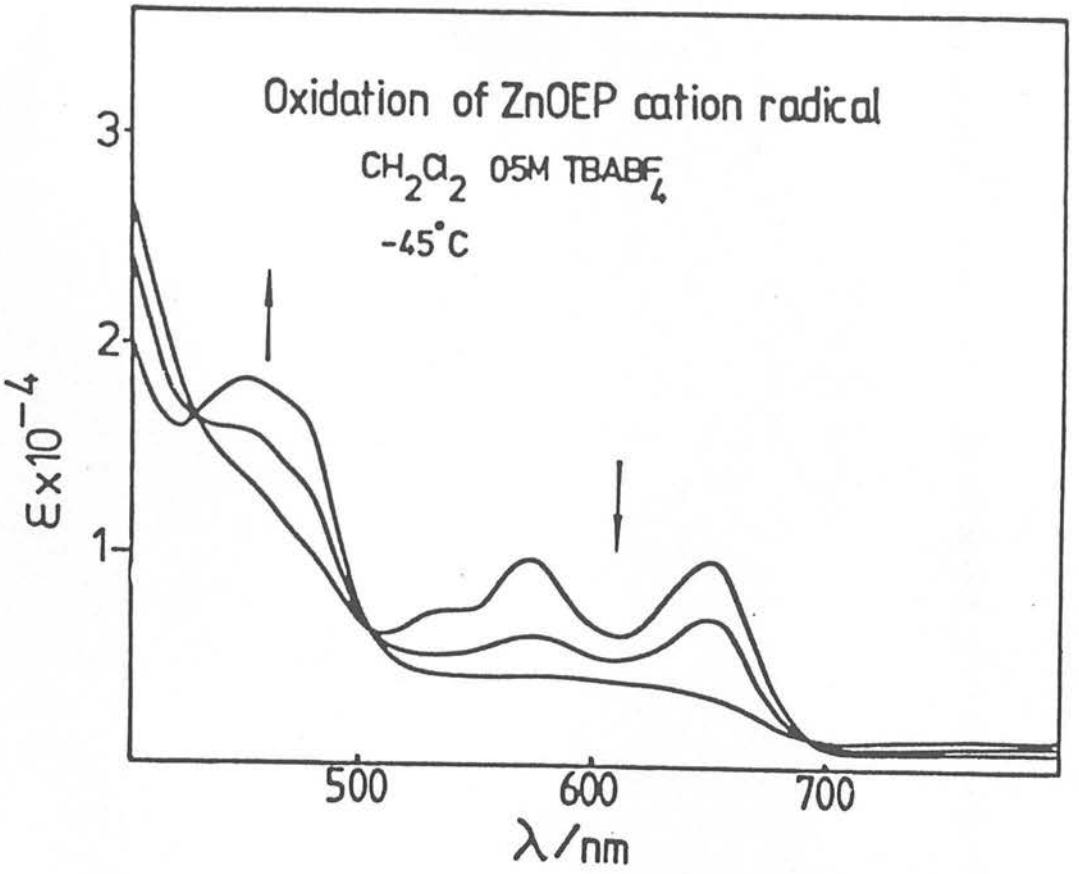

Figure 3.11 Optical progression during the second oxidation of ZnOEP

of $ZnOEP^{+\cdot}$ and $ZnOEP^{2+}$ are shown in Figure 12, and the data listed in Table 6.

The optical changes which occur during the first oxidation of ZnTPP are subtly different from those exhibited by ZnOEP. The absorption spectrum of the one electron oxidation product, $ZnTPP^{+\cdot}$, is shown in Figure 13. The visible spectrum has the same number of transitions as $ZnOEP^{+\cdot}$ but the energies and intensities of these bands are dissimilar. A weak band at 850nm is the most obvious difference. The Soret band undergoes a similar blue shift and decrease in intensity as observed for $ZnOEP^{+\cdot}$. The electronic spectral differences between the two cations, $ZnTPP^{+\cdot}$ and $ZnOEP^{+\cdot}$, can be explained by the different ground states possessed by each radical as discussed earlier. Previous ESR results[8] attribute a $^2A_{2u}$ ground state to $ZnTPP^{+\cdot}$ and a $^2A_{1u}$ ground state to $ZnOEP^{+\cdot}$. The ESR spectrum measured for $ZnTPP^{+\cdot}$ in the present work is similar to that reported previously.[10] Hyperfine splitting attributed to the four equivalent nitrogens, giving rise to a nine-line spectrum, is observed. No such hyperfine was observed for $ZnOEP^{+\cdot}$ (Figure 14).

$ZnTPP^{2+}$ was ESR silent and exhibited a similar optical spectrum to that of $ZnOEP^{2+}$. Upon oxidation of $ZnTPP^{+\cdot}$ the Soret band shifts considerably to higher energy and decreases markedly in intensity. The only observed feature of the visible

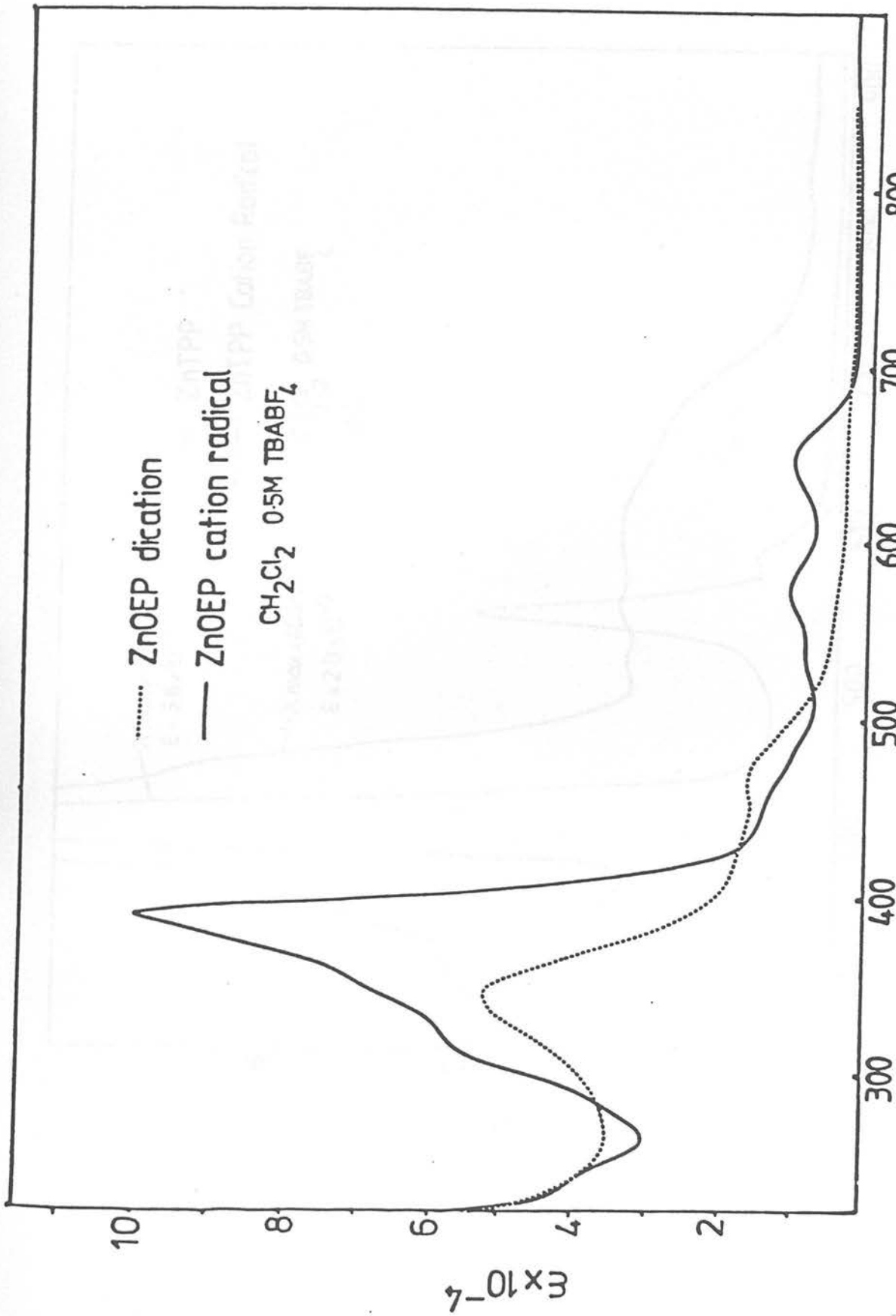

Figure 3.12 Optical absorption spectra of the anodic products of ZnOEP

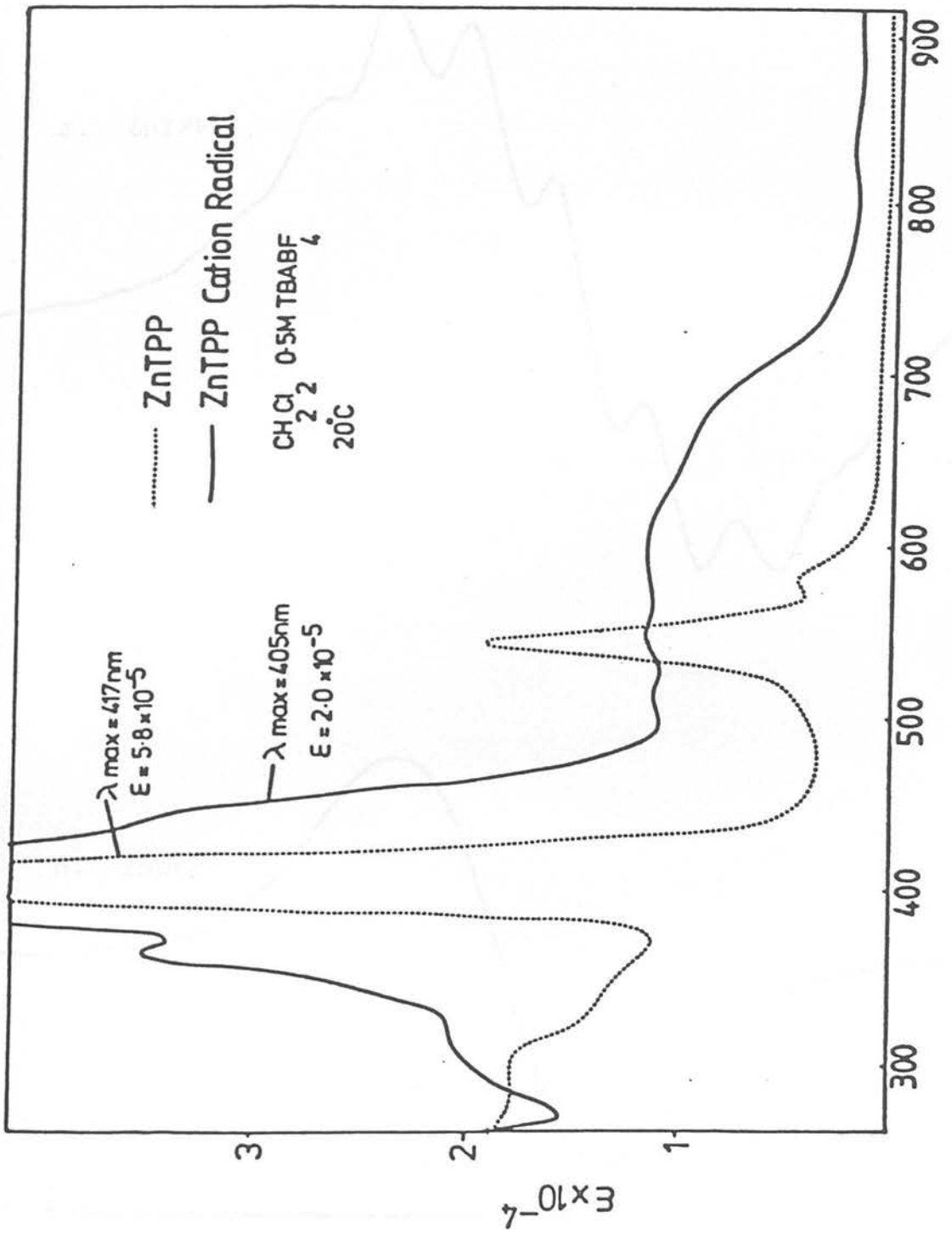

Figure 3.13 Optical absorption spectrum of $ZnTPP^{+}$

Figure 3.14 250K ESR spectra of zinc porphyrin π cation radicals

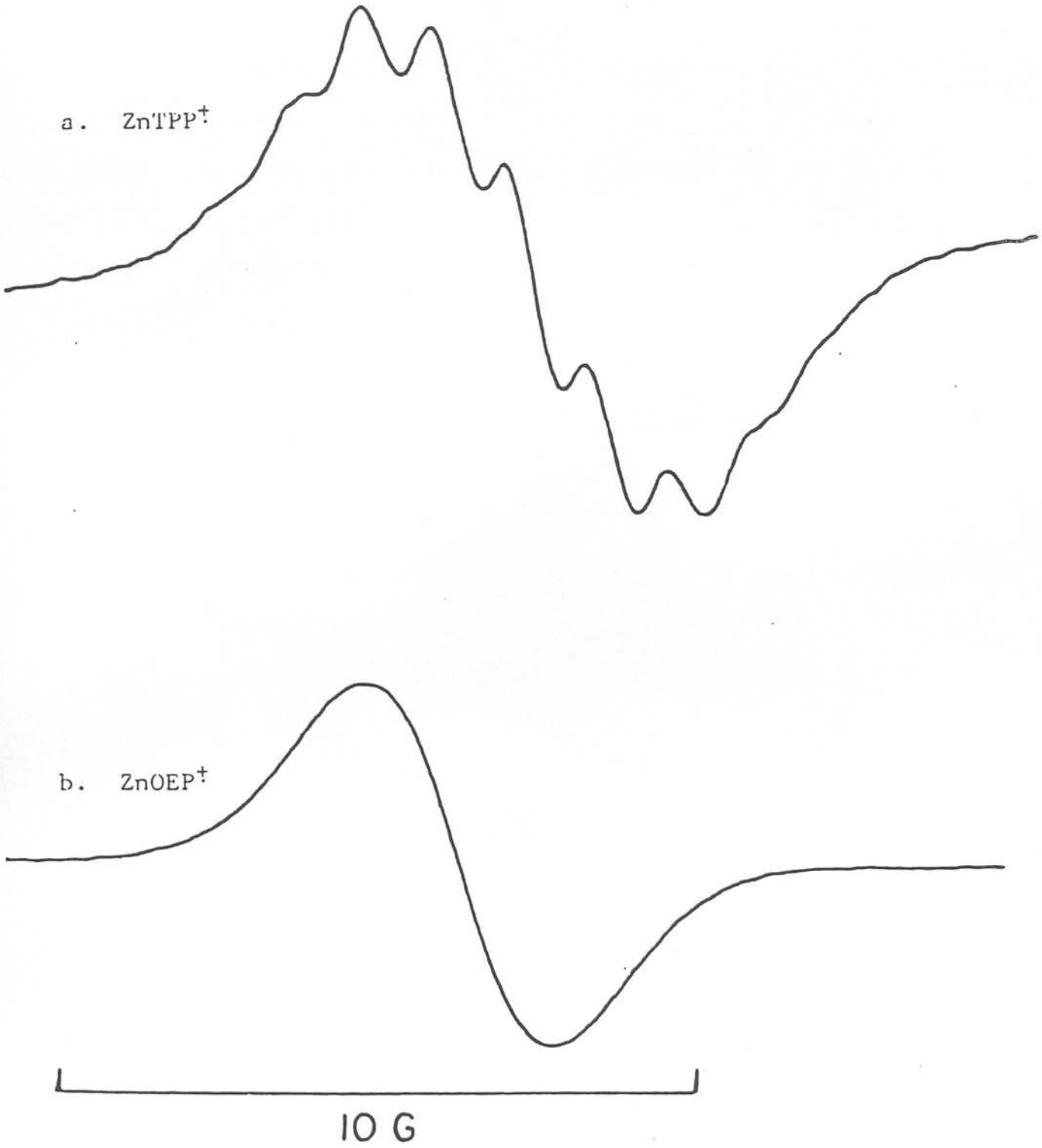

Table 3.6 Spectral data for the oxidation products of ZnOEP

	Wavelength maxima, nm (extinction coefficient x 10^{-3})
$ZnOEP^{+}$	880(broad), 648(9.9), 595(9.9), 560(9.0), 480(11.4), 454(15.0), 410(100.6), 320(5.9)
$ZnOEP^{2+}$	900-700(broad), 470(18.5), 456(19.0), 388(51.2)

Table 3.7 Spectral data for the oxidation products of ZnTPP

	Wavelength maxima, nm (extinction coefficient x 10^{-3})
$ZnTPP^{+}$	840(2.9), 694(7.6), 602(9.8), 555(9.9), 520(9.5), 405(200) 363(34)
$ZnTPP^{2+}$	850-700(broad), 510(14.0), 354(110.4)

spectrum is a broad unresolved shoulder around 500nm. Figure 15 shows the optical spectra of $ZnTPP^{+}$ and $ZnTPP^{2+}$ in full. The data are listed in Table 7.

The spectroelectrochemical results for the zinc porphyrins thus establish general qualitative diagnostic criteria for the presence of porphyrinato π cation radicals, π anion radicals, π dications and π dianions. The assignment of the optical transitions will be discussed at the end of the chapter with the main points summarised below-

1. Π anion radicals:

exhibit unstructured isotropic ESR signals with a g value close to the free spin value (2.0023). Broad optical absorptions in the near ir and visible region (900 - 600nm) of reasonable intensity ($\epsilon \sim 1 \times 10^{-4}$) and a split Soret band red-shifted from the Soret transition of the parent porphyrin.

2. Π dianions:

ESR silent; sharp visible bands ($\epsilon \sim 2 \times 10^{-4}$) around 600nm. No near ir bands. Single Soret transition of much lower intensity than the π anion radical, with small blue shift.

3. Π cation radicals:

a) $^{2}A_{2u}$ ground state: ESR shows ^{14}N coupling (a_N - 1.4G) Optical spectrum has weak band between 900 - 800nm and

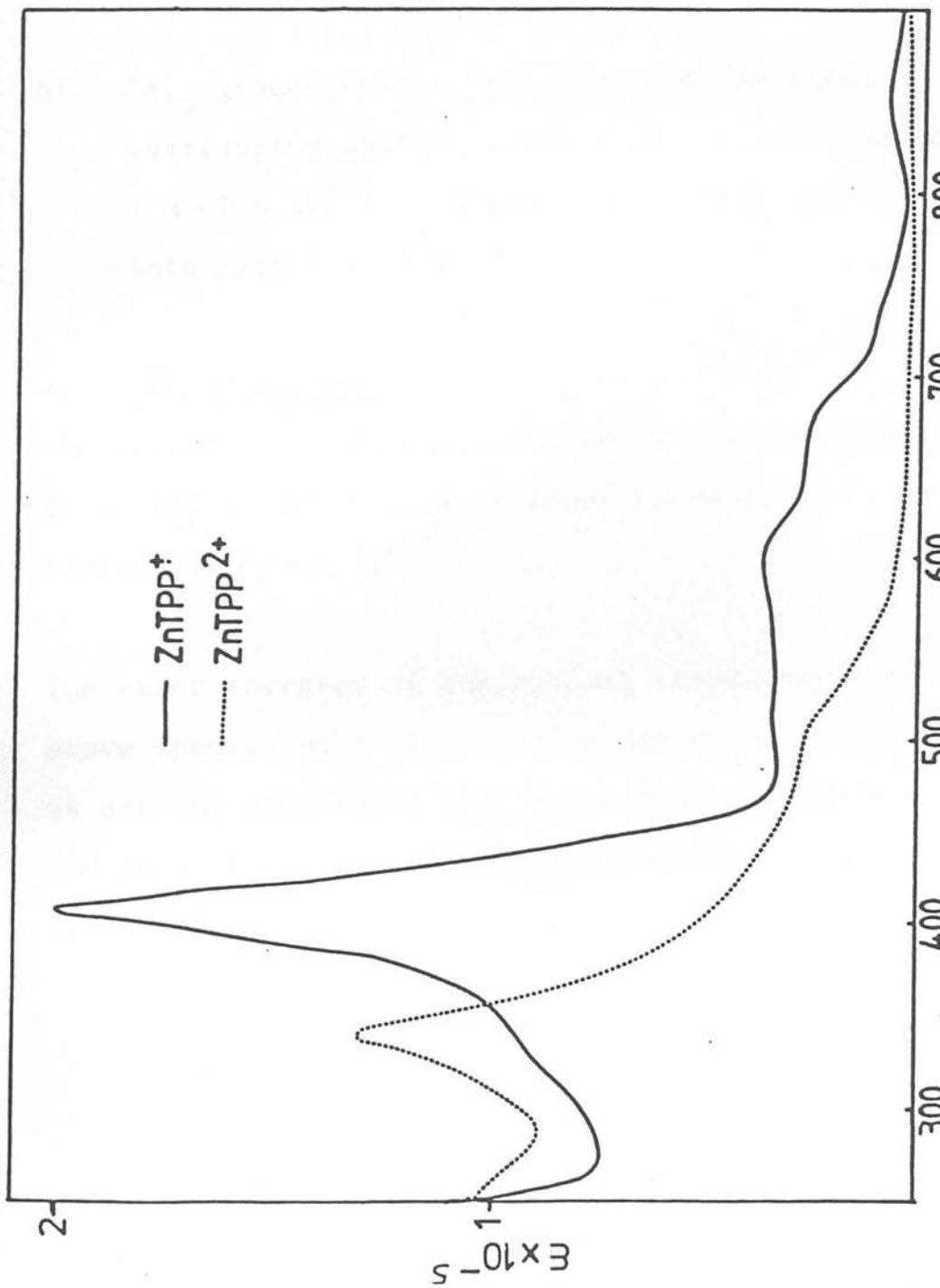

Figure 3.15 Optical absorption spectra of the anodic products of ZnTPP

more intense (ϵ - 1 x 10^{-4}) broad overlapping bands between 750 and 550nm. Broad Soret band of decreased intensity (ϵ-2 x 10^{-5}) from the parent porphyrin with small blue shift.

b) $^2A_{1u}$ ground state: unstructured ESR signal. Three overlapping optical transitions between 750 and 500nm (ϵ- 1 x 10^{-4}). Blue-shifted Soret band also of decreased intensity (ϵ - 1 x 10^{-5}).

4. Π dications:

ESR silent. Unstructured shoulder in visible spectrum, λ-500nm. Blue shifted Soret band of lower intensity than π cation radical (ϵ=8 x 10^{-4}).

The exact energies of the optical transitions for all the above species will of course be dependent on the metal centre, as are the spectra of the parent metalloporphyrins. However the general pattern should be applicable in the assignment of porphyrin ring-based redox steps.

3.3 THE d^9-METALLOPORPHYRINS

A number of studies into the redox behaviour of copper porphyrins and the valence isoelectronic silver and gold porphyrins have been reported [46-52]. Extensive ESR studies on the parent paramagnetic metalloporphyrins of Cu(II) and Ag(II)[53, 54] show the unpaired electron is in the uppermost d-orbital, $d_{x^2-y^2}$. Depending on the relative energy of the metal-based $b_{1g}(d_{x^2-y^2})$ orbital and the e_g π^* of the macrocycle then, oxidation and reduction of these complexes can occur either at the metal or the ligand. I.E.H. calculations[52] predict the energy of $d_{x^2-y^2}$ to rise through the series Cu(II) Por < Ag(II) Por < Au(II) Por, and thus Au(II) should be the most easily oxidised and Cu(II) the least likely to oxidise at the metal. Au(II) porphyrins are in fact unstable, oxidising in the presence of O_2 to (Au(III) porphyrins)$^+$ [55]. Gold porphyrins are not discussed further in this work. Copper and silver porphyrins are long known as having metal valence (II)[56]. In keeping with the M.O. calculations it is found here oxidation of Cu(II) porphyrins results in formation of porphyrin π cation radicals whereas Ag(II) porphyrins are preferentially oxidised at the metal.

Wolberg and Manassen[46] report the one electron oxidation product of Cu(II) TPP to be a π cation radical. This assignment was based largely on a linear plot of $E_{\frac{1}{2}}$(1st ox) vs 3rd

Ionisation Potential of the central metal. We have shown in this work (Chapter 2) that this correlation is extremely limited in its applicability. However the reported optical spectrum of $Cu(II)TPP^{+}$ confirms the first oxidation is indeed ligand based. Fuhrhop[47], contrastingly, reports the first oxidation of Cu(II)OEP to be metal-based as no ESR signal was observed for the primary anodic product. This is consistent with the formulation of the diamagnetic species $(Cu(III)OEP)^{+}$. Cu(III) is not a common oxidation state but related species such as $Cu(II)(dimethylglyoxime)_2$ do exhibit a $Cu^{II/III}$ couple at comparable potentials to that displayed by the copper porphyrins[57]. However it has since been calculated[58] that considerable exchange coupling between the electron 'hole' of d^9 Cu(II) and that of an oxidised porphyrin would result if the oxidation product was $(Cu(II)OEP^{+\cdot})^{+}$ and thus the lack of an ESR signal is not definitive.

An X-ray photoelectron spectroscopic study[59] on Ag(II)OEP determined binding energies of the silver d electrons for both the parent complex and the oxidised product. The binding energies were noted as being greater in the oxidised compound reflecting an increased positive charge on the metal. It was thus concluded the first oxidation was an $Ag^{II/III}$ couple. This was confirmed by Kadish et al.[48] who noted the visible absorption spectrum of the oxidised product was that expected from a metalloporphyrin with the π conjugative path-

way intact. We confirm these previously published results but also characterise the products of the subsequent oxidations of the d^9 metalloporphyrins.

Far less work has been previously carried out on the cathodic behaviour of copper and silver porphyrins. On the basis of the polarographic data alone Felton and Linschitz[22] concluded the one electron reduction of Cu(II)TPP and Cu(II) etioporphyrin *(I)* resulted in the formation of π-anion radicals. In direct contrast however, an X-ray photoelectron study[60] on the reduction of Cu(II) TPP by sodium vapour, concluded the product to be $(Cu(I)\ TPP)^-$. This assignment was based on the copper 2p binding energy changing upon reduction (Zn TPP 2p spectra remained constant under similar treatment). It is however necessary to assume a nearby positive sodium ion, to explain the <u>increased</u> binding energy on reduction and the product was thus formulated as $Na^+(Cu(I)\ TPP)^-$. More recent $X\alpha$ calculations by Case and Karplus[61] on copper porphin similarly predict reduction to take place at the metal centre. Gouterman et al.[52] report electrochemical reduction of Ag(II) TPP and Ag(II) OEP occurs at the macrocycle but no spectroscopic evidence for this assignment is presented.

Here, we compare both the anodic and cathodic electrochemistry of Cu(II) and Ag(II) porphyrins in CH_2Cl_2 and attempt to characterise the redox products in the same manner as described

previously. The redox potentials exhibited by these complexes are tabulated below

	$E_{\frac{1}{2}}$(3rd ox)*	$E_{\frac{1}{2}}$(2nd ox)	$E_{\frac{1}{2}}$(1st ox)	$E_{\frac{1}{2}}$(1st red)	$E_{\frac{1}{2}}$(2nd red)
CuTPP	-	1.03	0.70	-1.51	-1.95
CuOEP	-	0.84	0.51	-1.70	-2.19
AgTPP	1.50	1.31	0.32	-1.27	-2.23
AgOEP	1.46	1.18	0.30	-1.30	-2.23

* Volts vs Ag/AgCl reference

All waves correspond to a reversible one electron step. However reduction of the silver porphyrins proved fully reversible only at unusually high scan rates ($5Vs^{-1}$) due to very rapid decomposition of the electrode products. Characterisation of these products thus proved impossible for these complexes and assignment of reduction sites must therefore be based on the voltammetric data alone. As such these assignments are not definitive and further work is required on these complexes.

The observed electrochemistry of the copper porphyrins is quite different from that of the silver porphyrins. Whereas the Cu(II) porphyrins closely mimic the redox behaviour of the zinc porphyrins, the Ag(II) porphyrins exhibit three oxidations, not two. The cathodic behaviour is also quite different.

The value of ΔE(1st red/2nd red) for Ag(II) TPP (0.72V) and Ag(II) OEP (0.93V) are a good deal larger than that exhibited by both the copper and zinc porphyrins (typically ~ 0.4V). Also, Ag(II) OEP and Ag(II) TPP reduce at comparable potentials. In general due to their differing basicities, the OEP macrocycle is harder to reduce than the TPP moiety by ~ 200mV. This observation along with the fact the Ag(II) porphyrins are easier to reduce than their free-base derivatives, strongly indicates the first reduction occurs at the metal and not the macrocycle, as previously reported[52]. (The cathodic electrochemistry of the silver porphyrins is similar to that of the Co(II) porphyrins, where the first reduction product has been characterised as a Co(I) porphyrin; see later).

Spectral characterisation of the reduced products of copper porphyrins shows unequivically that two successive reductions of the macrocycle occurs with copper remaining in the divalent state throughout.

Both Cu(II) OEP and Cu(II) TPP reduce at far more cathodic potentials than related Cu(II) (N_4) macrocycles which exhibit a $Cu^{II/I}$ couple[62], exhibiting instead voltammetric behaviour consistent with the successive formation of a porphyrin π anion radical and π dianion, i.e. Cu(II) TPP is easier to reduce than Cu(II) OEP by 190mV and ΔE(1st red/2nd red) is 0.44V and 0.47V respectively.

Many ESR reports on copper (II) porphyrins exist[63] and detailed hyperfine splitting has been noted in a few polycrystalline studies at 77K[64]. However in CH_2Cl_2 at temperatures between 300 - 200K only an extremely broad anisotropic signal is detectable. This is similar to that noted by Blumberg and Peisach[65] for copper uroporphyrin in acetone at room temperature. Both the first and second reduction products of the copper porphyrins are ESR silent. As the first reduction proceeds the signal of the parent Cu(II) porphyrin gradually decays. This is non-informative however as although the absence of an ESR signal is consistent with a diamagnetic (Cu(I) porphyrin)$^-$ the presence of two unpaired electrons, one on the ring and one on the copper would lead to an extremely broad anisotropic signal which would be extremely difficult to detect.

Optical absorption spectral characterisation clearly distinguishes that reduction of both Cu(II) porphyrins occurs at the ligand and not the metal. Figure 16 shows the one electron reduction product of Cu(II) TPP. The resulting split Soret band and the growth of low energy transitions in the near ir region are all indicative of formation of a porphyrin π anion radical. The optical spectrum of (Cu(II) $OEP^{\cdot-}$)$^-$ is very similar to that of (Cu(II) $TPP^{\cdot-}$)$^-$. Spectral data for both π anion radicals are listed in Table 8. Table 8 also includes the peak positions of the doubly reduced

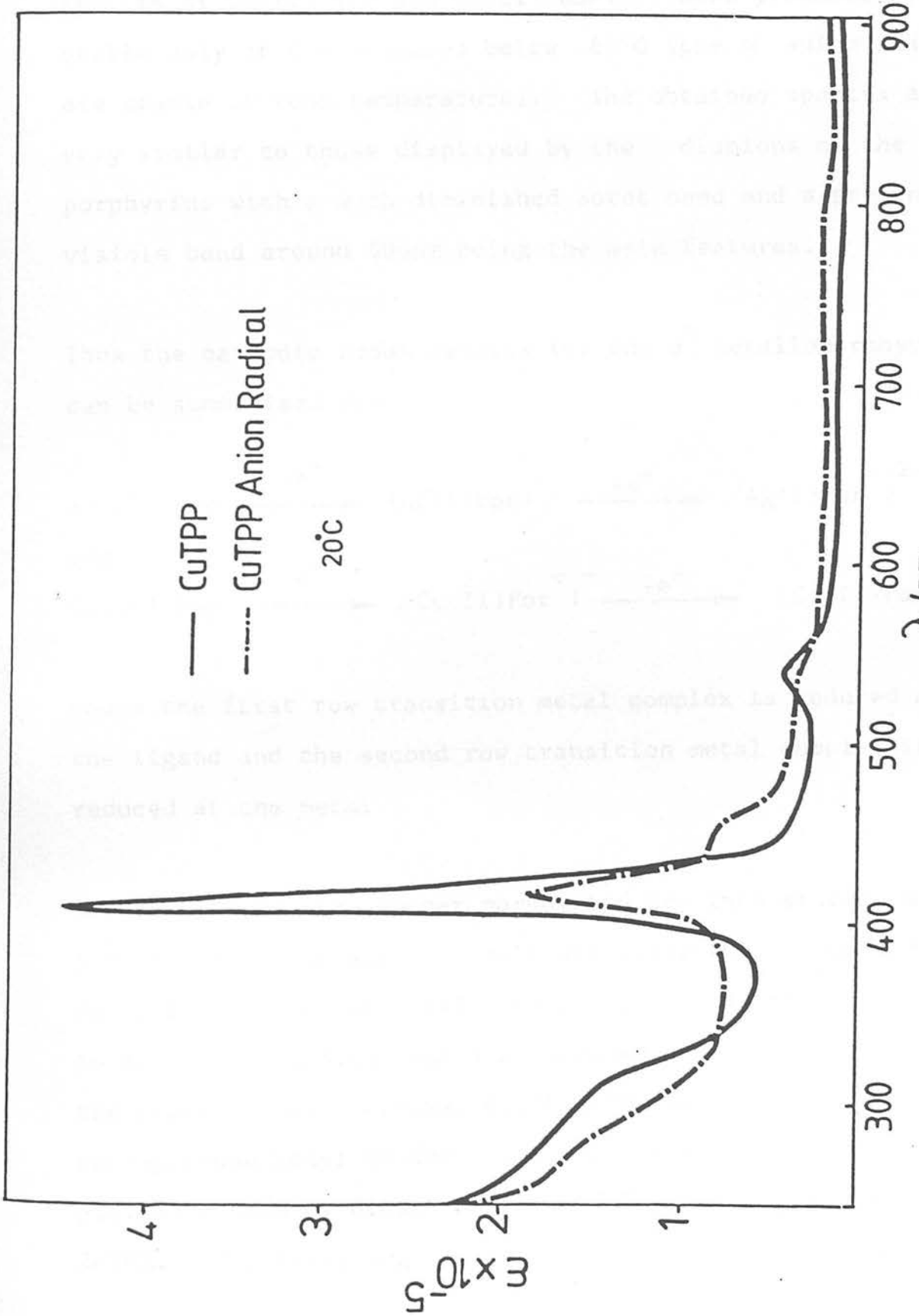

Figure 3.16 The one-electron reduction product of Cu(II)TPP

species of Cu(II) TPP and Cu(II) OEP. These products are stable only at temperatures below -60°C (the π anion radicals are stable at room temperature). The obtained spectra are very similar to those displayed by the dianions of the zinc porphyrins with a much diminished Soret band and a prominent visible band around 600nm being the main features.

Thus the cathodic redox results for the d^9 metalloporphyrins can be summarised as-

$$\text{Ag(II) Por} \xrightarrow{+e^-} (\text{Ag(I)Por})^- \xrightarrow{+e^-} (\text{Ag(I)Por}^{\cdot 2-})$$

and

$$\text{Cu(II) Por} \xrightarrow{+e^-} (\text{Cu(II)Por}^{\cdot -}) \xrightarrow{+e^-} (\text{Cu(II)Por}^{2-})$$

where the first row transition metal complex is reduced at the ligand and the second row transition metal complex is reduced at the metal.

The results for the copper porphyrins are inconsistent with the photoelectron spectroscopic determination of the first reduction product of Cu(II) TPP as $Na^+(Cu(I)\ TPP)^-$. In order to check that sodium ions are 'innocent' in determining where the reduction site occurs, Cu(II) TPP was treated with sodium benzophenone ketyl in THF following the same experimental procedure used by Closs and Closs[24] for the reduction of ZnTPP. The resulting spectrum is very similar to that measured

for the electrochemically generated Cu(II) $TPP^{\cdot-}$. Thus our electrochemical (and chemical) results seem to be in conflict both with the previous photoelectron spectroscopic work[60] and M.O. calculations[61] which predict the lowest acceptor orbital to be the metal-based b_{1g} ($d_{x^2-y^2}$). Here again then we must emphasise the fundamental difference between electronic spectroscopic data and electrochemical measurements, referred to earlier. Spectroscopic data measure 'vertical' transitions within a molecular orbital array and as such give rise to Franck-Condon excited states where by definition the geometry of the excited state and the ground state are identical. Electrochemistry, contrastingly, deals with fully thermally-equilibrated electrode products where the time scale of the electron-transfer is orders of magnitude greater than in the spectroscopic event. The photoelectron results[60] conclusively show the $d_{x^2-y^2}$ to be the lowest acceptor orbital, as predicted by Case and Karplus[61]. Electrochemistry lends insight however to the consequent geometric relaxation of the one-electron reduction product. One can envisage the following sequence of events. Firstly an electron is added to the b_{1g} ($d_{x^2-y^2}$) of the central copper to give initially $(Cu(I)\ TPP)^{-}$. The spin-spin repulsion term in this localised orbital must be great enough to make $d_{x^2-y^2}$ less stable than the ligand-based e_g π^* orbital. Consequently the $(Cu(II)\ TPP^{\cdot-})^{-}$ form of the reduced complex is more stable than when both electrons are paired in the

same orbital, and this thermally-equilibrated state will be the electrochemically observed redox product. Thus although usually we find that spectral and electrochemical results can be used in close conjunction to give information about say, the HOMO/LUMO gap, in this case careful consideration is necessary to show the results are complementary rather than inconsistent. The differences observed do show us the half-filled $d_{x^2-y^2}$ of Cu(II) is very close in energy to the lowest empty degenerate porphyrin π^* levels as predicted by Zerner and Gouterman[66].

Both copper complexes exhibit two oxidative redox couples at potentials slightly anodic to those of their zinc counterparts. As for the first reduction, the ESR signal of the copper porphyrins disappears during the one electron oxidation of these complexes. More interestingly the second oxidation of both porphyrins gives rise to a very broad anisotropic signal similar to that displayed by the parent neutral porphyrins-

	g factor*	ΔH/G
$(Cu(II)\ TPP)^{2+}$	2.2	220
$(Cu(II)\ OEP)^{2+}$	2.18	200

* at 250K

This is clear evidence that the doubly oxidised copper porphyrins have Cu(II) at their centre with both electrons having

been removed from the porphyrin moiety. This is not conclusive evidence however that the one electron oxidation product exists as (Cu(II) $Por^{+\cdot}$)$^{+}$. Optical absorption measurements though, confirm that this is indeed the case. Both (Cu(II) $TPP^{+\cdot}$)$^{+}$ and (Cu(II) $OEP^{+\cdot}$)$^{+}$ are green and display broad absorptions in the visible region and a blue-shifted Soret band of lower intensity to that of the parent neutral porphyrin. These spectra are temperature independent (20° to - 150°C). As for the first oxidation, the second oxidation of both copper complexes is fully reversible at room temperature. The spectrum obtained for Cu(II) TPP^{2+} is shown in Figure 17 and is typical of a porphyrin π dication spectrum, consistent with the ESR results. (Cu(II) OEP^{2+})$^{2+}$ also exhibits an optical spectrum which is assigned as a porphyrin π -dication. All spectral data for the anodic behaviour of the copper porphyrins are listed in Table 9.

The anodic behaviour of the silver porphyrins is quite different from that of the copper porphyrins. The presence of three one-electron oxidations for Ag(II) TPP and Ag(II) OEP immediately suggests the occurrence of a metal-based redox process as, has been previously described, only two electrons can be removed from the porphinato ligand. Both Ag(II) TPP and Ag(II) OEP are easier to oxidise than the corresponding copper complexes and $E_{\frac{1}{2}}$(1st ox) values for Ag(II) TPP and Ag(II) OEP are within 20mV of each other (cf. Cu(II) OEP is

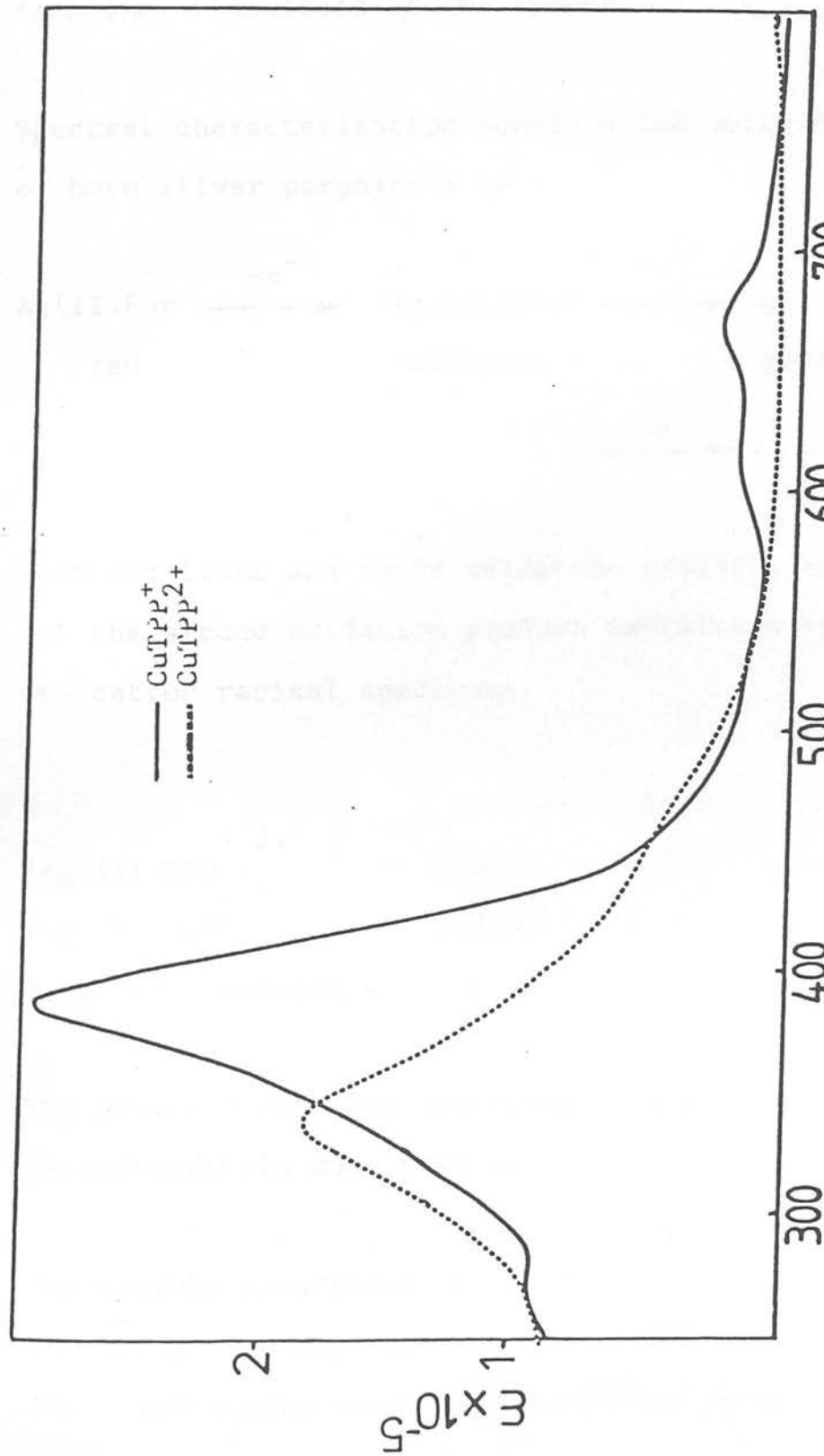

Figure 3.17 Optical absorption spectra of the anodic products of CuTPP

easier to oxidise than Cu(II) TPP by 190mV). The two subsequent oxidations of AgTPP and AgOEP have the voltammetric pattern expected for the stepwise removal of two electrons from the π manifold of the ligand.

Spectral characterisation confirms the voltammetric behaviour of both silver porphyrins as

$$\underset{\text{red}}{Ag(II)Por} \xrightarrow{-e^-} \underset{\text{red/brown}}{(Ag(III)Por)^+} \xrightarrow{-e^-} \underset{\text{green}}{(Ag(III)Por^{\cdot})^{+\,2+}} \xrightarrow{-e^-} \underset{\text{brown}}{(Ag(III)Por^{2+})^{3+}}$$

Both the first and third oxidation products are ESR silent but the second oxidation product exhibits a typical isotropic π - cation radical spectrum-

	g factor*	ΔH/G	a_N
$(Ag(III)TPP^{\cdot})^{+\,2+}$	2.0032	6	1.40
$(Ag(III)OEP^{\cdot})^{+\,2+}$	2.0030	7	1.45

* spectra measured at 200K

The observed nitrogen splitting is significant in that both cation radicals must have an $^2A_{2u}$ ground state.

The visible absorption spectrum of $(Ag(III)\ OEP)^+$ is similar to that previously reported by Kadish[48], and is shown in Figure 18. Isosbestic points during oxidation are noted at 560,

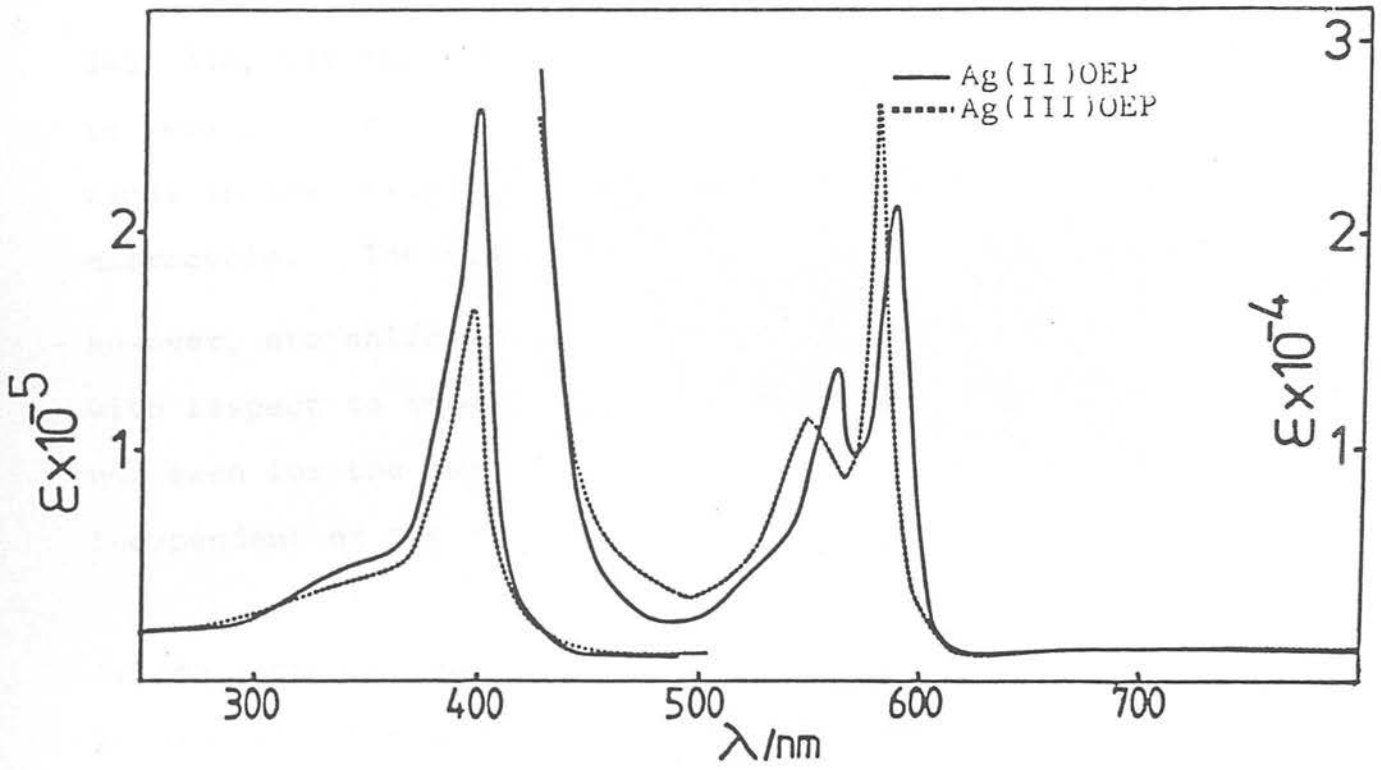

Figure 3.18 The one-electron oxidation of Ag(II)OEP in CH_2Cl_2/0.5M $TBABF_4$ (20°C)

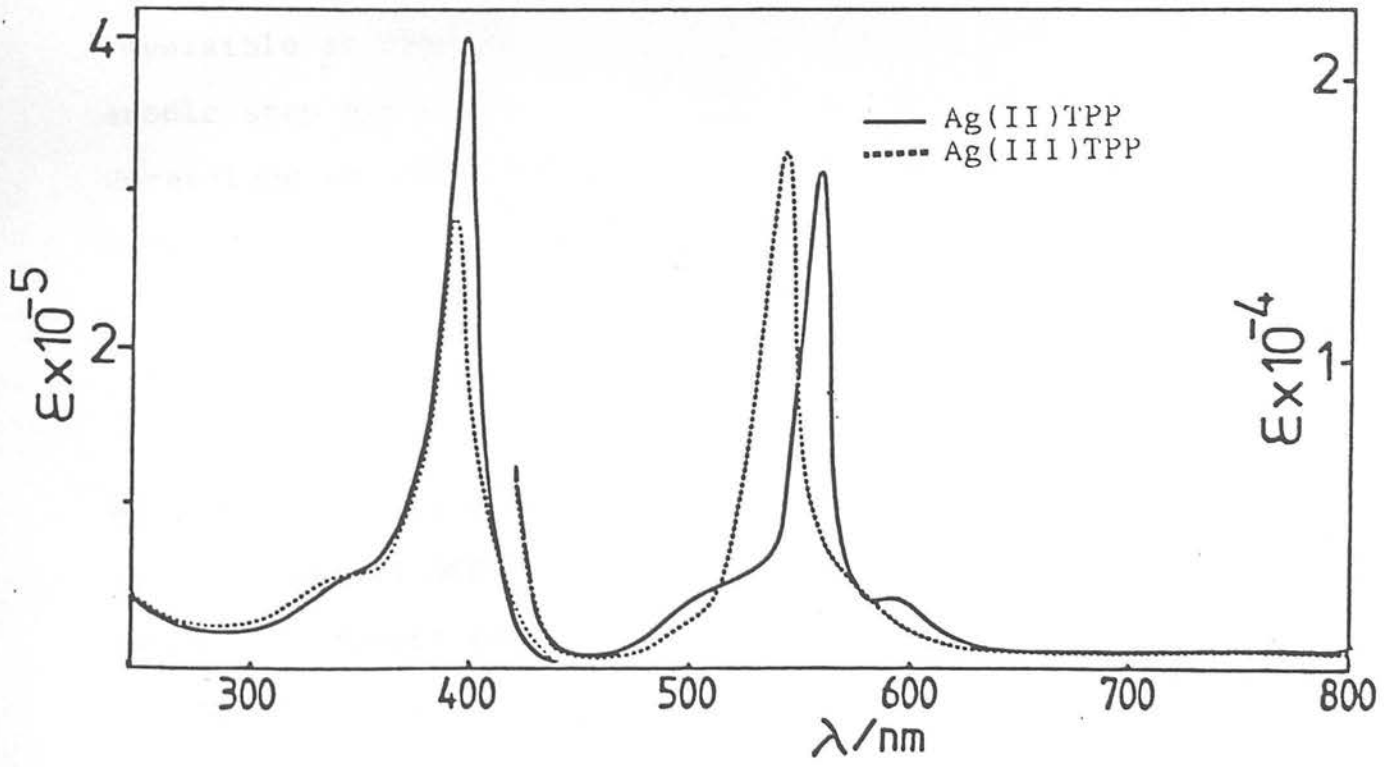

Figure 3.19 The one-electron oxidation of Ag(II)TPP in CH_2Cl_2/0.5M $TBABF_4$ (20°C)

545, 520, 425 and 360nm. The final spectrum of $(Ag(III)OEP)^+$ is very similar to that of the parent Ag(II) OEP, with 2 sharp bands in the visible region typical of a neutral porphyrin macrocycle. The visible bands displayed by $(Ag(III)\ OEP)^+$ however, are shifted to the blue by approximately $300cm^{-1}$ with respect to those of Ag(II) OEP. This blue shift is not seen for the Soret transition, the energy of which seems independent of the oxidation state of the central metal.

As the second oxidation proceeds, isosbestic points are noted at 575, 490, 420 and 380nm. The final spectrum shows broad visible bands and a blue shifted and broadened Soret band. This is shown to be a fully reversible redox step by the full recovery of $(Ag(III)\ OEP)^+$ on reversing the potential to an appropriate value. Likewise the third oxidation is also reversible at room temperature. The product of this final anodic step has a featureless visible spectrum with only an unresolved shoulder of 420nm and a Soret transition of much reduced intensity at 360nm. The second and third oxidation products of Ag(II) OEP then display typical π -cation and π dication optical properties.

Ag(II) TPP displays entirely similar optical changes in oxidation to Ag(II) OEP. Isosbestic points throughout the first oxidation process are noted at 572, 550, 520, 428 and 360nm, and Ag(II) TPP is fully regenerated when the potential is

reversed. Again a blue shift of the visible bands occurs on oxidation and a much smaller blue shift of the Soret also results (Figure 19).

The second oxidation results in collapse of the two sharp visible bands and the simultaneous growth of broad absorptions to lower energy. The third oxidation product of Ag(II) TPP is only stable at temperatures below -20°C. However at these lower temperatures Ag(II) TPP is recovered in its original concentration stepwise through the π cation radical and Ag(III) TPP. The final spectrum is typical of that displayed by a porphyrin π dication. A summary of the spectral data for the silver porphyrins appears in Table 10.

The d^9 metalloporphyrins are a very good example of how the central metal can grossly affect the redox chemistry of porphinato complexes. Whereas Cu(II) porphyrins display only macrocycle-based electron-transfer processes, primary reduction and primary oxidation of silver porphyrins occurs at the metal centre giving rise to Ag(I) and Ag(III) porphyrins respectively, thus delaying oxidation and reduction of the macrocycle to more extreme potentials.

Table 3.8 Spectral data for the cathodic products of CuTPP and CuOEP

	Wavelength maxima, nm (extinction coefficient x 10^{-3})
CuTPP	581(21.2), 410(420)
$CuTPP^-$	900(7.2), 806(3.4), 800-600 broad absorption, 451(96.2), 410(196)
$CuTPP^{2-}$	604(22.4), 560(14.0), 409 (152)
CuOEP	560(25.4), 522(13.1), 399 (300)
$CuOEP^-$	874(2.9), broad absorption 850-600, 429(102), 400(142)
$CuOEP^{2-}$	582(24.6), 557(15.4), 398(100.1)

Table 3.9 Spectra data for the anodic products of CuTPP and CuOEP

	Wavelength maxima, nm (extinction coefficient x 10^{-3})
$CuOEP^+$	620(4.6), 563(5.2), 512(5.0), 476(3.2), 382(99.9)
$CuOEP^{2+}$	495(14.0), 361(41.2)
$CuTPP^+$	810(1.4), 671(4.5), 600(6.2), 554(4.1), 400(190)
$CuTPP^{2+}$	480(10.1), 381(101)

Table 3.10 Spectral data for the oxidation products of AgOEP and AgTPP

	Wavelength maxima, nm (extinction coefficient x 10^{-3})
AgTPP	600(2.4), 564(17.6), 405(399)
$AgTPP^+$	552(18.1), 403(286)
$AgTPP^{2+}$	650-500 broad absorption, 400(111.1)
$AgTPP^{3+}$	498(10.0), 372(51.6)
AgOEP	584(21.6), 547(13.2), 398(249)
$AgOEP^+$	573(26.8), 537(11.3), 398(154)
$AgOEP^{2+}$	610(3.2), broad absorption 600-500, 385(94)
$AgOEP^{3+}$	490(5.6), 352(41.0)

3.4 THE d^8 METALLOPORPHYRINS

The electrooxidation and electroreduction of Ni(II) TPP has been the subject of several publications over the last 16 years. Wolberg and Manassen[32,67] first reported that Ni(II) TPP gave two closely overlapping one-electron oxidation steps in benzonitrile. The first of these steps was characterised by ESR as producing $(Ni(III)\ TPP)^{+}$ which gradually decayed via internal electron-transfer ($t_{\frac{1}{2}}$ - 45 min) to yield $(Ni(II)\ TPP^{\cdot})^{+}$. The product of the second oxidation was assigned as the cation radical $(Ni(III)\ TPP^{\cdot})^{2+}$. This assignment was based largely on a plot of Fe(II), Co(II), Ni(II), Cu(II) and Zn(II) porphyrin oxidation potentials vs. the third ionisation potential of each metal. Dolphin et al.[68] later reinvestigated this oxidation in CH_2Cl_2. In this study the initial one-electron anodic product was formulated by room temperature ESR as the π cation radical $(Ni(II)\ TPP^{\cdot})^{+}$. However when this green solution was frozen an internal electron-transfer occurred to produce an orange-red solid of $(Ni(III)\ TPP)^{+}$. This assignment was supported by a 77K anisotropic ESR spectrum with $g_{\perp} = 2.286$ and $g_{\parallel} = 2.086$. Further electrolysis of $(Ni(II)\ TPP^{\cdot})^{+}$ at a potential anodic of the second oxidation wave was reported to generate a brown solution which gave no ESR signal. Kadish and Morrison[69] reported half-wave potentials for the first oxidation and first reduction of a series of Ni(II) (p-X) TPP complexes in CH_2Cl_2. Similar to the earlier results, Ni(II) TPP gave two closely spaced oxidation waves by cyclic

voltammetry. As might be expected, these potentials were dependent on the nature of the substituent on the phenyl rings. The magnitude of the substituent effect was not equal for the two oxidations. Consequently, complexes containing electron-withdrawing substituents (such as $-COOCH_3$ or $-NO_2$) gave a single two electron transfer process, while those with electron-donating groups (such as $-CH_3$ or $-OCH_3$) had negatively shifted potentials such that two, well separated single electron oxidation processes were obtained. Based in large part on the substituent effects of the two electrode-processes, the room temperature mechanism was assigned as an initial oxidation to yield $(Ni(II)(p\text{-}X)\ TPP^{+\cdot})^{+}$, followed by further oxidation to yield $(Ni(III)(p\text{-}X)\ TPP^{+\cdot})^{2+}$.

Fuhrhop and Mauzerall[47] reported oxidation of Ni(II) OEP, by ferric perchlorate, provided a singly oxidised complex, the optical spectrum and g value of which were compatible with ring oxidation. A later electrochemical study showed Ni(II) OEP to undergo a reversible one-electron oxidation and a reversible one-electron reduction. From the $E_{\frac{1}{2}}$ values both redox couples were assigned as macrocycle-based electron-transfer steps.

Far less work has been done on the characterisation of the electrode products of Pd(II) and Pt(II) porphyrins and indeed the second and third row transition metal porphyrins in general. Fuhrhop reported Pd(II) OEP[47] to undergo a one-electron oxidation on treatment with ferric perchlorate in $CHCl_3/CH_3OH$.

An isotropic ESR signal, g = 1.9991 at -50°C, characterised this product as $(Pd(II)\ OEP^{+\cdot})^{+}$. The electrochemistry of Pd(II) TPP and Pt(II) TPP in CH_2Cl_2 has been briefly reported by Bard et al[70]. Their interest in these compounds arose primarily from the potential of these compounds as chemiluminescent agents. Two reversible oxidations and one reversible reduction were noted for Pd(II) TPP. Pt(II) TPP, however, exhibited quite different behaviour. Cyclic voltammetry showed Pt(II) TPP to undergo three oxidations and four reductions (occurring between -1.46 and -1.95 volts vs SCE reference). This is <u>not</u> the expected redox behaviour for a metalloporphyrin with a redox inert metal centre. The reported cathodic electrochemistry, in particular, suggests an impurity is present in solution. As coulometric experiments were not undertaken and no characterisation of the electrode products attempted it is impossible to comment on the validity of the electrochemical results presented.

In this study we were interested in the redox potentials of the $3d^8$, $4d^8$ and $5d^8$ metalloporphyrins to establish the importance of $d\pi - \pi^*$ back-bonding contributions to the redox behaviour of porphinato complexes. Full characterisation of the generated electrode-products should also help to settle the apparent controversy in the literature regarding the site of electron abstraction and electron addition in these complexes. The complete redox behaviour of Ni(II), Pd(II) and

Pt(II) complexes of both OEP and TPP is reported here. At room temperature all electron transfers were found to occur at the macrocycle, with only one exception. The initial oxidation site of Pt(II) TPP is surprisingly found to be at the metal centre giving rise to the unusual oxidation state Pt(III).

The anodic electrochemistry of the d^8 metallooctaethylporphyrins, as measured in CH_2Cl_2/0.5M $TBABF_4$, is summarised below.

	$E_{\frac{1}{2}}$(1st ox)/V*	$E_{\frac{1}{2}}$(2nd ox)/V	ΔE
NiOEP	0.56	1.08	0.52
PdOEP	0.63	1.31	0.68
PtOEP	0.68	1.40	0.72

* Volts vs Ag/AgCl reference

Stirred voltammetry and controlled-potential coulometry showed each oxidation to be a one electron step. The order of the $E_{\frac{1}{2}}$ (1st ox) values is as expected if all electron transfers are macrocycle based (i.e. the metalloporphyrin is harder to oxidise the more electronegative the central metal is). Exhaustive electrolysis at potentials anodic of the first oxidation wave at room temperature produced similar green/red solutions for all three metalloporphyrins with similar narrow, uncoupled, isotropic ESR signals at 250K, again indic-

ating oxidation of the macrocycle in all three cases.

	g value	$\Delta H/G$
$(NiOEP)^{+}$	2.0040	8.0
$(PdOEP)^{+}$	2.0048	8.5
$(PtOEP)^{+}$	2.0021	9.0

At temperatures below 160K the ESR signal for the oxidised product of Pt(II) OEP, although remaining isotropic exhibits a degree of hyperfine splitting. This is not present for the oxidation product of Ni(II) OEP or Pd(II) OEP, both of which exhibit singlet spectra at similar temperatures. The measured coupling constant of 6.0G for $(PtOEP^{+\cdot})^{+}$ is much larger than that normally found for ^{14}N splittings in porphyrin π cation radicals (typically 1.4 - 1.7G). We assign the hyperfine observed for $(PtOEP^{+\cdot})^{+}$ as coupling to ^{195}Pt (33.8% abundant, $I = \frac{1}{2}$), indicating some unpaired electron density has 'leaked' from the macrocycle to the metal. The hyperfine coupling constant of 6.0G however reflects only a very small electron density on the metal as the isotropic coupling constant for ^{195}Pt is 3692.6G. The fact that splitting is observed at all is indicative that considerable electron density must be present at the pyrrolic nitrogens, and $(PtOEP^{+\cdot})^{+}$ must therefore have an $^{2}A_{2u}$ ground state.

The visible optical progression during the first oxidation

of Ni(II) OEP is shown in Figure 20. The oxidation is fully reversible at room temperature and isosbestic points are maintained at 564, 504, 416 and 380nm throughout. The π -cation radical exhibits diffuse absorption throughout the visible region and three relatively intense absorptions between 620 and 500nm. An unresolved shoulder at 460nm is also present. In the uv region (Figure 21) the Soret band broadens and shifts to the blue on oxidation. Similar spectral changes accompany the oxidation of Pd(II) OEP (Figure 22) and Pt(II) OEP (Figure 23). The maintenance of isosbestic points at 558, 496, 422, 372 and 275nm for Pd(II) OEP and 548, 489, 415 and 370nm for Pt(II) OEP, and the full recovery of the parent metalloporphyrins at the appropriate potentials, show the oxidations to be reversible at room temperature. The second oxidation products of all three porphyrins are however unstable at temperatures above -30°C.

Optical characterisation of these products show them to be metalloporphyrin π dications. Blue shifts of the Soret transition occur with a simultaneous decrease in intensity. The only visible feature, in all three cases, is an unresolved shoulder in the visible, around 400nm. All anodic spectral data for Ni(II), Pd(II) and Pt(II) OEP are listed in Table 11.

The measured anodic redox potentials for the d^8 metallotetraphenylporphyrins are shown below-

Table 3.11 Spectral data for the oxidation products of NiOEP, PdOEP and PtOEP

	Wavelength maxima, nm (extinction coefficient x 10^{-3})
NiOEP	551(32.1), 515(14.2), 390(300)
$NiOEP^{+}$	570(8.2), 552(8.3), 524(9.7), 500(10.0), 386(176)
$NiOEP^{2+}$	465(14.5), 372(92.5)
PdOEP	545(30.4), 510(20.1), 392(310)
$PdOEP^{+}$	610(2.2), 572(10.1), 540(14.5), 516(13.0), 356(125)
$PdOEP^{2+}$	460(17.0), 350(78.6)
PtOEP	534(28.0), 500(18.2), 390(299)
$PtOEP^{+}$	610(3.2), 560(6.7), 520(8.2), 498(10.4), 360(129)
$PtOEP^{2+}$	460(13.5), 352(80.4)

Table 3.12 Spectral data for the oxidation products of NiTPP, PdTPP and PtTPP

	Wavelength maxima, nm (extinction coefficient x 10^{-3})
NiTPP	529(17.2), 414(210)
$NiTPP^{+}$	758(2.9), 641(11.4), 592(13.0), 524(10.0), 405(119)
$NiTPP^{2+}$	510(18.2), 336(71.2)
PdTPP	555(2.0), 524(17.1), 416(200)
$PdTPP^{+}$	741(3.1), 629(11.2), 588(10.0), 521(5.0), 405(131)
$PdTPP^{2+}$	508(20.0), 340(80.7)
PtTPP	537(6.2), 507(16.0), 402(300)
$(PtTPP)^{+}$	568(4.7), 532(1.39), 420(296)
$(PtTPP)^{2+}$	730(1.9), 640(10.0), 576(10.2), 516(11.4), 416(159)

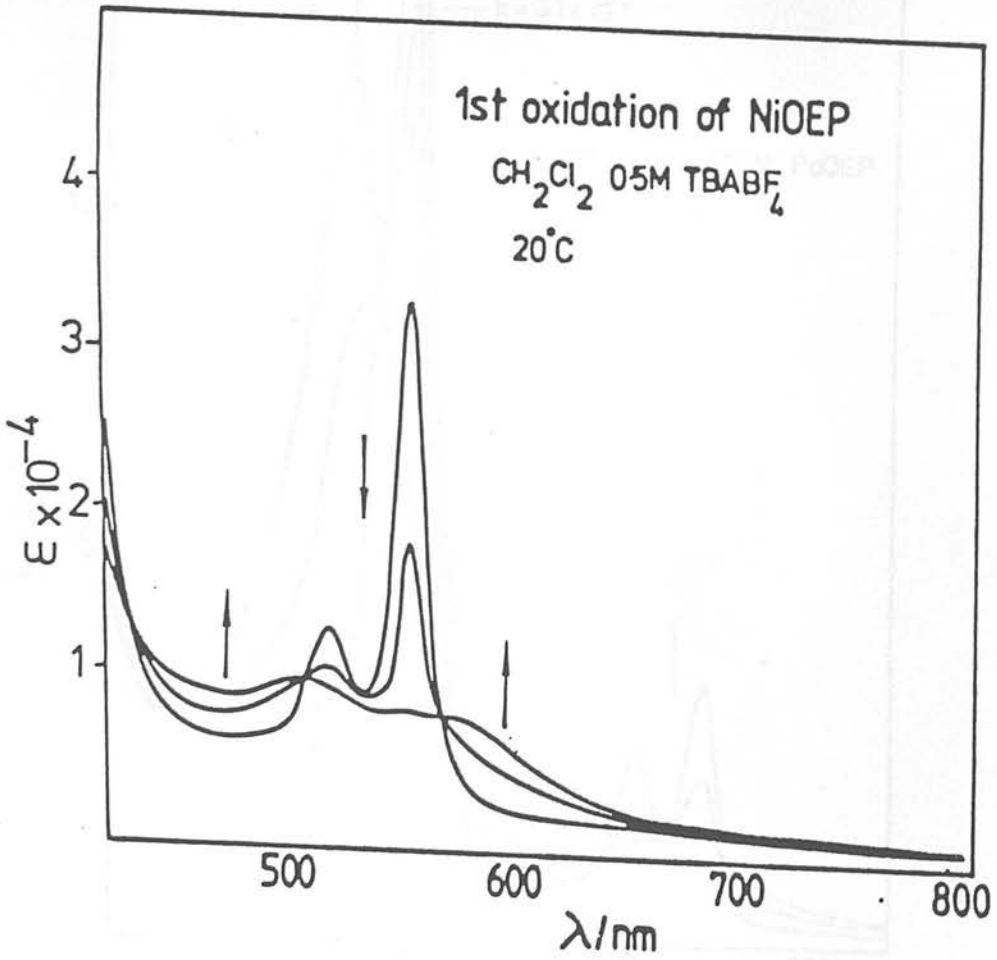

Figure 3.20 Optical progression during the first oxidation of Ni(II)OEP

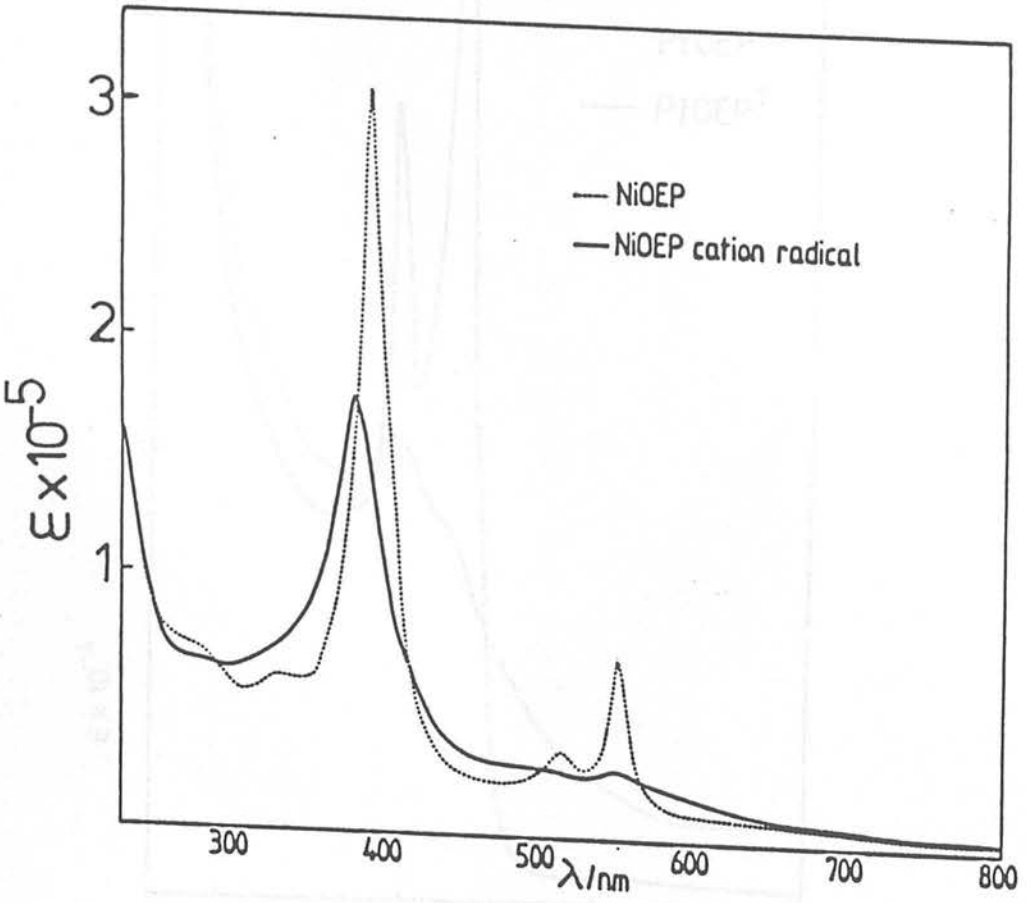

Figure 3.21 The one-electron oxidation product of Ni(II)OEP

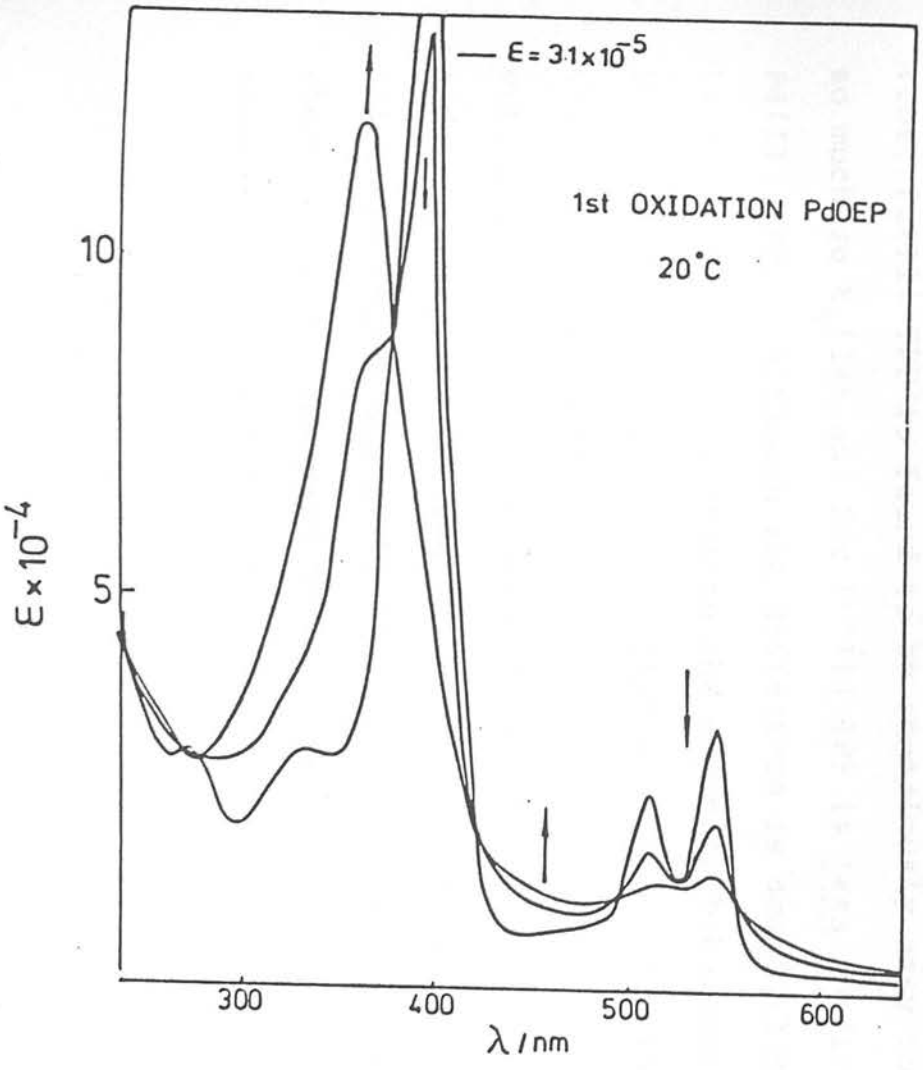

Figure 3.22 Optical progression during the first oxidation of Pd(II)OEP

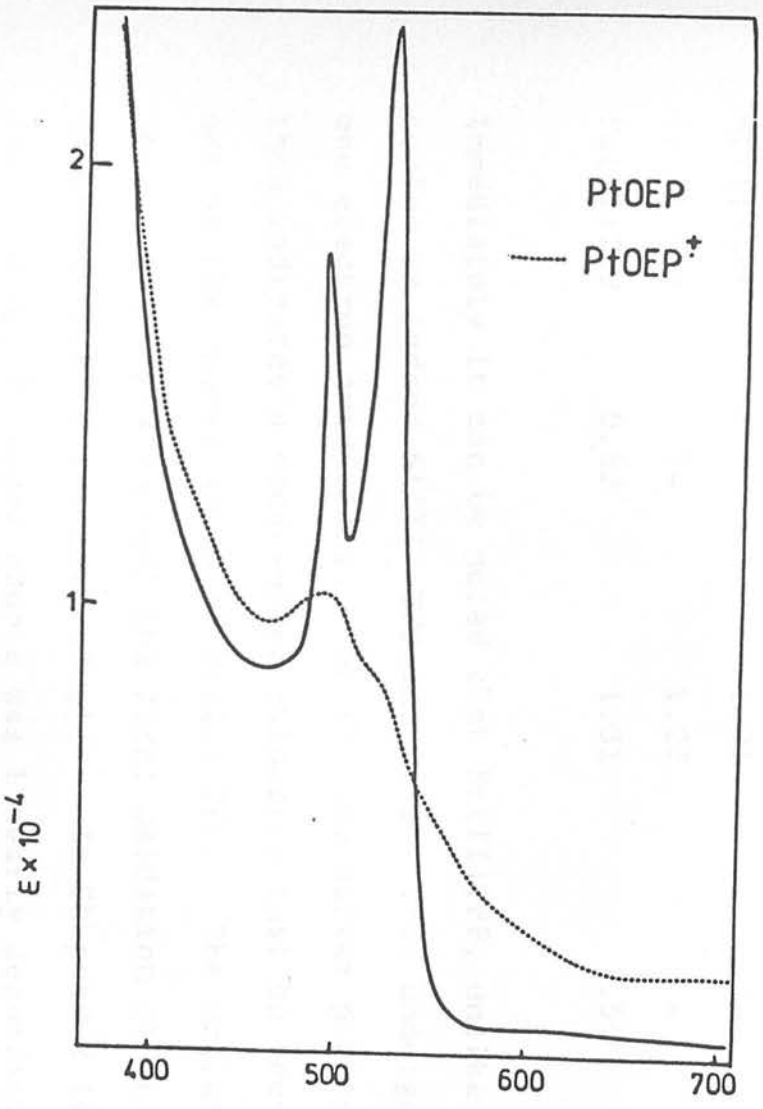

Figure 3.23 The one-electron oxidation product of Pt(II)OEP

	$E_{\frac{1}{2}}$(1st ox)/V	$E_{\frac{1}{2}}$(2nd ox)/V	$E_{\frac{1}{2}}$(3rd ox)V
Ni(II)TPP	0.77	1.01	-
Pd(II)TPP	0.84	1.27	-
Pt(II)TPP	0.82	1.31	1.54

Immediately it can be noted that Pt(II)TPP, unlike the d^8MOEP series or indeed Ni(II) TPP and Pd(II) TPP, undergoes <u>three</u> one electron oxidations. As for the silver porphyrins this then indicates a metal-based oxidation must be occurring at one of the anodic waves of Pt(II) TPP. The voltammetric results strongly suggest the first oxidation of Pt(II) TPP is not a macrocycle-based couple. In Chapter 2 it was shown that the MP/MP^{+} redox couple was linearly dependent on the elecronegativity (X) of the central metal. Whereas the first oxidation of Ni(II) TPP and Pd(II) TPP fit closely on this line, Pt(II) TPP is found to be anomalously easy to oxidise, so much so $E_{\frac{1}{2}}$(1st ox) for Pt(II) TPP is <u>less</u> anodic than for Pd(II) TPP. Although the difference is small (20mV), this is strikingly in contrast to the expected behaviour, as the Pauling electronegativity of platinum (X = 2.28) is greater than that of palladium (X = 2.20)[71]. Coulometric measurements over a sizeable concentration range (1.2×10^{-5} - 1×10^{-4}M), and complementary stirred voltammetric potential scans, showed all three oxidations of Pt(II) TPP to be reversible one electron steps, independent of concentration. Figure 24 shows the stirred d.c. voltammograms of Pt(II) TPP and its

Figure 3.24 Stirred d.c. voltammetry of the anodic products of Pt(II)TPP in CH_2Cl_2/0.5M $TBABF_4$ at -75°C

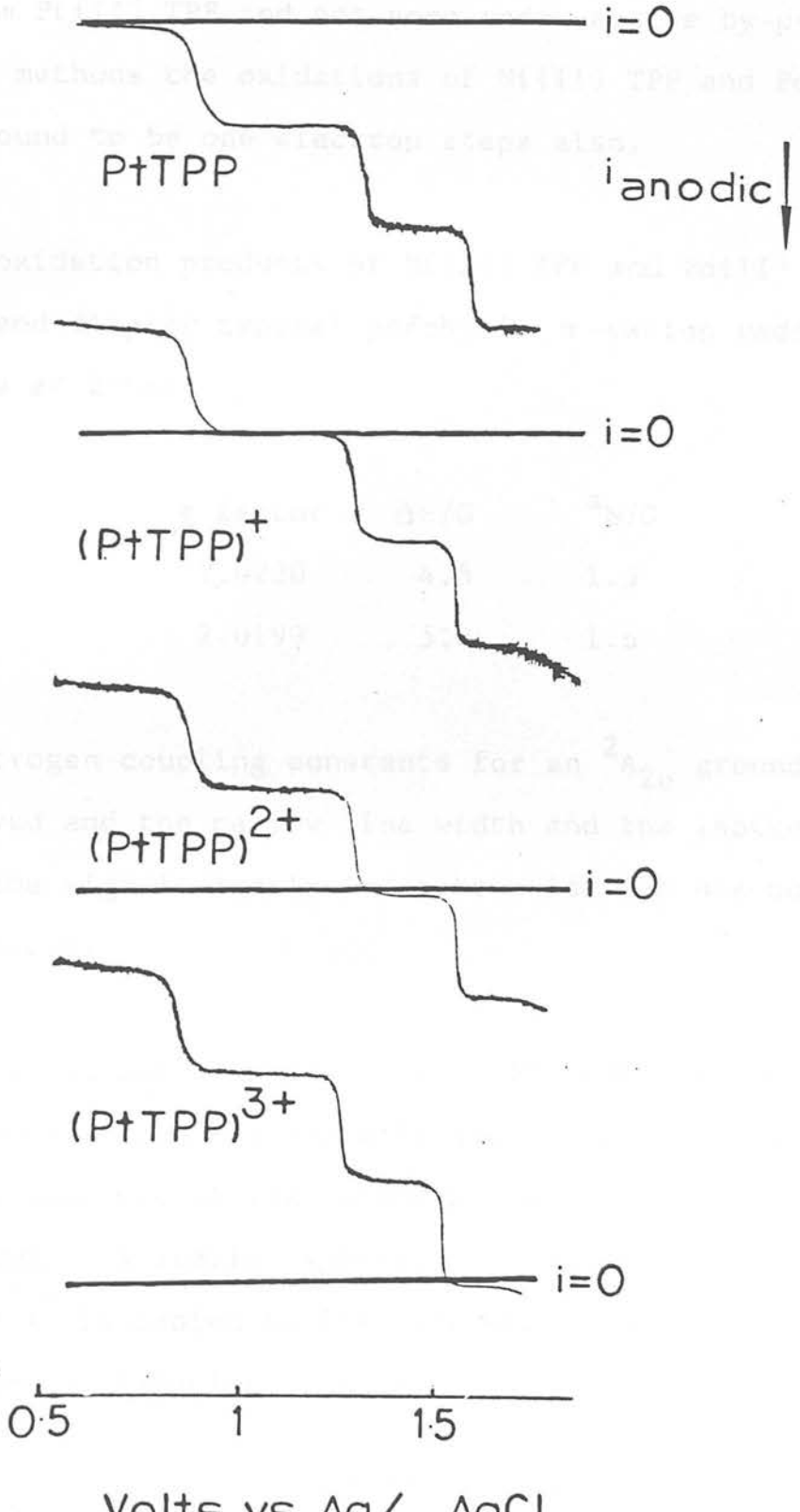

oxidation products. The highly charged third oxidation product is only stable at temperatures below -70°C. It is clear from the bulk electrogeneration results that all three waves result from Pt(II) TPP and not some redox-active by-product. By similar methods the oxidations of Ni(II) TPP and Pd(II) TPP were all found to be one electron steps also.

The first oxidation products of Ni(II) TPP and Pd(II) TPP are green and display typical porphyrin π-cation radical ESR spectra at 250K:-

	g factor	ΔH/G	^{a}N/G
$Ni(TPP^{\cdot +})^{+}$	2.0220	4.5	1.5
$Pd(TPP^{\cdot +})^{+}$	2.0199	5.0	1.6

Typical nitrogen coupling constants for an $^{2}A_{2u}$ ground state were resolved and the narrow line width and the isotropic nature of the signal clearly indicate oxidation has occurred at the macrocycle.

The red first oxidation product of Pt(II) TPP very contrastingly exhibits a much broader anisotropic signal (Figure 25) and is only observed at 77K, where $g_{\perp} = 2.0120$, $g_{\parallel} = 1.9282$ and $\Delta H = 50G$. A similar spectrum is obtained when $(Ni(II)\ TPP^{\cdot +})^{+}$ is cooled to 77K, whereupon the ESR isotropic singlet changes dramatically to an anisotropic signal ($g_{\perp} = 2.2100$

Figure 3.25 77K ESR spectra in CH_2Cl_2/0.5M $TBABF_4$ of a. $(Pd(II)TPP)^+$ and b. $(Pt(II)TPP)^+$

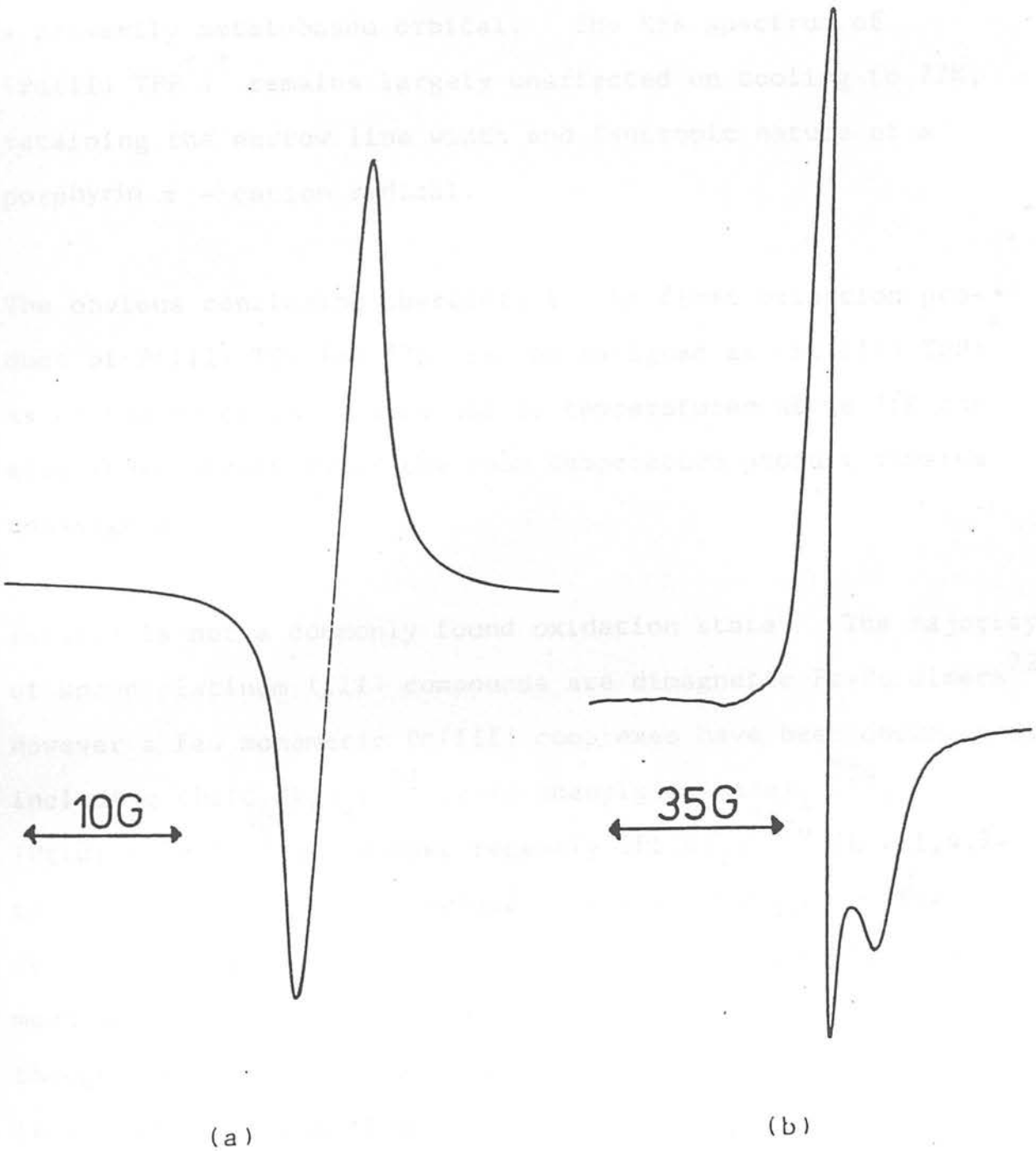

$g_{\parallel}$ = 2.0001). This is in good agreement with previous published results, where Felton[68] assigned this 77K product as $(Ni(III)\ TPP)^{+}$ where the unpaired electron is present in a primarily metal-based orbital. The ESR spectrum of $(Pd(II)\ TPP^{+\cdot})^{+}$ remains largely unaffected on cooling to 77K, retaining the narrow line width and isotropic nature of a porphyrin π - cation radical.

The obvious conclusion therefore is the first oxidation product of Pt(II) TPP (at 77K) can be assigned as $(Pt(III)\ TPP)^{+}$. As no ESR spectrum is obtained at temperatures above 77K the electronic structure of the room temperature product remains unassigned.

Pt(III) is not a commonly found oxidation state. The majority of known platinum (III) compounds are dimagnetic Pt-Pt dimers[72]. However a few monomeric Pt(III) complexes have been documented, including $(Pt(C_6Cl_5)_4)^{-}$[73] $(Pt(diphenylgloximate)_2)^{+}$[74], $(Pt(diamsar^{*}))^{3+}$[75], and most recently $(Pt(L)_2)^{3+}$[76] (L = 1,4,7-trithiacyclononane). Previously reported ESR spectra for Pt(III) are grossly similar to that reported here, displaying much the same g tensor values. A significant discrepancy though, does exist. If indeed the unpaired electron density is primarily at the Pt metal centre then coupling to ^{195}Pt should be observed. ^{195}Pt coupling constants have been

---

*diamsar = 1,8-diamino-3,6,10,13,16,19 hexa-azabicyclo (6.6.6) kosane.

observed for the pseudo-octahedral systems (Pt(III) diamsar)$^{3+}$[75] and (Pt(III)$(L)_2$)$^{3+}$ and are typically 30 - 100G. No such coupling is observed for the proposed square-planar (Pt(III)TPP) species, suggesting that considerable elecron density has been transferred, through the pyrrolic N atoms, to the porphyrin ring. This would result in a much smaller $a_{^{195}Pt}$ value. The extent of this electron transfer must be great enough at 77K to make the ^{195}Pt coupling constant unresolvable ($<$ 20G).

The further oxidation products of Pt(II) TPP and the nickel and palladium TPP complexes exhibit no ESR signal. The ESR results then indicate the initial oxidation of both Ni(II)TPP and Pd(II) TPP result in porphyrin π cation radicals. No ESR spectrum is detectable for the one electron oxidation product of Pt(II) TPP in solution and no assignment can thus be made. At 77K both $(NiTPP)^+$ and $(PtTPP)^+$ exhibit anisotropic spectra consistent with the electronic formulation of $(M(III)TPP)^+$ species. However the lack of hyperfine coupling for Pt(III) TPP indicates a considerable degree of electron density exists on the macrocycle.

Room temperature observations on the optical absorption spectra of the oxidised products clearly show that the first one-electron oxidation of the d^8 MTPP series in CH_2Cl_2 results in π cation radicals for nickel and palladium, but a metal-based oxidation for platinum giving rise to $(Pt(III)\ TPP)^+$.

The optical progress of the first oxidation of Ni(II) TPP is shown in Figure 26. Isosbestic points are noted at 544, 514, 440 and 402nm, and Ni(II) TPP is fully regenerated on returning the potential to a value immediately cathodic of $E_{\frac{1}{2}}$(1st ox). The final spectrum of the oxidised product is very similar to that displayed by $ZnTPP^{+\cdot}$, and is temperature independent (+20°C to -70°C). The second oxidation is also fully reversible at room temperature, and results in a typical porphyrin π dication specrum. Isosbestic points relating $(Ni(II)TPP^{+\cdot})^{+}$ and $(Ni(II)\ TPP)^{2+}$ are noted at 786, 540, 480 and 370nm. The optical changes (Figure 27) involve a sizeable blue shift of the Soret band (~ 4,000 cm^{-1}), collapse of the main visible bands of the π-cation radical spectrum and the continued growth of an unresolved shoulder at 500nm. Pd(II) TPP undergoes closely analogous changes to those exhibited by Ni(II) TPP. Figure 28 shows the optical changes during the Pd TPP/$Pd\ TPP^{+\cdot}$ redox couple. Again isosbestic points maintained at 540, 504, 430 and 400nm indicate the oxidation is fully reversible. The pattern of the visible bands and the small blue shift and broadening of the Soret bands characterise the product as a π-cation radical. The second oxidation product of Pd(II) TPP is very unstable at temperatures above -60°C. The lifetime of this species can however be extended at -70°C to allow optical characterisation. The resultant brown solution exhibits a typical porphyrin π-dication spectrum. The optical details of the anodic products of Pd(II) TPP and Ni(II) TPP are listed

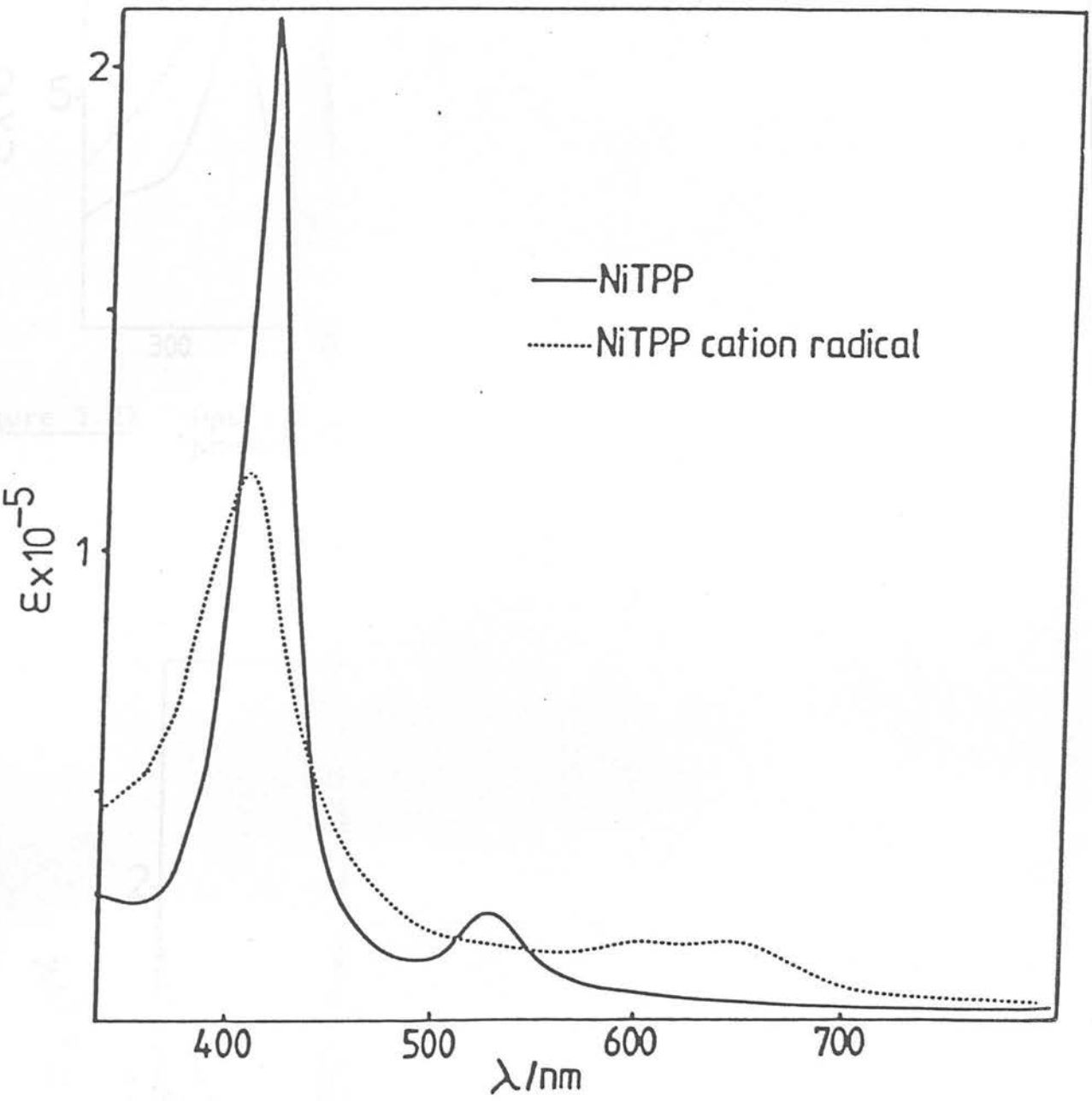

Figure 3.26 Optical absorption spectrum of the one-electron oxidation product of NiTPP

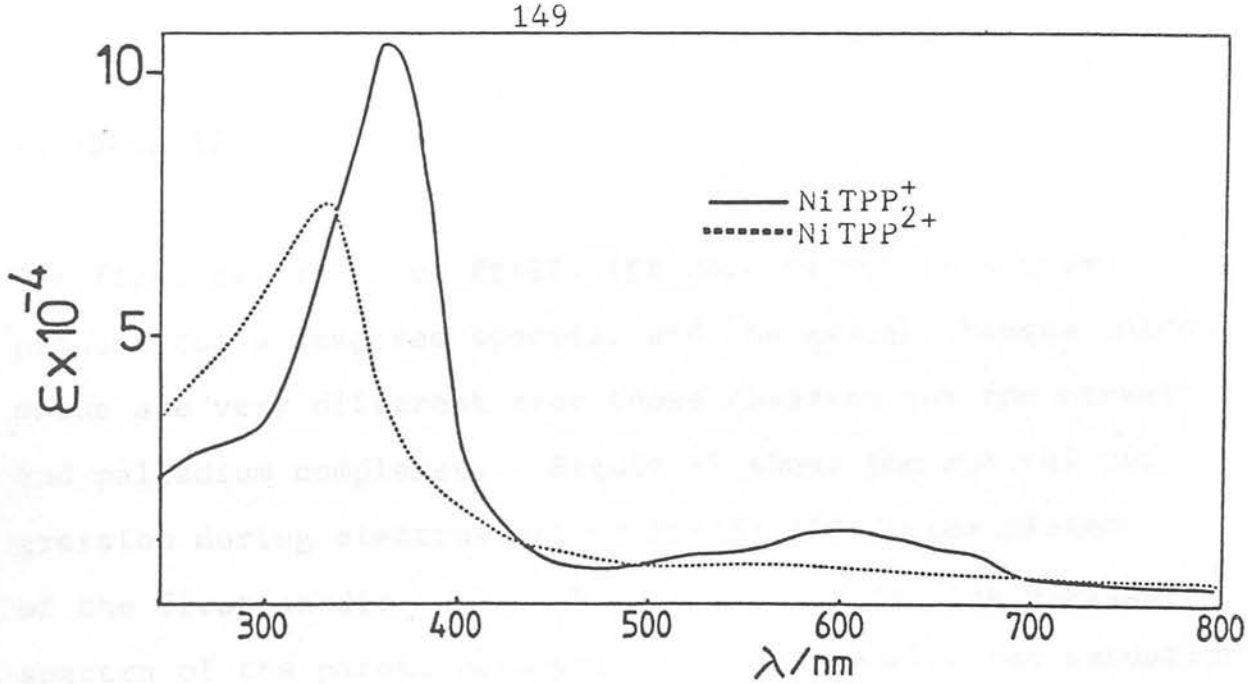

Figure 3.27 Optical absorption spectra of the anodic products of NiTPP

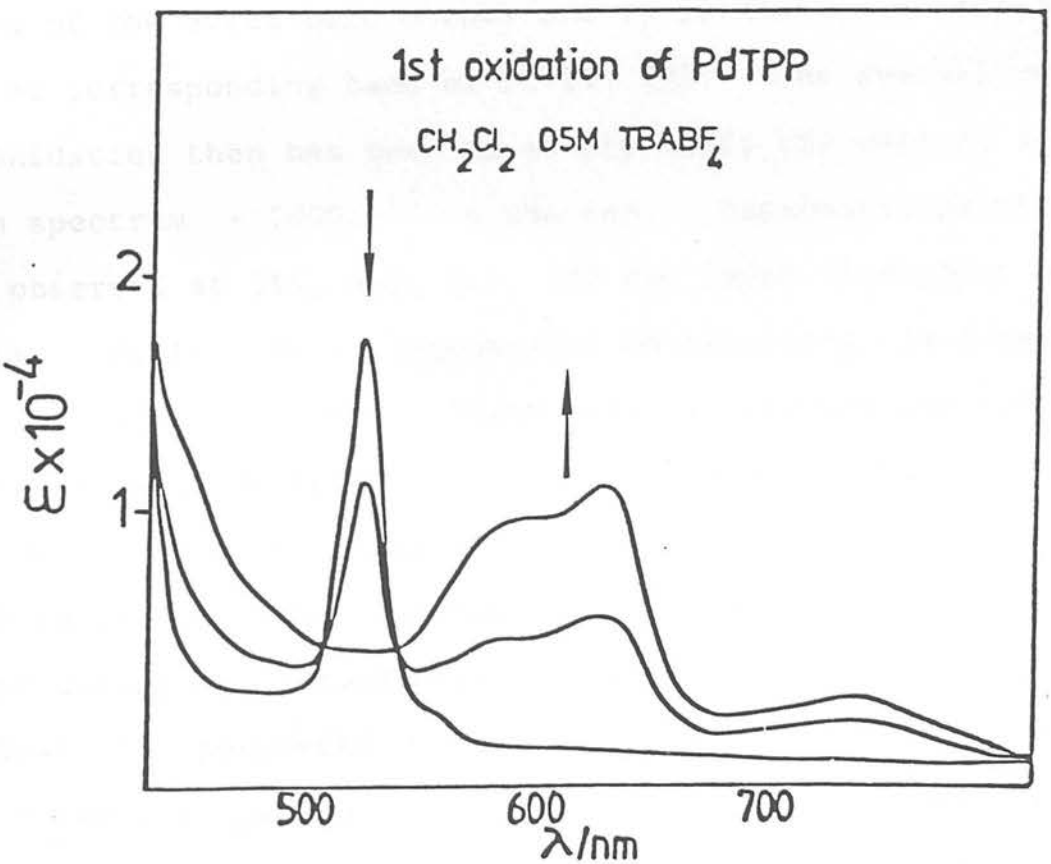

Figure 3.28 Optical progression during the one-electron oxidation of PdTPP

in Table 12.

The first oxidation of Pt(II) TPP results not in a green product but a deep red species, and the optical changes which ensue are very different from those observed for the nickel and palladium complexes. Figure 29 shows the optical progression during electrolysis of Pt(II) TPP at the plateau of the first anodic wave. Figure 30 compares the visible spectra of the parent porphyrin and the one-electron oxidation product. They are obviously very similar, with the oxidation product retaining the two-banded spectrum typical of a neutral porphyrin macrocycle. Oxidation has resulted in a red-shift of both the visible bands and the Soret transition. No broadening of the Soret band occurs and it is almost as intense as the corresponding band of Pt(II) TPP. The overall result of oxidation then has been to simply shift the optical absorption spectrum - $1000cm^{-1}$ to the red. Isosbestic points are observed at 516, 442, 410, 382 and 360nm throughout oxidation. Pt(II) TPP is regenerated on reversing the potential cathodic of $E_{\frac{1}{2}}$(1st ox). These spectral changes can only be interpreted as being the result of metal oxidation, with the π array of the porphyrin remaining intact. This assignment is given further support by the optical changes which occur during the second oxidation (Figure 31). Visible bands typical of a porphyrin π cation radical grow between 800 and 550nm accompanied by a broadening, blue shift and partial collapse of the Soret transition. These spectral changes

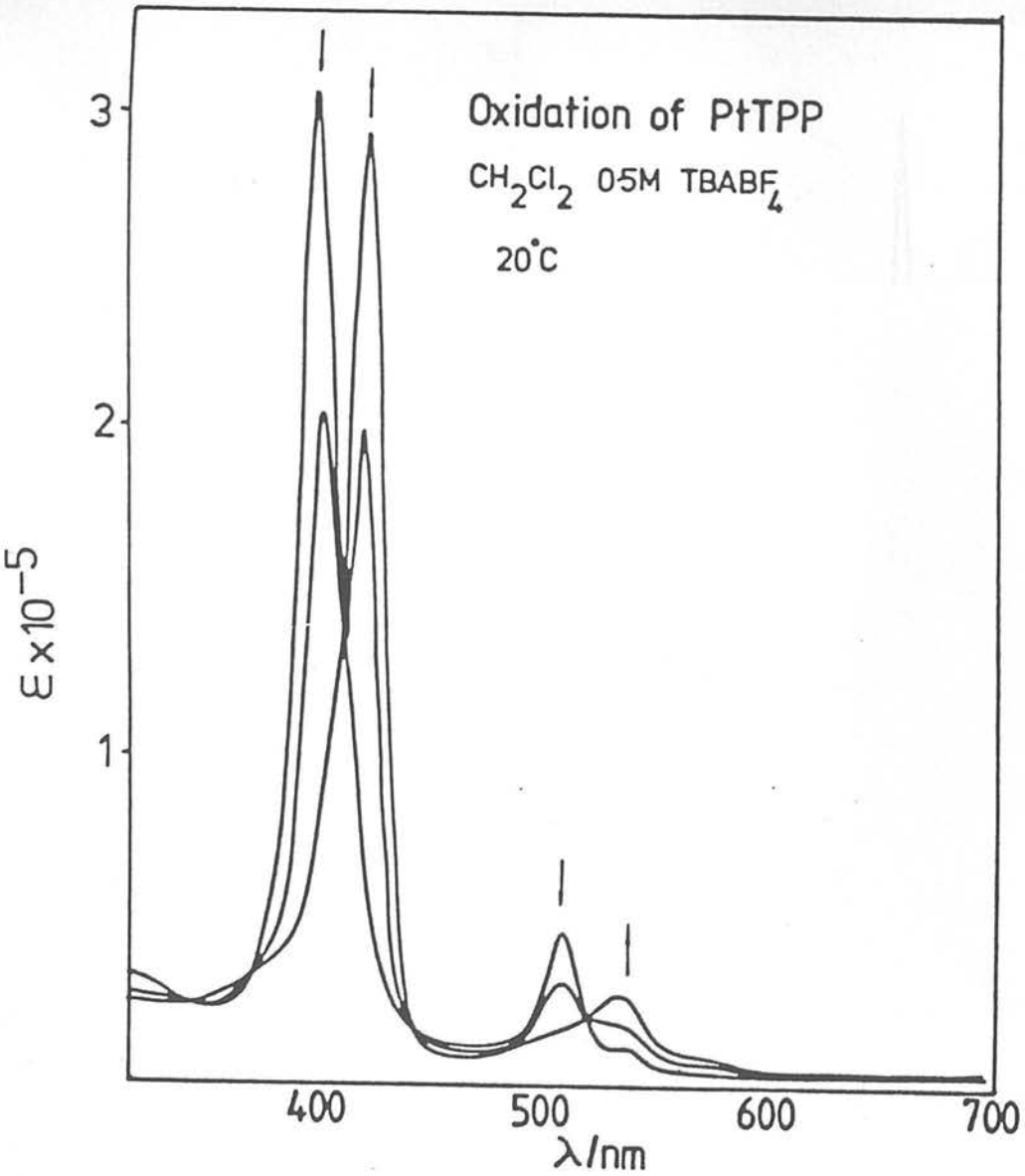

Figure 3.29 Optical progression during the first oxidation of Pt(II)TPP

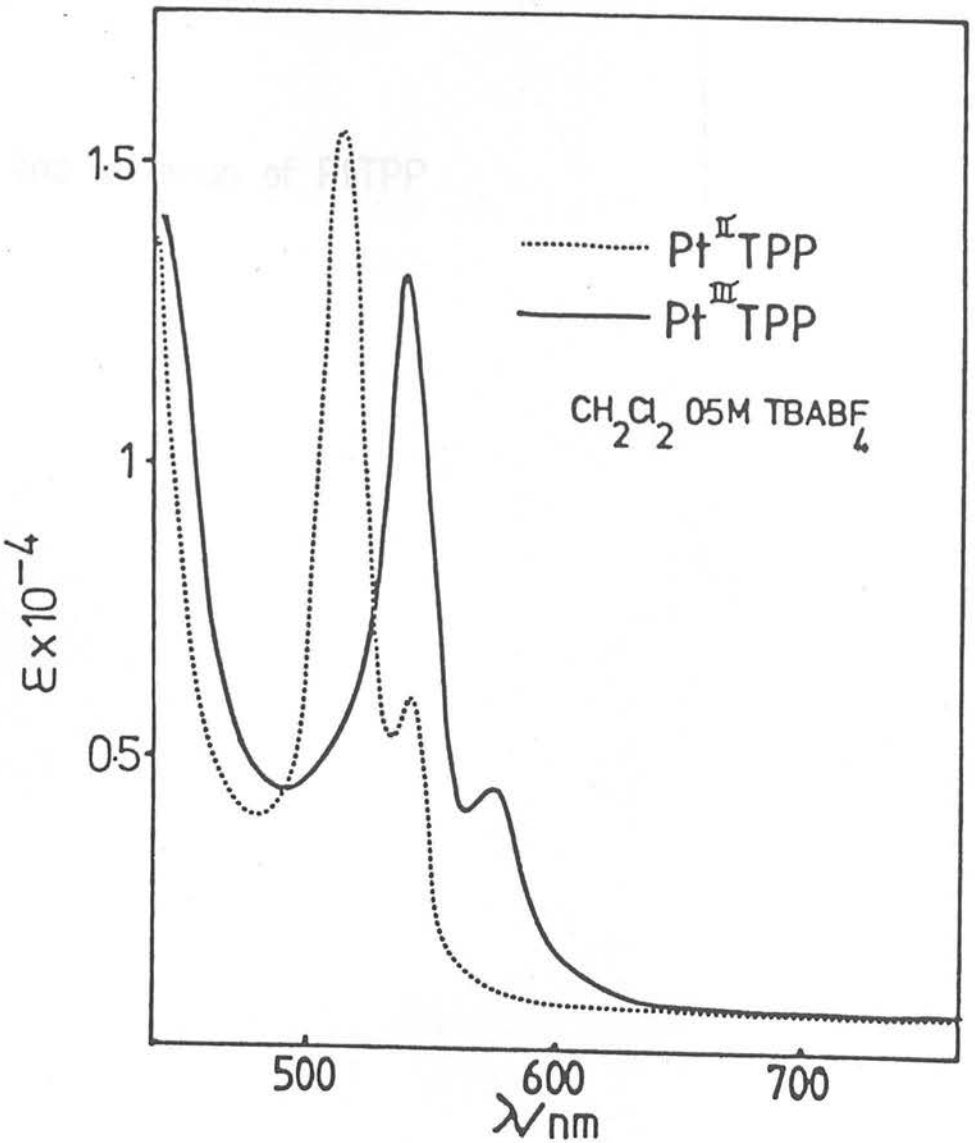

Figure 2.30 The one-electron oxidation product of Pt(II)TPP

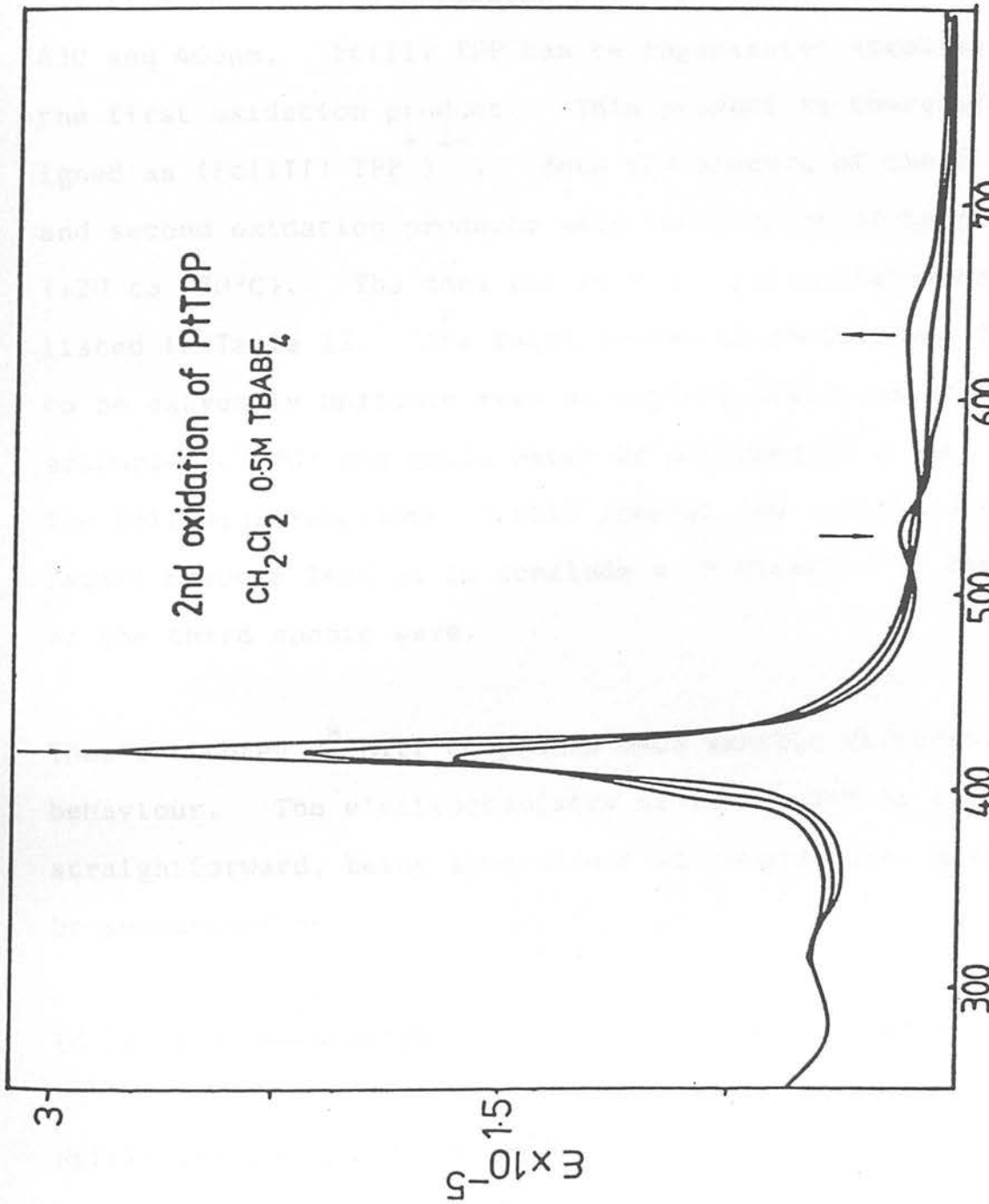

Figure 3.31 The one-electron oxidation of $(Pt(III)TPP)^+$

are all consistent with the formation of a porphyrin π cation radical at the second oxidation. Isosbestic points relating the first and second oxidation products appear at 550, 508, 430 and 406nm. Pt(II) TPP can be regenerated stepwise via the first oxidation product. This product is therefore assigned as $(Pt(III)\ TPP^{\cdot+})^{2+}$. Both the spectra of the first and second oxidation products were independent of temperature (+20 to -70°C). The data for both oxidation states are listed in Table 12. The third oxidation product was found to be extremely unstable even at experimentally extreme temperatures (-70°C) and could never be obtained in a pure state. The following reactions of this species (as will be discussed later) however lead us to conclude a π dication is formed at the third anodic wave.

Thus the three d^8 MTPP complexes each exhibit different anodic behaviour. The electrochemistry of Pd(II) TPP is the most straightforward, being independent of temperature, and can be summarised as-

$$Pd(II)\ TPP \xrightarrow{-e^-} (Pd(II)TPP^{\cdot+})^{+} \xrightarrow{-e^-} (Pd(II)\ TPP)^{2+}$$

Ni(II) TPP shows similar anodic behaviour to Pd(II) TPP at room temperature but the π-cation radical undergoes a thermally-controlled valence isomerism at 77K -

$$Ni(II)TPP \xrightarrow{-e^-} (Ni(II)\,TPP^{\cdot})^{+} \xrightarrow{-e^-} (Ni(II)\,TPP)^{2+}$$

$$(Ni(II)\,TPP^{\cdot})^{+} \xrightarrow{77K} (Ni(III)\,TPP)^{+}$$

Pt(II) TPP undergoes three one electron oxidations in CH_2Cl_2, the first being metal-based -

$$Pt(II)TPP \xrightarrow{-e^-} (Pt(III)TPP)^{+} \xrightarrow{-e^-} (Pt(III)TPP^{\cdot})^{2+}$$

$$(Pt(III)TPP)^{+} \xrightarrow{-e^-} (Pt(III)\,TPP)^{3+}$$

When the first oxidation product is cooled to 77K the ESR spectrum indicates considerable electron density has 'leaked' to the macrocycle and further temperature-dependent ESR studies are obviously required to accurately assign the electronic structure of $(PtTPP)^+$ at low temperatures.

When in solution however we confidently assign the oxidation site as a metal-based orbital. This is supported by the shift of $E_{\frac{1}{2}}(ox)$ of Pt(II) TPP in coordinating media. The redox potentials of Pt(II) TPP in acetonitrile and pyridine are shown below-

Solvent	$E_{\frac{1}{2}}$(1st ox)/V*	$E_{\frac{1}{2}}$(2nd ox)/V	$E_{\frac{1}{2}}$(3rd ox)/V
CH_2Cl_2	0.82	1.31	1.54
CH_3CN	0.75	1.30	1.52
pyridine	0.60	1.28	1.51

*volts vs Ag/AgCl reference, fully corrected for liquid junction potentials

It is noted the first oxidation shifts significantly to more cathodic values in coordinating media. While the qualitative shift of the second and third oxidations is similar, it is quantitatively much smaller. The electrochemistry of Pd(II)TPP similarly show only minimal shifts in coordinating solvents (< 30mV). The sizeable cathodic shift of the first oxidation of Pt(II) TPP is consistent with the stabilisation of the larger positive charge on the metal (Pt(III)), being stabilised by σ-donor solvents.

Further corroborative evidence for this assignment comes from the chemiluminescence study on Pd(II) TPP and Pt(II) TPP by Bard et al[70]. They found for Pd(II) TPP that when one cycled the potential between the first anodic and first cathodic waves, electrogenerated chemiluminescence (ECL) was observed. This they assigned as arising from the electron-transfer reaction-

$$PdTPP^{+} + PdTPP^{-} \longrightarrow PdTPP^{*} + PdTPP$$

The close agreement in the emitted frequency of the ECL excited state (PdTPP*) to that found in an earlier photo-excitation study by Gouterman[77] prompts assigning the ECL spectrum to be from the triplet state to the highest occupied π orbital of the porphyrin-

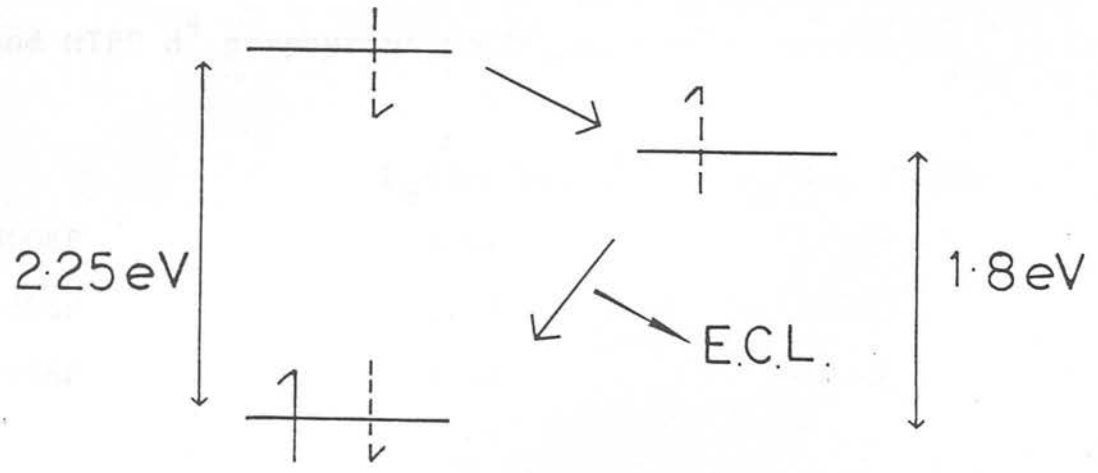

For these macrocyclic complexes to exhibit ECL then, a hole is required in the π core of the ligand. Interestingly when the potential was cycled between the first anodic and first cathodic wave for Pt(II) TPP no ECL was observed. It was not until the anodic limit is increased to encompass the second anodic wave that an ECL spectrum appeared. Although Bard did not comment on this, it implies that not until the second oxidation of Pt(II) TPP does the necessary hole appear in the π manifold allowing ECL to occur. It is thus indicative that the first oxidation of Pt(II) TPP occurs at a primarily metal-based orbital.

The anodic data shows that for the d^8 MTPP series the d_z2 orbital is very close in energy to the occupied a_{2u} orbital of the porphyrin ligand and thus oxidation can occur either at the metal or the macrocycle. All cathodic redox processes for the d^8 metalloporphyrins are however found to occur at the porphyrin moiety. The voltammetric data for the MOEP and MTPP d^8 porphyrins in CH_2Cl_2 are shown below-

	$E_{\frac{1}{2}}$(1st red)/V*	$E_{\frac{1}{2}}$(2nd red)/V
NiOEP	-1.68	-2.38
PdOEP	-1.75	-2.40
PtOEP	-1.78	-2.44
NiTPP	-1.49	-2.06
PdTPP	-1.54	-1.98
PtTPP	-1.56	-2.04

*Volts vs Ag/AgCl reference electrode

All waves were shown to be one electron steps either by coulometry or comparative stirred voltammetry. The second reduction of both Pt(II) OEP and Pd(II) OEP was found to be reversible only at extreme experimental conditions i.e. rapid scan rate ($5Vs^{-1}$) and very low temperatures ($< -60°C$).

The first reduction products of all six metalloporphyrins are stable and readily characterised spectrally. The ESR

results for these green species are listed below in Table 13-

Table 13: ESR data for the d^8 metalloporphyrin π anion radicals at 250K (in CH_2Cl_2)

	g factor	ΔH/G
$(NiOEP)^{\cdot-}$	2.0040	8.0
$(PdOEP)^{\cdot-}$	2.0002	5.5
$(PtOEP)^{\cdot-}$	2.0010	7.5
$(NiTPP)^{\cdot-}$	2.0032	11.5
$(PdTPP)^{\cdot-}$	2.0061	9.5
$(PtTPP)^{\cdot-}$	2.0045	10.0

The ESR spectra are largely independent of temperature, having only slightly narrower line widths at 77K. No hyperfine structure is observed for any of the cathodic products. The second reduction products of the MTPP series are blue and ESR silent. The doubly reduced products are all very unstable and have limited lifetimes even at -60°C. $(Ni(II)OEP)^{2-}$, $(Pd(II)\ OEP)^{2-}$ and $(Pt(II)\ OEP)^{2-}$ are not isolable in solution, rapidly protonating to give green by-products, the identity of which will be discussed later. This protonation is common to all doubly reduced species and is indicative of initial formation of a π dianion.

Optical characterisation of the electrode products confirms

that all electron-transfer processes occur at the porphinato moiety leaving the metal centre in the divalent state throughout. The monoanion π radicals of all six metalloporphyrins exhibit similar electronic spectra. The data are listed in Table 14. The spectral progression during reduction of Pd(II) TPP is shown in Figure 32. The final spectra are qualitatively similar to those exhibited by the zinc porphyrin π anion radicals.

Figure 33 shows the second reduction of Ni(II) TPP. The doubly-reduced products $(Ni(II)\ TPP)^{2-}$, $(Pd(II)\ TPP)^{2-}$ and $(Pt(II)\ TPP)^{2-}$ are stable at -60°C and are reversible through the π anion radical back to the neutral porphyrin. Table 14 also lists the available optical data for the π dianions.

The cathodic behaviour of the d^8 metalloporphyrins is thus straightforward and temperature independent with no evidence for Ni(I), Pd(I) or Pt(I).

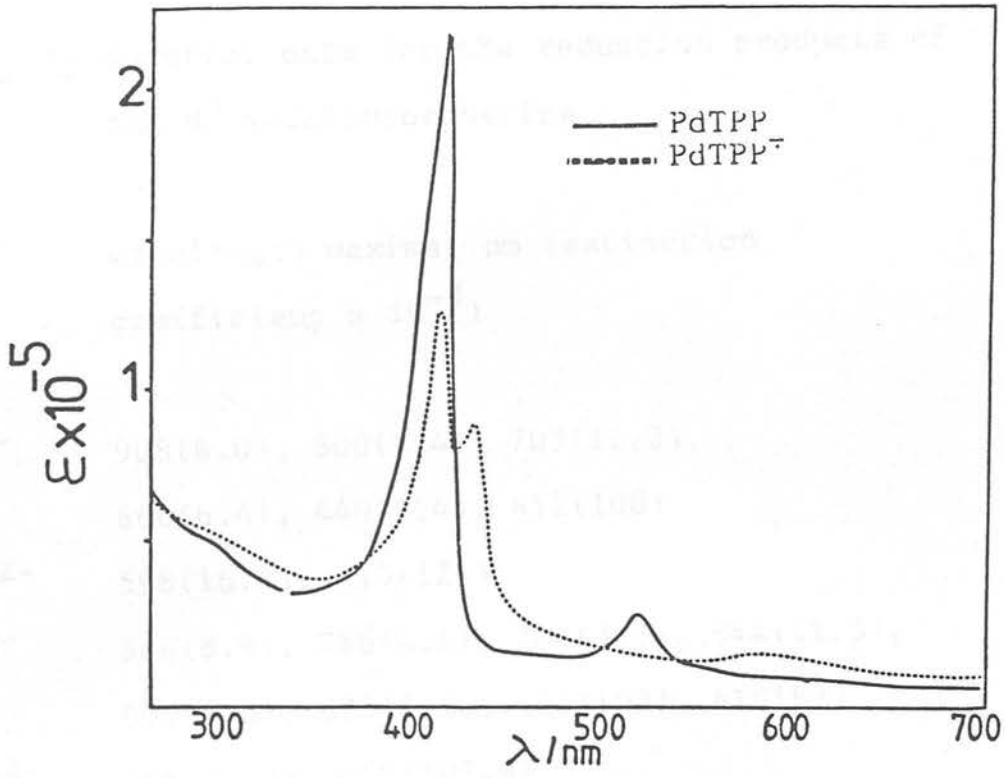

Figure 3.32 Optical absorption spectrum of the one-electron reduction product of PdTPP

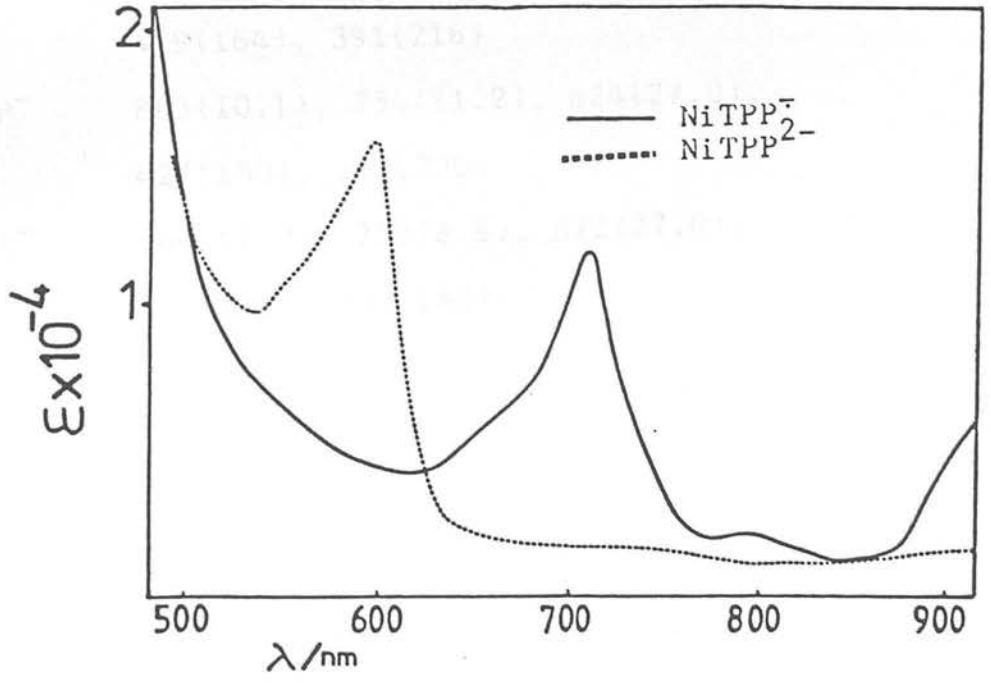

Figure 3.33 Optical absorption spectra of the cathodic products of NiTPP

Table 3.14 Spectral data for the reduction products of the d^8 metalloporphyrins

	wavelength maxima, nm (extinction coefficient x 10^{-3})
$NiTPP^-$	908(6.0), 800(1.4), 705(11.2), 666(6.4), 440(114), 412(100)
$NiTPP^{2-}$	598(16.4), 410(124)
$PdTPP^-$	886(8.9), 780(4.1), 704(3.0), 644(11.3), 600(8.3), 520(8.4), 440(102), 410(92)
$PdTPP^{2-}$	596(17.4), 409(102.6)
$PtTPP^-$	880(11.0), 770(3.2), 704(2.9), 640(10.9), 600(7.4), 516(7.4), 440(134), 402(114.6)
$PtTPP^{2-}$	590(18.3), 400(80.0)
$NiOEP^-$	864(9.4), 760(9.0), 624(24.1), 419(164), 391(216)
$PdOEP^-$	863(10.1), 754(11.2), 624(27.0), 427(150), 392(200)
$PtOEP^-$	860(12.0), 752(8.6), 622(27.0), 428(146), 389(182)

3.5 COBALT (d^7) PORPHYRINS

The redox behaviour of cobalt porphyrins is of great interest due to the close structural similarities with the biologically important cobalamins and especially Vitamin B_{12}. Electrochemical studies on Vit B_{12} have shown it undergoes a reversible reduction and a reversible oxidation which are intrinsically involved in its bioactivity[78]. Previous studies on the model cobalt porphyrin Co(II) TPP[79, 80] have concluded that, as for Vitamin B_{12}, both the first oxidation and the first reduction of the complex results in electron transfer at the metal centre to give $(Co(III)\ TPP)^+$ and $(Co(I)\ TPP)^-$ respectively.

The assignment of $(Co(I)\ TPP)^-$ was based on the lack of paramagnetism exhibited by the chemically reduced product of Co(II) TPP (by NaHg or $NaBH_4$), in full accord with the expected $d_{xy}^2\ d\pi^4\ d_{z^2}^2$ electron configuration of Co(I)[79]. (Co(II) is always present in its low spin state in these molecules)[81]. Later, the cathodic electrochemistry of Co(II) TPP in DMSO was studied by Felton and Linschitz[22] and the unusually high value of ΔE(1st red/2nd red) of approximately one volt led them to assign the order of reduction as-

$$Co(II)\ TPP \xrightarrow{+e^-} (Co(I)TPP)^- \xrightarrow{+e^-} (Co(I)\ TPP^{\cdot})^{2-}$$

The anodic electrochemistry of Co(II) TPP has also been studied. Truxillo and Davies[82] report three one-electron oxidations in benzonitrile and solely on the basis of the separation between the waves assign the order of oxidation as

$$\text{Co(II)TPP} \xrightarrow{-e^-} (\text{Co(III)TPP})^{+} \xrightarrow{-e^-} (\text{Co(III)TPP}_2^{2+}) \xrightarrow{-e^-} (\text{Co(III)TPP}^{3+})$$

Further electrochemical evidence the first oxidation did indeed occur at the metal centre rather than the macrocycle was presented by Kadish[83]. He reported that $E_{\frac{1}{2}}$(1st ox) was dependent to a large extent on the solvent employed, being as much as 0.7V more cathodic in pyridine than the value measured in benzonitrile. As no such solvent dependence was noted for macrocycle-based oxidations, Kadish concluded the first oxidation was a metal-based $Co^{II/III}$ redox couple. It was also reported the couple was irreversible in CH_2Cl_2.

The electrochemistry of Co(II) OEP has been studied to a far lesser extent than Co(II) TPP. Fuhrhop et al.[47] report a single reversible oxidation in benzonitrile which they attribute to oxidation of the macrocycle i.e. the opposite behaviour to that displayed by Co(II) TPP. Kadish[83] in a cathodic investigation of Co(II) OEP observed only one reduction which from the value of $E_{\frac{1}{2}}$ (1st red) he assigned as a Co(II)/I couple.

Our spectroelectrochemical characterisation of the electrode products of Co(II) TPP in CH_2Cl_2 confirm that both primary cathodic and anodic redox events do indeed occur at the metal. Further we find Co(II) OEP exhibits a similar redox pattern, contrary to the previous study.

Both Co(II) OEP and Co(II) TPP were shown to undergo three one-electron oxidations in CH_2Cl_2.

	$E_{\frac{1}{2}}$(1st ox)/V*	$E_{\frac{1}{2}}$(2nd ox)V	$E_{\frac{1}{2}}$(3rd ox)/V	ΔE(2nd ox/ 3rd ox)/V
CoTPP	0.41	0.83	1.02	0.19
CoOEP	0.43	0.64	0.92	0.28

*Volts vs. Ag/AgCl reference electrode

Each wave corresponds to a diffusion controlled step, fully reversible on the electrochemical time scale. The similarity in the values of $E_{\frac{1}{2}}$ (1st ox) for the two porphyrins strongly indicates the first oxidation takes place at the metal centre. It has been shown in this work that when the oxidation is macrocycle-based MOEP complexes are generally 160-200mV easier to oxidise than the corresponding MTPP complex. This difference is reflected not by the first oxidation of the cobalt porphyrins but by the second oxidation, which is 190mV more anodic for Co(II) TPP than Co(II) OEP. Additionally the values of $E_{\frac{1}{2}}$ (1st ox) for both Co(II) TPP and Co(II) OEP do not fit on the linear relationship of $E_{\frac{1}{2}}$ (1st ox) against

electronegativity of the central metal. The values extrapolated from Figure 2.8 for the Co(II) P/Co(II) $P^{+\cdot}$ redox step are +0.53V for Co(II) OEP and +0.70V for Co(II) TPP. These numbers are far more anodic than the observed experimental values and thus the voltammetric results indicate that the first oxidation of both porphyrins occurs at the metal centre giving rise to a Co(III) porphyrin.

The separation between the second and third oxidations of both porphyrins is consistent with the stepwise removal of electrons from the macrocycle. Spectroelectrochemical characterisation of all three electrode products support the above conclusions.

In situ esr measurements gave limited but consistent information. An esr signal for Co(II) TPP was only obtained at 77K. The observed spectrum in CH_2Cl_2/0.5M $TBABF_4$ was similar to that previously reported[81], with $g_{\parallel}$ = 2.1820 and $g_{\perp}$ = 2.0010. Both the first and third oxidation products of Co(II) TPP exhibited no paramagnetic signal at any temperature (77K - 300K). However the product of the second oxidation gave rise to a highly isotropic esr signal (g = 2.0047 at 290K). Similar behaviour is noted for the oxidation products of Co(II) OEP. Co(II) OEP itself exhibits a typical Co(II) d^7 esr signal at 77K with $g_{\parallel}$ = 2.200 and $g_{\perp}$ = 1.9976 in CH_2Cl_2/0.5MTBABF$_4$. Again, only the second oxidation product

is paramagnetic. A highly isotropic signal, with a g value of 2.0003 at 290K, is observed. The ESR data then supports the assignment that the second oxidation of both porphyrins results in a porphyrin π cation radical.

Uv/visible characterisation of all 3 oxidation products, of both Co(II) TPP and Co(II) OEP, proved possible at room temperature in CH_2Cl_2 using the OTTLE cell. Unlike most metalloporphyrins the electronic spectrum of Co(II) TPP in CH_2Cl_2 exhibits only one visible band. This has been assigned previously[84] as the Q(1,0) band, the Q(0,0) band being forbidden. Figure 34 shows the spectral changes which occur on oxidation at the plateau of the first wave. The spectral data are summarised in Table 15. Clearly, the observed spectral changes are <u>not</u> those which accompany the formation of a porphyrin cation radical. Instead a simple two banded spectrum results, similar to the starting spectrum but shifted to the red. This red shift is not uniform across the spectrum, the Soret band energy shift being greater than the shift of the visible band. Isosbestic points relating the oxidised species to Co(II) TPP are noted at 538nm and 420nm. Co(II) TPP is fully regenerated on reversing the applied potential. The final spectrum of the first oxidised product is consistent with the electronic formulation $(Co(III)TPP)^+$, with electron removal having occurred from the d_{z^2} orbital of the metal rather than from the a_{2u} or a_{1u} of the porphyrin. (Although it appears from Figure 34 that the Soret band is

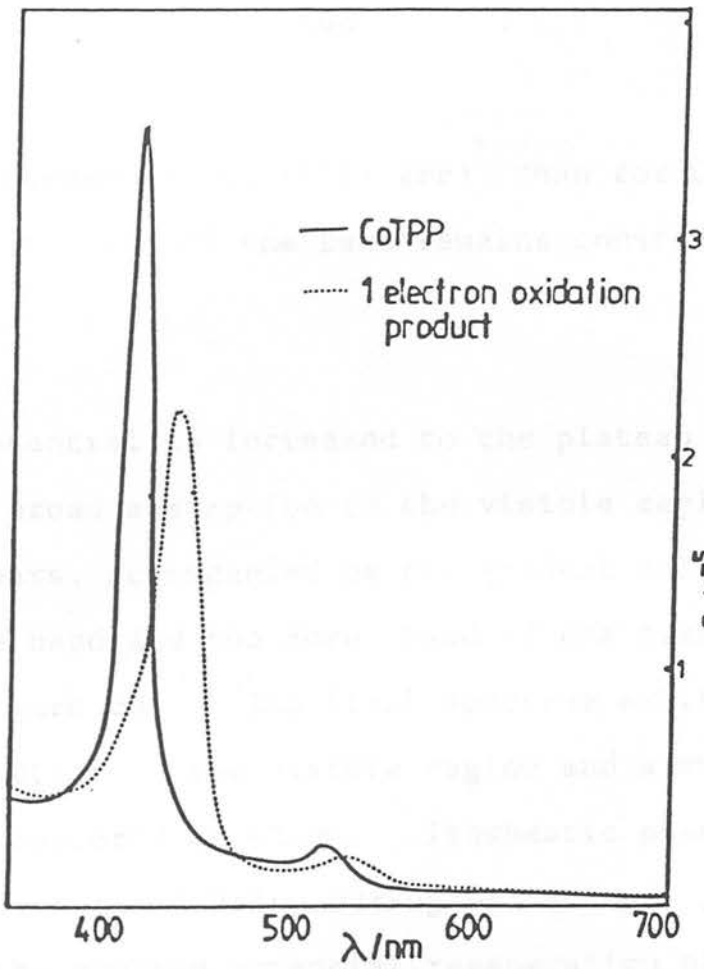

Figure 3.34 One-electron oxidation product of Co(II)TPP in CH_2Cl_2/0.5M $TBABF_4$ (20°C)

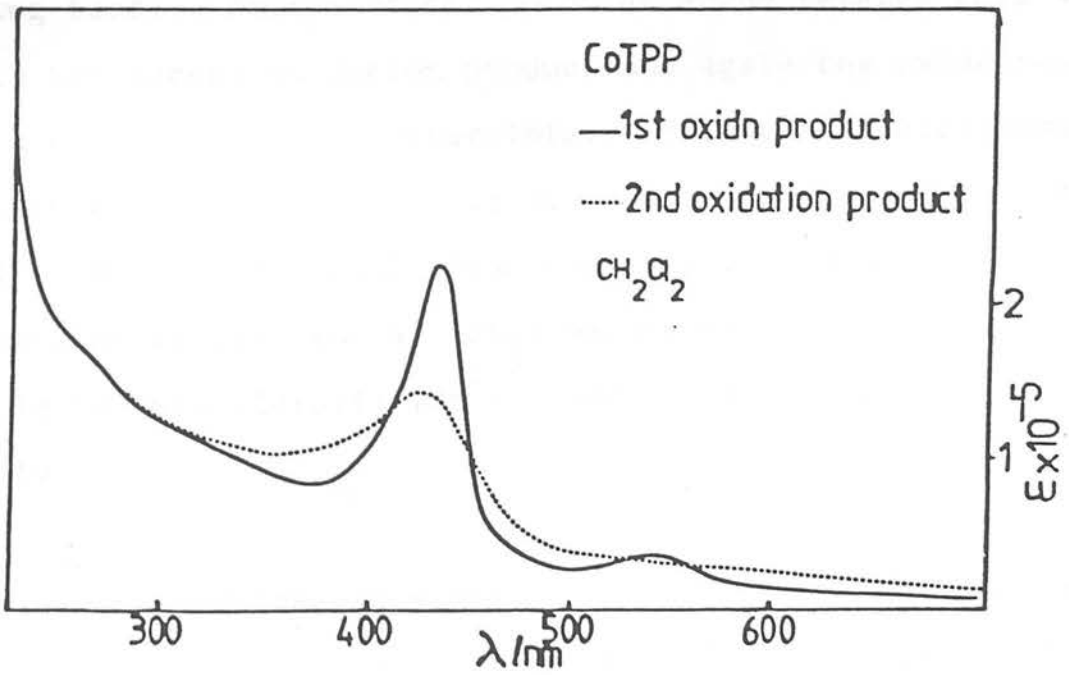

Figure 3.35 Optical absorption spectra of the anodic products of Co(II)TPP

much less intense for $(Co(III)\ TPP)^{+}$ than for Co(II) TPP the oscillator strength of the band remains constant on oxidation).

When the potential is increased to the plateau of the second oxidation, broad absorption in the visible region, from 700-600nm, appears, accompanied by the gradual collapse of both the visible band and the Soret band of the first oxidation product (Figure 35). The final spectrum exhibits broad absorption in the visible region and a much less intense Soret band centered at 430nm. Isosbestic points are noted at 558, 534, 448 and 388nm during oxidation. Again on reversing the applied potential regeneration of the first oxidised species was complete. Further oxidation at the third wave results in a featureless visible spectrum with a broad peak at 380nm ($\epsilon = 8.2 \times 10^{-4}$) as its only characterising band. An isosbestic point at 400nm relates this species with the second oxidation product and again the oxidation was found to be fully reversible. From the earlier results presented in this work it is clear both the second and third oxidised products result from the stepwise removal of electrons from a molecular orbital based mainly on the porphyrin macrocycle to form $(Co(III)\ TPP^{+\cdot})^{2+}$ and $(Co(III)\ TPP^{2+})^{3+}$ respectively.

Co(II) OEP undergoes a similar anodic redox sequence. The

spectral changes during the first oxidation of Co(II) OEP are shown in Figure 36 and summarised in Table 15. Isosbestic points at 552, 548, 512, 402 and 377nm relate the oxidation product to the neutral starting material. On reversing the potential to a value cathodic of $E_{\frac{1}{2}}(ox)$ full recovery of Co(II) OEP was obtained. The observed spectral changes are qualitatively similar to those noted during the first oxidation of Co(II) TPP with the spectrum undergoing a shift to the red. Therefore as for Co(II) TPP, we assign the first oxidation of Co(II) OEP as a metal-based redox step as the electronic spectrum shows none of the characteristic bands expected for a metalloporphyrin cation radical. On oxidation at the second wave this spectrum collapses and the growth of broad absorptions in the visible region between 700 - 580nm are noted. Isosbestic points relating the first oxidised and second oxidised products are noted at 578, 510 and 430nm. The product of the third oxidation has a featureless visible spectrum and a very weak Soret transition at 350nm. All three oxidations were shown to be fully reversible.

The uv/visible and esr spectral determinations confirm the earlier conclusions made from the voltammetric data. The first one electron oxidation occurs at the metal centre, followed by the consequent stepwise removal of two electrons from the macrocycle, to give firstly a Co(III) porphyrin cation radical and finally a Co(III) porphyrin dication.

Table 3.15 Spectral data for the oxidation products of CoTPP and CoOEP

	Wavelength maxima, nm (extinction coefficient x 10^{-3})
CoTPP	528(30.1), 415(330)
$(CoTPP)^{+}$	544(23.3), 432(210)
$(CoTPP)^{2+}$	broad absorption 700-500, 425(120.1)
CoOEP	551(21.5), 514(10.6), 392(194.1), 320(29.0)
$(CoOEP)^{+}$	548(16.6), 410(43.0), 380(53.0)
$(CoOEP)^{2+}$	broad absorption 700-500, 400(131.2)

Table 3.16 Spectral data for the reduction products of CoTPP and CoOEP

	Wavelength maxima, nm (extinction coefficient x 10^{-3})
$(CoTPP)^{-}$	520(32.4), 415(245)
$(CoTPP)^{2-}$	920(4.2), 690(3.4), 600(2.1), 454(96.5), 416(129.2)
$(CoOEP)^{-}$	541(22.6), 401(172.4)

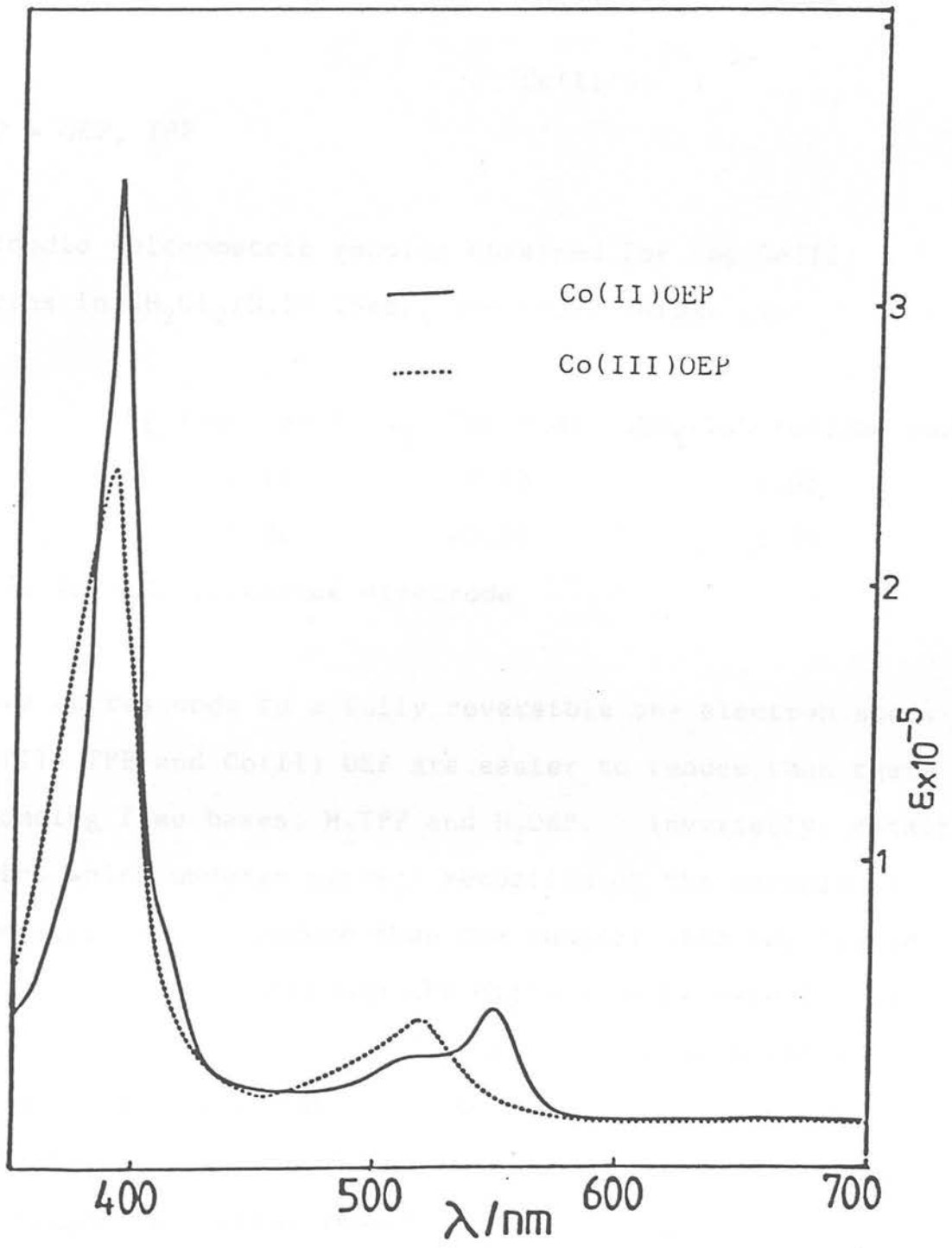

Figure 3.36 Optical absorption spectrum of the one-electron oxidation product of Co(II)OEP

$$Co(II)P \xrightarrow{-e^-} (Co(III)P)^{+} \xrightarrow{-e^-} (Co(III)P^{\cdot})^{+\,2+} \xrightarrow{-e^-} (Co(III)P^{2+})^{3+}$$

where P = OEP, TPP.

The cathodic voltammetric results obtained for the Co(II) porphyrins in CH_2Cl_2/0.5M $TBABF_4$ are shown below-

	$E_{\frac{1}{2}}$ (1st red)*	$E_{\frac{1}{2}}$ (2nd red)	$\Delta E_{\frac{1}{2}}$(1st red/2nd red)
CoTPP	-1.11	-2.16	1.05
CoOEP	-1.26	-2.51	1.25

*Volts vs Ag/AgCl reference electrode

Each wave corresponds to a fully reversible one electron step. Both Co(II) TPP and Co(II) OEP are easier to reduce than their corresponding free bases, H_2TPP and H_2OEP. Invariably, metalloporphyrins which undergo primary reduction at the macrocycle are more difficult to reduce than the unmetallated macrocycle (see Table 2). Thus although the difference between $E_{\frac{1}{2}}$ (1st red) for Co(II) TPP and Co(II) OEP of 150mV is as expected if both complexes were reduced at the macrocycle (cf $\Delta E_{\frac{1}{2}}$ (1st red) for ZnTPP and ZnOEP of 160mV), the voltammetric results suggest the first reduction occurs at the metal giving rise to a Co(I) porphyrin. No information to the electronic structure of the product from the second reduction is available from the electrochemistry alone. Three possible redox sequences exist -

1) $Co(II)P \xrightarrow{+e^-} (Co(I)P)^- \xrightarrow{+e^-} (Co(I)P^{2-})$

2) $Co(II)P \xrightarrow{+e^-} (Co(I)P)^- \xrightarrow{+e^-} (Co(0)P)^{2-}$

3) $Co(II)P \xrightarrow{+e^-} (Co(I)P)^- \xrightarrow{+e^-} (Co(II)P^{2-})^{2-}$

The third possibility above has a precedent. Hush and Woolsey[85] found for the related 1-19-diethoxycarbonyl-tetrahydrocorrin an internal redox reaction occurred in which both added electrons are in the ligand π^* orbital in the doubly reduced compound.

Spectroelectrochemical determination of the cathodic products of Co(II) TPP confirmed the reduction order to be that shown in (1) above. Unfortunately the second reduction product of Co(II) OEP was not sufficiently stable to allow characterisation. When Co(II) TPP is reduced at a potential on the plateau of the first cathodic wave, the product exhibits no esr signal. This is consistent with reduction of the Co(II) centre to Co(I), but is not conclusive evidence in itself. Further reduction at the second wave gives rise to an isotropic signal, g = 2.0001 (250K). As described earlier this is typical of a porphyrin anion radical.

Following the two reduction processes using uv/visible spectroscopy gives corroborative support to the esr results (Table 16). Firstly the one electron reduction of Co(II) TPP results in a small blue shift of the visible bands and a broadening of the Soret band. Isosbestic points at 540,

456 and 398nm are noted throughout reduction. No peaks in the near ir are observed. The shift of the visible π / π^* transition is of course the opposite to the red shift observed during oxidation of Co(II) TPP to Co(III) TPP. The spectral changes which occur during the second reduction are shown in Figure 37. Broad visible bands are noted and the Soret band splits. These changes are consistent with the formation of a porphyrin anion radical.

The spectral changes which occur during the first reduction of Co(II) OEP are similar to those observed for Co(II) TPP. The first reduction product has a similar uv/visible spectrum to that of Co(II) OEP, with only a small blue shift ($200cm^{-1}$) of the whole spectrum occurring (Table 16). This product exhibits no esr signal and is assigned as $(Co(I)\ OEP)^-$. Although no spectral characterisation of the second reduced product is available, we tentatively assign this species as $(Co(I)\ OEP^{\cdot 2-})$ from the voltammetric data above. The value of ΔE(1st red/2nd red) for Co(II) OEP is 200mV greater than that for Co(II) TPP. This is consistent with the second reduction occurring at the porphyrin macrocycle in both cases as the OEP ring is generally 160 - 200mV more difficult to reduce than the TPP ring for a given metal centre in a given oxidation state (see Table 2.2).

Thus the order of reduction for both Co(II) porphyrins is-

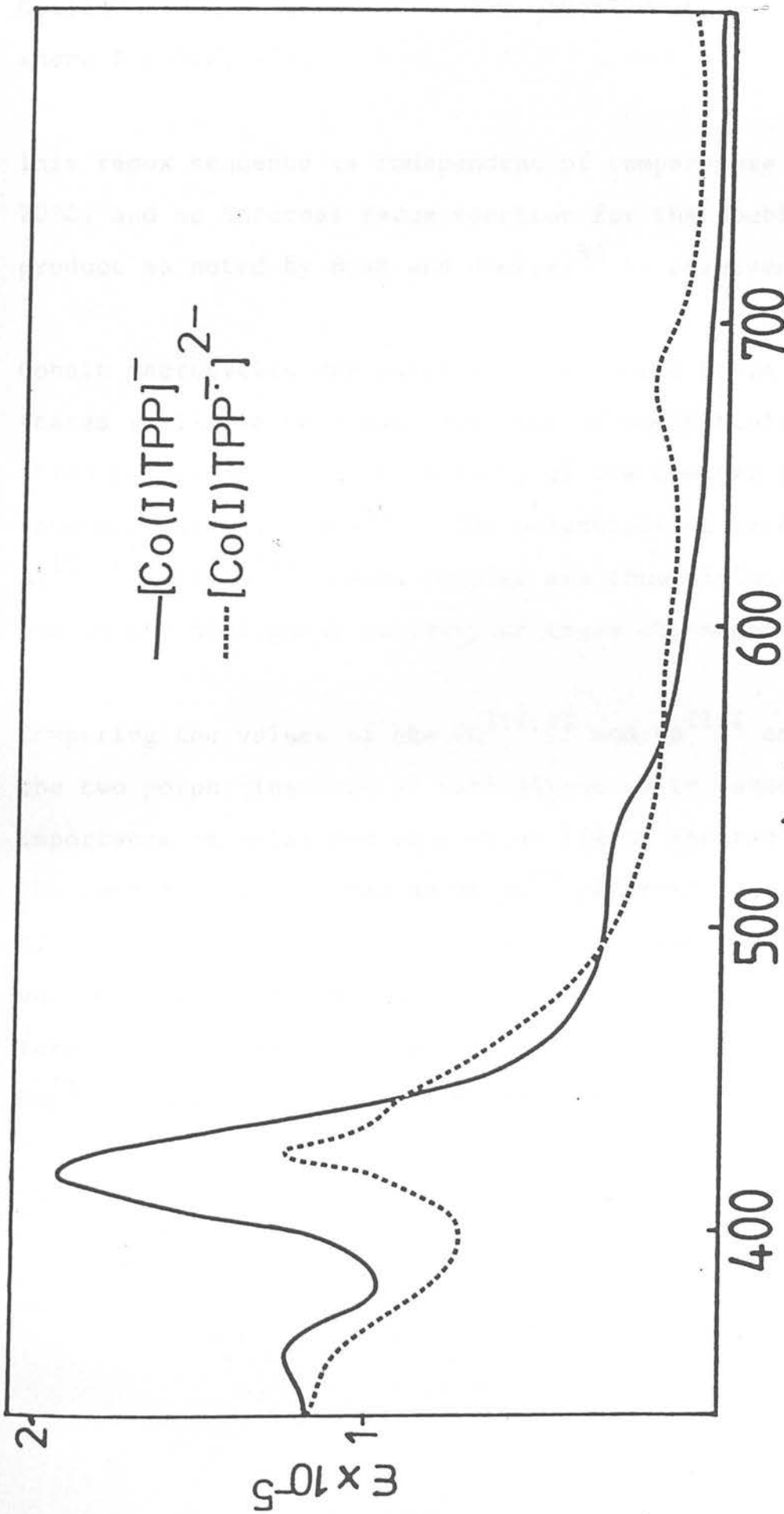

Figure 3.37 Optical absorption spectra of the cathodic products of Co(II)TPP in CH_2Cl_2/0.5M $TBABF_4$ at - 30°C

$$Co(II)P \xrightarrow{+e^-} (Co(I)P)^{-} \xrightarrow{+e^-} (Co(I)P^{\cdot})^{2-}$$

where P = OEP, TPP.

This redox sequence is independent of temperature (-70°C to 20°C) and no internal redox reaction for the doubly reduced product as noted by Hush and Woolsey[85] is observed.

Cobalt macrocycles can exist in vivo in all three oxidation states available to cobalt and much of their biological function is dependent on the ability of the complex to undergo internal redox changes[86]. The potentials of both the $Co^{III/II}$ and $Co^{II/I}$ redox couples are thus ultimately important in the biological activity of these chromophores.

Comparing the values of the $Co^{III/II}$ and $Co^{II/I}$ couples for the two porphyrins studied here allows us to comment on the importance of axial and equatorial ligand interaction with the central metal. Kadish et al.[83] reported the potential of the $Co^{III/II}$ redox step of Co(II) TPP was highly dependent on the solvent it was measured in. A similar study was undertaken here but extended to include both the $Co^{III/II}$ and the $Co^{II/I}$ couples. The results are shown in Table 17 below.

	Solvent	$Co^{III/II}/V$*	$Co^{II/I}/V$
	CH_2Cl_2	0.43	-1.11
CoTPP	DMF	0.05	-1.11
	DMSO	-0.05	-1.10
	pyridine	-0.10	-1.12
	CH_2Cl_2	0.41	-1.26
CoOEP	DMF	0.05	-1.28
	DMSO	0.00	-1.27
	pyridine	-0.09	-1.28

Table 17: Electrochemical data for Co(II) TPP and Co(II) OEP in Various Non-aqueous Solvents

* Volts measured vs Ag/AgCl and fully corrected for liquid junction potentials

In coordinating solvents such as DMSO and pyridine, cobalt porphyrins have been shown[87] to exist in an octahedral environment with ligation of two solvent molecules at the vacant axial sites. The results above strongly suggest that axial ligation of this type stabilises Co(III) porphyrins to a greater degree than Co(II) porphyrins as the $Co^{III/II}$ couple shifts to considerably more cathodic values in coordinating media. Basolo et al.[88] have reported that the ease of oxidation of cobalt (II) complexes is directly proportional to

the base strength of the bound axial ligand and that a plot of $E_{\frac{1}{2}}$ vs pKa yielded a linear relationship. In the present study we observe a similar qualitative relationship between the half-wave potential for the oxidation of Co(II)/Co(III), and the coordinating ability of aprotic solvents. The coordinating ability[89] of aprotic solvents for cations decreases in the following order: pyridine > DMSO > DMF > CH_2Cl_2. This follows the ease of Co(II) oxidation in each solvent. The similarity of the values of the $Co^{III/II}$ couple between Co(II) TPP and Co(II) OEP in each solvent shows that axial ligand electronic interactions are far more important than the equatorial interaction of the porphyrin macrocycle. Quite the opposite is true for the $Co^{II/I}$ couple where the $E_{\frac{1}{2}}$ value is largely independent of the solvent employed. Thus Co(II) OEP is consistently more difficult to reduce than Co(II) TPP by approximately 160mV, regardless of solvent. For the $Co^{II/I}$ couple then the equatorial ligand electronic interaction between the metal and the porphyrin ring dominates the relative stability of Co^{II} and Co^{I}. Axial ligand effects are negligible. Uv/visible data obtained for the redox products of Co(II) PL_2 (where L = DMSO, DMF, pyridine and P = OEP, TPP), by similar methods to those described earlier, also reflect the relative importance of solvent coordination to Co(I), Co(II) and Co(III). The spectra of Co(I)PL_2 and Co(II)PL_2 are seen to be largely independent of solvent, with both the position and intensity of the bands varying little. The energies of the π / π^* transitions for Co(III)PL_2

are also constant in all solvents. However when the oscillator strength of both the Q and Soret bands for $Co(III)PL_2$ are compared it is observed they change dramatically with solvent. In coordinating media the oscillator strength of both $\pi/\ \pi^*$ transitions greatly increases on oxidation of $Co(II)\ PL_2$ to $Co(III)PL_2$ (see Figure 38). This is not observed in CH_2Cl_2. We attribute this increase in oscillator strength to a lowering of symmetry of the Co(III) species in coordinating media. Whereas in CH_2Cl_2 the oxidised product will have a strict square-planar symmetry, coordinating solvents will decrease this to a pseudo-octahedral geometry. As a direct result of the lower symmetry of the complex as a whole, the macrocycle $\pi/\ \pi^*$ transitions consequently have less symmetry restrictions to obey and become more 'allowed' in nature. Moreover we note the increase in oscillator strength of the $\pi\ /\ \pi^*$ bands is greater the more coordinating the solvent is. Therefore the more coordinating the solvent, the more cathodic is the $Co^{III/II}$ redox couple and the more intense are the intra-ligand transitions of the porphyrin macrocycle. While this could be an exceedingly important observation in that a spectroscopic handle exists to estimate the importance of axial ligation in natural cobalt porphyrin systems, further study is obviously required to quantify the above effects.

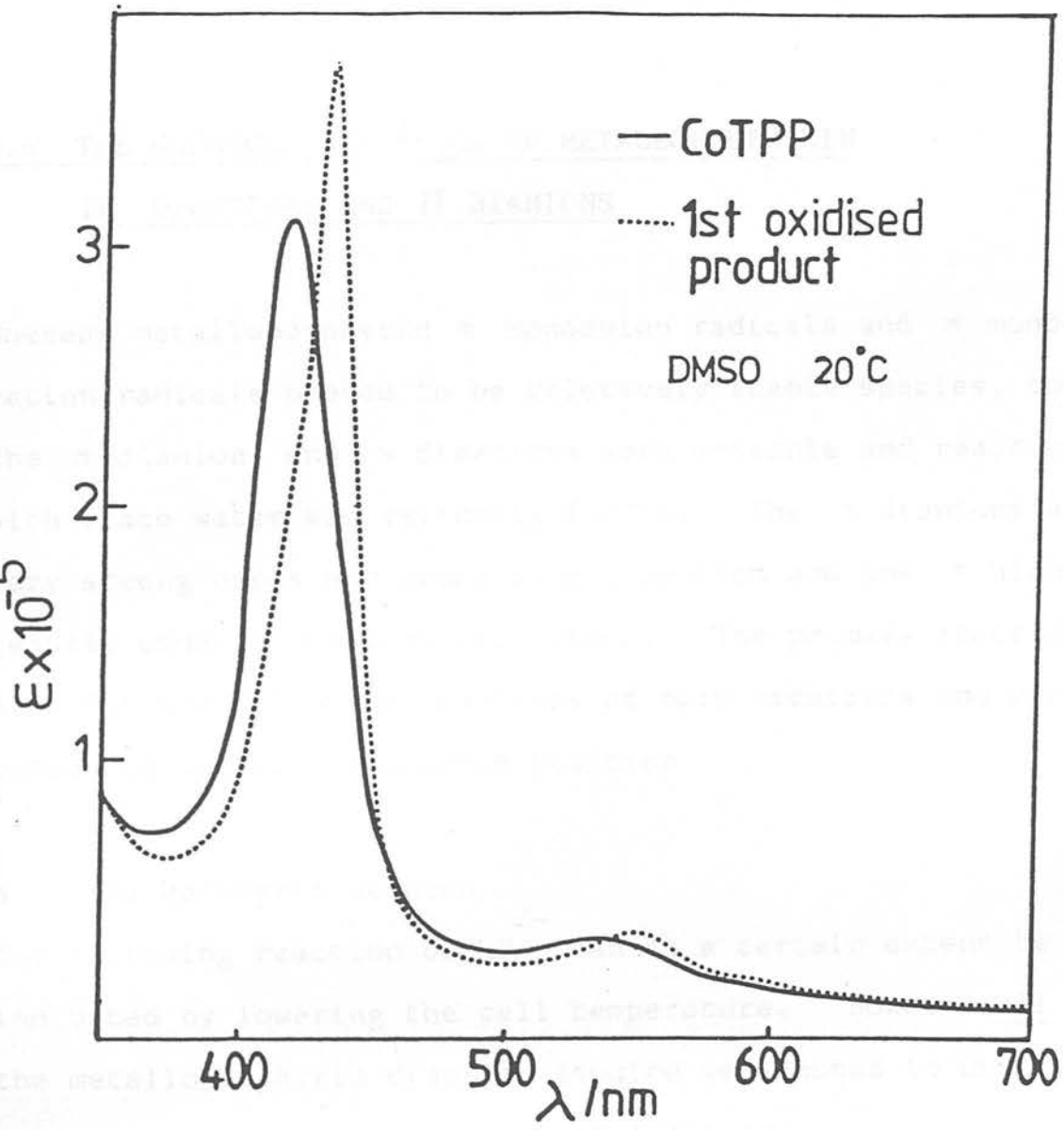

Figure 3.38 One-electron oxidation product of Co(II)TPP in DMSO/0.1M $TBABF_4$ (cf Figure 3.34)

The extinction coefficient of the Soret band for the Co(III) species are-

	ϵ (B band)
pyridine	400,000
DMSO	370,000
DMF	300,000
CH_2Cl_2	210,000

3.6 THE CHEMICAL REACTIONS OF METALLOPORPHYRIN Π DICATIONS AND Π DIANIONS

Whereas metalloporphyrin π monoanion radicals and π monocation radicals proved to be relatively stable species, both the π dianions and π dications were unstable and reaction with trace water was extremely facile. The π dianions are very strong bases and prone to protonation and the π dications readily undergo nucleophilic attack. The primary reaction site for the following reactions of both dications and dianions proved to be the meso-carbon position.

a) The Porphyrin Dianion

The following reaction of MP^{2-} can to a certain extent be inhibited by lowering the cell temperature. However <u>all</u> the metalloporphyrin dianions studied were noted to undergo the following reaction at room temperature-

$$MP^{2-} + H^{+} \longrightarrow MPH^{-}$$

Figure 39 shows the electrochemistry of the ultimate product of the second reduction of Pd(II) TPP when the electrogeneration is carried out at room temperature. This green product exhibits an irreversible two-electron oxidation at -0.60V, and a semi-reversible one-electron reduction at -2.06V. Electrogeneration at -0.40V resulted in full recovery of Pd(II) TPP. The green product is ESR silent and no ESR signal

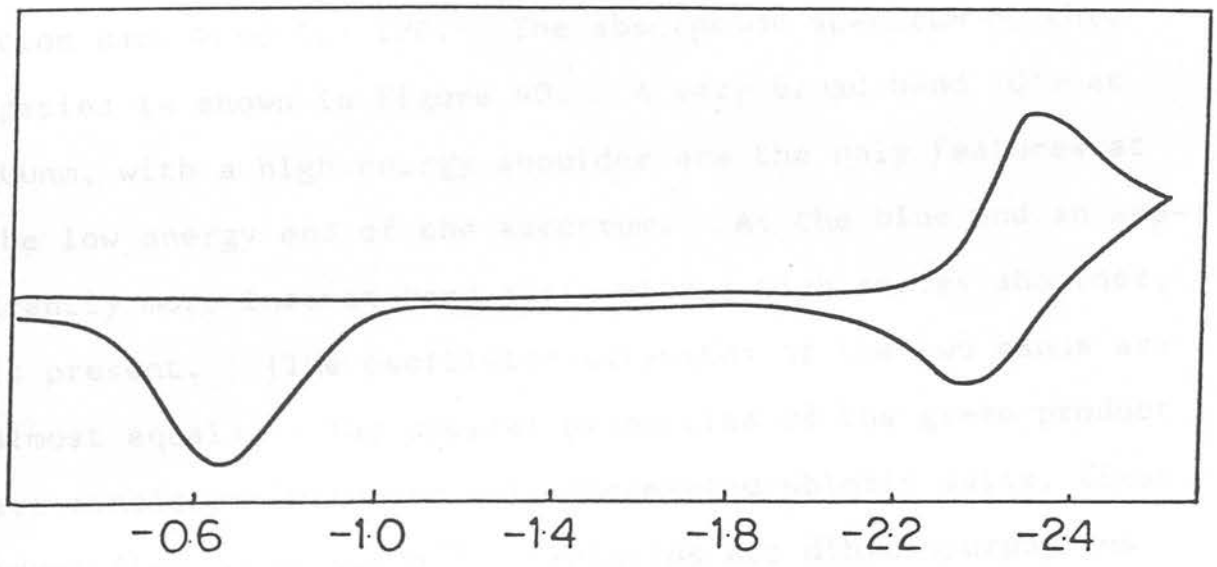

Figure 3.39 Cathodic electrochemistry of the phlorin salt of PdTPP ($PdTPPH^-$) in CH_2Cl_2/0.5M $TBABF_4$ at 20°C

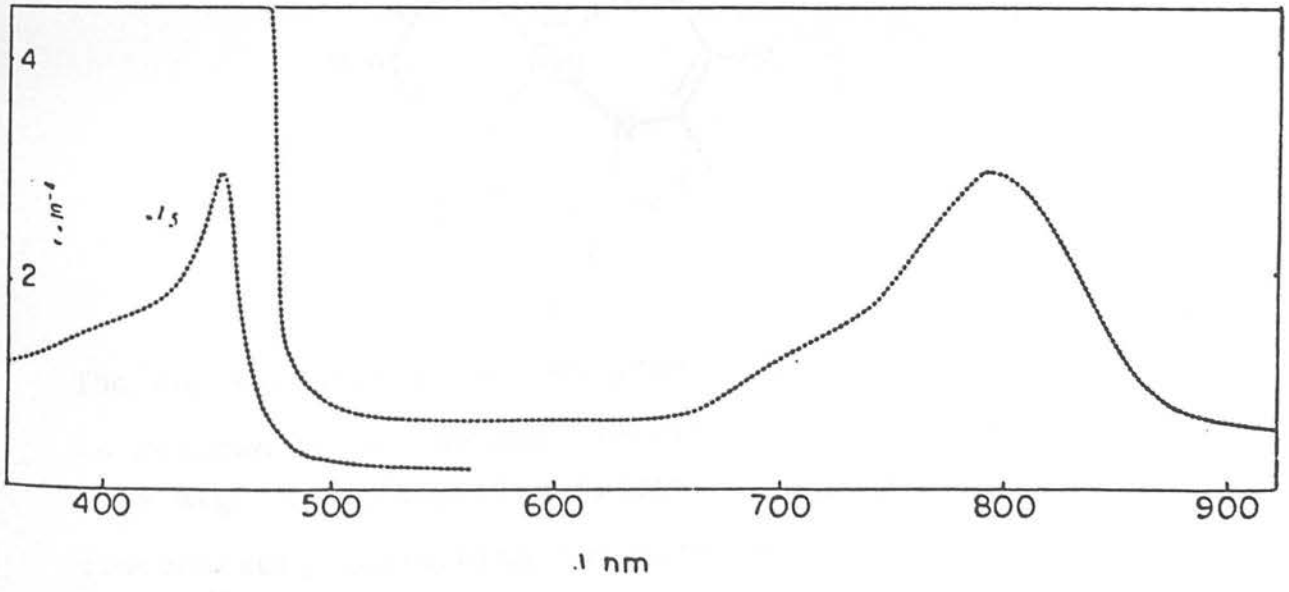

Figure 3.40 Optical obsorption spectrum of $(PdTPPH)^-$ in CH_2Cl_2/0.5M $TBABF_4$ at 20°C

was detected throughout the course of the two-electron oxidation back to Pd(II) TPP. The absorption spectrum of this species is shown in Figure 40. A very broad band (Q') at 800nm, with a high energy shoulder are the only features at the low energy end of the spectrum. At the blue end an apparently more intense band again with a high energy shoulder, is present. (The oscillator strengths of the two bands are almost equal). The optical properties of the green product are consistent with the well documented phlorin salts, first identified by Woodward[90]. Phlorins are dihydroporphyrins where protonation has occurred at a meso-carbon atom. Thus the product arising from the second reduction of Pd(II) TPP is assigned as (3) below.

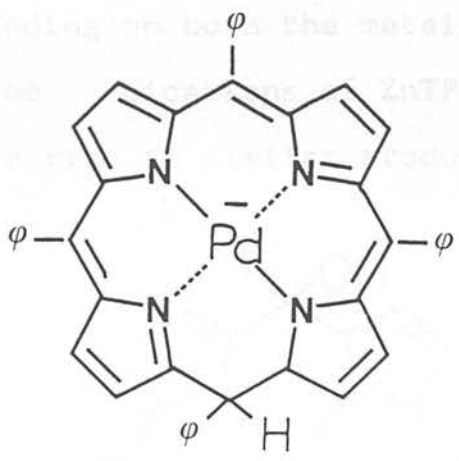

(3)

The one electron reduction product of (3) is unstable but is assumed to be the metallophlorin radical $(Pd(II)\ TPPH)^{2-\cdot}$. This highly nucleophilic species is presumed to undergo further protonation, explaining the semi-reversibility of the redox wave. Behaviour of this sort is common to all the studied

metallophlorins. The electrochemical data for the metallophlorins are listed in Table 18. The MPH^-/MP two-electron couple is largely independent of the metal centre. The MPH^-/MPH^{2-} couple however shows the same qualitative trend as the MP/MP^- couple suggesting π back-bonding is also present for the metallophlorins. This is also reflected in the energy of the Q' band in the absorption spectrum (Table 19). The MPH^- species are very stable under these experimental conditions and no rearrangement to the metallochlorin, as reported elsewhere[91], was noted here.

b) The Porphyrin Dication-

The further reactions of porphyrin dications leads to several products depending on both the metal centre and the macrocycle. Reaction of the dications of ZnTPP, CuTPP and NiTPP with trace H_2O gave rise to similar products with the general structure (4) -

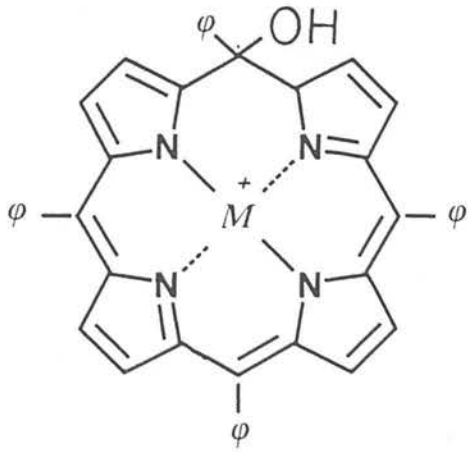

(4)

The optical data for these metallo-isoporphyrin species have

Table 3.18 Redox potentials of the Metallophlorins in CH_2Cl_2/0.5M $TBABF_4$ at 20°C (Volts vs. Ag/AgCl)

	$E_{\frac{1}{2}}(ox)^+$	$E_{\frac{1}{2}}$(1st red)
$ZnTPPH^-$	-0.61	-1.97
$CuTPPH^-$	-0.60	-1.95
$NiTPPH^-$	-0.58	-2.10
$PdTPPH^-$	-0.60	-2.06
$PtTPPH^-$	-0.58	-2.09
$ZnOEPH^-$	-0.64	-2.31
$CuOEPH^-$	-0.63	-2.29
$NiOEPH^-$	-0.63	-2.30
$PdOEPH^-$	-0.65	-2.37
$PtOEPH^-$	-0.63	-2.44

+Irreversible two-electron step

Table 3.19 Spectral data for the Metallophlorins in CH_2Cl_2/0.5M $TBABF_4$

	Q'/nm	S'/nm
$ZnTPPH^-$	847	471
$CuTPPH^-$	846	470
$NiTPPH^-$	810	469
$PdTPPH^-$	800	456
$PtTPPH^-$	794	455
$ZnOEPH^-$	808	454
$CuOEPH^-$	804	452
$NiOEPH^-$	774	446
$PdOEPH^-$	760	442
$PtOEPH^-$	751	440

been previously reported[92], and good agreement with these results is obtained here. The electrochemical properties of these species are quite different from the parent metalloporphyrins. They exhibit a semi-reversible one-electron oxidation (at ~ 1.0V) and a fully reversible <u>two</u> electron reduction (at ~ 0.4V). The one-electron oxidation product is not stable and characterisation of this product proved impracticable. The two-electron reduction of the metalloisoporphyrin results in full recovery of the parent porphyrin. This has not been reported previously.

The π dications of Pd(II) TPP and Pt(III) TPP undergo quite different chemistry in the presence of water, resulting in a previously unknown prophyrin structure. $(Pd(II)\ TPP^{2+})^{2+}$ and $(Pt(III)\ TPP^{2+})^{3+}$ are highly reactive species at room temperature. The optical progression of the second oxidation of Pd(II) TPP is shown in Figure 41. The maintenance of isosbestic points throughout oxidation shows the π dication to be short-lived. The final green product exhibits quite different optical properties from the isoporphyrin-type structure. This product is in fact air stable and has been isolated in solid form in complementary studies in our laboratory[93]. FAB mass spectrometry, ^{1}H and ^{13}C nmr and ir studies have characterised this product as palladium 14, 15-dihydroxy-14,15-dihydro-tetraphenylporphyrin (5).

Figure 3.41

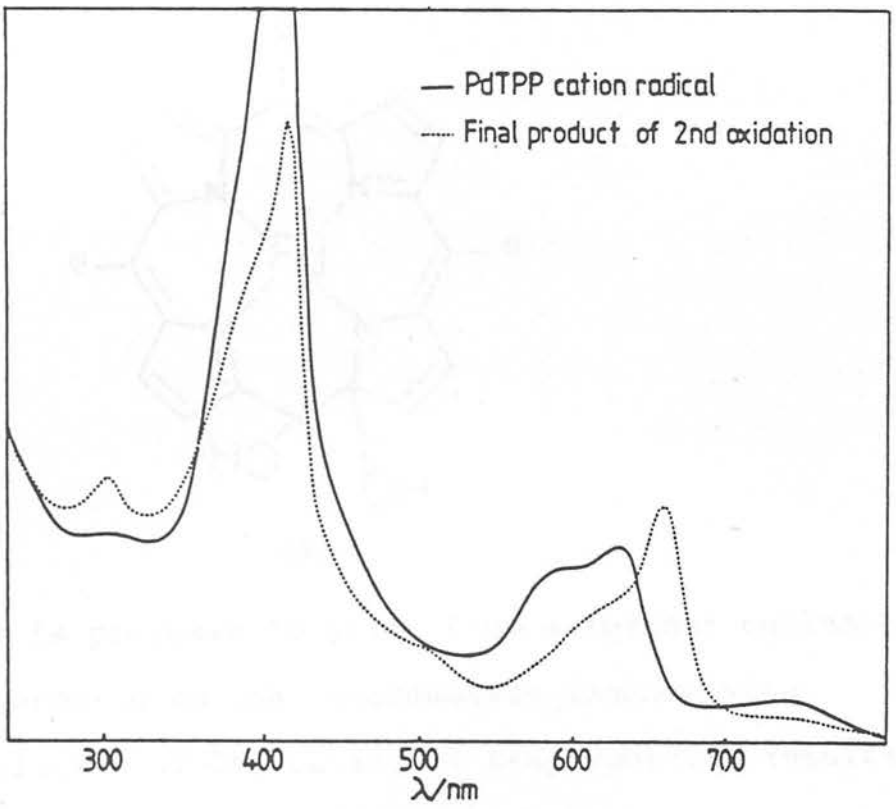

a) Optical absorption spectrum of the 2-electron oxidation product of PdTPP at room temperature in the presence of trace hydroxide ion.

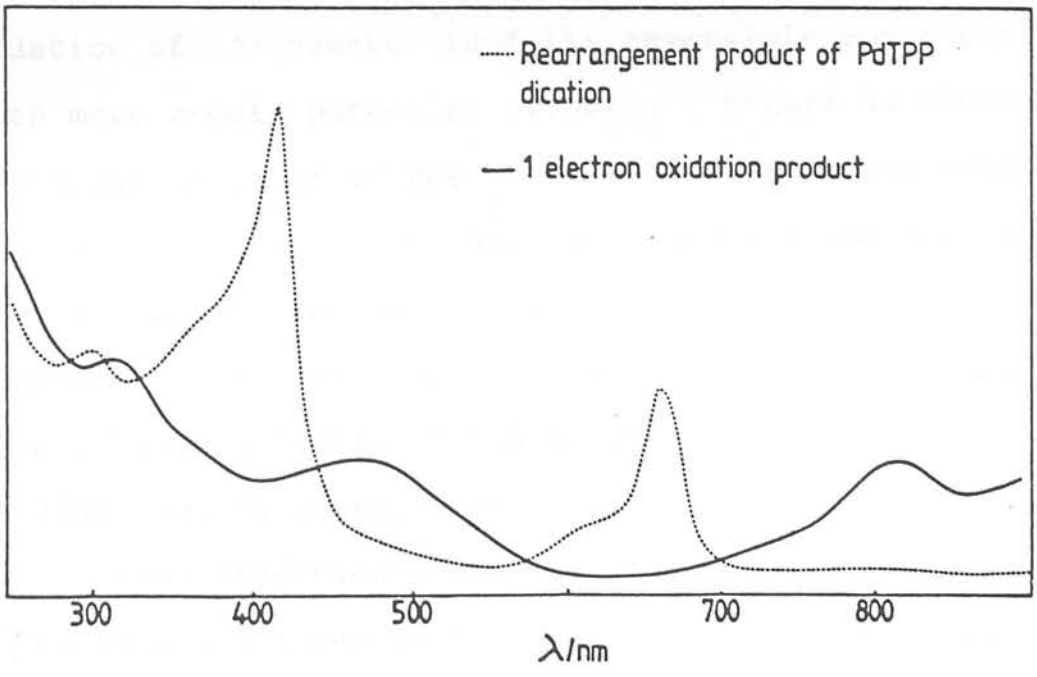

b) Optical absorption spectrum of the one-electron oxidation product of (5)

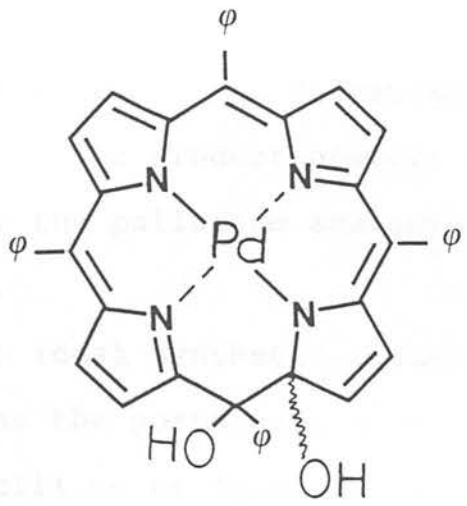

(5)

This species is proposed to arise from a further nucleophilic attack by hydroxide on the intermediate isoporphyrin. Further hydroxylation of Zn, Cu and Ni isoporphyrins results in cleavage of the ring.

Similar to the metallo-isoporphyrins the dihydroxy-derivative (5) exhibits a one-electron oxidation and a two-electron reduction. The oxidation of (5) however is fully reversible and occurs at a much more anodic potential (1.50V). Figure 41 shows the uv/visible spectrum of the one-electron oxidation product of (5). Broad peaks at 810, 480 and 312nm are the only transitions observed and isosbestic points at 700, 582, 429, 320 and 293nm are maintained throughout oxidation. This oxidised species displays an isotropic ESR signal ($g = 2.0005$, $\Delta H = 6.5G$ at 250K) and is assigned as the π cation radical of (5). The two electron reduction occurs at a similar potential (-0.4V) to that displayed by the isoporphyrins and results in full regeneration of Pd(II) TPP. Oxidation of Pt(II) TPP

also ultimately results in a dihydroxy-derivative at the third oxidation wave. The product however is far less stable than is the case for the palladium analogue and is not isolable.

Here then is an ideal synthetic route into a unique substitution pattern at the porphinato moiety, the applicability of which has still to be fully investigated.

The π dications of the MOEP series undergo yet another reaction pathway which is well documented elsewhere[94]. For the MTPP series the meso-substituent, phenyl, is an extremely poor leaving group and the isoporphyrin structure is relatively stable. In contrast, rapid proton loss after nucleophilic attack occurs during reaction of the $MOEP^{2+}$ species, yielding a meso-substituted porphyrin. Dolphin[95] and Smith[96, 97] have utilised the oxidised porphyrin ring as a synthetic intermediate in the preparation of a variety of meso-substituted porphyrins.

3.7 DISCUSSION

In Chapter 2 we observed the electrochemical redox potentials measured for metalloporphyrin complexes were largely dependent on the 'fit' of the metal in the macrocycle cavity. Whereas $E_{\frac{1}{2}}$ (1st ox) was found to vary linearly with the electrostatic effect of the central metal on the porphyrin π array, $E_{\frac{1}{2}}$(1st red) was significantly affected by the π acceptor properties of the ring. The extent of π back-bonding, of course, depends on the compatability of the metal d-orbitals and the macrocycle-based LUMO, both in energy terms and in geometric overlap. The degree of π back-bonding present in each metalloporphyrin was reflected spectroscopically in the hypso-nature of the visible spectrum. Thus the energy of the Q transition is a measure of the 'fit' of the metal in the porphyrin cavity. For the metal-based redox steps observed in this chapter, the optical spectral changes can also be rationalised in terms of π back-bonding.

In the general case of a one-electron oxidation occurring at the metal one would predict a red-shift in the visible spectrum. Removal of a d electron will result in a decrease in the energy of the d-orbitals. This energy decrease will result in less mixing of the dπ and e_g π^* orbitals and consequently the a_{1u} a_{2u} (π) $\longrightarrow$ e_g (π^*) transition will occur at lower energy. This is indeed the change in

the visible spectrum noted during the first oxidation of Co(II) TPP and Pt(II) TPP where the Q band is observed to shift by ~ $1000cm^{-1}$ to the red in both cases.

Reduction of the metal centre would, by the same argument, result in a blue shift of the visible π / π * bands i.e. the d(π)/e_g(π *) overlap will increase on addition of an electron into the d-manifold. For reduction of Co(II) TPP to $(Co(I)\ TPP)^-$, a blue shift of the Q band was noted. The observed shift of the visible band during reduction (~ $300\ cm^{-1}$) is however far smaller than that noted during metal oxidation.

For the metal-based redox steps of Pt(II) and Co(II) porphyrins then, the qualitative energy shift of the visible bands is as predicted. However the Ag(II)/Ag(III) oxidation-couple of Ag(II) TPP and Ag(II) OEP results in a <u>blue</u> shift of the Q bands. Oxidation of Ag(II) in a square planar environment results in removal of an electron from $d_x2 - y^2$. This change in site of oxidation (as opposed to d_z2 for Pt(II)/(III) and Co(II)/(III) does not explain why the visible π/ π * bands should shift to higher energy as both d_z2 and $d_x2 - y^2$ are symmetry-forbidden from mixing with the π manifold of the porphyrin ring for a complex of D_{4h} symmetry.

The porphyrin ring, as mentioned previously, is a rigid, flat macrocycle and as such the geometric parameters of the central

cavity are sterically fixed. It has been estimated[98] that the radius of the central hole which minimises radial strain in the porphinato core is 2.01Å. X-ray studies[98] on a wide range of planar metalloporphyrins have shown that the M-N distances can vary between 1.958 - 2.098Å. The metal which allows the minimisation of equatorial strain within the porphinato moiety is Pd(II), which has an M-N bond length of 2.009Å. For complexes such as ZnTPP (pyridine)[99], the zinc ion is displaced from the plane of the ring by 0.33Å to relieve macrocyclic radial strain. Typically, Ag(II) has a far larger ionic radius than any of the other divalent metals studied in this work (eg Pd(II) ionic radius = 0.80Å, Ag(II) ionic radius = 0.89Å)[100]. An early structural study[101] on a molecular solid solution of Ag(II) TPP suggested the silver ion was in the plane of the ring and the porphyrin ring remained largely unruffled. However a subsequent crystallographic study by Hoard[98] on the same complex showed it to have a distinctly non-planar confirmation in which two oppositely situated pyrrole rings are each tilted 6.6° from the mean plane and Ag(II) occupies a capped position. The measured Ag-N distance of 2.101Å is larger than any of the planar M-N bond lengths. The optical spectral results suggest that Ag(III) fits in the porphyrin cavity better than Ag(II). Therefore although upon oxidation the d-orbitals fall in energy the geometric overlap of the d π orbitals with the e_g (π^*) degenerate pair must improve upon removal

of an electron. Ag(III), being smaller than Ag(II), can be envisaged as occupying the centre of the macrocyclic cavity (or closer to the centre than Ag(II)).+

Therefore although one can predict the direction of the energy shift of the porphyrin π / π^* bands during oxidation or reduction of the central metal, one must limit such predictions to complexes where the metal occupies the central cavity. If the metal is sterically hindered from sitting in the plane of the ring then further considerations as to changes in ion size, must also be taken into account.

When the redox step under investigation results in a change in oxidation state of the porphyrin macrocycle, rather than the metal, the observed optical spectral changes are far more complicated. The porphyrin cation radical spectra generally consist of very broad absorptions throughout the visible/near uv region. A crystal structure of Zn $TPP^{+}C10_4^{-}$[103] has shown that the porphyrin macrocycle retains D_{4h} symmetry upon oxidation. We can therefore assume the electronic transitions exhibited by the cation radical are similar to those observed for the neutral porphyrin complex i.e. $1\ a_{1u}(\pi) \longrightarrow 4e_g(\pi^*)$ and $3\ a_{2u}(\pi) \longrightarrow 4e_g(\pi^*)$ transitions. Extra electronic transitions will also occur as

---

+ The ionic radius of Ag(III) is estimated as 0.75Å. This number arises from a crystal structure of $NaAg(III)F_4$[102].

electrons can now be promoted to the semi-occupied $3a_{2u}$ or $1a_{1u}$ orbital, depending on the ground state of the π cation radical. SCF-MO calculations[104] have shown that the energetic order of orbitals is unaltered from that encountered in neutral porphyrin. For a cation radical of ground electronic state $^2A_{2u}$ the ground state configuration is thus $(2e_g)^4 (2a_{2u})^2 (2b_{2u})^2 (3e_g)^4 (1a_{1u})^2 (3a_{2u})^1$. Allowed transitions (optically accessible states are ^2E_g) which are predicted[104] to fall in the studied spectral range (8,000 - 32,000cm^{-1}) are $3a_{2u} \longrightarrow 4e_g$, $3e_g \longrightarrow 3a_{2u}$, $1a_{1u} \longrightarrow 4e_g$ and $2e_g \longrightarrow 3a_{2u}$. The energetic order in which these transitions occur is less clear. Also it can be expected that there will be extensive configuration interaction (CI) between these transitions (as in the spectrum of neutral porphinato complexes). Exact characterisation of each electronic transition is thus impossible from straightforward solution electronic spectroscopy as measured in this work. However the hypso-behaviour exhibited by the visible π / π * bands in neutral metalloporphinato complexes should also be reflected in the spectra of the one-electron oxidised products. Transitions resulting in promotion of an electron to the $4e_g$ level then, should be dependent upon the metal at the centre of macrocycle. The energies of the $3a_{2u} \longrightarrow 4e_g$ and $1a_{1u} \longrightarrow 4e_g$ transitions for instance should follow a similar trend to that displayed by the neutral metalloporphyrins, while transitions to the half-empty a_{2u} or a_{1u} orbital should be largely

independent of the metal centre. From this rationalisation we can assign the transition contributing most to each band in the π cation radical spectrum. If we compare the spectra of Zn(II) $TPP^{+\cdot}$, Pd(II) $TPP^{+\cdot}$ and Ni(II)$TPP^{+\cdot}$ then the electronic transitions to the $4e_g$ level should occur to higher energy through the series Zn(II) < Ni(II) < Pd(II). The main visible transitions exhibited by these three metalloporphyrins are listed in Table 20 below-

Table 20 The energies (in wavenumbers) of the visible bands displayed by the porphyrin cation radicals of Pd(II), Ni(II) and Zn(II)

	$PdTPP^{+\cdot}$	$NiTPP^{+\cdot}$	$ZnTPP^{+\cdot}$
A	13,500	13,200	11,900
B	15,900	15,600	14,400
C	17,000	16,900	16,600
D	-	-	18,000
E	19,200	19,100	19,200

All three cation radicals have been assigned as having an $^2A_{2u}$ electronic ground state. The lowest energy transition (A) shows a considerable dependence on the central metal, as does transition B. Also an almost constant energy difference between transitions A and B exists for all three metalloporphyrins (~ 2500cm^{-1}). These two findings lead us to assign

transition A as $3a_{2u} \longrightarrow 4e_g$ and transition B as $1a_{1u} \longrightarrow 4e_g$. The energy difference between the $3a_{2u}$ and $1a_{1u}$ orbital (not accounting for CI) can be estimated as approximately 0.3eV. Estimates from SCF-MO calculations[104] vary between 0.2 and 0.25eV. Importantly, the dependence of transitions A and B on the central metal is found to be greater for the porphyrin cation radicals than is the case for the neutral metalloporphyrins (the Q band of the parent complexes occur at 16,900 (ZnTPP), 17,800 (NiTPP)and 18,000cm^{-1} (PdTPP)). Thus the porphyrin π cation radical, perhaps not surprisingly, must be a better π acceptor than the neutral macrocycle.

The energy of transition E, contrastingly, is independent of the metal centre, suggesting it involves promotion of an electron to the $3a_{2u}$ orbital. We assign this band as a $2e_g \longrightarrow 3a_{2u}$ transition. Moreover the mixing of this transition with transitions to the $4e_g$ level must be minimal. The energy of band C does not show the same degree of independence from the metal centre as band E. However the degree of dependence upon the metal ion is less pronounced than that observed for bands A and B. SCF-MO calculations[104] have shown the transition $3e_g \longrightarrow 3a_{2u}$ is predicted to undergo significant CI with the $3a_{2u} \longrightarrow 4e_g$ transition. This would explain the dependence of band C on the central metal. An approximate quantitative idea of what percentage each pure configuration contributes to band C can be obtained from the differing degrees of dependence on the divalent metal shown

by band A and band C. If band A is considered as a pure $3a_{2u} \longrightarrow 4e_g$ transition then we can estimate band C as ~ 30% $3a_{2u} \longrightarrow 4e_g$ and ~ 70% $3e_g \longrightarrow 3a_{2u}$. Band D is only noted in the spectrum of $ZnTPP^+$ and remains unassigned.*

The above assignments are for the main transitions only. More comprehensive assignment to account for all the visible optical density exhibited by the porphyrin cation radicals would require deconvolution of the overlapping bands. Also we have failed to take into consideration doubly excited states.

As in the neutral metalloporphyrin electronic spectra the bands in the near uv displayed by the cation radical are far more intense than the visible bands. This difference in intensity is a measure of the degree of CI between the $3a_{2u} \longrightarrow 4e_g$ and $1a_{1u} \longrightarrow 4e_g$ transitions[105]. The ratio of oscillator strength of the Q bands to oscillator strength of the Soret band does in fact increase for the porphyrin cation suggesting there is less CI present than in the neutral metalloporphyrin. The oscillator strength of the Soret

---

* It is probable this band is a vibrational overtone of band C as the relative intensities of the two bands change upon cooling the solution to -70°C, where band C grows at the expense of band D.

transition displayed by the cation radical is also less intense than that of the neutral porphyrin. In the radical, of course, only three electrons can be promoted rather than the four available in neutral porphyrin. This simple model thus predicts a cation Soret band three-quarters as intense as the porphyrin Soret band. SCF-MO calculations[104] predict a ratio of 0.7. Experimentally we find the ratio to be 0.58 - 0.66 depending on the metal centre.

Further evidence as to the assignment of the lowest energy transition in the $^2A_{2u}$ ground state porphyrin cation radical as a $3a_{2u} \longrightarrow 4e_g$ transition comes from the spectra of the $MOEP^{+\cdot}$ species which have a similar ground state. All the visible bands in the optical spectra of these radicals occur at higher energy than the corresponding $MTPP^{+\cdot}$ transitions (this parallels the behaviour of the neutral metalloporphyrins). However band A is shifted considerably more than band B. When comparing the spectra of $NiTPP^{+\cdot}$ and $NiOEP^{+\cdot}$ for instance band B shifts $2500cm^{-1}$. A similar comparison for the palladium π radicals also gives a figure of $2500cm^{-1}$. Band A, though, shifts $3300cm^{-1}$ and $4100cm^{-1}$ for the nickel and palladium porphyrin cations respectively. The $3a_{2u}$ orbital has considerable electron density at the porphyrin meso-positions and thus it would be expected that transitions from this orbital would be greatly affected by substitution at the meso-carbon atom. Replacing a proton (MOEP) with a phenyl group

(MTPP) results in a sizeable shift in the lowest energy transition supporting the assignment of this band as a $3a_{2u} \longrightarrow 4e_g$ transition.

Further oxidation of the porphyrin cation radical to the π dication results in largely unstructured absorption in the visible region, precluding assignment. Broad absorptions are observed in most of the π dication spectra between 450 and 500nm. These absorptions are more intense than the transitions noted for the π cation radical in the similar region of the spectrum, a fact consistent with the bands arising from a $3e_g \longrightarrow 3a_{2u}$ transition (simple statistical reasoning predicts that this transition should be twice as intense for the π dication). SCF-MO calculations[104] however predict the electronic ground state of the π dication to be $^1A_{2g}$, arising from the configuration $(2e_g)^4\ (2a_{2u})^2\ (2b_{2u})^2\ (3e_g)^4\ (1a_{1u})^1\ (3a_{2u})^1$ and thus this assignment is, at best, tentative.

D_{4h} symmetry is assumed to have been retained in both the singly oxidised and the doubly oxidised porphyrin macrocycle. However the optical data for the π anion and π dianion suggest a degree of distortion from D_{4h} symmetry occurs. The addition of electrons into the porphyrin moiety has previously been viewed as the stepwise process shown below-

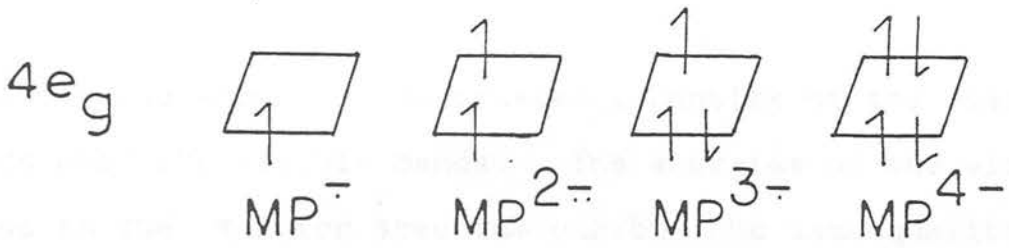

where the degeneracy of the $4e_g$ level is assumed to remain and D_{4h} symmetry is retained. We propose however electron addition proceeds as follows-

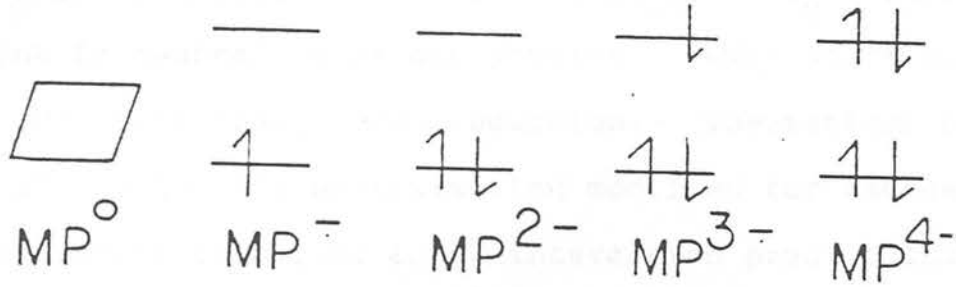

where the degeneracy of the $4e_g$ level is lifted on addition of an electron. Adding an electron to the lowest unfilled molecular orbital would result in a ^2Eg ground state and excited states of $^2A_{1u}$, $^2A_{2u}$, $^2B_{1u}$ and $^2B_{2u}$ symmetry if the anion radical retains D_{4h} symmetry. The lowest energy transition is predicted[27] to be $4e_g \longrightarrow 2b_{1u}$. However analysis of the energy of this band for both $MOEP^-$ and $MTPP^-$ shows it to depend to some extent on the metal centre (eg for $ZnTPP^-$ the band occurs at 11,000cm$^-$ and for $PdTPP^-$, 11,400cm^{-1}). Thus this transition must have some metal character and mix with the a_{1u} $a_{2u} \longrightarrow e_g$ transitions responsible for the typical metalloporphyrin spectrum. Configurational interaction must then also be present for the transitions of the monoanion radical.

This is also shown by the greater intensity of the near uv bands over the visible bands. The energies of the visible bands in the π anion spectrum exhibit the same qualitative trend as the Q band of the neutral metalloporphyrins. A constant energy difference between the two lowest energy transitions ($\sim 1400 cm^{-1}$) suggests both originate from the same orbital i.e. $4e_g$. The bands in the 740 - 600nm range must arise primarily from the $3a_{2u}\ 1a_{1u} \longrightarrow 4e_g$ transitions present in neutral metalloporphyrins. They shift significantly to lower energy upon reduction. Theoretical calculations[27] in the PPP approximation modified for radicals[106] and including configurational interaction predict that <u>two</u> electronic states, $^2A_{1u}$ and $^2B_{2u}$, are responsible for these absorptions. In the spectrum of $ZnTPP^{\cdot-}$ two distinct absorptions are noted in this region (Figure 9). The band at 550nm in this spectrum is tentatively assigned as a triplet transition of the monoanion radical Soret band. The intense absorption in the Soret region is calculated[27] to arise from four electronic transitions ($^2A_{1u}$, $^2A_{2u}$, $^2B_{1u}$ and $^2B_{2u}$). The same calculations predict the total intensity of the monoanion to be less than that of the neutral porphyrin. Here, we observe the total intensity of the monoanion is <u>greater</u> than that of the parent compound. The ground state of the monoanion is of course Jahn-Teller[107] unstable and formally forbidden transitions may gain intensity by coupling of electronic and vibrational motion of the molecules. Maslov[108]

has reported that the polarisation of the first electronic transition for the Zn etioporphyrin anion radical is the same as that found in the intense Soret absorption. This observation is consistent with only one component of the ^2Eg ground state contributing to the transition, which in turn implies a distorted geometry for the anion. We, in fact, note a significant splitting of the Soret band into two separate electronic transitions in CH_2Cl_2/0.5M $TBABF_4$ medium. The high energy band (S') occurs at almost exactly the same energy as the parent porphyrin Soret band and the less intense lower energy band (S) occurs at 1000 - 1200cm^{-1} to the red. The degree of splitting is dependent upon the metal suggesting the higher energy band is not merely a vibrational overtone of band S. The π anion radical spectra are also temperature independent (-70° to 20°C). These observations are consistent with the doubly-degenerate $4e_g$ orbital splitting and consequently two transitions, one to the semi-occupied orbital and another to the empty orbital at higher energy can occur. The red shift of band S, as compared to the energy of the parent porphyrin Soret band, is consistent with the energy of the π * anti-bonding orbital decreasing in energy on addition of an electron. Whereas some evidence for distortion exists for the porphyrin π monoanion radical, the optical properties of the doubly reduced π dianion can only be explained by invoking a departure from D_{4h} symmetry. PPP calculations[27] predict that the π dianion (D_{4h}) should

display a very strong band at high energy (Soret region) a weak band in the visible and absorption of medium intensity in the far red. We note from the optical spectra of the π dianion

1) Strong absorption in the Soret region but only twice as intense as the visible bands and
2) There is no evidence of transitions in the far red.

The ground state of the dianion is predicted[27] to be the triplet state which is calculated to be 1,600cm^{-1} more stable than the singlet state. The energy gap separating each of the four reductions of CuTPP, NiTPP and ZnTPP were noted as -0.4V, -0.7V and -0.4V. This voltammetric pattern indicates that at the second and fourth reductions spin-pairing occurs, the resulting spin-spin repulsion term being reflected in the $E_{\frac{1}{2}}$ values. The ESR evidence also suggests the ground-state is a singlet. Figure 42 shows the in situ monitoring of the second reduction of PdTPP. No broadening of the mono-anion isotropic signal occurs i.e. no triplet ESR signal was detected. An nmr spectrum[24] of $ZnTPP^{2-}$ also shows the proton resonances are not paramagnetically contact-shifted. Felton[27] has suggested in plane distortions, where alternate bonds are shortened and lengthened around the aromatic core, could occur in the dianion. These pseudo Jahn-Teller distortions would reduce the symmetry to D_{2h}. This lowering of the symmetry

Figure 3.42 ESR of a porphyrin π dianion

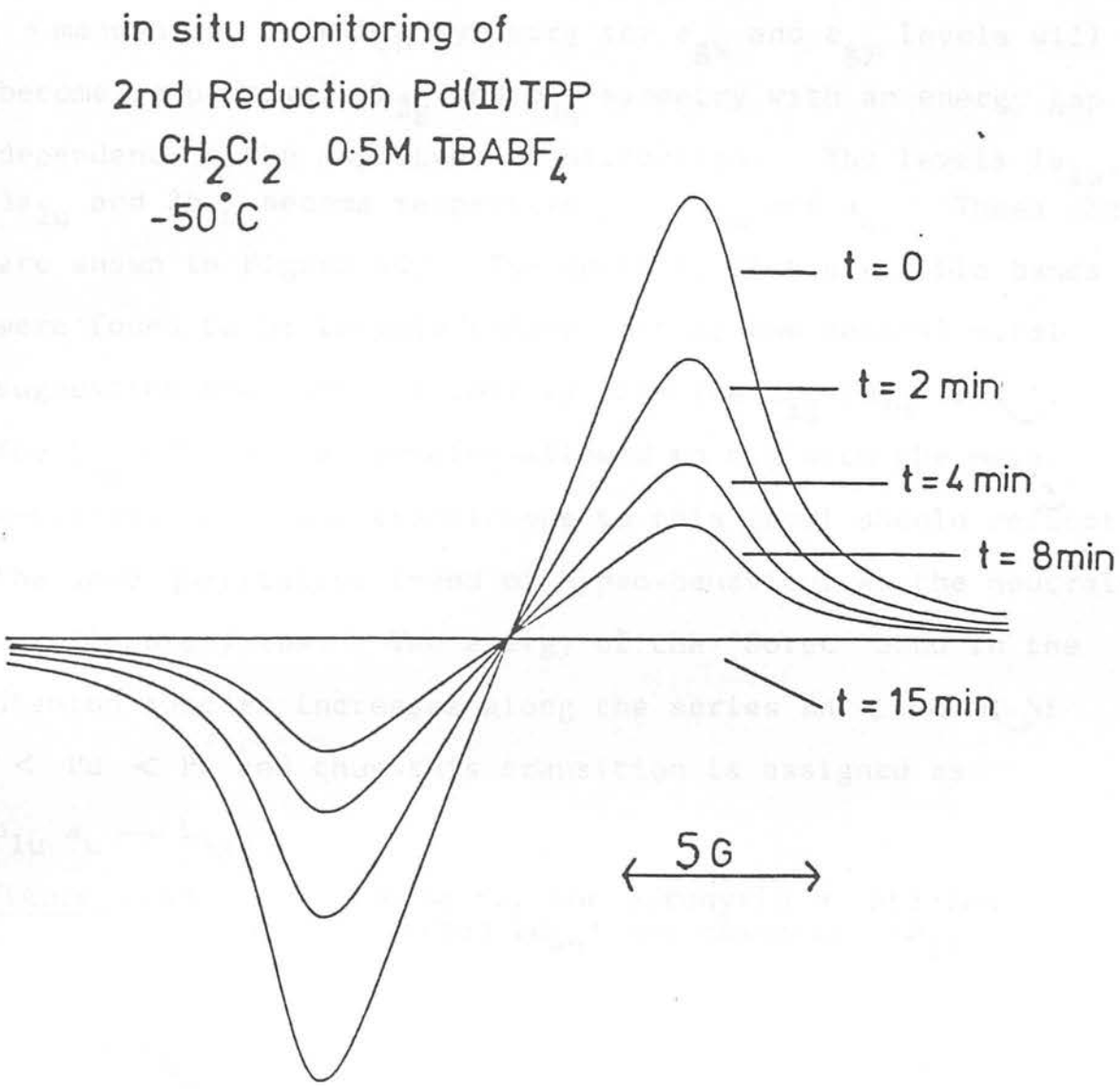

would tend to stabilise the singlet state. Interestingly the calculated splitting of the $4e_g$ level of $1400cm^{-1}$ is very close to the value obtained from the optical data for the π monoanion. In D_{2h} symmetry the e_{gx} and e_{gy} levels will become respectively b_{2g} and b_{3g} symmetry with an energy gap dependent on the magnitude of distortion. The levels $1a_{1u}$, $3a_{2u}$ and $2b_{1u}$ become respectively a_u, b_{1u} and a_u. These charges are shown in Figure 43. The energies of the visible bands were found to be largely independent of the central metal, suggesting they arise primarily from the b_{2g} (D_{2h}) level. The b_{3g} orbital is symmetry-allowed to mix with the metal d-orbitals and thus transitions to this level should reflect the same qualitative trend of hypso-behaviour as the neutral metalloporphyrins. The energy of the 'Soret' band in the dianion spectra increases along the series Zn < Cu < Ni < Pd < Pt and thus this transition is assigned as $b_{1u}\ a_u \longrightarrow b_{3g}$.

Figure 3.43 M.O. scheme for the porphyrin π dianion - undistorted (D_{4h}) and distorted (D_{2h})

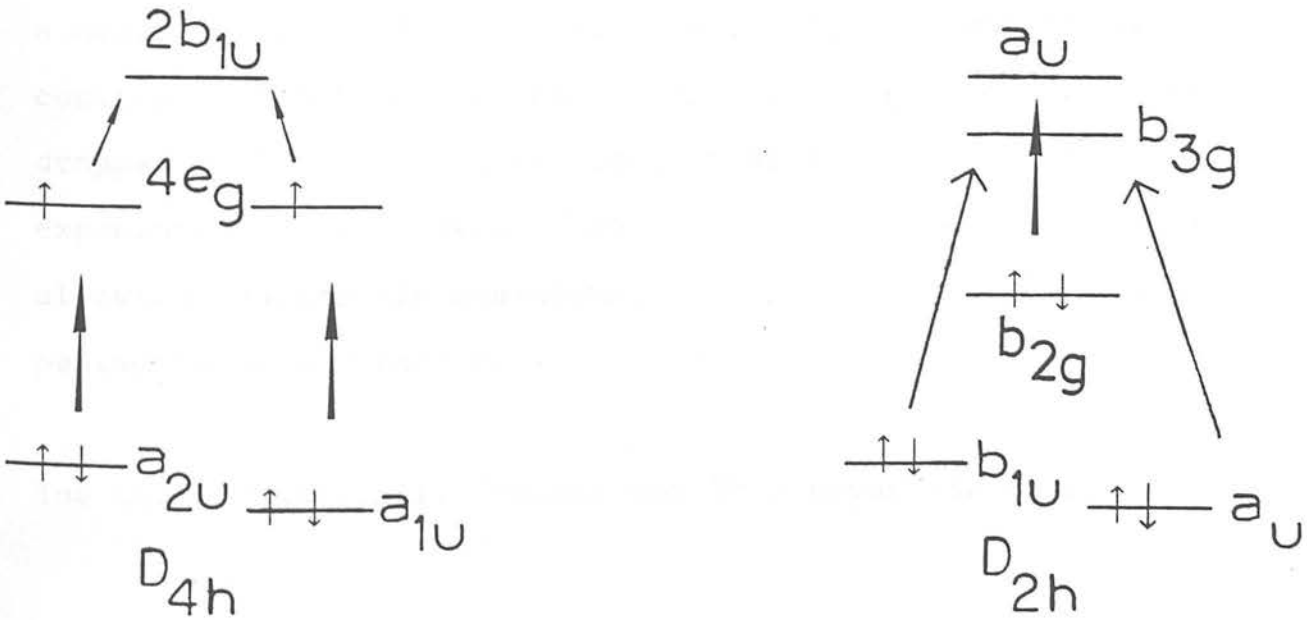

3.8 EXPERIMENTAL

Synthesis of the metalloporphyrins and basic voltammetric techniques in CH_2Cl_2/0.5M $TBABF_4$ have been described in Chapter 2. DMSO, DMF and pyridine were used without further purification. Bulk electrosyntheses were carried out in a three compartment cell as shown in Figure 44. The working electrode compartment is separated from the counter electrode compartment by two porous glass frits to prevent cross-contamination. The working electrode compartment contains a large Pt basket at which the bulk electrogeneration is carried out, a Pt mini-disc electrode to voltammetrically monitor the course of the reaction and a normal Ag/AgCl reference electrode. A large Pt basket is employed as the counter electrode to facilitate maximum current flow. Temperature control was achieved by immersing the entire cell in a methanol/dry ice slush bath. Potentials were applied using a Hi-Tek waveform generator type PPRI in conjunction with a Hi-Tek potentiostat type DT2101. Current was monitored as a function of time using a Hewlett-Packard 704A X-Y recorder. Electrogeneration was considered complete when the current flowing in the cell had dropped to less than 1% of its initial value. Classical exponential decay curves of current vs. time were integrated, allowing coulometric measurement of the number of electrons passed to an accuracy of ± 0.05 electrons.

The chilled Optically Transparent Thin Layer Electrode (OTTLE)

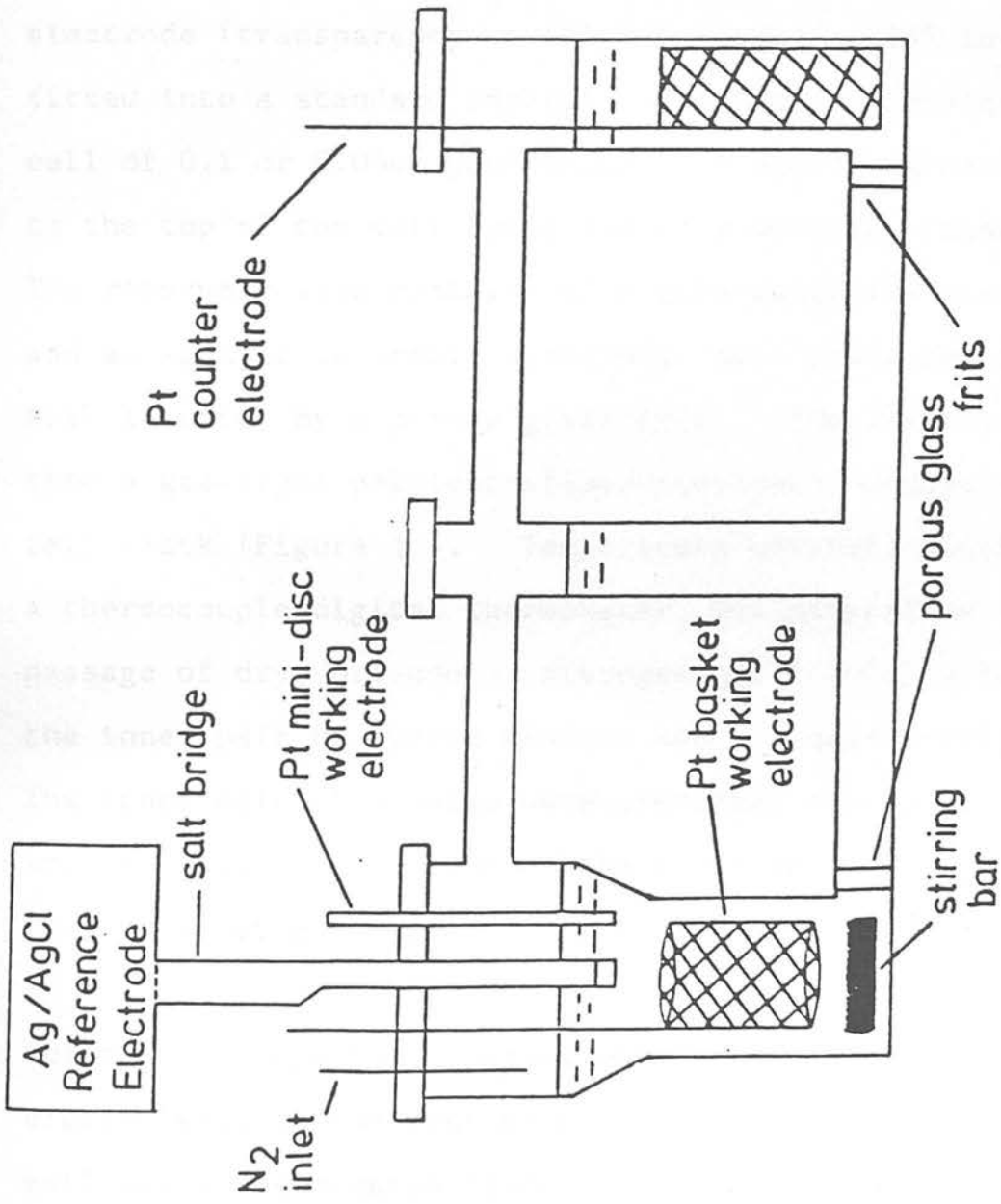

Figure 3.44 Bulk Electrogeneration cell

cell was designed and built in the Department of Chemistry, University of Edinburgh, in accordance with the original principles of Murray et al[109].

The OTTLE cell consists of a fine Pt (or Pt/Rh) gauze working electrode (transparency - 40% for Pt and - 25% for Pt/Rh) fitted into a standard Infrasil quartz uv/visible/near ir cell of 0.1 or 0.05cm pathlength. A quartz extension fitted to the top of the cell functions as a solution reservoir. The reservoir also contains a Pt wire auxiliary electrode and an Ag/AgCl reference electrode, both protected from the bulk solution by a porous glass frit. The assembly is fitted into a gas-tight poly(tetrafluoroethylene), double glazed, cell block (Figure 2). Temperature control, monitored by a thermocouple/digital thermometer, was maintained by the passage of dry, pre-cooled nitrogen gas (-70°C to 20°C) between the inner pair of quartz windows and the quartz cell assembly. The inner pair of windows were prevented from fogging by passing dry nitrogen gas between the inner and outer windows, thus preventing contact of air with any cooled surface.

Solutions of the test species were purged with dry argon and electrolysed at the mini-grid working electrode of the OTTLE cell which was mounted directly in the beam of a Pye-Unicam SP8-400 or Perkin-Elmer Lamda 9 spectrophotometer. The progress of the electrolysis was monitored both spectroscop-

ically, to the limiting spectrum, and more essentially by the decay of the current to a constant residual value. Standard practice was to return the test species to the original state by reverse electrolysis in order to ensure that the process was chemically reversible and to confirm that degradation of the complex was negligible. Importantly, these reverse electrolyses were conducted at potentials immediately (~ 200mV) cathodic (for a re-reduction) or anodic (for a re-oxidation) of the measured $E_{\frac{1}{2}}$ value of the redox couple under investigation.

Electron spin resonance measurements were carried out on a Bruker ER 200D-SRC Q band spectrometer (employing 100KHz magnetic field modulation) in conjunction with a 4107 WZ cylind rical wide-bore cavity. The cell designed for <u>in situ</u> electrogeneration is shown in Figure 45. A commercial ESR quartz tube (8 mm outside diameter; 6 mm inside diameter) is employed as the basic reaction vessel. A porous quartz frit (porosity 1) is sealed into the tube and a Quickfit B_{10} cone attached to the bottom of the tube. The quartz frit is sufficient to isolate the counter electrode compartment and prevent cross-contamination. The working electrode is a 10cm long Pt hollow tube (3mm o.d.) passed down the long axis of the cylind rical esr tube. Both the reference electrode salt-bridge (Luggin capillary) and an N_2 inlet (1mm teflon tubing) are passed down the centre of the Pt tube and

Figure 3.45 In situ ESR electrogeneration cell

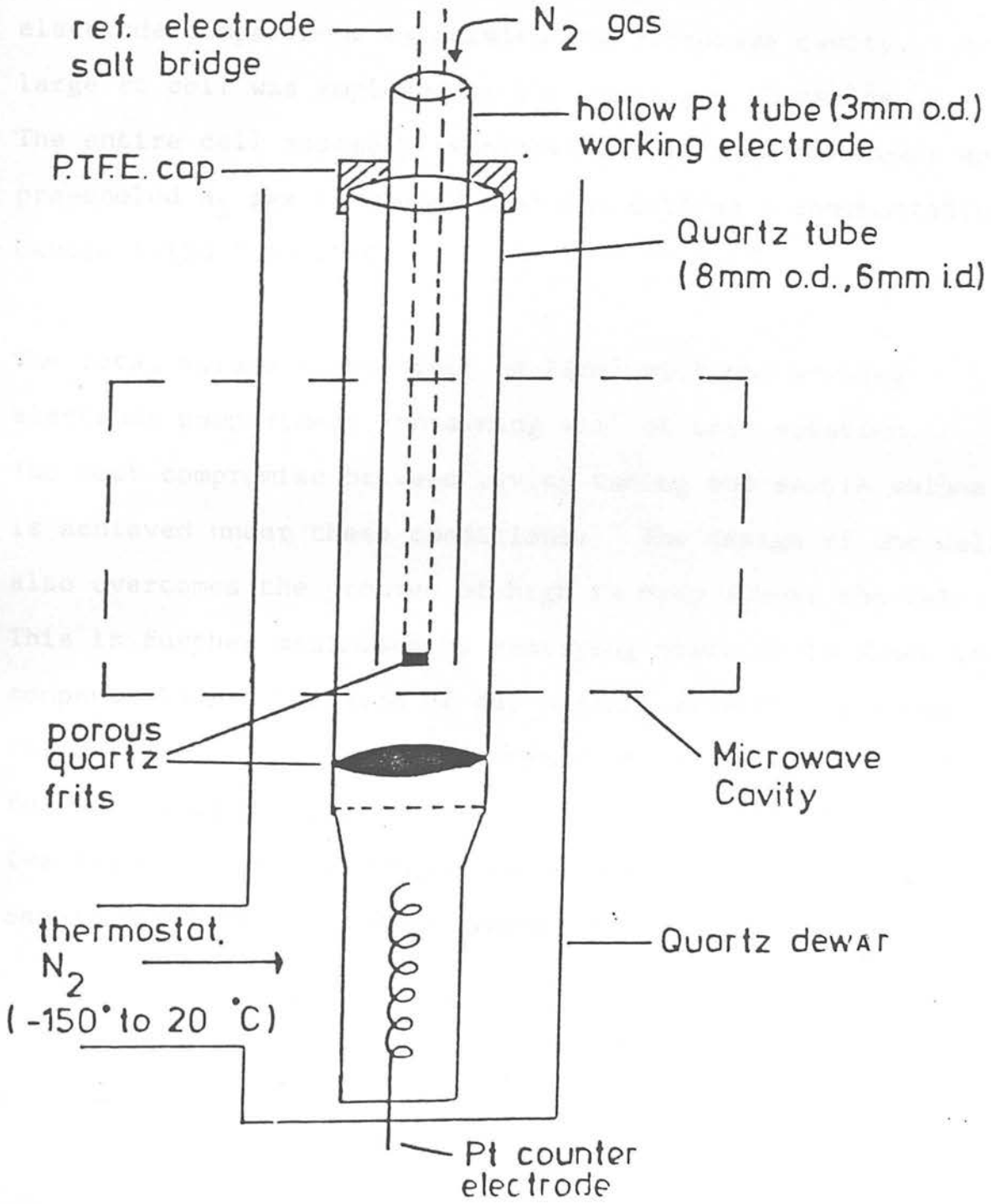

remain undetected in the microwave cavity. Efficient diffusion of the substrate to the working electrode is achieved by the slow passage of N_2 down the centre of the electrode. The counter electrode compartment is attached through a Quickfit B_{10} socket. Care was taken to ensure the entire counter electrode compartment is outwith the microwave cavity. A large Pt coil was employed as the auxiliary electrode. The entire cell assembly is placed within a quartz dewar and pre-cooled N_2 gas is passed over the cell as a thermostating device (-150°C to 20°C).

The total volume of the cell is $10cm^3$ with the working electrode compartment containing $4cm^3$ of test solution. The best compromise between cavity tuning and sample volume is achieved under these conditions. The design of the cell also overcomes the problem of high iR drop across the cell. This is further minimised by employing positive feedback ohmic compensation. The size of the working electrode and the relatively small diffusion distance to the electrode allows full electrogeneration to take place. Thus several successive electron-transfer steps can be monitored successfully. Sample concentrations were typically 5×10^{-4}M.

REFERENCES : CHAPTER 3

1. H.C. Longuet-Higgins, C.W. Rector and J.R. Platt, J. Chem. Phys., 1950, 18, 1174.
2. A. Antipas, J.W. Buchler, M. Gouterman and P.D. Smith, J. Am. Chem. Soc., 1978, 100, 3015.
3. M. Gouterman, L.K. Hanson, G.E. Khalil, W.R. Leenstra and J.W. Buchler, J. Chem. Phys., 1975, 62, 2343.
4. M. Symons, "Chemical and Biochemical Aspects of E.S.R.", Van Nostrand Rheinold, England, 1978.
5. H.M. Swartz, J.R. Bolton and D.C. Borg, "Biological Applications of E.S.R.", Wiley (Interscience), New York, N.Y., 1972.
6. "E.S.R. of Metal Complexes", Ed Te Fu Yen, Plenum Press, New York, N.Y., 1969.
7. A. MacCragh, C.B. Storm and W.S. Voski, J. Am. Chem. Soc., 1965, 87, 1470.
8. J. Fajer, D.C. Borg, A. Forman, A.D. Adler and V. Vareldi, J. Am. Chem. Soc., 1974, 96, 1238.
9. Yu. V. Glazkov, P.V. Kuzulov and A.M. Shul'ga, Zh. Prikl. Spectrosk, 1973, 18, 320.
10. J. Fajer and M.S. Davis, "The Porphyrins", Ed. D. Dolphin, Academic Press, New York, N.Y., 1969, Chapter 4.
11. Yu V. Glazkov, A.G. Zhurzalev, P.V. Kuzovkov and A.M. Shul'ga Zh. Prikl. Spectrosk., 1973, 19, 305.
12. D. Lexa and M. Reix, J. Chim. Phys., 1974, 71, 24.

13. A. Forman, D.C. Borg, R.H. Felton and J. Fajer, J. Am. Chem. Soc., 1971, 93, 2790.

14. J. Fajer, D.C. Borg, A. Forman, R.H. Felton, L. Vegh and D. Dolphin, Ann. N.Y. Acad. Sci., 1973, 206, 349.

15. Yu. V. Glazokov, P.V. Kuzulov and A.M. Shul'ga, Zh. Prikl. Spectrosk., 1973, 18, 117.

16. D. Dolphin, A. Forman, D.C. Borg, J. Fajer and R.H. Felton, Proc. Nat. Acad. Sci., U.S., 1971, 68, 614.

17. L.D. Spaulding, R.G. Filler, J.A. Bertrand and R.H. Felton, J. Am.Chem. Soc., 1974, 96, 982.

18. K.M. Kadish, M.M. Morrison, L.A. Constant, L. Dickens and D.G. Davis, J. Am. Chem. Soc., 1976, 98, 8387.

19. M.H. Barley, J.Y. Becker, G. Domazetis, D. Dolphin and B.R. James, J. Chem. Soc. Chem. Commun., 1981, 982.

20. M.H. Barley, J.Y. Becker, G. Domazetis, D. Dolphin and B.R. James, Can. J. Chem., 1983, 61, 2389.

21. C.M. Guzy, J.B. Raynor, L.P. Stodulski and M.C.R. Symons, J. Chem. Soc., 1969, 997.

22. R.H. Felton and H. Linschitz, J. Am. Chem. Soc., 1966, 88, 1113.

23. V.G. Maslov, Opt. Spectrosc., 1974, 37, 580.

24. G.L. Closs and L.E. Closs, J. Am. Chem. Soc., 1963, 85, 818.

25. V.E. Kholmogorov and V.G. Maslov, Opt. Spectrosc., 1975, 31, 195.

26. M. Zerner, M. Gouterman and H. Kobayashi, Theor. Chim. Acta., 1966, 6, 363.

27. R.H. Felton, PhD. Thesis, Harvard University, U.S.A., 1964.

28. J.-H. Fuhrhop, "Porphyrins and Metalloporphyrins" Ed. K.M. Smith, Elsevier, Amsterdam, 1975, Chapter 14.

29. G.A. Heath, L.J. Yellowlees and P.S. Braterman, J. Chem. Soc., Chem Commun., 1981, 287.

30. W.J. Aubrey, R.G. Compton and C.C. Jones, J. Am. Chem. Soc., 1984, 106, 469.

31. R.N. Bagchi, A.M. Bond, G. Brain, R. Colton, T.L.E. Henderson and J.E. Kevekordes, Organomet., 1984, 3, 4.

32. A. Wolberg and J. Manssen, J. Am. Chem. Soc., 1970, 92, 2983.

33. M. Gouterman, J. Mol. Spectrosc., 1961, 6, 138.

34. J.-H. Fuhrhop, "Porphyrins and Metalloporphyrins", Ed. K.M. Smith, Elsevier, Amsterdam, 1975, Chapter 15.

35. R.H. Campbell, G.A. Heath, G.T. Hefter and R.C.S. McQueen, J. Chem. Soc., Chem. Commun., 1983, 1123.

36. R.C.S. McQueen , PhD. Thesis, Edinburgh University, 1983.

37. K.M. Kadish, K.L. Thomson, D. Berioz, L.A. Bottomley in "Electrochemical Studies of Biological Systems", A.C.S. Symposium Series 38, Washington, 1977, 51.

38. D.M. Collins and J.L. Hoard, J. Am. Chem. Soc., 1970, 92, 3761.

39. M. Nappa and J.S. Valentine, J. Am. Chem. Soc., 1978, 100. 5075.

40. J.-H. Fuhrhop and D. Mauzerall, J. Am. Chem. Soc., 1968, 90, 3875.

41. J. Fajer, D.C. Borg, A. Forman, D. Dolphin and R.H. Felton J. Am. Chem. Soc., 1970, 92, 3451.

42. J.-H. Fuhrhop, P. Wasser, D. Reisner and D. Mauzerall, J. Am. Chem. Soc., 1972, 94, 7996.

43. K.H. Hausser and J.N. Murrel J. Chem. Phys., 1957, 27, 500.

44. V.A. Umrikhin and Z.P. Gribova, Biofizika, 1974, 19, 640.

45. G.M. Cheniae, Annu. Rev. Plant. Physiol., 1970, 21, 467.

46. J. Manassen and A. Wolberg, J. Am. Chem. Soc., 1970, 92, 2982.

47. J.-H. Fuhrhop and D. Mauzerall, J. Am. Chem. Soc., 1969, 91. 4174.

48. K.M. Kadish, D.G. Davis and J.-H. Fuhrhop, Angew. Chem., Int. Ed., Engl. 1972, 11, 1014.

49. M.E. Jamin and R.T. Iwamoto, Inorg. Chim. Acta., 1978, 27, 135.

50. J.-H. Fuhrhop, Struct. Bonding (Berlin), 1974, 18, 1.

51. A. Stanienda and G. Biebl, Z. Phys. Chem (Frankfurt am Main) [N.S.], 1967, 52, 254.

52. A. Antipas, D. Dolphin, M. Gouterman and E.C. Johnson, J. Am. Chem. Soc. 1978, 100, 7705.

53. F.K. Kneubuhl, W.S. Koski and W.S. Daughey, J. Am. Chem. Soc., 1961, 83, 1607.

54. E.M. Roberts and W.S. Koski, J. Am. Chem. Soc., 1960 82, 3006.

55. E.B. Fleischer and A. Laszlo, Inorg. Nuc. Chem. Lett., 1969, 5, 373.

56. G.D. Dorough, J.R. Miller and F.M. Huennekens, J. Am. Chem. Soc., 1951, 73, 4315.

57. M.R. Low, unpublished results.

58. R.L. Ake and M. Gouterman, Theor. Chim. Acta., 1969, 15, 20.

59. D. Karweik, N. Winograd, D.G. Davis and K.M. Kadish, J. Am. Chem. Soc., 1974, 96, 591.

60. Y. Niwa, J. Chem. Phys., 1975, 62, 737.

61. D.A. Case and M. Karplus, J. Am. Chem. Soc., 1977, 99, 6182.

62. R.R. Gagné, J.L. Allison and G.C. Lisensky, Inorg. Chem., 1978, 17, 3563.

63. W.C. Lin, "The Porphyrins" Ed. D. Dolphin, Academic Press (1980) Vol IV p. 358.

64. C.M. Guzy, J.B. Raynor and M.C.R. Symons, J. Chem. Soc., 1969, A2299.

65. W.E. Blumberg and J. Peisach, J. Biol. Chem., 1965, 240, 870.

66. M. Zerner and M. Gouterman, Theor. Chim. Acta., 1966, 4, 44.

67. A. Wolberg and J. Manassen, Inorg. Chem., 1970, 9, 2365.

68. D. Dolphin, T. Niem, R.H. Felton and I. Fujita, J. Am. Chem. Soc., 1975, 97, 5288.

69. K.M. Kadish and M.M. Morrison, Inorg. Chem. 1976, 15, 980.

70. N.E. Tokel-Takvoryan and A.J. Bard, Chem. Phys. Lett., 1974,25, 235.

71. F.A. Cotton and G. Wilkinson, "Advanced Inorganic Chemistry", Wiley, U.S.A., 1972, 3rd Edition, p. 115.

72. T.V. O'Halloran and S.J. Lippard, Isr. J. Chem., 1985, 25, 130.

73. R. Uson, J. Fornies, M. Tomas, B. Menjon, K. Sunkel and R. Bau, J. Chem. Soc., Chem. Commun., 1981, 751.

74. H. Endres, H.J. Keller, H. van de Sand and V. Dong, Z. Naturforsch, Teil B., 1978, 33, 843.

75. H.A. Boucher, G.A. Lawrence, P.A. Lay, A.M. Sargeson, A.M. Bond, D.F. Sangster and J.C. Sullivan, J. Am. Chem. Soc., 1983, 105, 4652.

76. A.J. Blake, R.O. Gould, A.J. Holder, T.I. Hyde, A.J. Lavery, M.O. Odulate and M. Schroder, J. Chem. Soc., Chem. Commun., 1987, 118.

77. D. Eastwood and M. Gouterman, J. Mol. Spectrosc., 1970, 35, 359.

78. H.A.O. Hill, J.M. Pratt and R.J.P. Williams, J. Chem.Soc., 1964, 5149.

79. H. Kobayashi, T. Hara and Y. Kaizu, Bull. Chem. Soc. Jpn., 1972, 45, 2148.

80. H.W. Whitlock and B.K. Bower, Tetrahedron Lett., 1965, 4827.

81. D.V. Stynes, H.C. Stynes, B.R. James and J.A. Ibers, J. Am. Chem. Soc., 1973, 95, 1796.

82. L.A. Truxillo and D.G. Davis, Anal. Chem., 1975, 47, 2260.

83. F.A. Walker, D. Beroiz and K.M. Kadish, J. Am. Chem.Soc., 1976, 98, 3484.

84. M. Gouterman, "The Porphyrins" Ed. D. Dolphin, Academic Press (1980), Vol III, p.1.

85. N.S. Hush and I.S. Woolsey, J. Am. Chem. Soc., 1972, 94, 4107.

86. R.W. Hay, "Bio-inorganic Chemistry", Wiley, New York, N.Y., 1984.

87. D.P. Rillema, C.M. Wicker, Jr., R.D. Morgan, L.F. Barringer and L.A. Scism, J. Am. Chem. Soc., 1982, 104, 1276.

88. M.J. Carter, D.P. Rillema and F. Basolo, J. Am. Chem.Soc. 1974, 96, 392.

89. D.T. Sawyer and J.L. Roberts, "Experimental Electrochemistry of Chemists", Wiley, New York, N.Y., 1974.

90. R.B. Woodward, Angew. Chem., 1960, 72, 651.

91. H.W. Whitlock and M.Y. Oester, J. Am. Chem. Soc., 1973, 95, 5738.

92. D. Dolphin, R.H. Felton, D.C. Borg and J. Fajer, J. Am. Chem. Soc., 1970, 92, 743.

93. G.S. Smith, PhD Thesis, Edinburgh University, 1987.

94. G.H. Barnett, M.F. Hudson, S.W. McCombie and K.M. Smith, J. Chem. Soc., Perkin Trans 1, 1973, 691.

95. D. Dolphin, Z. Muljiani, K. Rousseau, D.C. Borg, J. Fajer and R.H. Felton, Ann. N.Y. Acad. Sci., 1973, 206, 177.

96. J.A.S. Cavaleiro and K.M. Smith, J. Chem. Soc., Perkin Trans. 1., 1973, 2149.

97. G.H. Barnett, B. Evans and K.M. Smith, Tetrahedron., 1975, 31, 2711.

98. J.L. Hoard "Porphyrins and Metalloporphyrins", Ed. K.M. Smith, Elsevier, Amsterdam, 1975, Chapter 8.

99. C.H. Kirksey, P. Hambright and C.B. Storn, Inorg. Chem., 1969, 8, 2141.

100. "Handbook of Chemistry and Physics" Ed. R.C. Weast, CRC Press, 1974, F. 198.

101. M.L. Schneider, J. Chem. Soc., Dalton Trans., 1972, 1093.

102. Von. R. Hoppe and R. Homann, Zeit. Anorg. Allge. Chem., 1970, 379, 193.

103. L.D. Spowlding, P.G. Eller, J.A. Bertrand and R.H. Felton, J. Am. Chem. Soc., 1974, 96, 982.

104. J. Fajer, D.C. Borg, A. Forman, D. Dolphin and R.H. Felton, J. Am. Chem. Soc., 1970, 92, 3451.

105. M. Gouterman, G.H. Wagniere and L.C. Snyder, J. Mol. Spectrosc., 1963, 11, 108.

106. H.C. Longuet-Higgins and J. Pople, Proc. Phys. Soc., (London), 1955, A68, 591.

107. H.A. Jahn and E. Teller, Proc. Roy. Soc (London), 1937, A.161.

108. V.G. Maslov, Opt. Spectrosc., 1976, 40, 275.

109. W.R. Heinemann, R.W. Murray and G.W. O'Dom, Anal. Chem. 1973, 45, 165.

CHAPTER 4 : THE ELECTROCHEMICAL BEHAVIOUR OF SOME IRON AND RUTHENIUM PORPHYRINS

4.1 INTRODUCTION

By far the most important metalloporphyrins in biological systems are the iron complexes. They are the prosthetic groups of such haemoproteins as haemoglobin, myoblogin, cytochromes, catalases, and some peroxidases. The haemoproteins are responsible for the transportation and storage of oxygen, the transfer of electrons in the 'respiratory chain', hydrogen peroxide elimination, and possibly as intermediates in the formation of high energy bonds in the mitochondria.

The use of synthetic porphyrins and metalloporphyrins such as Fe(II) OEP and Fe(II) TPP to model these naturally occurring porphyrin systems is well established[1-3]. Interest has increased recently in the ruthenium analogues of these compounds, as otherwise reactive intermediates are expected to be more stable for the ruthenium complexes than for the iron complexes.[4,5] This is particularly relevant in the study of porphyrin cation radicals, which have been suggested as intermediates in a number of natural porphyrin systems such as cytochrome P450[6] and horse-radish peroxidase[7].

It is surprising then that the oxidation of iron porphyrins

is still an area of current interest and controversy. The anodic behaviour of ferric porphyrins in particular has led to much disagreement in the literature. It has been reported[8] that Fe(III)TPPCl yields a π -cation radical at the first oxidation wave on the basis of the measured magnetic susceptibility (S = 1). A subsequent, contrary, view of the electron distribution in the oxidised product has been advanced by Felton et al[9]. They assigned the oxidation product of ferric porphyrins as an Fe(IV) species (Fe(IV) PCl (ClO_4); P = TPP, OEP).

The Fe(IV) assignment was based on the electronic spectrum of the oxidised product, where the oscillator strength of the Soret band was noted to change less than was observed for formation of a genuine cation radical ($ZnTPP^{+\cdot}$), and there was an apparent lack of characteristic π cation radical visible bands. The magnetic susceptibility (200 - 300 K) measured by Felton of S = 2 was also quite different from the previous measurement.

The proposed change from d^5 (S = 5/2) ferric ion to a d^4(S = 2) tetravalent iron with weak ligands (Cl^- and ClO_4^-) is perhaps not surprising. However if the oxidised species were $Fe(III)P^{+\cdot}$, then antiferromagnetic exchange coupling between the five iron spins and the porphyrin ring spin would also yield S = 2. This coupling picture results in a spin pairing

of the ring π electron and one of the iron d electrons and this might also explain the observed nmr results[9], where the shift of the proton resonances was smaller than expected for the formation of a π cation radical.

Supporting the Fe(IV) assignment, Kadish et al[10] report Fe(III) TPPCl to undergo three one-electron oxidations in CH_2Cl_2 (at 1.14, 1.42 and 1.63V vs. SCE). They attribute the order of oxidation as-

$$\text{Fe(III) TPPCl} \xrightarrow{-e^-} (\text{Fe(IV) TPPCl})^{+} \xrightarrow{-e^-} (\text{Fe(IV) TPP}^{\cdot+}\text{Cl})^{2+} \xrightarrow{-e^-} (\text{Fe(IV) TPP}^{2+}\text{Cl})^{3+}$$

In direct contrast a recent study[11] on twelve Fe(III) TPPX species found $E_{\frac{1}{2}}$ (1st ox) to be virtually independent of the charge and ligand character of the axial ligand (X). The iron electronic structure is known to be affected by these parameters and if indeed the first oxidation was metal-based a greater dependence of $E_{\frac{1}{2}}$ (1st ox) on X would have been expected.

The one-electron oxidation product of the μ-oxo dimer $(Fe(III)TPP)_2O$ has been assigned[12] as containing the unit $(Fe(IV) - O - Fe(III))^+$. Extended Huckel calculations[13] on the μ -oxo-dimer shows strong mixing of oxygen 2p orbitals with Fe d_{xz} and d_{yz} orbitals. Thus the added charge in the

oxidised complex can be envisaged as being stabilised by distribution over three centres. The assignment also finds support in the preparation of an isoelectronic TPP Fe(III)-N-Fe(III) TPP dimer[14].

We report here on a reinvestigation of the anodic electrochemistry of the monomers Fe(III) TPPCl and Fe(III) OEPCl in non-coordinating media. We find both undergo two one-electron oxidations, the products of which are best described as the stepwise formation of π cation radicals and π dications.

Anodic studies on ruthenium porphyrins have thus far been limited to Ru(II)(P)(CO)L and Ru(II)(P)L_2 complexes; where L = pyridine, CH_3CN, THF and PR_3 : P = OEP, TPP[15-18]. Oxidation of the L_2 species is reported to give a Ru(III) complex[15]. In contrast, the complexes incorporating CO undergo a one-electron oxidation to give a π cation radical. This assignment was based largely on the small changes occurring in $\bar{\upsilon}_{CO}$ during oxidation (15 - 33cm^{-1}). (The site of the one electron oxidation of Os(II) OEPCO is the metal[16] and $\bar{\upsilon}_{CO}$ shifts considerably from 1898 cm^{-1} to 2014cm^{-1}).

Rillema et al.[18] have assigned a second oxidation of Ru(II) TPPCO in CH_2Cl_2 as a $Ru^{II/III}$ couple. The assignment was based primarily on the potential separation of the first and second wave (0.42V), which was considered to be larger than that

observed for successive oxidations of the porphinato moiety. This argument has been used extensively in porphyrin electrochemistry for many years, the accepted limits, as set down by Fuhrhop[19], being 290±50mV between the oxidation steps. However, as was shown in Chapter 2, this gap can be much larger for the second and third row transition-metal complexes. This then seriously undermines the assignment of the second oxidation as a $Ru^{II/III}$ couple and reopens the question as to whether the subsequent oxidation of the cation radical is metal or ligand-based. It was proposed therefore to study afresh the electrochemistry of both Ru(II) TPPCO and Ru(II)OEPCO in non-coordinating media and attempt to elucidate the site of oxidation throughout.

The cathodic electrochemistry of Fe(III)TPPCl in aprotic media (DMF, DMSO) is rather better defined than the oxidative sequence. Three one-electron reductions are reported[20-22], the first two of which have been assigned as metal-based processes. The $Fe^{III/II}$ couple, central to the bioactivity of cytochromes, has been well documented[23] for other model systems of the general formula Fe(III) TPPX (where X = Br^-, SCN^-, OEt^-, OH^-). Chemical reduction at the second wave in DMF yields an Fe(I) species[24], characterised by its magnetic moment at 77K ($S = \frac{1}{2}$) and ESR spectrum. The third reduction has not been fully investigated but the product has tentatively been assigned[24] as ($Fe(I)\ TPP^{\cdot-}$).

The sequence of electrocnemical reduction of $(Fe(III)\ TPP)_2O$ in DMF has been investigated by d.c. and cyclic voltammetry[25]. At the first reduction dimer cleavage occurs, with uptake of two electrons and one proton, resulting in Fe(II) TPP and $(Fe(II)\ TPP\ OH)^-$. A transient intermediate in this reduction step snows an ESR signal with a g value of 1.95 at 77K and has been assigned as tne mixed $(Fe(II)\ Por-O-Fe\ (III)\ Por)^-$ dimer, prior to cleavage.

The reduction site of Ru(II) TPPCO has been reported[18] as being macrocycle-based solely upon the measured value of ΔE(1st ox/1st red) of 2.19V. However the possible stabilisation of Ru(I) in the reduced complex has also been recently proposed[26].

The cathodic electrochemistry of Fe(III) TPPCl, Fe(III) OEPCl, Ru(II) TPPCO and Ru(II) OEPCO in CH_2Cl_2 is reported here. The iron porpnyrins exhibit four one electron reductions, the first two of which are assigned as metal-based and tne latter two, macrocycle-based. The ruthenium porphyrins exhibit only one irreversible reduction in CH_2Cl_2. In DMSO however two reductions are observed both of which are assigned as macrocycle-based redox steps.

In addition we also report on the electrochemical behaviour of the ruthenium μ-oxo dimers $(Ru(IV)\ TPPOH)_2O$ (1) and $(Ru(IV)\ OEP\ OH)_2O$.

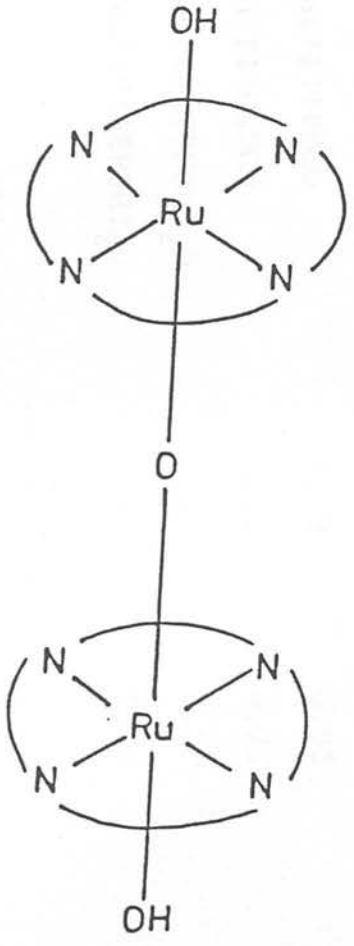

(I)

Table 1 lists the redox potentials for all the iron and ruthenium porphyrins studied.

4.2 ANODIC ELECTROCHEMISTRY OF FERRIC PORPHYRINS

Both Fe(III)TPPCl and Fe(III)OEPCl exhibit two oxidations in CH_2Cl_2/0.5M $TBABF_4$ values for which are listed below-

	$E_{\frac{1}{2}}$(1st ox)/V*	$E_{\frac{1}{2}}$(2nd ox)/V	ΔE(1st ox/2nd ox)
Fe(III)TPPCl	0.87	1.16	0.29
Fe(III)OEPCl	0.70	1.12	0.42

*Volts vs Ag/AgCl

Table 4.1 Redox Potentials of some Iron and Ruthenium Porphyrins in CH_2Cl_2/0.5M $TBABF_4$ at 20°C (Volts vs Ag/AgCl)

	$E_{\frac{1}{2}}$(2nd ox)	$E_{\frac{1}{2}}$(1st ox)	$E_{\frac{1}{2}}$(1st red)	$E_{\frac{1}{2}}$(2nd red)	$E_{\frac{1}{2}}$(3rd red)	$E_{\frac{1}{2}}$(4th red)
Fe(III)TPPCl	1.16	0.87	-0.59	-1.32	-1.91	-2.33
Fe(III)OEPCl	1.12	0.70	-0.63	-1.44	-2.03	-2.46
Ru(II)TPPCO	1.33	0.92	-1.58+	-	-	-
Ru(II)OEPCO	1.25	0.72	-1.79+	-	-	-
$(Ru(IV)TPPOH)_2O$	-	1.09	0.20	-1.22	-1.98+	-
$(Ru(IV)OEPOH)_2O$	-	0.08	0.11	-1.20	-2.06+	-

+ irreversible

Coulometry (at -40°C) shows all the oxidative steps to be diffusion-controlled, one-electron, reversible steps. Figure 1 shows the a.c. and cyclic voltammograms of Fe(III) OEPCl at room temperature. A third oxidation wave for Fe(III) TPPCl at 1.36V is observed at room temperature (as reported by Kadish[10]). However this wave was not present at -40°C and is thus assigned as arising from a by-product of the second oxidation which is not fully reversible at room temperature. This is confirmed by bulk electrogeneration, at room temperature, at the plateau of the second oxidation wave of Fe(III) TPPCl. This gives rise to a product which is itself oxidised at +1.36V. The identity of this product will be discussed later.

The first oxidation of both ferric porphyrins exhibits classical voltammetric behaviour for a fully reversible one-electron step at room temperature. Plots of Ip vs $W^{\frac{1}{2}}$ (a.c. frequency dependence) and Ip vs $v^{\frac{1}{2}}$ (cyclic voltammetry sweep rate dependence) are linear and (Epc - Epa) was found to equal 59mV in both cases (see section 2.5).

The $E_{\frac{1}{2}}$ (1st ox) values for the ferric porphyrins are more anodic than any of the corresponding metalloporphyrins studied in Chapter 2, reflecting the greater positive charge at the metal centre. Comparisons with these metalloporphyrins are however non-informative as to the site of oxidation, due to

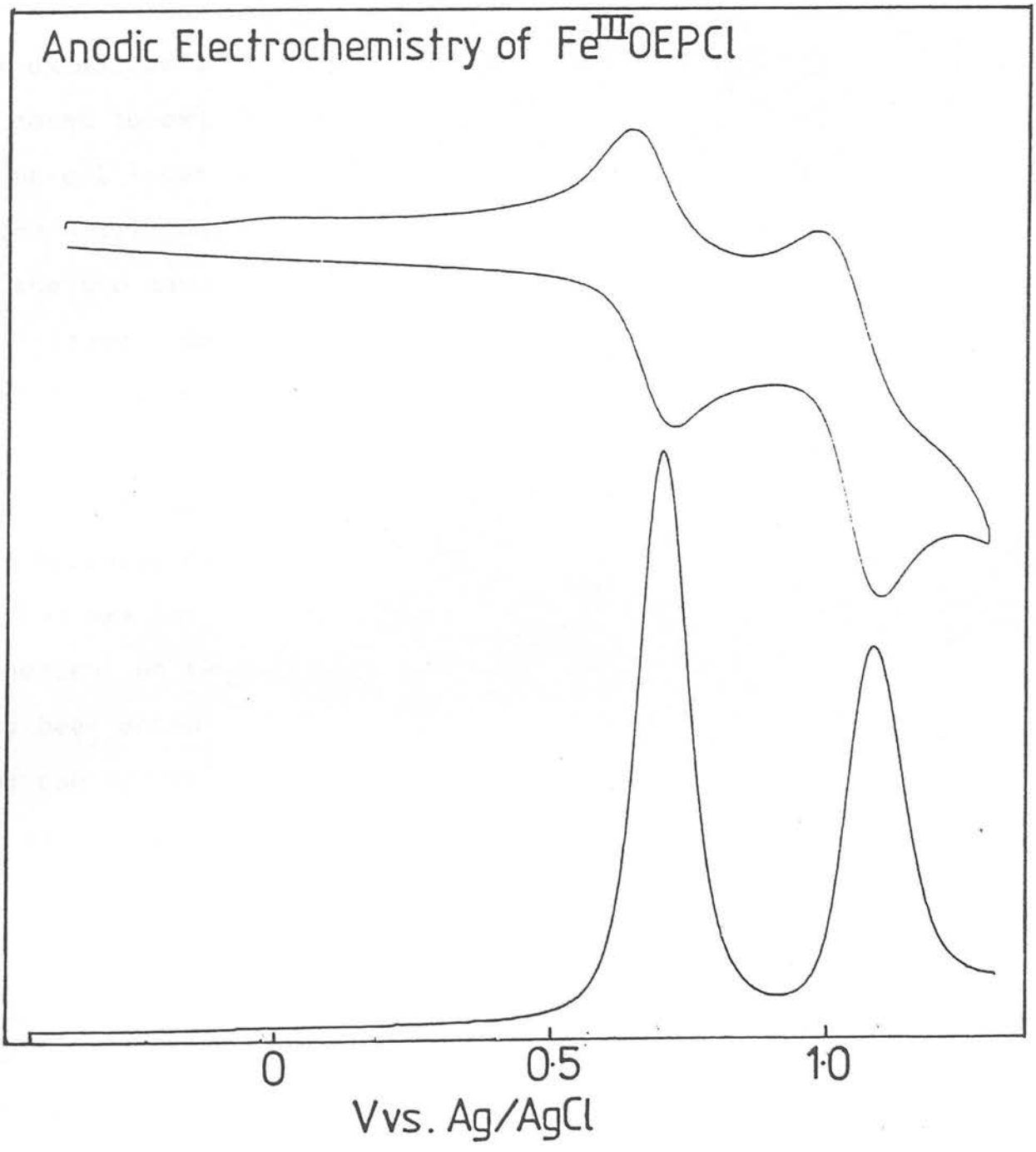

Figure 4.1 Oxidative redox chemistry of Fe(III)OEPCl in CH_2Cl_2/0.5M $TBABF_4$

the presence of the axially-coordinated chloride ion. An internal comparison of $E_{\frac{1}{2}}$ (1st ox) between the two iron porphyrins though, does offer indirect evidence as to whether the oxidation is macrocycle or metal-based. Fe(III) OEPCl is noted to oxidise more easily than Fe(III) TPPCl by 170mV. Identical internal comparisons for the other first-row transition metal porphyrins, reflecting the different basicities of the two macrocycles, give rise to similar values (e.g. Zn : 160mV; Cu : 190 mV). This then indicates that oxidation of the iron porphyrins might well be based at the ring. Further the value of $E_{\frac{1}{2}}$ (2nd ox) for the two ferric porphyrins leads us to conclude that both the first and second oxidations are macrocycle-based. Although we have shown $\Delta E_{\frac{1}{2}}$ (1st ox/2nd ox) for two successive macrocycle oxidations is strongly dependent on the 'fit' of the metal in the macrocycle, it has been noted that $\Delta E_{\frac{1}{2}}$ (1st ox/2nd ox) is generally larger for the OEP ring than the TPP ring (see Chapter 2). This is again the case here, where ΔE(1st ox/2nd ox) is 100mV larger for Fe(III) OEPCl than Fe(III) TPPCl. Figure 2 shows a comparative a.c. voltammogram of the two complexes, where the second oxidations are virtually coincident.

If indeed the first oxidation was metal-based then the proposed second macrocycle-based oxidation of these ferric compounds should reflect the difference in basicity of the two macrocycles. This it clearly does not do and, moreover, no third

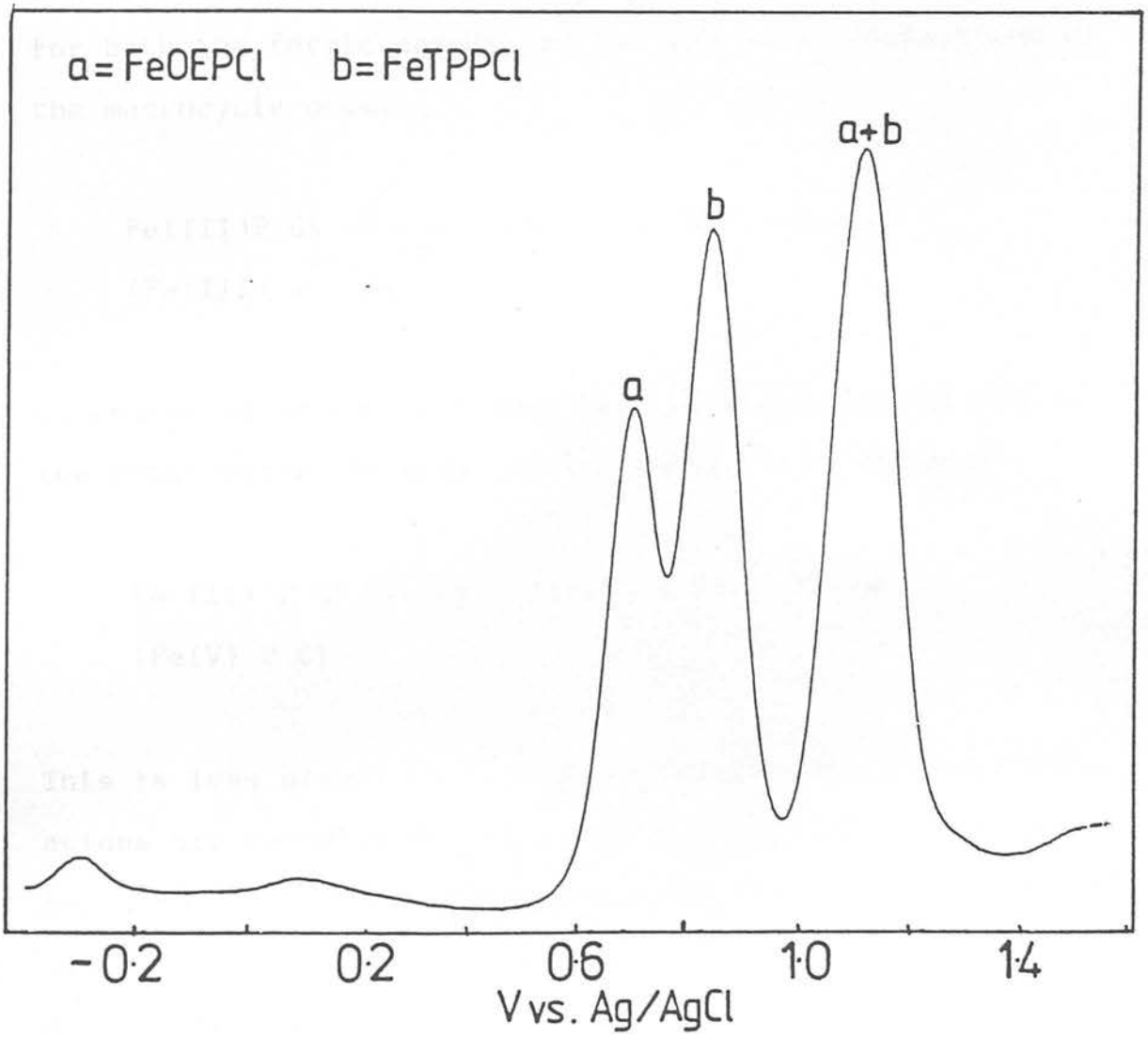

Figure 4.2 A.c. voltammogram of Fe(III)OEPCl and Fe(III)TPPCl in CH_2Cl_2/0.5M $TBABF_4$

oxidation wave is observed for either Fe(III) TPPCl or Fe(III) OEPCl up to the solvent front (+ 2.05V).

The voltammetric results in CH_2Cl_2 then strongly suggest that for both the ferric porphyrins two successive oxidations of the macrocycle occur.

$$\text{Fe(III)P Cl} \xrightarrow{-e^-} \underset{\text{(Fe(III) P Cl)}}{\overset{2+}{\text{(Fe(III) P}^{\cdot}\text{Cl)}}} \overset{2+}{} \xrightarrow{+-e^-}$$

Of course it is possible that two successive oxidations of the metal occur, to give the following redox sequence-

$$\underset{\text{(Fe(V) P Cl)}}{\overset{2+}{\text{Fe(III) P Cl}}} \xrightarrow{-e^-} \text{(Fe(IV) P Cl)}^{+} \xrightarrow{-e^-}$$

This is less plausible in that successive metal-based oxidations are normally separated by a much larger energy gap and also d^3 Fe(V) is an extremely unlikely stable oxidation state of iron. Additionally, both the first and second oxidation potentials of the Fe(III) P Cl complexes are largely unaffected by axial ligation by coordinating solvents. Doping the CH_2Cl_2 with CH_3CN, pyridine or THF shifted the oxidation potentials no more than 20mV. Similar shifts are noted for the $MP/MP^{+\cdot}$ and $MP^{+\cdot}/MP^{2+}$ couples of metalloporphyrins with a redox inert metal centre. It is extremely unlikely that

the stabilities of Fe(III), Fe(IV) and Fe(V) would all be equally affected (or unaffected) by the occupation of the sixth ligand site.

The voltammetric behaviour of the ferric chlorins Fe(III) TPCCl (TPC = meso-tetraphenylchlorin) and Fe(III) OECCl (OEC = octaethylchlorin), which is discussed fully in Chapter 5, also suggests that oxidation of the corresponding porphyrin complexes occurs at the macrocycle. The chlorin macrocycle is found to be easier to oxidise than the porphyrin macrocycle with the same substitution pattern by approximately 300mV for complexes with a redox inert metal centre. Fe(III) OEC Cl and Fe(III) TPC Cl are easier to oxidise than their corresponding porphyrin analogues by 290mV and 285mV respectively. This shift in oxidation potential is identical for the second wave. This significant dependence of $E_{\frac{1}{2}}$ (ox) on the chelating macrocycle is unlikely if either or both of the oxidations of ferric porphyrins is metal-based.

The voltammetric results then indicate the oxidative sequence of both Fe(III) TPP Cl and Fe(III) OEPCl involves two successive macrocycle-based redox steps, resulting in a π cation radical then a π dication. Spectroelectrochemical characterisation of the anodic electrode products supports this proposed behaviour.

No ESR signals were observed for any of the oxidation products

of Fe(III) TPPCl or Fe(III) OEPCl. This is non-informative for reasons outlined previously.

The optical absorption spectra of Fe(III) P Cl complexes contain extra bands both in the visible region and the near u.v. region. These transitions are assigned as charge transfer bands from both the porphyrin and the Cl^- axial ligand to Fe(III), and their presence dictates that Fe(III) P Cl spectra are classified as hyper. Koybayashi and co-workers[27] have carried out extensive studies on the optical spectra and MCD spectra of Fe(III) complexes of TPP. Since d_{xy} appears to be the first d-orbital to be doubly occupied the Fe(III) porphyrins then have a vacancy in the e_g ($d\pi$) shell. Thus the possibility of allowed charge-transfer transitions a_{1u} (π), a_{2u} (π) $\longrightarrow$ e_g ($d\pi$) occurs and extra bands are noted in the optical spectrum. The visible bands around 680nm in the spectrum of Fe(III) TPPCl (see Figure 3) are just such transitions. The 'extra' intense band at 380 nm (Fig. 4) is assigned in this work as a $Cl^- \longrightarrow$ Fe(III) charge transfer band for reasons which will become apparent later. Figure 3 also shows the visible spectrum of the green one electron oxidation product of Fe(III) TPPCl. Isosbestic points are noted at 520, 500, 442 and 336 nm throughout oxidation. The resulting spectrum is independent of temperature (+20°C to -70°C) and full regeneration of Fe(III) TPPCl is achieved at the appropriate potential.

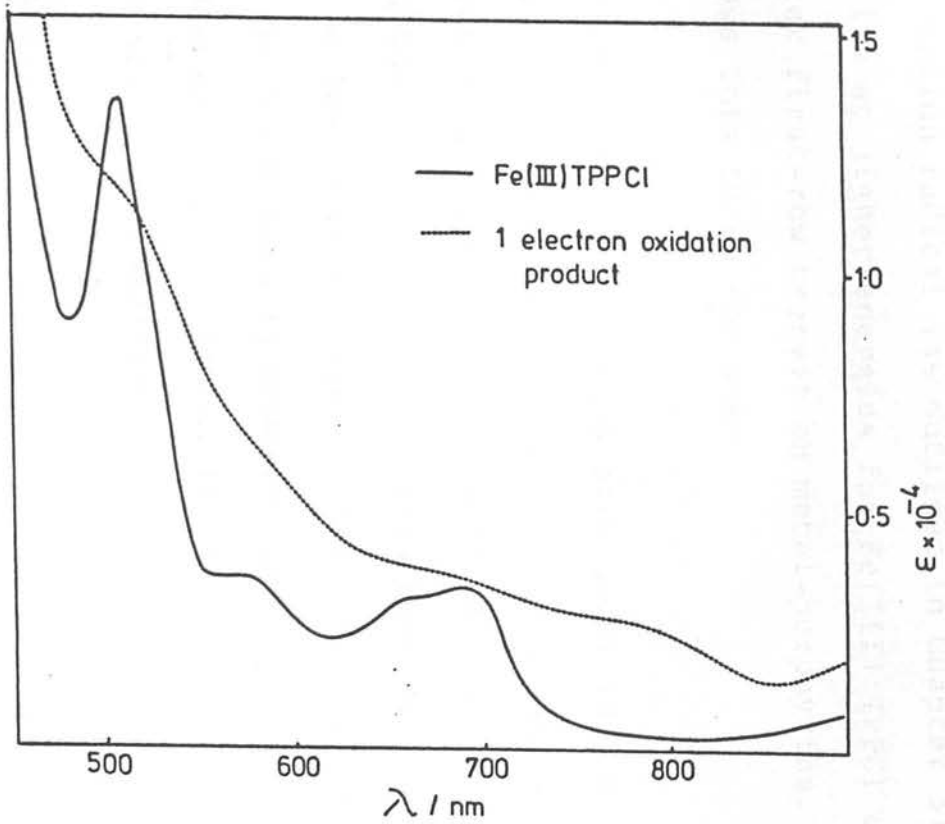

Figure 4.3 Visible absorption spectrum of the one-electron oxidation product of Fe(III)TPPCl

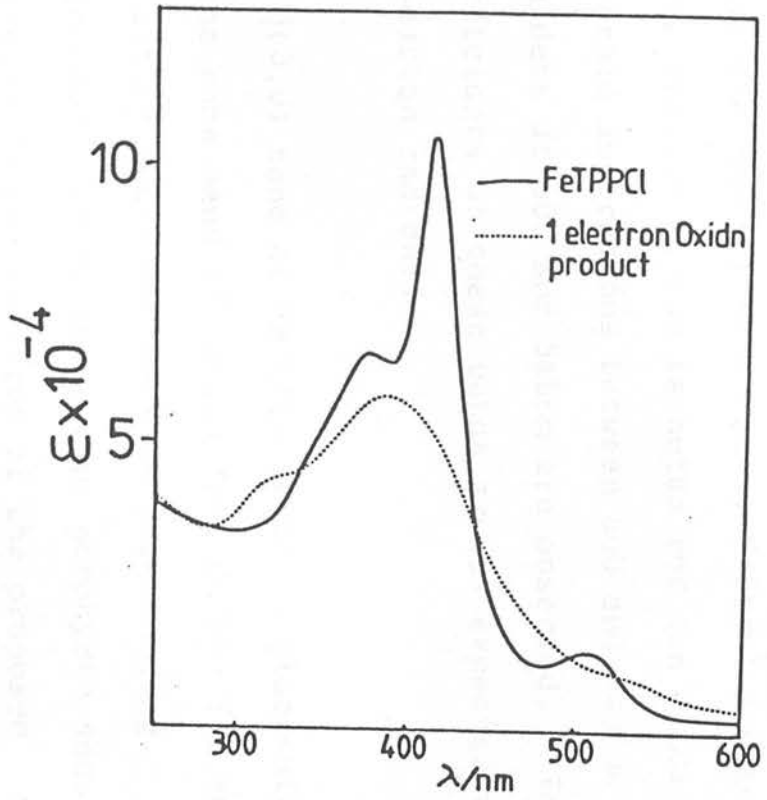

Figure 4.4 Near uv spectrum of the one electron oxidation product of Fe(III)TPPCl

Unlike the results reported by Felton[9] considerable absorption in the visible region is noted for the oxidised product. Two broad absorptions between 660 and 640 nm and ill-defined shoulders at 600 and 510nm are observed. The extinction coefficients of these bands are as expected for a porphyrin π-cation radical.

The Q(0,0) band of Fe(III) TPPCl is blue-shifted compared to the same band of Ni(II) TPP, Cu(II) TPP and Zn(II) TPP, indicating increased $d\pi - \pi^*$ back bonding. This increased hypso-character of the parent porphyrin should also be reflected in the spectrum of the proposed π-cation radical. Thus the characterising visible bands for the porphyrin π-cation radical (as outlined in Chapter 3) are predicted to lie at higher energies for Fe(III) TPPCl compared to the later first-row transition metal-porphyrins. Table 2 clearly shows this to be the case.

Dramatic spectral changes also occur in the Soret region upon oxidation, with an apparent collapse and blue shift of the Soret band (Figure 4). The resulting band is very broad and the low energy tail of this band causes the visible bands to be less well resolved. The decrease in oxcillator strength of the Soret band is however less than expected for the formation of a cation radical (as reported by Felton et al[9]). However we rationalise this anomaly by proposing the $Cl^- \longrightarrow$ Fe(III

Table 4.2 Spectral data for the oxidation products of Fe(III)TPPCl in CH_2Cl_2/0.5M $TBABF_4$

	Wavelength maxima, nm (extinction coefficient x 10^{-3}
Fe(III)TPPCl	690(3.0, 660(2.8), 575(3.0) 510(13.2), 418(110), 380(69.0)
$(Fe(III)TPP^{+}Cl)^{+}$	800(2.7), 600(5.3), 520(11.4) 395(60), 310(42)
$(Fe(III)TPP^{2+}Cl)^{2+}$	broad absorption 800-500 375(42)
Ferric chloride dihydroxydihydroporphyrin	602(15), 576(9.2), 400(39.4)

Table 4.3 Spectral data for the oxidation products of Fe(III)OEPCl in CH_2Cl_2/0.5M $TBABF_4$

	Wavelength maxima, nm (extinction coefficient x 10^{-3})
Fe(III)OEPCl	636(4.2), 532(8.4), 500(8.5) 376(99.2)
$(Fe(III)OEP^{+}Cl)^{+}$	630(3.0), 580(4.8), 514(7.9) 356(69.0)
$(Fe(III)OEP^{2+})^{2+}$	broad absorption 800-500, 330(40.6)

charge-transfer transition (originally at 376nm) lies under the Soret transition. This CT band then will contribute an unknown amount towards the total oscillator strength of the 'Soret' band of the oxidised product and thus Felton's argument is invalid.

The visible band pattern and the blue-shifted Soret transition lead us to assign the one-electron oxidation product of Fe(III)TPPCl as the π cation radical $(Fe(III)TPP^{\cdot}Cl)^{+}$, with an $^{2}A_{2u}$ ground state.

The second oxidation of Fe(III) TPPCl at -40°C results in the spectral changes shown in Figure 5. The Soret transition again shifts to the blue and continues to broaden. The low energy tail of this band reaches 600nm and consequently no visible transitions are resolved. This oxidation is reversible at -40°C with isosbestic points at 450 and 300nm maintained throughout. However if this brown product is warmed to room temperature (20°C) analogous spectral changes to those reported earlier (section 3.6) for the second oxidation product of Pd(II) TPP result : i.e. the formation of a ferric chloride dihydroxydihydroporphyrin (2).

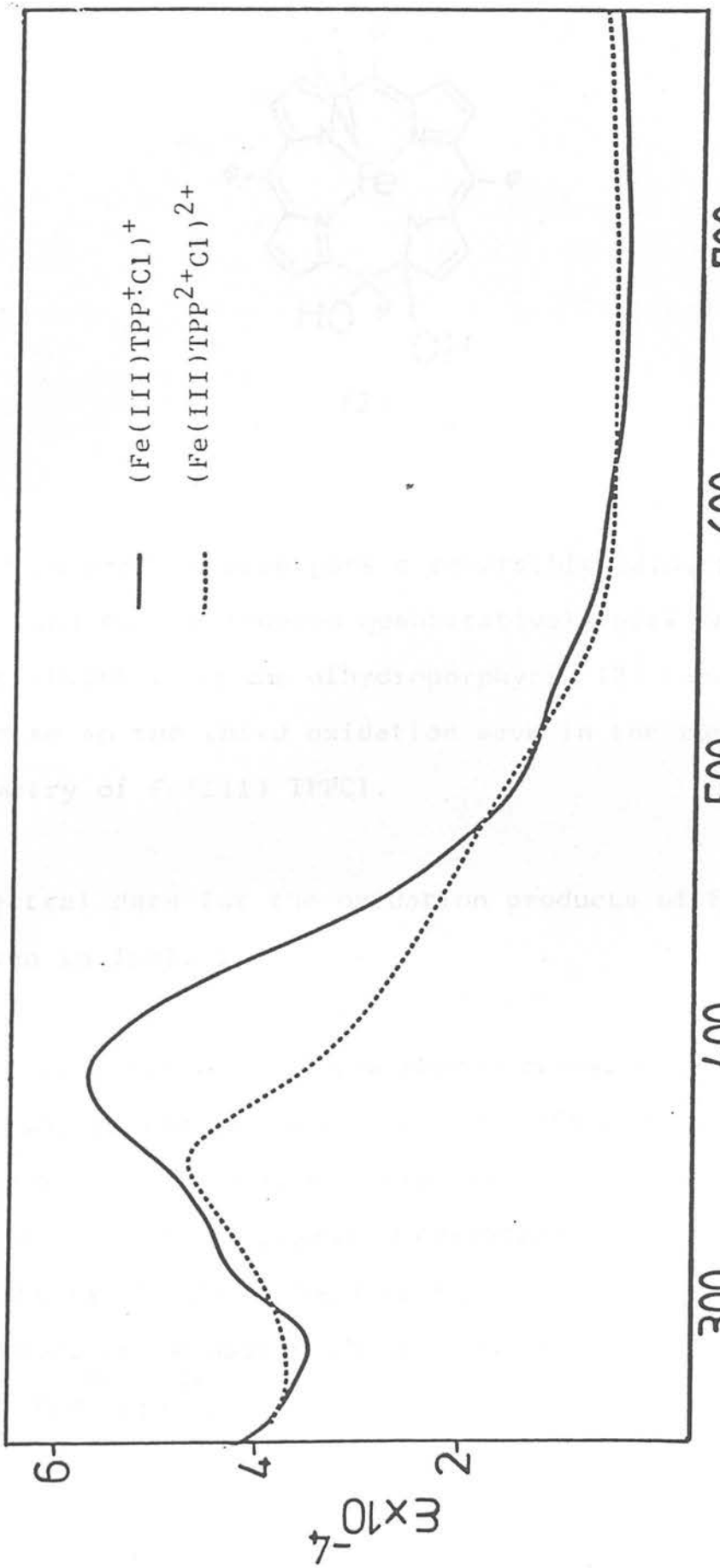

Figure 4.5 Optical absorption spectra of the oxidised products of Fe(III)TPPCl at -50°C in CH_2Cl_2/0.5M $TBABF_4$

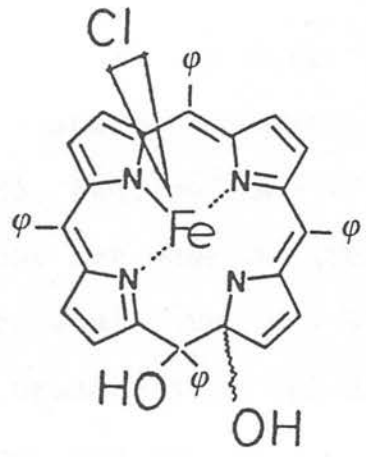

(2)

This green product undergoes a reversible oxidation (at +1.36V) and can be reduced quantitatively back to Fe(III) TPPCl at -0.30V.It is the dihydroporphyrin (2) then which gives rise to the third oxidation wave in the room temperature voltammetry of Fe(III) TPPCl.

All spectral data for the oxidation products of Fe(III) TPPCl are given in Table 2.

The following reaction of the second oxidation product is significant in that it has been shown (Chapter 3) the formation of the dihydroxydihydroporphyrin results from nucleophilic attack on a metalloporphyrin π-dication. This, with the blue shift of the Soret band during the second oxidation at -40°C, leads us to assign the second oxidation product as $(Fe(III)\ TPP\ Cl)^{2+}$ $^{2+}$.

The spectral progression of the first oxidation of Fe(III)OEPCl is shown in Figures 6 and 7. Isosbestic points are observed at 650, 613, 554, 485, 420, 362 and 292nm. Very broad long wavelength absorptions are seen to grow as was the case for Fe(III) TPPCl. Once again the main visible bands are ill-resolved due to the broadness of the Soret transition but three main transitions can be distinguished at 630, 580 and 525nm. The decrease in intensity of the Soret transition on oxidation is noted to be less than expected for the formation of a genuine π-cation radical. However this can be explained, as for Fe(III) TPPCl, by the super-imposition of a $Cl^- \longrightarrow$ Fe(III) CT band. Also the Soret band is seen to shift to the blue. As such, the first oxidation product is assigned as $(Fe(III)\ OEP^{+\cdot}\ Cl)^+$. The ground state is tentatively ascribed as $^2A_{1u}$ from the pattern of the visible bands (very similar to $ZnOEP^{+\cdot}$).

The second oxidation product is stable at room temperature. A blue shift of the Soret band occurs, with a further decrease in intensity. Weak broad absorptions in the visible are also noted. These spectral changes are indicative of π dication formation. Isosbestic points at 350nm and 296nm are maintained throughout oxidation and Fe(III) OEPCl is fully regenerated, through the π cation radical, at the appropriate potentials. The spectral data for the oxidation products of Fe(III) OEPCl are listed in Table 3.

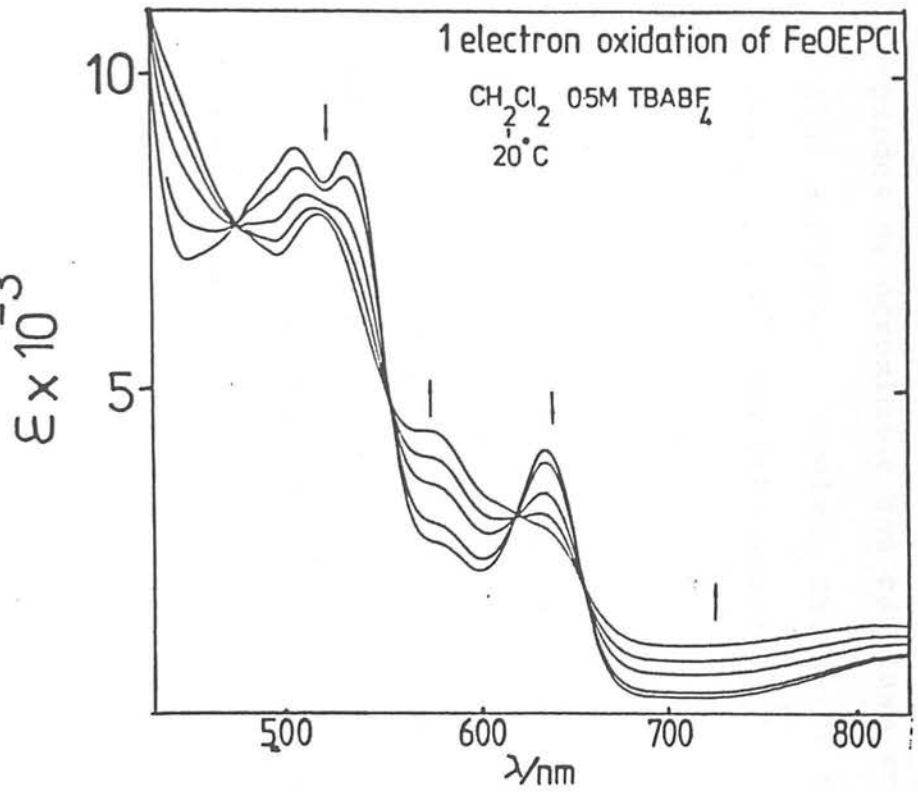

Figure 4.6 Optical progression during the first oxidation of Fe(III)OEPCl

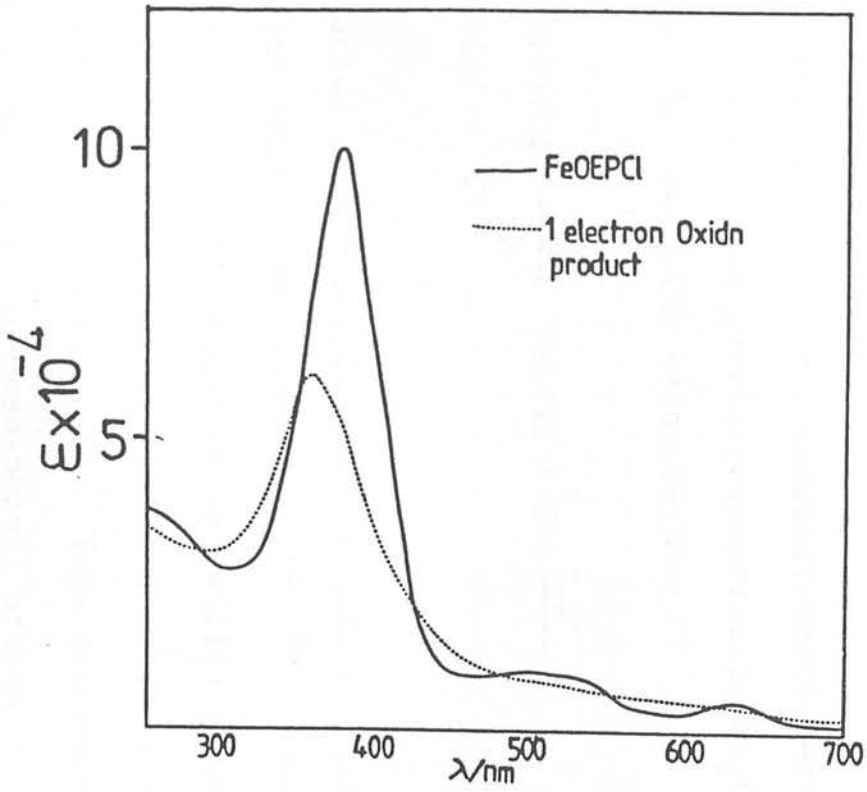

Figure 4.7 Optical spectrum of the first oxidation product of Fe(III)OEPCl

The voltammetric and optical spectral characterisation of the anodic products of ferric porphyrins in CH_2Cl_2 lead us to propose the following redox sequence -

$$Fe(III)PCl \xrightarrow{-e^-} \underset{(Fe(III)P^{2+}Cl)}{Fe(III)P^{+\cdot}Cl} \xrightarrow{-e^-}$$

The formation of a π cation radical and π dication contrasts with recent studies by Groves et al[28, 29]. They report the two electron chemical oxidation of Fe(III) porphyrins, by m-chloroperoxy-benzoic acid, yields a species best described as an Fe(IV) π cation radical. This assignment arises mainly from the large porphyrin meso-phenyl proton nmr shift values. Reactivity patterns and facile $H_2{}^{18}O$ exchange suggest a ferryl linkage, $Fe^{IV}{=}O$. The degradation of hydrogen peroxide and organic peroxides by peroxidase and catalase involve a catalytic cycle that also apparently involves oxidation of the haem prosthetic group to the iron (IV) state[30-32].

Extended Huckel calculations by Gouterman[33] have indicated that the lowest lying d-orbitals of Fe(III) are very similar in energy to the filled porphyrin orbitals a_{2u} and a_{1u}. It would be expected therefore that the site of oxidation would be subtly affected by the axial-ligand field environment at the iron centre. Our observations therefore do not challenge formulation of an Fe(IV) intermediate in haemoproteins.

Rather they support the presumed necessity for an oxo or hydroxo ligand for stabilisation of metal-centered oxidation. The radical compounds characterised in this work are more appropriate models for the proposed π -cation radicals involved in the bioactivity of horse-radish peroxidase.

4.3 CATHODIC ELECTROCHEMISTRY OF FERRIC PORPHYRINS

Fe(III) TPPCl and Fe(III) OEPCl are found to exhibit four one-electron reductions in CH_2Cl_2/0.5M $TBABF_4$, the $E_{\frac{1}{2}}$ values of which are listed below-

	$E_{\frac{1}{2}}$(1st red)/V*	$E_{\frac{1}{2}}$ (2nd red)	$E_{\frac{1}{2}}$ (3rd red)	$E_{\frac{1}{2}}$ (4th red)
Fe(III) OEPCl	-0.63	-1.44	-2.03	-2.46
Fe(III) TPPCl	-0.59	-1.32	-1.91	-2.33

*Volts vs Ag/AgCl

At room temperature waves 2 - 4 are found to be fully reversible on a voltammetric time scale, for both porphyrins. The first wave however is totally irreversible at room temperature. Figure 8 shows a room temperature cathodic cyclic voltammogram of Fe(III) TPPCl. Stirred d.c. voltammetry shows all the redox couples to involve the same number of electrons. Bulk coulometric measurements on the first two reductions show both to be one electron steps. The latter two reductions give products which are not stable on the

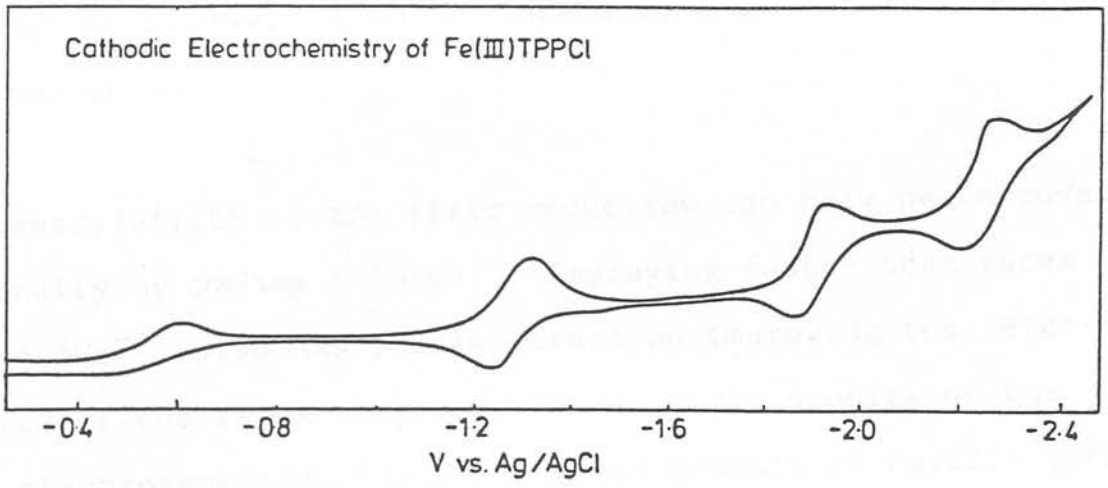

Figure 4.8 Room temperature cyclic voltammogram of Fe(III)TPPCl in CH_2Cl_2/0.5M $TBABF_4$

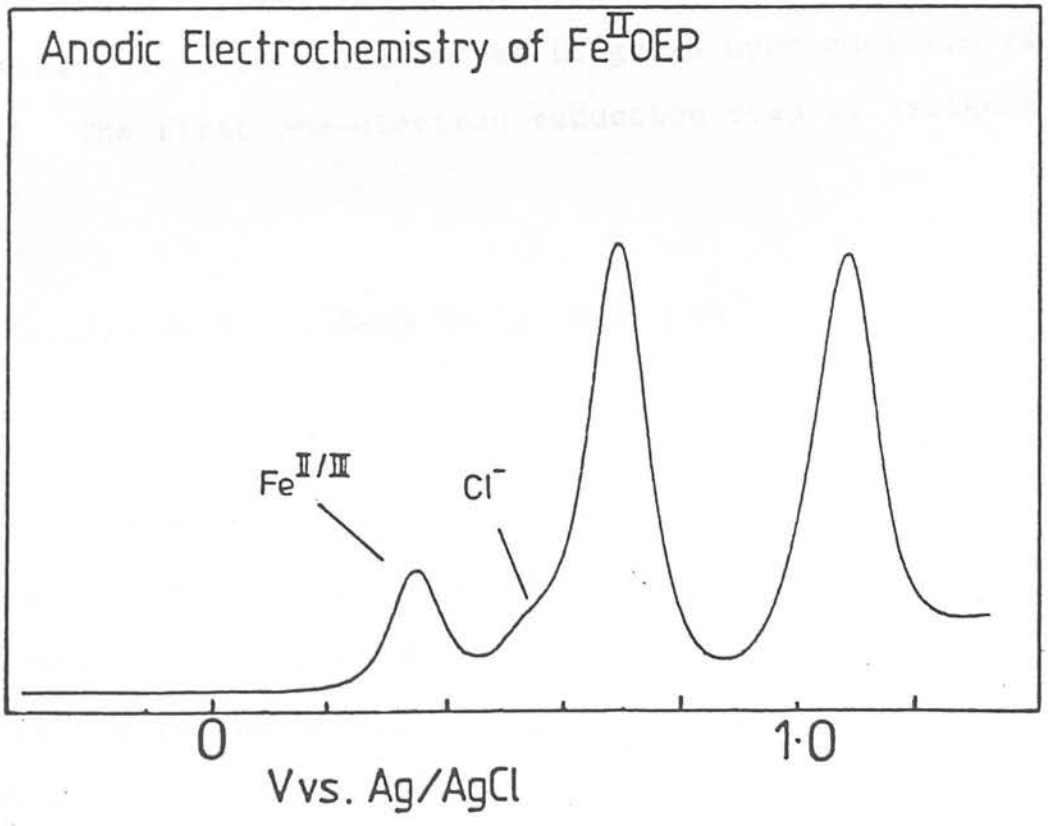

Figure 4.9 Oxidative electrochemistry of Fe(II)OEP in CH_2Cl_2/0.5M $TBABF_4$ at 20°C

coulometric time-scale but by inference they too must be one-electron steps.

The reversibility of the first reduction can only be improved marginally by cooling (-70°C). Employing faster scan rates (up to $5Vs^{-1}$) also has little affect on improving the reversibility of the redox couple. Voltammetric studies on the bulk-electrogenerated first reduction product of Fe(III) OEPCl show this species to exhibit four oxidation waves, the latter two of which correspond exactly to the two reversible oxidations of Fe(III) OEPCl. Additional waves are noted at +0.37V and - +0.6V, both of which are irreversible (see Figure 9). The wave at approximately +0.6V is assigned as the oxidation of chloride ion as it grows upon addition of TBACl. The first one-electron reduction step is assigned as-

$$\text{Fe(III) OEPCl} \xrightarrow{+e^-} \text{Fe(II) OEP} + Cl^-$$

The irreversible oxidation at +0.37V must then be the $Fe^{II/III}$ couple, in the absence of coordinated chloride. Electrogeneration anodic of this potential realises the starting material Fe(III) OEPCl, chloride rapidly recoordinating to the iron centre in the 3+ oxidation state. The effect of the chloride ion on the $Fe^{III/II}$ couple is very dramatic indeed then, shifting the redox couple exactly one volt to more neg-

ative potential i.e.

$$\text{Fe(III) OEPCl} \xrightarrow{+e^-} \text{Fe(II) OEPCl} \qquad E_{\frac{1}{2}} = -0.63\text{V}$$

$$\text{Fe(III) OEP} \xrightarrow{+e^-} \text{Fe(II) OEP} \qquad E_{\frac{1}{2}} = +0.37\text{V}$$

This is a measure of the stabilisation offered to the higher oxidation state of iron, by the axial ligation of chloride. Exactly analogous results are found for Fe(III) TPPCl.

Fe(II) OEP gives no ESR signal at temperatures between -150°C to 20°C. The optical spectral progression at room temperature of this reduction is shown in Figure 10. Isosbestic points are noted at 682, 610, 550, 490, 416, 400, 350 and 292nm, suggesting the dissociation of $(\text{Fe(II) OEPCl})^-$ is extremely rapid. A red shift of the visible π / π^* bands is noted and the two-banded structure is retained. The band at 638nm in the spectrum of Fe(III) OEPCl is seen to collapse upon reduction. This band is ascribed as an a_{2u}, $a_{1u} \longrightarrow e_g$ ($d\pi$) charge transfer transition due to the appearance of a similar band in Fe(III) TPPCl, which has previously been assigned[27] as such. The total collapse of this band (no other CT band is seen to grow upon reduction) suggests the $d\pi$ shell of Fe(II) OEP is full and therefore this species must be a low spin d^6 system. The red-shift of the visible π / π^* bands indicate the mixing of the e_g ($d\pi$) and e_g (π^*) orbitals is less efficient for the reduced product

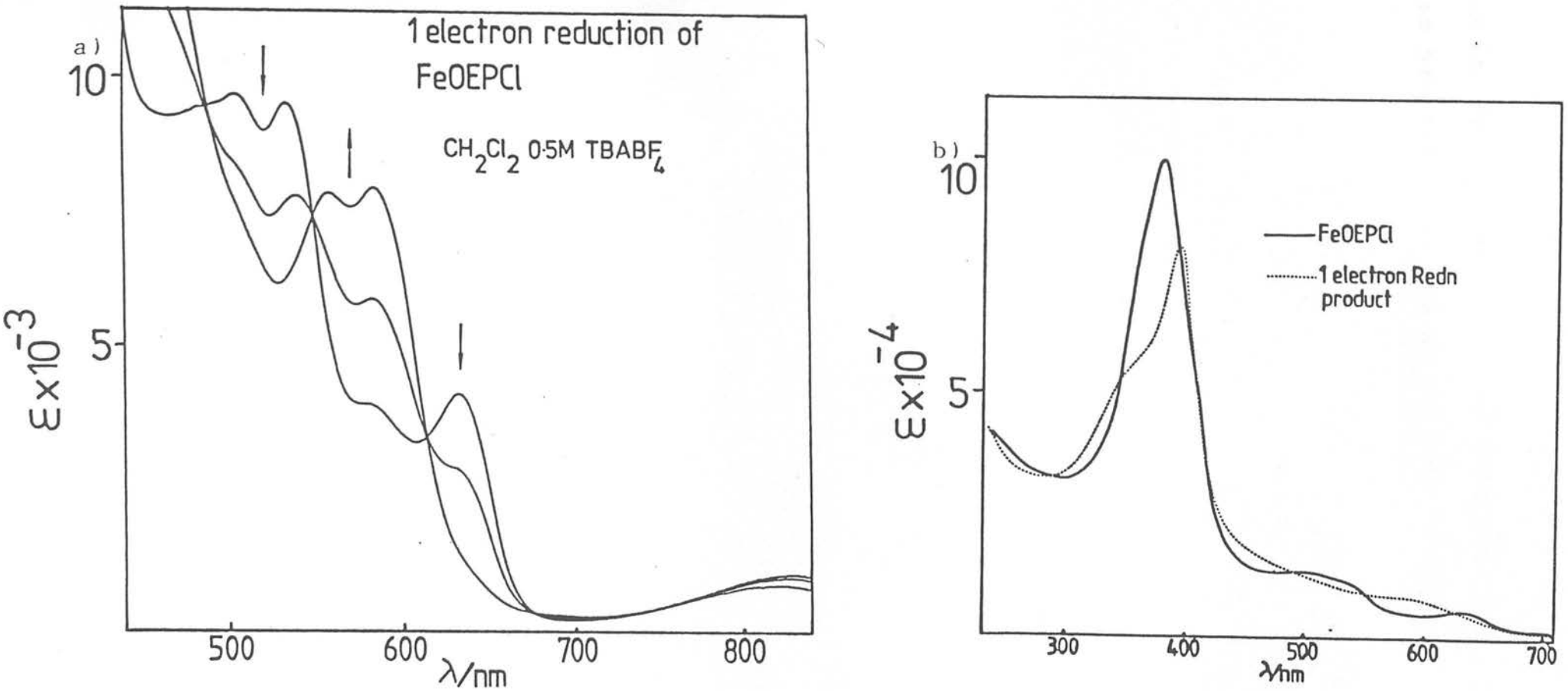

Figure 4.10 a) Optical progression during the first reduction of Fe(III)OEPCl

b) Optical absorption spectrum of the first reduced product of Fe(III)OEPCl

than for Fe(III) OEPCl. (The energy of the d-orbitals will also have been affected by the loss of chloride and reduction of the metal centre cannot be viewed in the same manner as in Chapter 3). The Soret band also shifts to the red upon reduction. The oscillator strength of the band decreases significantly and this is attributed to the loss of the underlying $Cl^- \longrightarrow$ Fe(III) charge transfer band. The visible band pattern, alone, is good evidence reduction has occurred at the metal to give Fe(II) OEP.

Fe(III) TPPCl undergoes similar optical changes upon reduction. Figure 11 shows the spectrum of Fe(III) TPPCl and the one-electron reduction product. The visible π / π^* bands shift to the red and the $a_{1u}\ a_{2u} \longrightarrow e_g(d\pi)$ CT bands collapse completely. The Soret band shifts only slightly to the red. The collapse of the 376 nm band is in keeping with the assignment of this band as a chloride to metal charge-transfer transition.

The spectral data for the first reduction of Fe(III) TPPCl and Fe(III) OEPCl are listed in Table 4.

The subsequent cathodic waves must then be considered as arising from the Fe(II) porphyrin and can be compared directly with the reduction behaviour of the other transition metal porphyrins studied in Chapter 2.

Table 4.4 Spectral data for the reduction products of Fe(III)OEPCl and Fe(III)TPPCl in CH_2Cl_2/0.5M $TBABF_4$

	Wavelength maxima, nm (extinction coefficient x 10^{-3})		
Fe(II)TPP	610(4.2),	580(7.0),	420(115)
	322(38)		
$(Fe(I)TPP)^-$	609(6.8),	582(10.1),	430(120)
	410(72.4)		
Fe(II)OEP	590(7.8),	555(7.6),	400(81.0)
	360(52.6)		
$(Fe(I)OEP)^-$	586(6.2),	548(9.1),	410(90.3)
	390(61.3)		

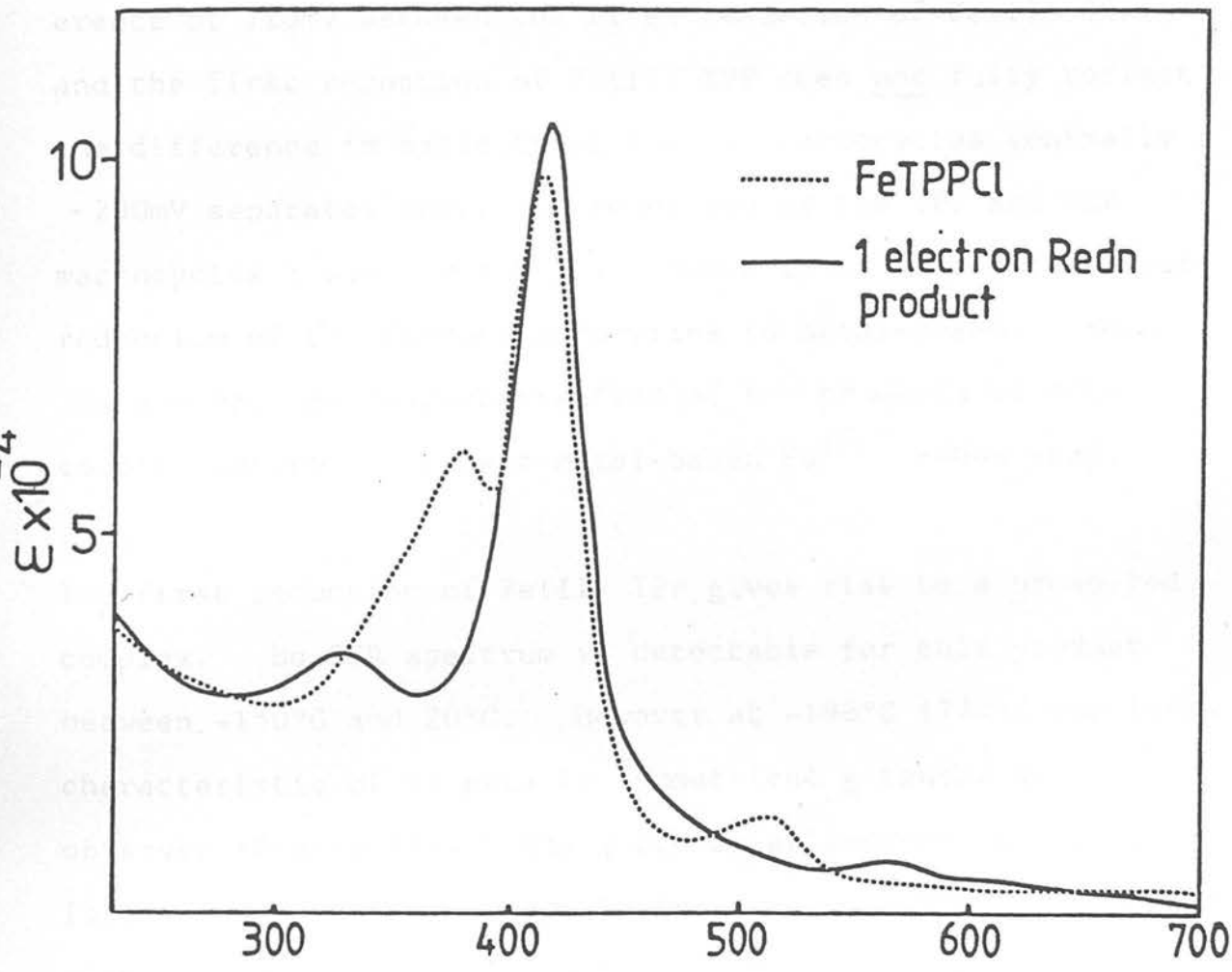

Figure 4.11 Optical absorption spectrum of the one-electron reduction product of Fe(III)TPPCl

It is observed the first reduction of both ferrous porphyrins occurs at too anodic a potential to be a porphyrin-based wave, i.e. the $E_{\frac{1}{2}}$ values are less negative than the first reduction potential of the corresponding free-bases. Also the difference of 120mV between the first reduction of Fe(II) OEP and the first reduction of Fe(II) TPP does not fully reflect the difference in basicity of the two macrocycles (normally -200mV separates the first reduction of the TPP and OEP macrocycles : see Table 2.2). Hence it is likely the first reduction of the ferrous porphyrins is metal-based. Both ESR and optical characterisation of the products of this couple confirm it to be a metal-based $Fe^{II/I}$ redox step.

The first reduction of Fe(II) TPP gives rise to a brown-red complex. No ESR spectrum is detectable for this product between -150°C and 20°C. However at -196°C (77K), two lines characteristic of an axially symmetrical g tensor were observed (Figure 12). The g tensor anisotropy is much too large to arise from an organic free radical with the unpaired electron residing mostly on the porphyrin ring. A similar spectrum arises from the chemical reduction of μ-oxo-bis (Fe(III) TPP) which Cohen et al.[34] assign to a low spin, $S = \frac{1}{2}$, d^7 iron porphyrin. It is also qualitatively similar to that reported by Lexa et al.[35] for the chemical reduction of Fe(III) TPPCl in THF by sodium or potassium anthracene ($g_{\perp} = 2.30$ $g_{\parallel} = 1.43$ $A_{\perp} = 30G$) although no hyperfine

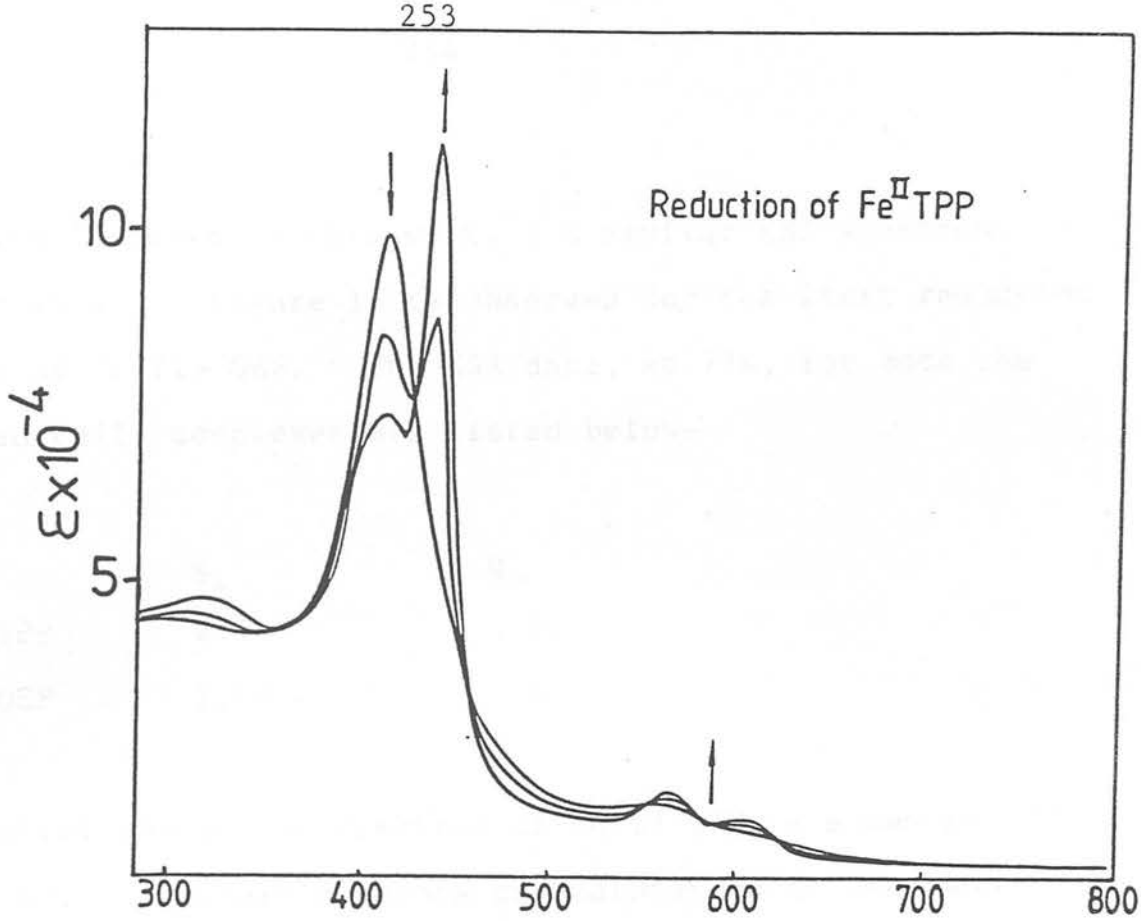

Figure 4.13 Optical progression during the second reduction of Fe(III)TPPCl in CH_2Cl_2/0.5M $TBABF_4$

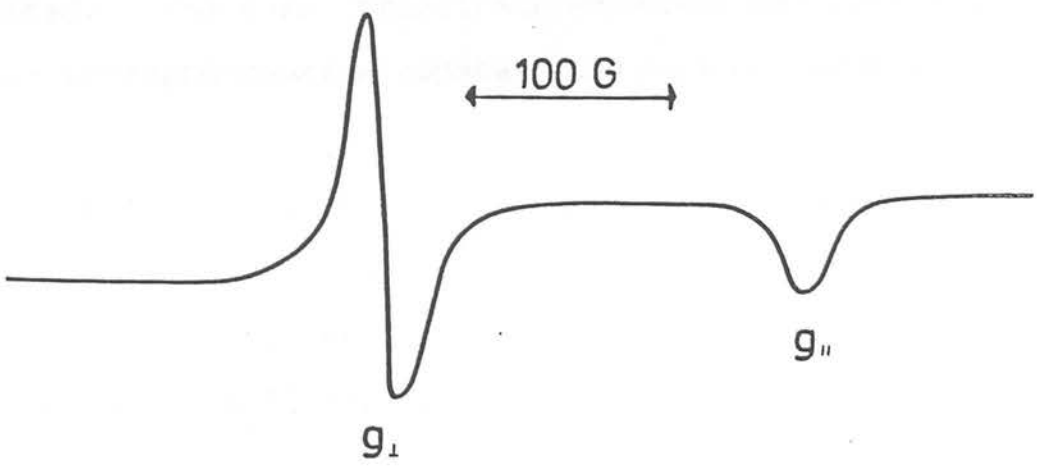

Figure 4.12 77K ESR spectrum of Fe(I)TPP in CH_2Cl_2/0.5M $TBABF_4$

splitting is noted in this work. A similar ESR spectrum to that shown in Figure 12 is observed for the first reduction product of Fe(II) OEP. The ESR data, at 77K, for both the proposed Fe(I) complexes are listed below-

	$g_{\perp}$	$g_{\parallel}$
Fe(I) TPP	2.41	1.96
Fe(I) OEP	2.40	1.98

The optical absorption spectrum of Fe(I) TPP is shown in Figure 13. Isosbestic points are maintained at 540, 460 and 390nm throughout reduction and Fe(II) TPP is fully regenerated on reverse electrolysis. The visible π / π^* bands are seen to move to the blue on reduction (qualitatively similar to those observed during the $Co^{II/I}$ reduction : Section 3.5). The spectral changes in the Soret region are however more complicated. The Soret transition broadens and splits, although the oscillator strength remains constant throughout reduction.

The appearance of this extra band suggests Fe(I) TPP should be classed as a hyper-type metalloporphyrin. Fe(I) OEP exhibits similar optical properties. The spectral data for both Fe(I) complexes are listed in Table 4.

The unusual optical behaviour of the Fe(I) porphyrins in the Soret region is extremely difficult to rationalise using

Gouterman's 4-orbital model for the porphyrin moiety.[36] The electronic spectrum of a Rh(I) porphyrin, (Rh(I) OEP $(I)_2(CO)_2Cl)^-$ is also reported[37] to show two Soret bands at 376nm and 444nm and thus this unusual behaviour is not unique to the Fe(I) porphyrins.

The further reduction products of the proposed Fe(I) complexes proved to be too unstable for full spectral characterisation to be achieved. Reduction of the red Fe(I) complexes initially gave rise to a yellow-green species which rapidly decomposed to an unknown product(s) at temperatures between -70°C and 20°C. The pattern of reduction potentials however suggests that the two one-electron reductions of the Fe(I) species result first in an Fe(I) (porphyrin π anion radical) then subsequently an Fe(I) (porphyrin π dianion) (ΔE(1st red/2nd red equals 0.43V for Fe(I) TPP and 0.42V for Fe(I) OEP).

4.4 ELECTROCHEMISTRY OF RuOEPCO and RuTPPCO

The ruthenium (II) porphyrins RuOEPCO and RuTPPCO both exhibit two reversible one-electron oxidations and an irreversible one-electron reduction in CH_2Cl_2/0.5M $TBABF_4$. The $E_{\frac{1}{2}}$ values for each redox step are summarised below-

	$E_{\frac{1}{2}}$(1st ox)/V*	$E_{\frac{1}{2}}$(2nd ox)	$E_{\frac{1}{2}}$(1st red)
Ru(II) OEPCO	+0.72	+1.25	-1.79^{+}
Ru(II) TPPCO	+0.92	+1.33	-1.58^{+}

* Volts vs Ag/AgCl reference $^{+}$ irreversible

Figure 14 shows the full electrochemical behaviour of Ru(II) OEPCO. The comparative anodic voltammetric behaviour of these complexes is consistent with two successive ring oxidations occurring i.e. RuOEPCO is easier to oxidise by 200mV and ΔE(1st ox/2nd ox) is significantly smaller for RuTPPCO (0.43V) than RuOEPCO (0.53V). The absolute values of ΔE (1st ox/2nd ox) are larger than those exhibited by the corresponding first row transition metal porphyrins, as was noted previously by Rillema[18]. However they are very similar to the differences for the two oxidations of the palladium (II) porphyrins, where the products were previously assigned in Chapter 3 as π cation radicals and π dications.

ESR and optical spectral characterisation of the electrode products confirms the two oxidations of both ruthenium porphyrins also to be macrocycle-based.

The visible electronic spectral changes which occur during the first one-electron oxidation of Ru(II) TPPCO are shown in Figure 15. Ruthenium (II) porphyrins are classed as hypso-porphyrins and as such are blue-shifted from the regular

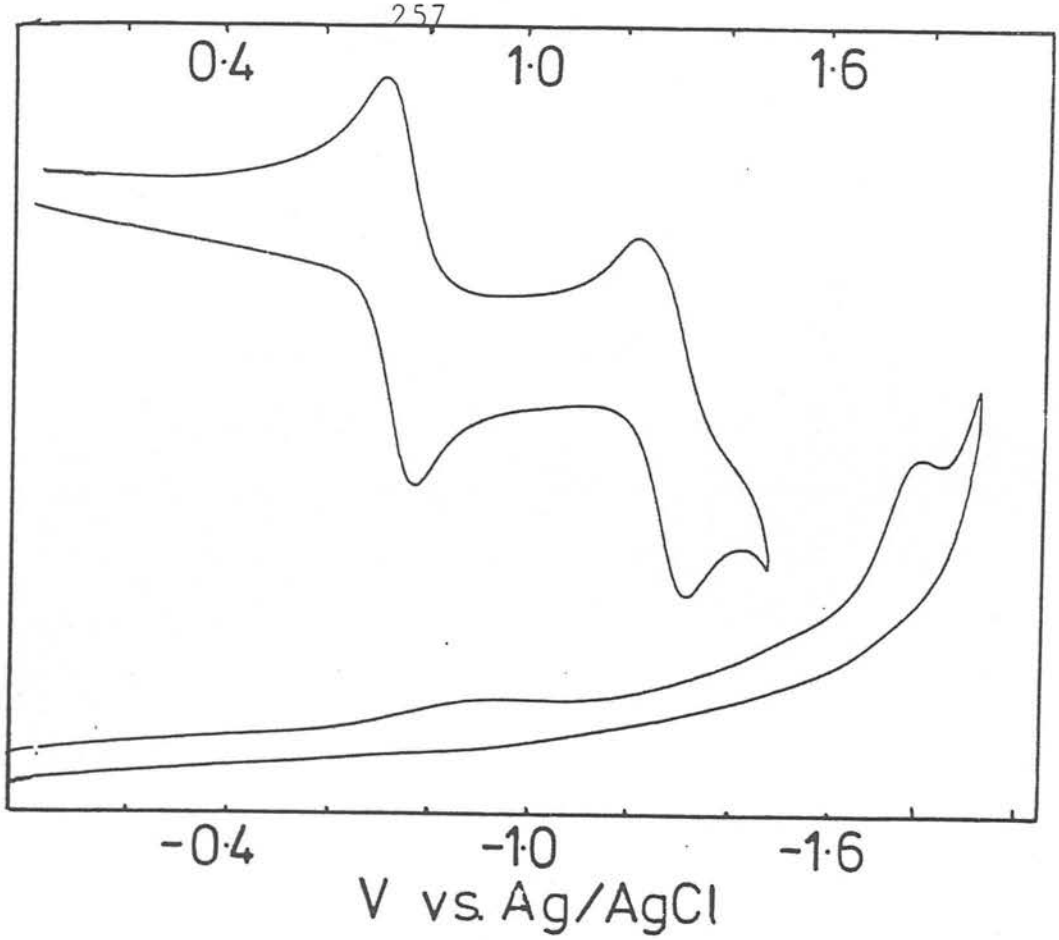

Figure 4.14 Electrochemistry of RuOEPCO in CH_2Cl_2/0.5M $TBABF_4$ at 20°C

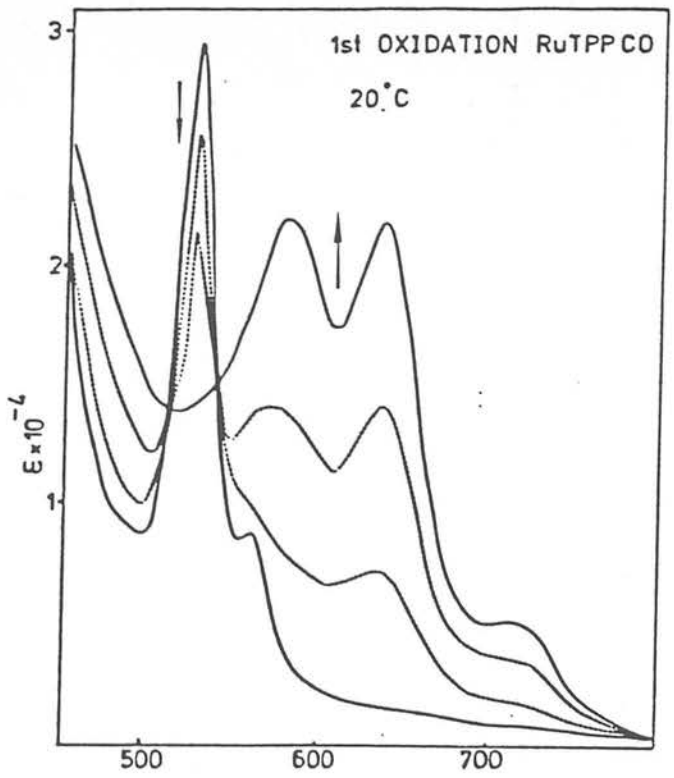

Figure 4.15 Optical progression during the one-electron oxidation of RuTPPCO in CH_2Cl_2/0.5M $TBABF_4$

porphyrins. For Ru(II) TPPCO for instance the Q(0,0) and Q(1,0) transitions occur at 560 and 528nm respectively as compared with 584 and 546nm for the same bands of ZnTPP. As oxidation of Ru(II) TPPCO proceeds the collapse of the Q transitions is accompanied by the simultaneous growth of broader bands in the 750 - 550nm range. The Soret band partially collapses and shifts to the blue. This spectrum is temperature independent (-70°C to 20°C). Isosbestic points are maintained throughout oxidation at 528, 512 and 420nm. The green oxidised species gives an isotropic nine-line esr signal (g = 2.0071, a_N = 1.4G) at 77K. Both the esr and optical data are consistent with the formulation of the oxidation product as $(Ru(II)\ TPP^{+\cdot}CO)^{+}$ with an $^2A_{2u}$ ground state (similar to $ZnTPP^{+\cdot}$).

When the potential is increased to the plateau of the second oxidation wave the esr signal decays completely, and no accompanying growth of another paramagnetic signal is detected. Far more instructive are the observed electronic spectral changes. The Soret band again decreases in intensity and shifts to higher energy during oxidation. The growth of an unresolved shoulder at 560nm and the general decay of all the visible bands are noted. Weak diffuse absorption is observed above 800nm. These spectral changes, from conclusions drawn in Chapter 3, allow the identification of the second oxidation product as $(Ru(II)\ TPP^{2+}\ CO)^{2+}$. This species is

stable in CH_2Cl_2 at temperatures below -30°C. An isosbestic point at 796nm relates the first and second oxidation products. Full recovery of Ru(II) TPPCO is achieved at the appropriate potential.

Exhaustive electrolysis at the plateau of the first oxidation of Ru(II) OEPCO results in the visible spectral changes shown in Figure 16. The final product is a very deep dark green in colour. The limiting spectrum of the oxidation has four overlapping peaks in the visible region from 650 - 500nm and a less intense Soret band shifted to the blue ($\sim 900\ cm^{-1}$). These spectral changes are very like those observed during the one-electron oxidation of NiOEP and PdOEP. Thus we assign the product as $(Ru(II)\ OEP^{+\cdot}\ CO)^{+}$ with an $^2A_{2u}$ ground state. This species is stable at room temperature.

Figure 17 shows the uv/visible spectrum of both $(Ru(II)\ OEP^{+\cdot}CO)^{+}$ and the oxidation product arising from the second anodic wave. The doubly-oxidised brown product again exhibits a typical π dication spectrum. This product is stable at temperatures below -40°C and full regeneration of Ru(II) OEPCO is achieved at this temperature on reversing the applied potential. Spectral data for all the oxidation products are listed in Table 5.

No ESR signal for $(Ru(II)\ OEP^{+\cdot}CO)^{+}$ is detectable at temper-

Table 4.5 Spectral data for the oxidation products of RuOEPCO and RuTPPCO

	Wavelength maxima, nm (extinction coefficient x 10^{-3})		
RuTPPCO	556(8.0),	526(29),	408(301)
$(RuTPP^{+}CO)^{+}$	716(5.2),	636(22.7),	575(22.8), 416(120)
$(RuTPP^{2+}CO)^{2+}$	560(15.2),	400(45.6)	
RuOEPCO	544(28.6),	512(15.7),	393(316)
$(RuOEP^{+}CO)^{+}$	610(6.9),	586(9.4),	540(9.6)
	514(8.0),	391(94.2)	
$(RuOEP^{2+}CO)^{2+}$	520(6.8),	340(50.0)	

Table 4.6 Spectral data for the reduction products of RuOEPCO and RuTPPCO in DMSO/0.1M $TBABF_4$

	Wavelength maxima, nm (extinction coefficient x 10^{-3})		
$(RuTPP^{-}CO)^{-}$	920(8.0),	704(8.5),	680(9.1),
	592(10.6),	524(12.0),	427(106.2)
	407(146.4)		
$(RuOEP^{-}Co)^{-}$	910(7.4),	701(8.0),	680(7.2),
	562(11.4),	544(10.9),	410(152)
	393(119.6)		

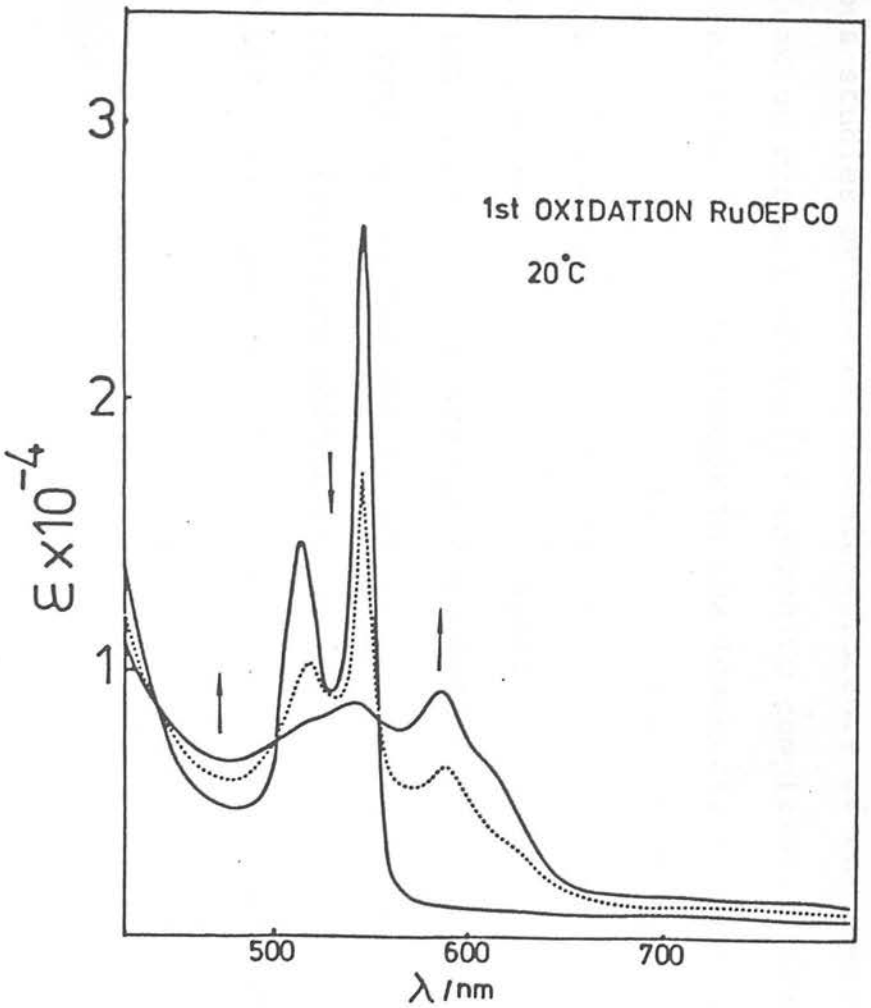

Figure 4.16 Optical progression during the first oxidation of RuOEPCO in CH_2Cl_2/0.5M $TBABF_4$

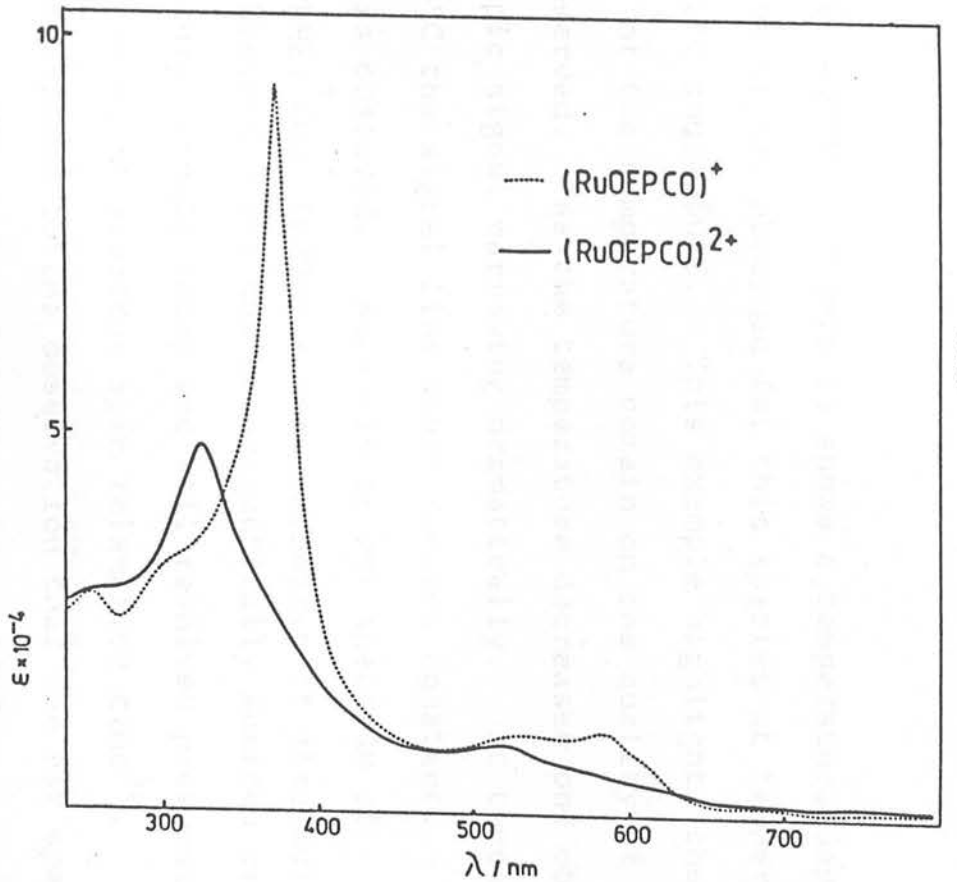

Figure 4.17 Optical absorption spectra of the oxidised products of RuTPPCO

atures above -50°C. Figure 18 shows a temperature-dependent study on the signal obtained for this species at temperatures between -50°C and -150°C. This example highlights the importance of the temperature domain on the quality of ESR signals observed. As the temperature decreases one observes the isotropic signal narrowing dramatically. At temperatures below -135°C the signal line width remains constant. No hyperfine is observed. Recently an nmr spectrum of $(Ru(II)(MPDME)^{+}CO)^{+}$ (MPDME = meso-porphyrin IX dimethyl ester) has been obtained where the paramagnetically shifted proton peaks are surprisingly sharp and well resolved presumably due to a very short electron spin relaxation time[38]. This finding corresponds to the observation that the esr spectrum was not detectable at temperatures above -50°C.

Our results in non-coordinating media, then, agree with previous studies on the electronic structure of the one-electron oxidation product of Ru(II) (porph)CO complexes. They do differ significantly though in the identification of the subsequent one-electron oxidation product of the π cation radical. Rillema[18] and Kadish[39] have independently suggested the product is a $(Ru(III)(porph)^{+}CO)^{+}$ species. The esr results obtained in this work are non-informative as Goodman[40] has referred to the difficulty of obtaining Ru(III) esr spectra. Extensive spin-spin coupling could also render the biradical species esr silent. The electronic spectral

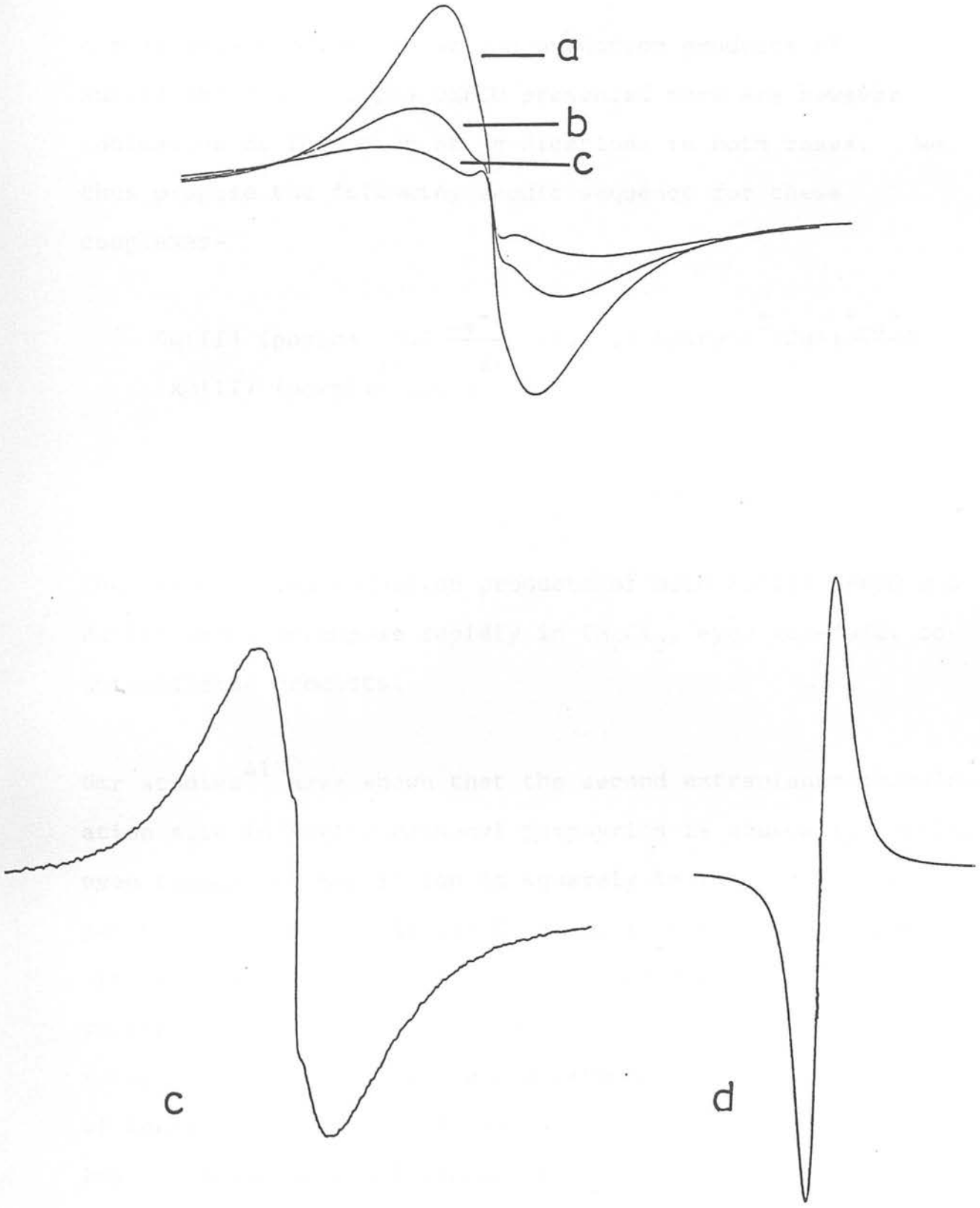

Figure 4.18 ESR spectra of $RuOEPCO^{+}$ at various temperatures
a. -60°C b. -100°C c. -150°C d. -196°C

characterisation of the second oxidation products of Ru(II) TPPCO and Ru(II) OEPCO presented here are however indicative of formation of π dications in both cases. We thus propose the following anodic sequence for these complexes-

$$\text{Ru(II) (porph) (CO)} \xrightarrow{-e^-} \underset{\text{(Ru(II) (porph) (CO))}^{2+}}{\text{(Ru(II) (porph)}^{+}\text{(CO))}^{2+}} \xrightarrow{+-e^-}$$

The one-electron reduction products of both Ru(II) TPPCO and Ru(II) OEPCO decompose rapidly in CH_2Cl_2, even at -70°C, to unidentified products.

Nmr studies[41] have shown that the second extraplanar coordination site in Ru(II) carbonyl porphyrins is unusually labile, even though the Ru(II) ion is squarely in the plane of the porphyrin. Apparently the CO group in the ruthenium complexes exerts a strong trans-labilising effect. This observation is supported in this work by the effect a coordinating solvent such as DMSO has on the cathodic electrochemistry of these complexes. Two reversible one electron reductions are noted for Ru(II) TPPCO and Ru(II) OEPCO in DMSO/0.1M $TBABF_4$. The $E_{\frac{1}{2}}$ potentials for these redox couples are listed below-

	$E_{\frac{1}{2}}$(1st red)/V*	$E_{\frac{1}{2}}$(2nd red)
Ru(II) TPPCO	-1.49	-1.94
Ru(II) OEPCO	-1.70	-2.19

* Volts vs Ag/AgCl : corrected for solvent junction-potential.

The voltammetric pattern of redox potential suggest both reductions are macrocycle-based. Spectral characterisation of the products confirms this.

The visible spectrum of the one electron reduction product of Ru(II) TPPCO, in DMSO, is shown in Figure 19. The yellow-green product displays a typical metalloporphyrin π anion radical spectrum and is stable at room temperature. This species displays a fully isotropic esr signal at -40°C ($g = 2.0020$ $\Delta H = 12.5G$). No hyperfine is observed. Reduction at the second wave is not reversible on the time scale of the bulk electrolysis. The final green product displays a typical metallophlorin anion visible spectrum indicating initial formation of the π dianion (Section 3.6).

Ru(II) OEPCO behaves exactly in the same manner. The stable first reduction product displays the characteristic peaks of the π anion radical in the near ir/visible region of the optical spectrum and an isotropic esr signal ($g = 2.0000$ $\Delta H = 15G$ at -40°C). The second reduction again results in a metallophlorin anion. Spectral data for the reduction

Figure 4.19 Optical progression during the first one-electron reduction of RuTPPCO in DMSO/0.1M $TBABF_4$ at 20°C

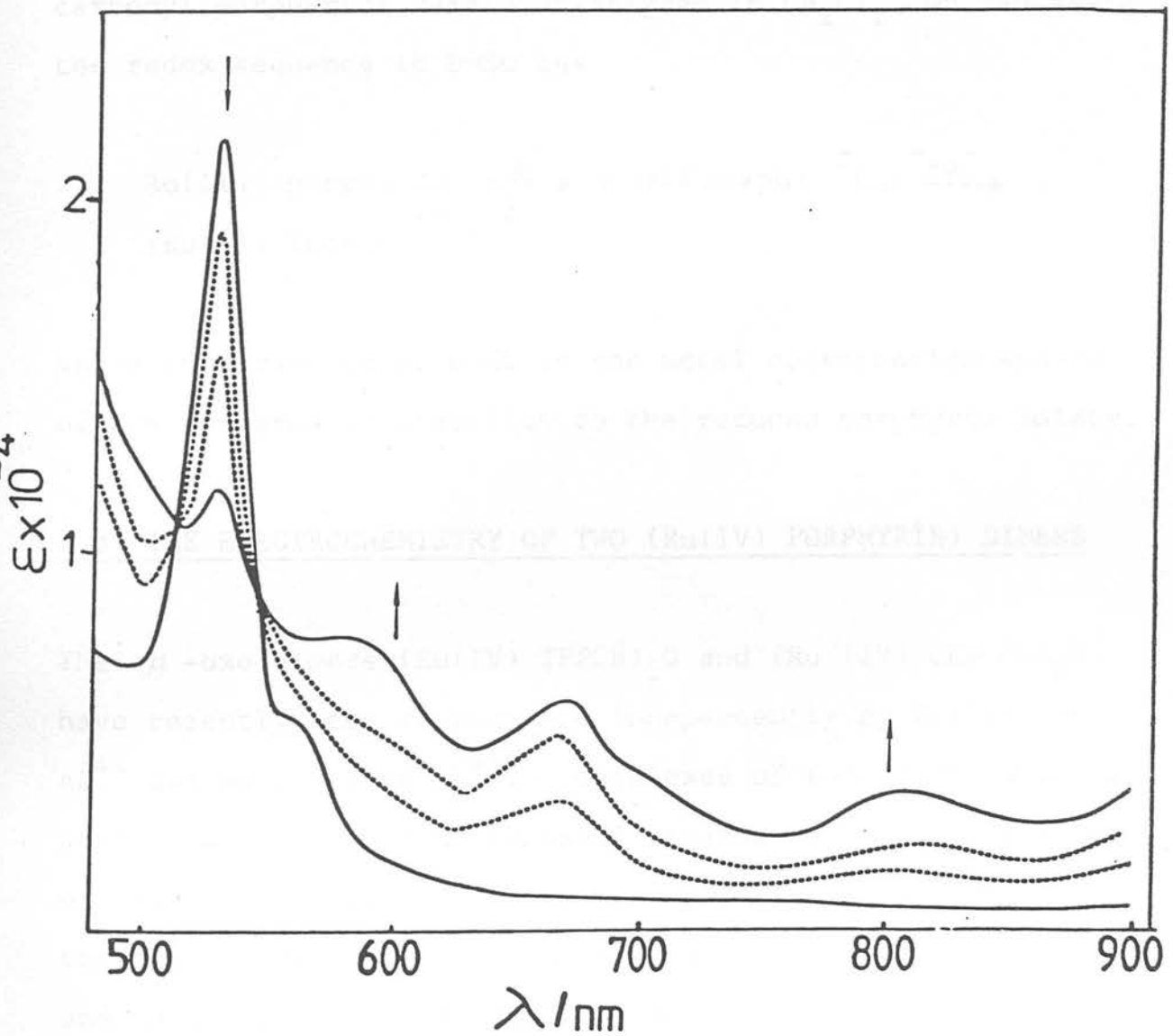

products of both Ru(II) TPPCO and Ru(II) OEPCO are listed in Table 6.

Therefore although the cathodic products of the ruthenium carbonyl porphyrins remain unassigned in CH_2Cl_2, we can assign the redox sequence in DMSO as-

$$\text{Ru(II) (porph) CO} \xrightarrow{+e^-} \underset{\text{(Ru(II) (porph) CO)}^{2-}}{\text{(Ru(II)(porph)}^{-}\text{CO)}^{2-}} \xrightarrow{+e^-}$$

where the presence of DMSO in the metal coordination sphere offers far greater stability to the reduced porphyrin moiety.

4.5 THE ELECTROCHEMISTRY OF TWO (Ru(IV) PORPHYRIN) DIMERS

The μ -oxo dimers $(Ru(IV)\ TPPOH)_2O$ and $(Ru\ (IV)\ OEP\ OH)_2O$ have recently been synthesised independently by Collman et al[42] and Sugimoto et al.[43]. Complexes of this form have the attraction of having no CO axial ligands to direct the site of oxidation or reduction. They are also likely models for the highly oxidised Fe(III) μ -oxo dimers discussed previously, and thus indirectly the oxidised form of cytochrome P450.

X-ray studies[44] have shown the Ru(IV)-O-Ru(IV) linkage to be almost exactly linear, with the mean planes of the porphinato cores 3.17Å apart. Contrastingly iron porphyrin μ -oxo dimers contain a bent FeOFe bond. For example in $(Fe(III)\ TPP)_2O$, the FeOFe angle is 174.5°[45].

Sugimoto has reported[43] on the electrochemical behaviour of complexes of the general formula $(M(IV)OEPX)_2O$ (where X = OH^-, Cl^-, Br^-, OCH_3^- and M = Ru, Os). All of the complexes were found to display two quasi-reversible reductions and one quasi-reversible oxidation in CH_2Cl_2. Each wave was assigned as a two-electron step from coulometric measurements. The two reductions were assigned as metal-based redox steps and the oxidation as a macrocycle-based step-

$$(M(IV)OEPX)_2O \xrightarrow{+2e^-} ((M(III)OEPX)_2O)^{2-} \xrightarrow{+2e^-} ((M(II)OEPX)_2O)^{4-}$$

$$(M(IV)OEPX)_2O \xrightarrow{-2e^-} ((M(IV)OEP^{+}X)_2O)^{2+}$$

The reported redox behaviour of the tervalent iron μ-oxo bridged dimers is quite different from that above. Phillipi and Goff[46] observed the electrochemical oxidation of $(Fe(III)TPP)_2O$ gave rise to both one-electron oxidised $(Fe(III)\text{-}O\text{-}Fe(IV))^{+}$ and two-electron oxidised $(Fe(IV)\text{-}O\text{-}Fe(IV))^{2+}$ species. Sugimoto rationalised the different behaviour of the iron complexes, to that exhibited by the ruthenium and osmium complexes, by suggesting that the redox properties were dependent on the geometry of the dimer i.e. for the iron complex he predicted there would be a weaker electronic interaction between the two porphyrin moieties (through the oxygen bridge) due to the non-linearity of the Fe-O-Fe linkage.

It should be noted no spectral characterisation of the electrode products of the $(M(IV)OEPX)_2O$ complexes was carried out. In a re-examination of the electrochemistry of $(Ru(IV)TPPOH)_2O$(1) and $(Ru(IV)OEPOH)_2O$(2) we find a quite different redox sequence for these complexes, to that proposed previously.

(1) and (2) exhibit two fully reversible reductions and a fully reversible oxidation in CH_2Cl_2/0.5M $TBABF_4$. The potentials of the redox steps of (2) are similar to those reported previously[43]. A further irreversible reduction is noted for both complexes at more cathodic potentials.

The $E_{\frac{1}{2}}$ values for each wave are tabulated below-

	$E_{\frac{1}{2}}$(ox)/V*	$E_{\frac{1}{2}}$(1st red)	$E_{\frac{1}{2}}$(2nd red)	$E_{\frac{1}{2}}$(3rd red)
(1)	+1.09	+0.20	-1.22	-1.98^{+}
(2)	+0.80	+0.11	-1.20	-2.06^{+}

* Volts vs. Ag/AgCl reference electrode. $^{+}$irreversible

A stirred d.c. voltammogram of (1) is shown in Figure 20, clearly showing each of the reversible redox steps to involve the same number of electrons. Careful coulometric measurements on the two reduction waves, at room temperature, showed

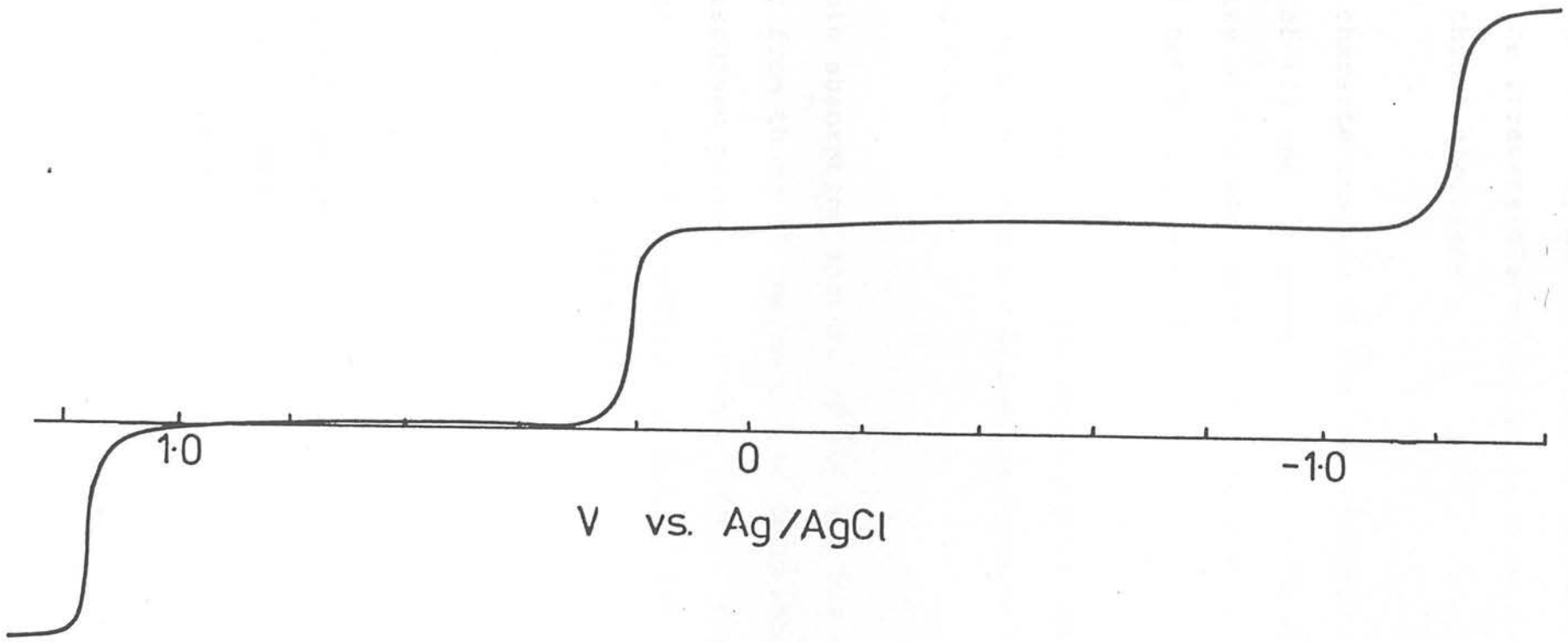

Figure 4.20 Stirred d.c. voltammogram of (1) in CH_2Cl_2/0.5M $TBABF_4$ (20°C)

each to involve only one electron. The oxidation product proved to be unstable on the extended bulk-electrolysis time-scale. The irreversible reduction is a multi-electron step (greater than 4 electrons).

Spectral characterisation of the one-electron oxidation products of (1) and (2) proved impracticable due to the instability of the electrode products, even at -70°C. This wave will not be discussed further.

The initial complexes, and the one electron and two-electron reduction products were esr silent at temperatures between -150°C and 20°C.

The visible absorption spectra of (1) and (2) are considerably different from those of the monomeric metalloporphyrin complexes discussed previously in this work. Figure 21 shows the visible electronic spectrum of (1). The Q(0,0) and Q(1,0) bands are considerably broadened. Other dimeric ruthenium complexes with a μ-oxo linkage also show intense anomolous light absorption in the visible region; e.g. $((Ru(bipy)_2Cl)_2O)^{2+}$ λ_{max} = 672, ϵ = 17,900[47] and $((RuCl_5)_2O)^{4-}$ λ_{max} = 500nm[48]. These extraneous bands have been assigned[49] as transitions arising from orbitals involved in the -Ru-O-Ru-bridge and it is likely this is the cause of the broadening observed in the porphyrin analogues studied

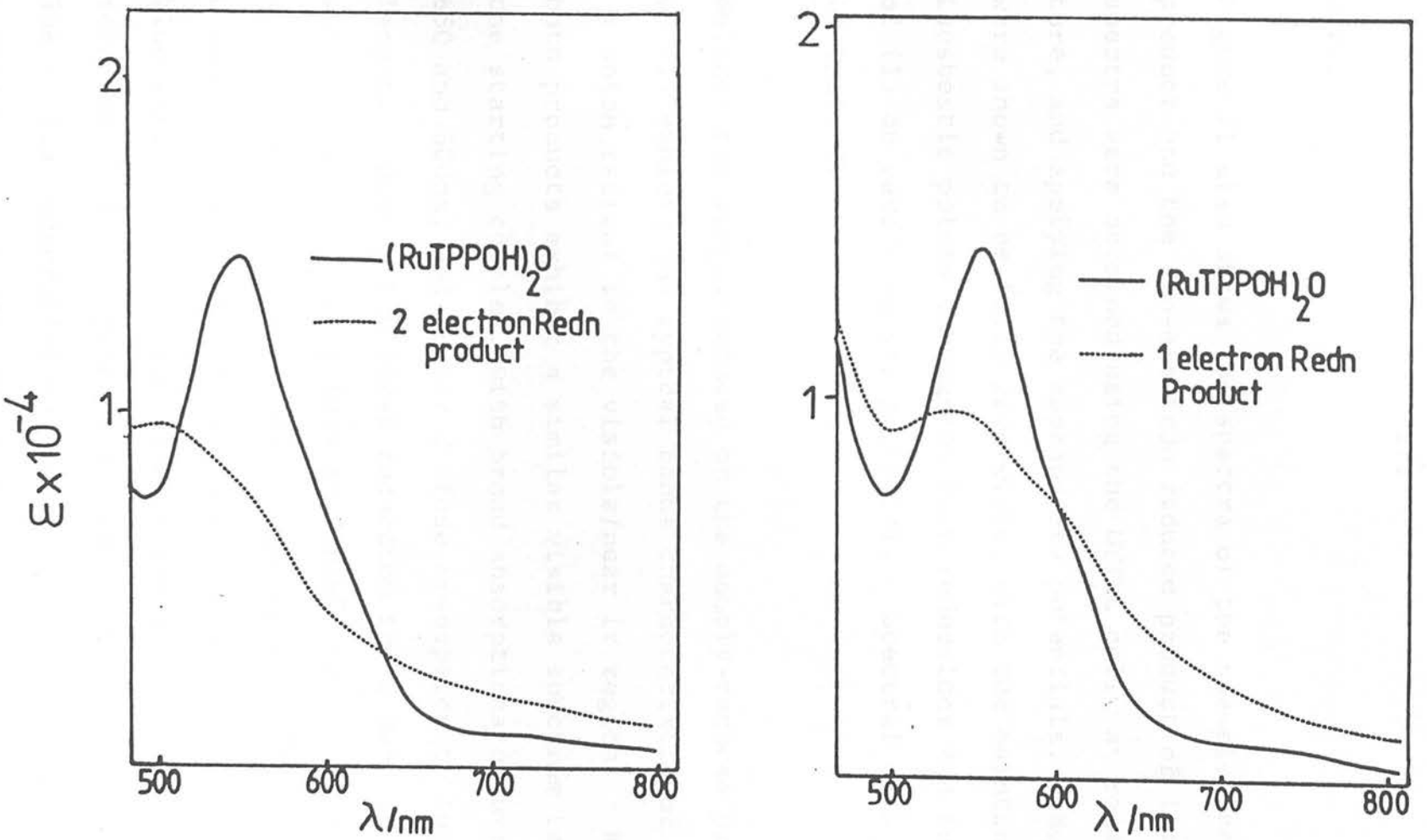

Figure 4.21 Visible spectra of the reduced products of complex (1) in CH_2Cl_2/0.5M $TBABF_4$ at 20°C

here.

Figure 21 also shows the spectra of the one-electron reduced product and the two-electron reduced product of (1). These spectra were obtained using the OTTLE cell, at room temperature, and applying the appropriate potentials. Both steps were shown to be fully reversible, with the maintenance of isosbestic points throughout both reductions and full recovery of (1) on reversing the potential. Spectral data are listed in Table 7.

Neither the singly-reduced or the doubly-reduced products of (1) exhibit the typical bands characteristic of a porphyrin π anion radical in the visible/near ir region. Rather, both products exhibit a similar visible spectrum to that of the starting complex, with broad absorptions occurring between 650 and 500nm, and weaker diffuse absorption to longer wavelength. During the first reduction the Q band is seen to shift to higher energy from 18,200cm^{-1} to 18,900 cm^{-1}. A similar shift occurs during the second reduction where the Q band of the final limiting spectrum is at 19,650cm^{-1}. The blue shift of the Q band is consistent with two successive metal reductions, rather than reduction of the porphyrin ring. The optical absorption changes in the Soret region also follows a systematic pattern, supporting the assignment of a metal-based redox site. The Soret band does <u>not</u> split during the

Table 4.7 Spectral data for the reduction products of $(Ru(IV)TPPOH)_2O$ and $(Ru(IV)OEPOH)_2O$ in CH_2Cl_2/0.5M $TBABF_4$

	Wavelength maxima, nm (extinction coefficient x 10^{-3})
$(Ru(IV)TPPOH)_2O$	550(15.2), 406(200)
$(Ru(IV)TPPOH)_2O^-$	610(8.2), 529(9.9), 408(246)
$(Ru(IV)TPPOH)_2O^{2-}$	600(8.6), 509(10.1), 411(287)
$(Ru(IV)OEPOH)_2$ O	582(20.9), 511(13.2), 377(205)
$(Ru(IV)OEPOH)_2O^-$	640(11.4), 547(16.9), 380(220)
$(Ru(IV)OEPOH)_2O^{2-}$	632(9.2), 515(18.0), 385(261)

first one-electron reduction. Instead it gains in intensity and shifts to the red. These spectral changes are repeated during the second one-electron reduction. Figure 22 shows the Soret region of the initial complex (1) and the two reduction products. Although the extinction coefficient of the Soret band increases upon initial reduction and again after the second reduction, the oscillator strength of the band remains constant throughout. The general observation then is that the Soret band shifts to the red and simultaneously sharpens during both reduction steps. The spectra of the reduced products are temperature independent (20°C to -70°C).

Complex (2) undergoes exactly analogous spectral changes upon reduction. The two reversible reductions occur at very similar potentials to that observed for (1). Spectral data for the singly and doubly reduced products of (2) are listed in Table 7. Again the oxidation product proved extremely unstable and spectral characterisation of this species proved impossible.

Both the voltammetric and spectral data suggest that the two reversible reductions occur at a metal-based site. We thus propose the following reduction sequence-

Figure 4.22 Near uv spectra of the reduced products of complex (1) in CH_2Cl_2/0.5M $TBABF_4$ at 20°C

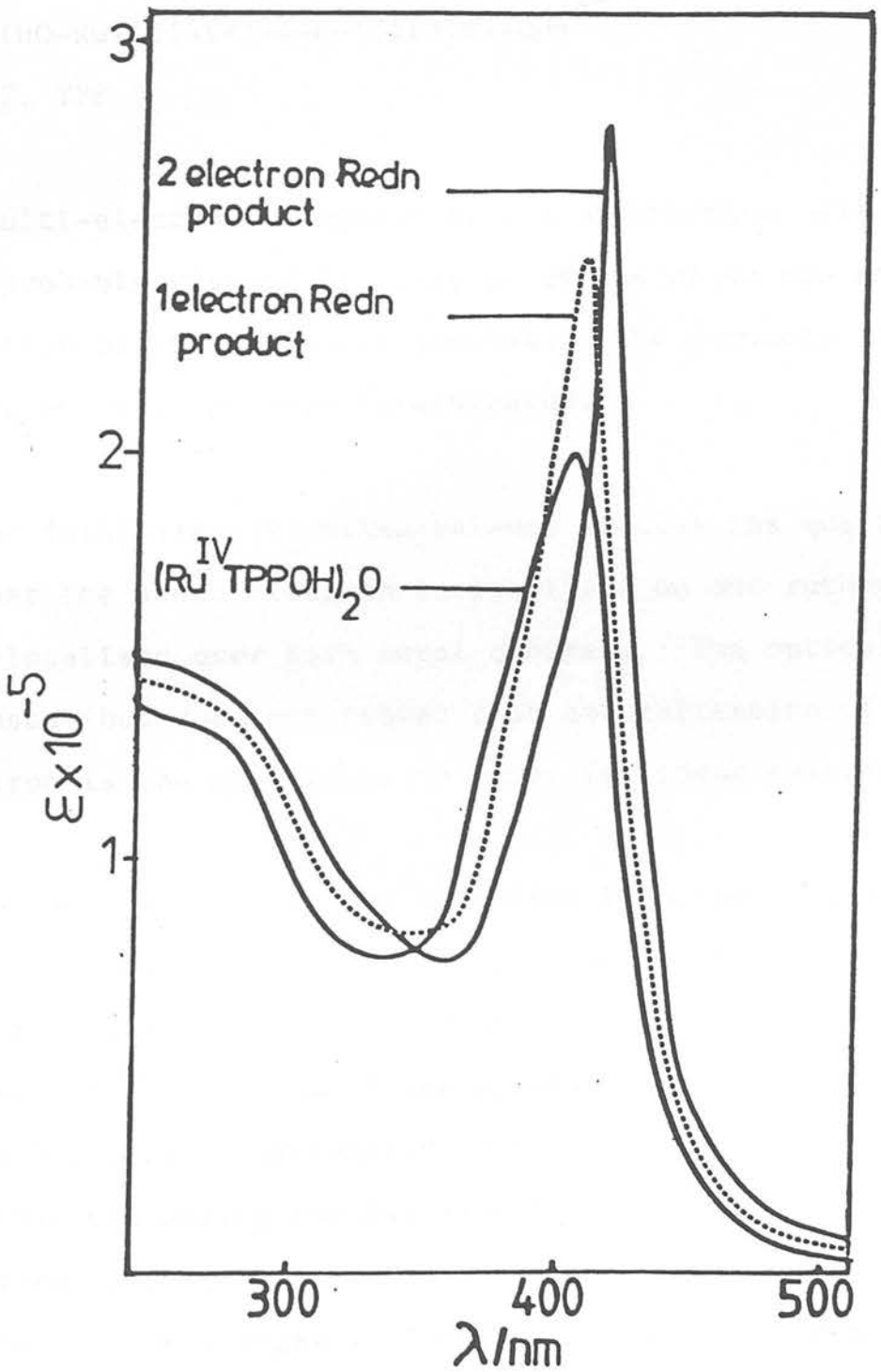

$$HO\text{-}Ru(IV)(P)\text{-}O\text{-}Ru(IV)(P)\text{-}OH \quad ^{0}$$

$$\downarrow +e^{-}$$

$$(HO\text{-}Ru(IV)(P)\text{-}O\text{-}Ru(III)(P)\text{-}OH)^{-}$$

$$\downarrow +e^{-}$$

$$(HO\text{-}Ru(III)(P)\text{-}O\text{-}Ru(III)(P)\text{-}OH)^{2-}$$

P= OEP, TPP

The multi-electron reduction of the diruthenium (III) species most probably results in cleavage of the dimer and then further reduction of the monomeric species. The products of this reduction have not been investigated.

In the Ru(III)/Ru(IV) mixed valence species the question arises whether the added electron is localised on one ruthenium atom or delocalised over both metal centres. The optical data suggests (but does not prove) that delocalisation of the added electron is the more accurate model for these systems.

If indeed the electron was localised then the mixed-valence complex should exhibit two distinct types of porphyrin π / π^{*} transitions, one for the Ru(III) metal centre and one for the Ru(IV) end of the dimer. This does not appear to be the case as systematic changes in the optical spectrum are observed during the two reductions. The visible band shape remains constant for the singly and doubly reduced species. The changes in the near uv also indicate the unpaired electron is delocalised over both metal-centres,

as the mixed-valence complex exhibits only a single Soret transition. In addition no Ru(III) ⟶ Ru(IV) charge-transfer transition is noted in the electronic spectrum (down to 8000 cm^{-1}).

Other mixed-valence complexes of this type have also been assigned as having the odd electron delocalised over the three atoms in the bridge. Dunitz and Orgel[48] were the first to envisage a series of delocalised molecular orbitals arising from Ru-O-Ru mixing for the diruthenium (IV) species, $((RuCl_5)_2O)^{4-}$. The ground state for this complex was assigned as $(E_u)\ (B_{2g}(B_{2u})(E_g))(E_u^*)$, where the lowest unfilled orbital is an E_u antibonding orbital (arising from interaction of a ruthenium-based E_u orbital and an E_u orbital based on O_2^-). Molecular orbital schemes of this sort help to rationalise why no esr signal is detectable for the parent complexes (1) and (2). For these lower symmetry porphyrin complexes a more appropriate M.O. scheme will be that proposed by Meyer et al[49]. Figure 23 shows the M.O. scheme for $((Ru(bipy)_2Cl)_2O)^{2+}$, where the degeneracy of the LUMO has been lifted. The lowest unfilled levels are then largely Ru d π^* antibonding in character.

M.O. schemes such as these have been used to explain the physical properties of other mixed-valence complexes. $((Ru(NH_3)_5)_2O)^{4+}$ [49] has been shown to undergo a one-electron

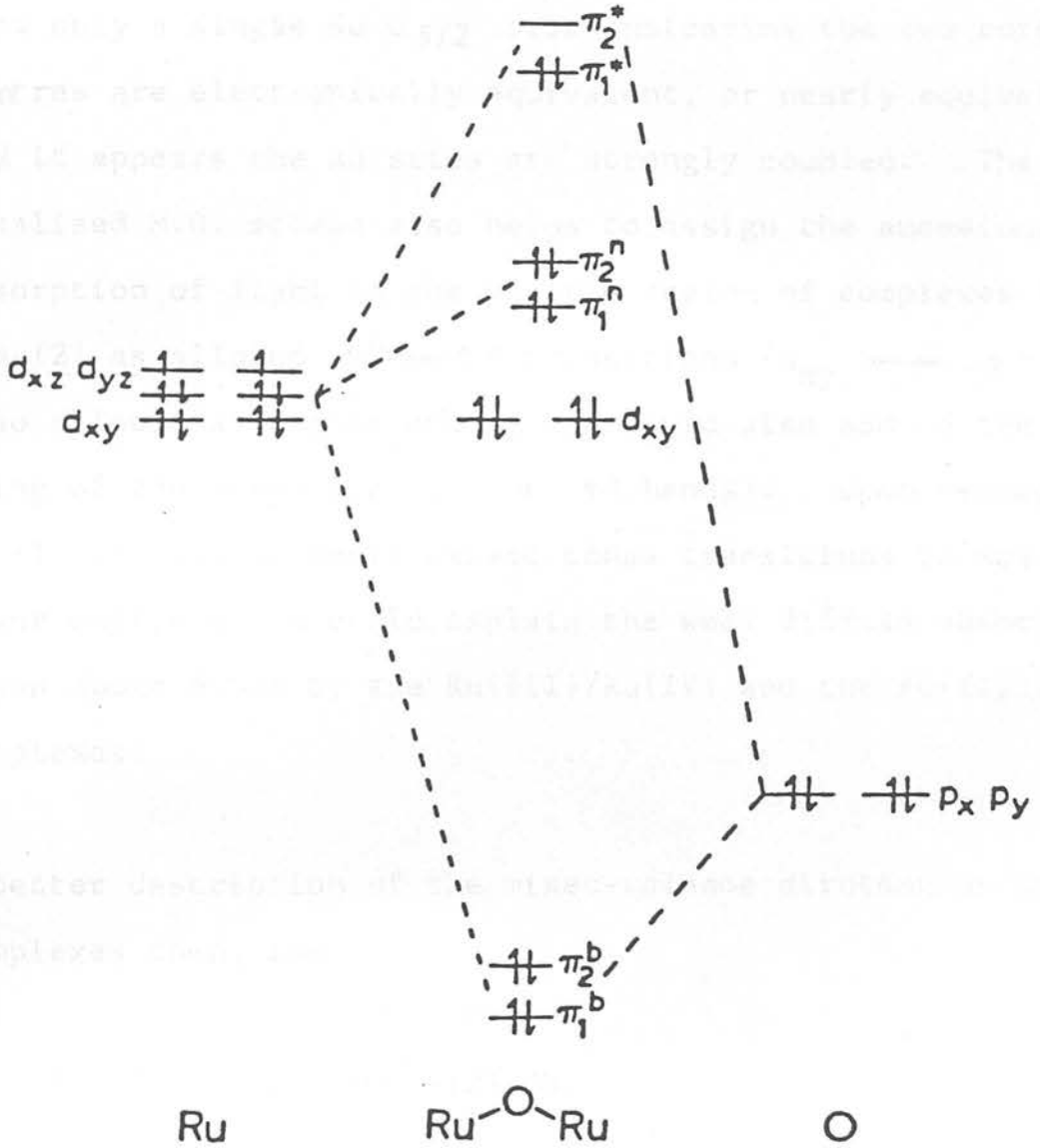

Figure 4.23 M.O. scheme for a Ru-O-Ru bridged complex (from ref. 49)

oxidation to give a mixed valence Ru(III)/Ru(IV) species. X-ray photoelectron spectral data of the oxidised complex show only a single Ru $d_{5/2}$ peak indicating the two ruthenium centres are electronically equivalent, or nearly equivalent, and it appears the Ru sites are strongly coupled. The delocalised M.O. scheme also helps to assign the anomalous absorption of light in the visible region of complexes (1) and (2) as allowed $\pi^n \longrightarrow \pi^*$ transitions ($d_{xy} \longrightarrow \pi^*$ are also allowed at higher energy and could also add to the broadening of the porphyrin π / π^* bands). Upon reduction of (1) and (2) we would expect these transitions to move to lower energy which could explain the weak diffuse absorption shown above 600nm by the Ru(III)/Ru(IV) and the Ru(III)/Ru(III) complexes.

A better description of the mixed-valence diruthenium porphyrin complexes then, is-

$$(HO(P) - (Ru\text{-}O\text{-}Ru)^{-} - (P)\ OH)^{-}$$

where the formal charge on the rutheniums, as seen by the porphyrin moieties, is 3.5.

This contrasts sharply with the localised model assigned to the $(TPP\ Fe\ (III)\ -O-Fe(IV)\ TPP)^{+}$ moiety, where the iron centres are magnetically distinct[46].

Finally, it is worth mentioning the remarkable stability afforded to Ru(IV) in these complexes. Other Ru(III) Ru(III)/ Ru(III) Ru(IV) redox couples have been noted for ruthenium μ-oxo dimers. The $((Ru(NH_3)_5)_2O)^{4+/5+}$ couple for instance occurs at +0.32V[49] (vs SCE reference) and the $((Ru(bipy)_2Cl)_2O)^{2+/3-}$ couple at +0.68V[47]. Both these couples are far more anodic than the equivalent couples exhibited by (1) and (2). This is possibly due to the linear geometry of the Ru-O-Ru bridge in (1) and (2) allowing a greater degree of delocalisation of charge in these complexes. The fixed geometry of the porphyrin ring has been suggested as an important factor in the linearity of the Ru-O-Ru linkage[43]. It can be said that the diruthenium (IV) dimers studied here certainly display far more delocalisation of charge than does (TPP Fe(III)-O-Fe(IV) TPP)$^+$, very probably due to the lesser d-orbital radial extension of the first-row transition metal.

4.6 EXPERIMENTAL

The iron porphyrins Fe(III) TPPCl and Fe(III) OEPCl were synthesised using well established literature procedures[50]. Ru(II) TPPCO and Ru(II) OEPCO were prepared by the method of Whitten et al[15]. (Ru(IV) TPPOH)$_2$O and (Ru(IV) OEPOH)$_2$O were prepared by the method of Collman[42] and Sugimoto[43] respectively. Voltammetric and spectroelectrochemical techniques are discussed adequately in Chapters 2 and 3.

REFERENCES : CHAPTER 4

1. C.H. Welborn, D. Dolphin and B.R. James, J. Am. Chem.Soc. 1981, 103, 2869.
2. T. Mashiko, C.A. Reed, K.J. Haller, M.E. Eastner and W.R. Scheidt J. Am. Chem. Soc 1981, 103, 5758.
3. J.W. Buchler "The Porphyrins" Ed. D. Dolphin, Academic Press, New York, 1978, Vol. 1. p. 453 and references therein.
4. N.P. Farrell, D. Dolphin and B.R. James, J. Am. Chem.Soc. 1978, 100, 324.
5. H. Masuda, T. Taga, K. Osaki, H. Sugimoto, M. Mori and H. Ogoshi, J. Am. Chem. Soc., 1981, 103, 2199.
6. J.T. Groves, R.L. Haushalter, M. Nakamura, T.E. Memo and B.J. Evans, J. Am. Chem. Soc., 1981, 103, 2884.
7. D. Dolphin, A. Forman, D.C. Borg, J. Fajer and R.H. Felton, Proc. Natl. Acad. Sci. USA, 1971, 68, 614.
8. A. Wolberg and J. Manassen, J. Am. Chem. Soc., 1970, 92, 2982.
9. R.H. Felton, G.S. Owen, D. Dolphin, A. Forman, D.C. Borg and J. Fajer, Ann. N.Y. Acad. Sci., 1973, 206, 504.
10. K.M. Kadish, J.S. Cheng, I.A. Cohen and D. Summerville, A.C.S. Symp. Ser., 1977, 38 (Electrochem. Stud. Biol. Syst. Sump., 1976), p. 65.
11. M.A. Phillippi, E.T. Shimomura and H.M. Goff, Inorg.Chem 1981, 20, 1322.

12. R.H. Felton, G.S. Owen, D. Dolphin and J. Fajer, J. Am. Chem. Soc., 1971, 93, 6332.

13. R.H. Felton "The Porphyrins" Ed. D. Dolphin, Academic Press, New York, 1978, Vol. V, p. 92.

14. D.A. Summerville and I.A. Cohen, J. Am. Chem. Soc., 1976, 98, 1747.

15. G.M. Brown, F.R. Hopf, J.A. Ferguson, T.J. Meyer and D.G. Whitten J. Am. Chem. Soc., 1973, 95, 5939.

16. G.M. Brown, F.R. Hopf, T.J. Meyer and D.G. Whitten, J. Am. Chem. Soc., 1975, 91, 5385.

17. T. Malinski, D. Chang, L.A. Bottomley and K.M. Kadish, Inorg. Chem., 1982, 21, 4248.

18. D.P. Rillema, J.K. Nagle, L.F. Barringer, Jr. and T.J. Meyer, J. Am. Chem. Soc., 1981, 103, 56.

19. J.-H. Fuhrhop, K.M. Kadish and D.G. Davis, J. Am. Chem.Soc., 1973, 95, 5140.

20. G. Caquis and G. Marback, Bioelec. Bioenerg., 1974, 1, 23.

21. K.M. Kadish and D.G. Davis Ann. N.Y. Acad. Soc., 1973, 206, 495.

22. A. Wolberg, Isr. J. Chem., 1974, 12, 1031.

23. D. Lexa, M. Momenteau, J. Mispelter and J.M. Lhoste, Bioelec. Bioenerg., 1974, 1, 108.

24. L.A. Constant and D.G. Davis, Anal. Chem., 1975, 47, 2253.

25. K.M. Kadish, G. Larson, D. Lexa and M. Momenteau. J. Am. Chem. Soc., 1975, 97, 282.

26. T. Boschi, G. Bontempelli and G.A. Mazzocchin, Inorg. Chim. Acta., 1979, 37, 155.

27. H. Kobayashi, T. Higuchi and K. Eguchi, Bull. Chem. Soc.Jpn. 1975, 48, 3137.

28. J.T. Groves, T.E. Meno and R.S. Myers, J. Am. Chem. Soc., 1979, 101, 1032.

29. J.T. Groves, R.C. Haushalter, M. Nakamura, T.E. Nemo and B.J. Evans, J. Am. Chem. Soc., 1981, 103, 2884.

30. L.K. Hanson, C.K. Chang, M.S. Davis and J. Fajer, J. Am. Chem. Soc., 1981, 103, 663.

31. H.B. Dunford and J.S. Stillman, Coord. Chem. Rev. 1976, 19, 187.

32. W.D. Hewson and L.P. Hagler, "The Porphyrins" Ed. D. Dolphin, Academic Press, New York, 1979, Vol VII p. 295.

33. M. Gouterman, Vol. III, p. 1 of reference 32.

34. I.A. Cohen, D. Ostfield and B. Lichtenstein, J. Am. Chem. Soc., 1972, 94, 4522.

35. D. Lexa, M. Momenteau and J. Mispelter, Biochim. Bio-Phys. Acta., 1974, 338, 151.

36. M. Gouterman, G.H. Wagniere and L.C. Snyder, J. Mol. Spectrosc., 1963, 11, 108.

37. Z. Yoshida, H. Ogoshi, T. Omura, E. Watanabe and T. Kurosaki, Tetrahedron Lett., 1972, 1077.

38. I. Morishima, Y. Shiro and Y. Takamuki, J. Am. Chem. Soc., 1983, 105, 6168.

39. T. Malinski, D. Chang, L.A. Bottomley and K.M. Kadish, J. Am. Chem. Soc., 1982, 21, 4248.

40. B.A. Goodman and J.B. Raynor, Adv. Inorg. Chem. Radiochem., 1978, 13, 278.

41. S.S. Eaton, G.R. Eaton and R.H. Holm, J. Organometal. Chem., 1972, 39, 179.

42. J.P. Collman, C.E. Barnes, T.J. Collins, P.J. Brothers, J. Galluci and J.A. Ibers, J. Am. Chem. Soc., 1981, 103, 7030.

43. H. Sugimoto, T. Higashi, M. Mori, M. Nagano, Z. Yoshida and H. Ogoshi, Bull. Chem. Soc. Jpn., 1982, 55, 822.

44. H. Masuda, T. Taga, K. Osaki, H. Sugimoto, M. Mori, and H. Ogoshi, J. Am. Chem. Soc., 1981, 103, 2199.

45. (a) E.B. Fleischer and T.S. Srivastava, J. Am. Chem. Soc., 1969, 91, 2403.

(b) A.B. Hoffman, D.M. Collins, V.W. Day, E.B. Fleischer, T.S. Srivastava and J.L. Hoard, J. Am. Chem. Soc., 1972, 94, 3620.

46. M.A. Phillippi and H.M. Goff, J. Am. Chem. Soc., 1979, 101, 7641.

47. T.R. Weaver, T.J. Meyer, S. Adeyemi, G.M. Brown, R.P. Eckberg, W.E. Hatfield, E.C. Johnson, R.W. Murray and D. Untereker, J. Am. Chem. Soc., 1975, 97, 3039.

48. J.D. Dunitz and L.E. Orgel, J. Chem. Soc., 1953, 2594.

49. J.A. Baumann and T.J. Meyer, Inorg. Chem., 1980, 19, 345.

50. A.D. Adler, F.R. Longo and V. Varadi, "Inorganic Synthesis", Ed. F. Basolo, McGraw-Hill, New York, 1976, Vol. 16, p. 213.

CHAPTER 5 SPECTROELECTROCHEMICAL STUDIES ON CHLORINS AND BACTERIOCHLORINS

5.1 INTRODUCTION

In the previous three chapters we have dealt extensively with the effect the central metal has on the frontier orbitals of the porphinato moiety. Also of great importance is how structural modifications at the periphery of the macrocycle affect the basic 18 π electron core. Of particular interest is the redox chemistry of the reduced porphyrins such as the chlorin and bacteriochlorin rings (see Chapter 1). Despite their great natural abundance surprisingly little work has been undertaken to define and characterise the electrochemical properties of these pigments. Studies on chlorin derivatives such as the chlorophylls and the pheophytins have been reported[1-5], but more as isolated compounds as befits their biochemical role, rather than as a direct attempt to correlate the redox potentials of a series of complexes. Fuhrhop,[6] in a potentiometric study on the oxidation of a series of metallo-octaethylchlorin (MOEC) derivatives (M = Zn, Cu, Ni, Pd and Mg), concluded that the chlorin ring was approximately 300 mV easier to oxidise than the corresponding porphyrin. A subsequent electrochemical study on ZnOEC by Stolzenberg et al.[7] reported the complex to undergo two one-electron oxidations in acetonitrile.

The products were assumed to be the π -cation radical and π dication, although no spectral characterisation was presented. However, no reduction waves were observed. More recently Kadish et al.[8] have reported on the electrochemistry of nickel meso-tetramethylchlorin. This complex displayed two reversible one-electron oxidations and one reversible one-electron reduction, in CH_2Cl_2. Electronic spectral characterisation of all three redox products was presented. Interestingly, the one-electron reduction product exhibited no absorption in the visible region, unlike the porphyrin analogue. Even more recently Ryan et al.[9] have reported on the cathodic electrochemistry of chloro-iron meso-tetraphenylchlorin (Fe(III) TPCCl). They were primarily interested in the kinetics of the first reduction wave in the presence of various amines. Again no spectroelectrochemical characterisation of the electrode products was attempted.

Here, we present the electrochemical behaviour of a series of first-row transition metal complexes incorporating both the OEC and TPC ligands in strictly non-coordinating aprotic media. In addition we report on the electrochemistry of the free-base meso-tetraphenylbacteriochlorin (H_2TPBC). The spectroelectrochemical results obtained for these model complexes proved invaluable in rationalising the redox behaviour of two naturally occurring chlorin

macrocycles, bonellin (1) and methyl pheophorbide a.(2).

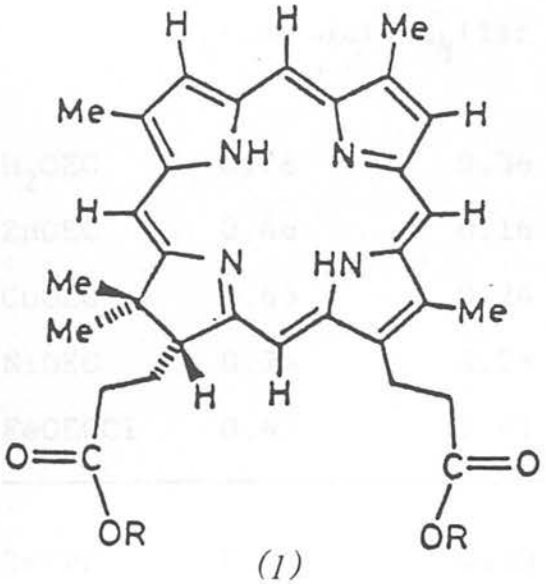

(1)

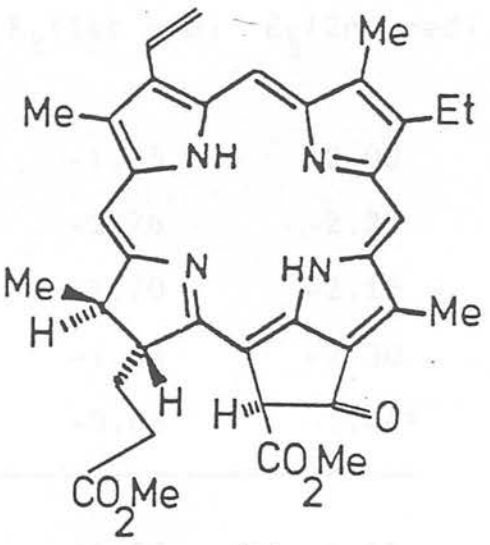

(2)

5.2 RESULTS

In contrast to previous reports, voltammetric and coulometric measurements showed the metallochlorins to exhibit very similar redox properties to the metalloporphyrins. In CH_2Cl_2/0.5M $TBABF_4$ all the complexes studied exhibited two one-electron oxidations. The Zn(II), Cu(II), Ni(II) and Co(II) complexes displayed two one-electron reductions. Four one-electron reductions were observed for FeTPCCl and FeOECCl (as was the case for FeTPPCl and FeOEPCl). The $E_{\frac{1}{2}}$ values for all the waves are listed in Table 1. Both the first oxidation and the first reduction of all the complexes were fully reversible on the voltammetric time-scale at room temperature. The second oxidation and the second reduction were only fully reversible at

Table 5.1 Redox Potentials of Metallochlorins and H_2TPBC in CH_2Cl_2/0.5M $TBABF_4$ at 20°C (Volts vs Ag/AgCl)

	$E_{\frac{1}{2}}$(2nd ox)	$E_{\frac{1}{2}}$(1st ox)	$E_{\frac{1}{2}}$(1st red)	$E_{\frac{1}{2}}$(2nd red)
H_2OEC	0.76	0.36	-1.55	-2.00
ZnOEC	0.46	0.16	-1.76	-2.22
CuOEC	0.63	0.24	-1.70	-2.15
NiOEC	0.74	0.28	-1.68	-2.30
FeOECCl	0.83	0.41	-0.63	-1.44*
ZnTPC	0.63	0.30	-1.57	-1.95
CuTPC	0.79	0.39	-1.52	-1.94
CoTPC	0.71	0.40	-1.11	-2.17
FeTPCCl	0.88	0.58	-0.59	-1.32*
H_2TPBC	0.67	0.27	-1.42	-1.80
H_2TPC	0.91	0.57	-1.41	-1.79
H_2TPP	1.00	0.76	-1.41	-1.78

*Fe(III)TPCCl exhibits two further one-electron reductions at -1.90 and -2.33V

Fe(III)OEPCl also exhibits two further one-electron reductions at -2.04 and -2.48V.

very low temperatures ($<$ -50°C).

When comparing the $E_{\frac{1}{2}}$ (1st red) and $E_{\frac{1}{2}}$ (2nd red) values obtained for the chlorins with the same values for the porphyrin complexes, a remarkable coincidence is observed. The reduction potentials of both series are virtually coincident e.g. ZnTPC reduces at exactly the same potential as ZnTPP. This is true not only of the macrocycle-based reductions but also the metal-based cathodic electron-transfers. For instance the first reductions of both CoTPC and CoTPP occur at -1.11V. These are important observations in that the chemical bonding between the metal ion and the chlorin ring must be exactly analogous to the bonding between the same metal ion and the porphyrin ring i.e. saturation of one of the peripheral double bonds does not affect either the energy of the macrocycle-based LUMO or the metal ion d-manifold. The π-acceptor properties of the porphyrin and the chlorin must also be identical. In addition it was noted that the $E_{\frac{1}{2}}$ (1st red) and $E_{\frac{1}{2}}$ (2nd red) values of H_2TPP, H_2TPC and H_2TPBC occur at exactly the same potentials. This confirms that peripheral saturation does not affect the energy of the lowest acceptor orbital of the π array.

The oxidative behaviour of the metallochlorins however differs significantly from that displayed by the metallo-

porphyrins. The Zn(II), Cu(II) and Ni(II) chlorins oxidise at much less anodic potentials than the corresponding porphyrins. The observed difference in $E_{\frac{1}{2}}$ (1st ox) for the MC and MP species is relatively constant (280 - 300mV) eg ZnOEC; 0.16v:ZnOEP; 0.44v). This is consistent with the potentiometric results reported previously[6]. A similar difference in first oxidation potentials was noted between the ferric chlorins and the ferric porphyrins. Spectroelectrochemical characterisation confirmed the primary oxidation product of Fe(III) TPCCl and Fe(III)OECCl to be a chlorinato π-cation radical (see later). This is consistent with the site of oxidation in the ferric porphyrins also to be the macrocycle. One must be extremely careful however with this type of analysis. The first oxidations of Co(II)TPC (0.40V) and Co(II) TPP (0.41V) are extremely close in energy. This, initially, would suggest the cobalt chlorin undergoes a metal-based Co(II)/(III) couple upon oxidation, similar to Co(II)TPP (as the cathodic electrochemistry showed the energy of the metal d-orbitals to be invariant whether TPC ro TPP was the chelating ligand). However, from Figure 2.8, where $E_{\frac{1}{2}}$ (1st red) of the MTPP series was plotted against central metal electronegativity, a theoretical value for the Co(II) TPP/$(Co(II)TPP^{+\cdot})^{+}$ couple can be extrapolated. The value thus obtained of 0.70V is 300 mV more positive than the measured Co(II)TPC/$(Co(II)TPC)^{+}$

couple. Indeed a plot of $E_{\frac{1}{2}}$ (1st ox) vs. central metal electronegativity for ZnTPC, CuTPC and CoTPC yields a linear relationship. Spectroelectrochemical characterisation confirmed that oxidation of all three metallochlorins results in π-cation radicals (see later). The trend in oxidation potentials for H_2TPP, H_2TPC and H_2TPBC clearly shows the effect peripheral saturation of the double bonds has on the HOMO of the macrocycles. H_2TPC is easier to oxidise than H_2TPP by 290mV and similarly H_2TPBC is easier to oxidise than H_2TPC by exactly the same amount. Thus, while the energy of the π^* LUMO is largely unaffected by the structural modifications present in chlorins and bacteriochlorins, the energy of the HOMO increases systematically through the series $H_2TPP < H_2TPC < H_2TPBC$. As the energy of the metal d -orbitals remains independent of the chelating macrocycle, ring-based electron transfer will be relatively more favoured for the more saturated ligands. Graphs of the type shown in Figure 2.8 will obviously then be very useful in predicting whether oxidation is likely to be metal or macrocycle based for other metalloporphyrin/chlorin/bacteriochlorin systems.

Spectroscopic mapping of the frontier orbitals also clearly indicates the decrease in the HOMO/LUMO gap through the series $H_2TPP > H_2TPC > H_2TPBC$. The Q band gradually

moves to lower energy as the macrocycle becomes more saturated. The absolute energies of the Q band agree very closely with the voltammetric results-

	Q(0,0)/eV	ΔE(1st ox-1st red)/V
H_2TPC	1.90	1.98
H_2TPBC	1.67	1.69

The optical absorption spectra of the chlorin and bacteriochlorin macrocycles do in fact show some distinct differences from porphyrin spectra. The lower symmetry of the reduced macrocycles results in a splitting of the Q band and the B band, into non-degenerate x and y polarised transitions[10]. Saturation of peripheral bonds of the porphyrin macrocycle will raise the energy of the π orbitals with electron density at these positions. Therefore the energy of the a_{1u} orbital will increase whereas the energy of the a_{2u} orbital will remain largely unaffected as it has very little electron density at the peripheral positions (see Chapter 3).[+] An obvious consequence of the resulting energy difference between the two highest occupied orbitals is that configurational interaction between the $3a_{2u} \longrightarrow 4e_g$ and $1a_{1u} \longrightarrow 4e_g$ electronic

---

+ For clarity the D_{4h} symmetry labels of a_{1u} and a_{2u} for the two highest filled π orbitals of porphyrins have been retained for the two lower-symmetry macrocycles.

transitions will decrease, as peripheral saturation increases. This is apparent from the electronic spectrum of H_2TPBC where the Q band and the Soret band have almost equivalent intensities (see Table 2). The lowest energy band (Q_y) in both the chlorin and bacteriochlorin electronic spectra can thus be viewed as mainly a $1a_{1u} \longrightarrow 4e_g$ transition. As the voltammetric value ΔE(1st ox - 1st red) agrees closely with the energy of the Q_y transition, oxidation of both H_2TPC and H_2TPBC must involve removal of an electron from the a_{1u} orbital. This is as predicted by recent extended Huckel M.O. calculations on the porphyrin, chlorin and bacteriochlorin moieties[11]. The same calculations also predict the energy of the LUMO to be invariant for all three macrocycles. This is consistent with the observed voltammetric results.

Characterisation of whether the electron-transfer steps of the metallated chlorins are macrocycle or metal based can be viewed in exactly the same manner as described previously for the metalloporphyrins. If an electron is removed from the highest occupied π orbital then the pattern of visible bands will be greatly affected. If the site of oxidation is the metal then the visible band structure should remain the same. The reduction site of the metallochlorins should be exactly analogous to the behaviour exhibited by the metalloporphyrins.

Table 5.2 Spectral data for the oxidation and reduction products of the metallochlorin+

	Wavelength maxima, nm (extinction coefficient x 10^{-3})
ZnOEC	615(64), 566(11.2), 530(6.2), 498(9.4), 400(225)
$ZnOEC^+$	700(7.2), 620(10.6), 550-480 broad absorption (12.2), 395(101.2)
$ZnOEC^-$	750(24.2), 710(10.1), 620(20.4), 576(16.2), 524(14.6), 450(34.5), 416(84.2), 400(77.6)
CuOEC	613(48), 560(14.2), 526(7.4), 494(6.2), 396(156)
$CuOEC^+$	694(5.2), 614(10.1), 547(11.2), 492(10.9), 392(90.1)
$CuOEC^-$	744(16.8), 700(11.2), 614(20.1), 440(30.3) 410(70.2), 396(66.6)
NiOEC	609(48), 556(10.1), 520(6.3), 395(162)
$NiOEC^+$	broad absorption 680-500, 390(84.6)
$NiOEC^-$	740(15.0), 696(8.6), 609(10.2), 440(29.4), 412(62.6), 396(64.2)
ZnTPC	614(55), 596(18.4), 562(12.4), 520(9.6), 423(314)
$ZnTPC^+$	broad absorption 650-500 410(162)
$ZnTPC^-$	770(19.6), 680(8.9), 610(22.4), 580(14.2), 545(14.7), 450(60), 424(150)
CuTPC	613(39.2), 576(11.6), 538(14.0), 508(9.2), 421(300)
$CuTPC^+$	broad absorption 620-500, 408(112)
$CuTPC^-$	760(14.2), 611(18.2), 560(8.4), 440(62), 421(106.4)
CoTPC	610(28.8), 540(9.7), 496(9.9), 432(221)
$CoTPC^+$	broad absorption 610-500, 409(87)
$CoTPC^-$	592(22.6), 500(6.5), 430(172)
FeOECCl	604(29), 560(14.2), 390(292)
FeOEC	664(10.2, 566(10.9), 460(13.2), 396(170.2)
$(FeOEC)^-$	624(31.2), 580(9.6), 520(6.3), 420(152.1)
H_2TPBC	742(120), 521(60), 378(161), 356(130)
H_2TPBC^+	820(10.4), broad absorption 700-500, 350(80.2)

Table 5.2 cont.

H_2TPC	651(42.0), 597(6.0), 542(11.0), 517(16.2), 418(189)
H_2TPC^+	broad absorption 700-500, 410(82.4)

Footnote$^+$ - oxidation data measured in CH_2Cl_2/0.5M $TBABF_4$

- reduction data measured in DMSO/0.1M $TBABF_4$

The one-electron oxidation products of the metallochlorins all displayed similar optical absorption properties and ESR spectra. Figure 1 shows the room temperature visible electronic spectrum of the π-cation radical of ZnOEC. During oxidation, where the observed colour change is from blue to green, the Q_y band is observed to collapse and broad bands are noted to grow throughout the visible region. The Soret band also partially collapses and shifts slightly to the blue. These spectral changes upon oxidation are very similar to those observed during the first oxidation of ZnOEP (see Figure 3.10). The overlapping nature of the bands in the lower symmetry (C_{2v}) metallochlorin π-cation radical spectrum however, precludes assignment of the bands. The green oxidation products of CuOEC, NiOEC, ZnTPC, CuTPC and CoTPC display similar electronic absorption spectra to $ZnOEC^{+}$. Isosbestic points are maintained throughout oxidation at room temperature and the parent metallochlorin was recovered in full upon rereduction at the appropriate potential. The spectra of the metallochlorin π-cation radicals proved to be temperature independent (+20°C to -70°C). Importantly, the one-electron oxidation products of Fe(III)TPCCl and Fe(III)OECCl displayed exactly similar optical behaviour. Thus the oxidation products of both ferric chlorins are also assigned as π-cation radicals. The spectral data for all the metallochlorin π-cation

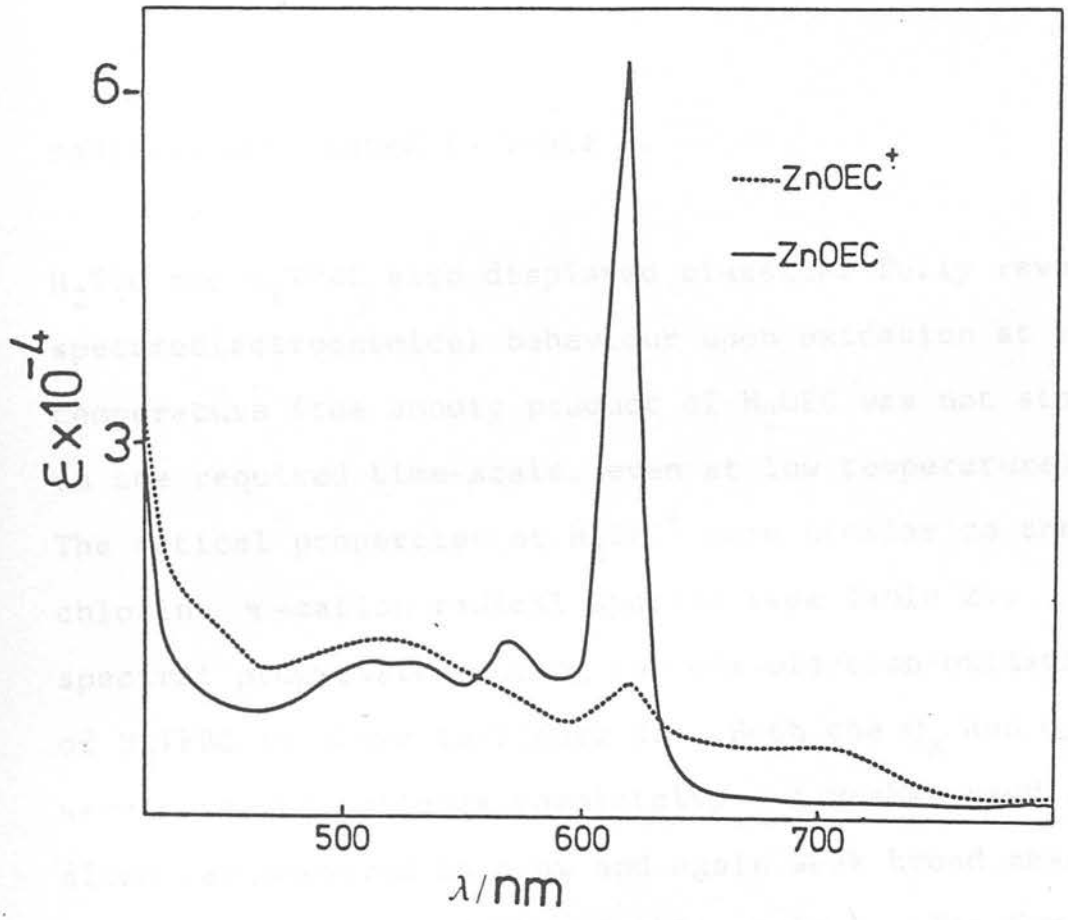

Figure 5.1 One-electron oxidation product of ZnOEC at 20°C (CH_2Cl_2/0.5M $TBABF_4$)

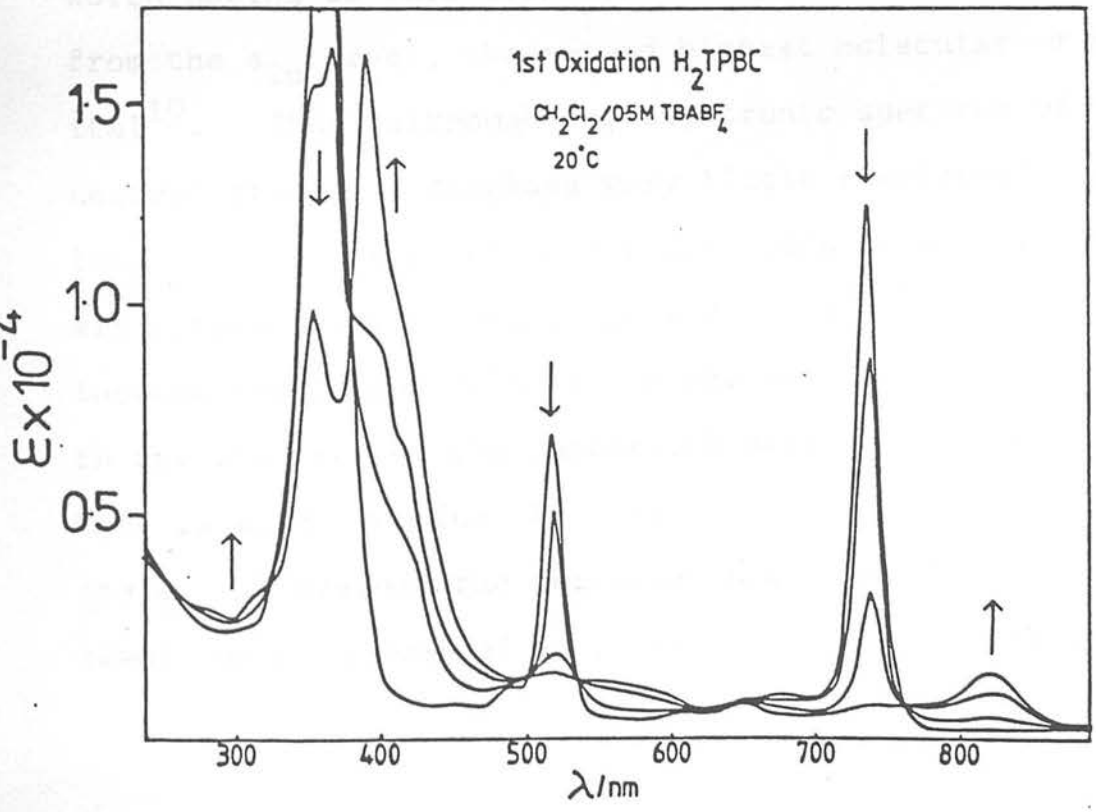

Figure 5.2 Optical progression during the one-electron oxidation of H_2TPBC

radicals are listed in Table 2.

H_2TPC and H_2TPBC also displayed classical fully reversible spectroelectrochemical behaviour upon oxidation at room temperature (the anodic product of H_2OEC was not stable on the required time-scale, even at low temperature). The optical properties of H_2TPC^+ were similar to the metallochlorin π-cation radical spectra (see Table 2). The spectral progression during the one-electron oxidation of H_2TPBC is shown in Figure 2. Both the Q_x and Q_y were noted to collapse completely. A weaker band at 820nm was observed to grow and again weak broad absorptions were noted throughout the visible region. The Soret band too, was noted to partially collapse and shift to lower energy. The collapse of the Q_x band is particularly worth noting as this transition is predicted to arise from the a_{2u} level, the second highest molecular π orbital[10]. Thus, although the electronic spectrum of the neutral free-base displays very little configurational interaction, the electronic transitions of H_2TPBC^+ must mix extensively. This is reflected by the much more intense Soret band relative to the bands at lower energy in the spectrum of the bacteriochlorin π-cation radical. This is also true for the metallochlorin π-cation radicals. Therefore the decrease in energy of the a_{1u} level, upon removal of an electron, must be sufficient

for the a_{1u} and a_{2u} levels to mix extensively in both the chlorin and bacteriochlorin complexes.

The ESR spectrum of $ZnTPC^{+\cdot}$ has previously been reported[5]. A five-line signal was observed, which after selective deuteration experiments, was assigned as being due to splitting by the four equivalent protons of the saturated ring. Similar five-line signals were observed in this work for $ZnOEC^{+\cdot}$, $NiOEC^{+\cdot}$, $ZnTPC^{+\cdot}$ and $H_2TPC^{+\cdot}$ at temperatures below -50°C. Table 3 lists the available ESR data.

Table 3 220K ESR data for the metallochlorin π-cation radicals in CH_2Cl_2/0.5M $TBABF_4$

	g value	a_H/G
$ZnTPC^{+\cdot}$	2.0020	6.0
$H_2TPC^{+\cdot}$	2.0020	6.0
$ZnOEC^{+\cdot}$	2.0028	7.0
$NiOEC^{+\cdot}$	2.0020	7.5

Unlike the previous study[5], the proton splittings were found to be independent of temperature. No nitrogen splitting was observed. No ESR signals were observed for the copper, cobalt and iron chlorin π-cation radicals. This is non-informative, as was outlined in Chapter 3. The ESR spectrum of the bacteriochlorin π-cation radical

moiety has also been reported previously[5,12]. Splittings due to both the hydrogens of the saturated rings and the pyrrolic nitrogens were noted. This indicates unpaired electron density exists at the nitrogen atoms and supports the conclusion drawn from the optical data, that the a_{1u} and a_{2u} orbitals mix.

The second oxidation products of the metallochlorins and H_2TPBC were all unstable. However the decomposition products were identifiable by electronic spectral methods. The second oxidation of H_2TPBC gave rise, quantitatively, to H_2TPC. The second oxidation of the metallochlorins led to formation of the corresponding metalloporphyrin -

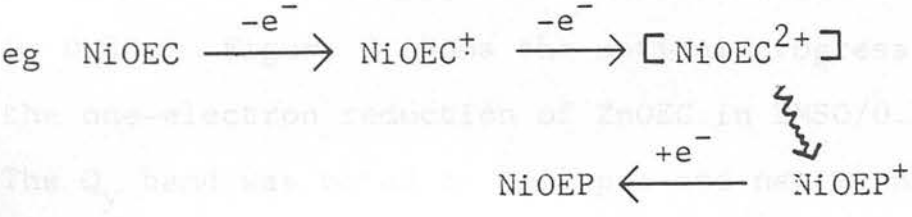

As the potential of the metallochlorin second oxidation was anodic of the metalloporphyrin first oxidation, it was unclear whether the primary product of the rearrangement of the metallochlorin π-dication was the metalloporphyrin or the metalloporphyrin π-cation radical. The important factor to note for the above rearrangements is that the metalloporphyrin is quantitatively generated at the rest potential. The future possibility exists therefore for the electrochemical bulk electrosynthesis of metalloporphyrins from metallochlorin π-dications.

This synthetic route must also be considered as a likely route for the in vivo conversion of bacteriochlorins to chlorins and chlorins to porphyrins.

The reduction products of the metallochlorins were found to be unstable in CH_2Cl_2. The unidentified ultimate product of the first one-electron reduction in CH_2Cl_2 displayed the same optical properties as those previously assigned as arising from the metallochlorin π -anion radical[8]. However this species is not reversible back to the neutral metallochlorin at the appropriate potential or indeed, at any potential. This species cannot therefore be the π -anion radical. The one-electron reduction products of the metallochlorins were found to be stable in DMSO. Figure 3 shows the optical progression during the one-electron reduction of ZnOEC in DMSO/0.1M $TBABF_4$. The Q_y band was noted to collapse and new transitions were observed to grow to higher and lower energy. The final spectrum consists of five bands between 800 and 500nm, one of which coincides with the Q_y band of the parent, neutral metallochlorin. The changes in the Soret region are similar to those which occur during reduction of a metalloporphyrin to a π -anion radical. Figure 4 shows the full electronic spectrum of $ZnTPC^-$. The one-electron reduction products of the copper chlorins and NiOEC display similar optical absorption spectra to

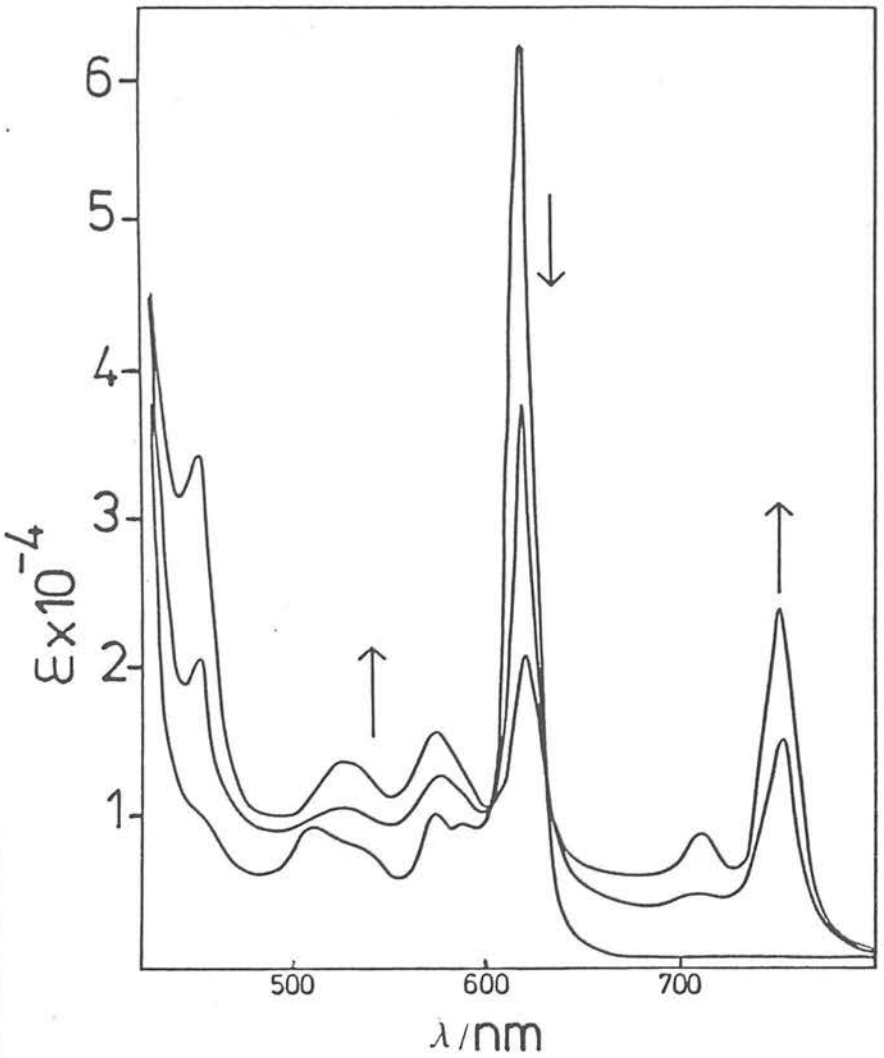

Figure 5.3 Optical progression during the one-electron reduction of ZnOEC at 20°C (DMSO/0.1M $TBABF_4$)

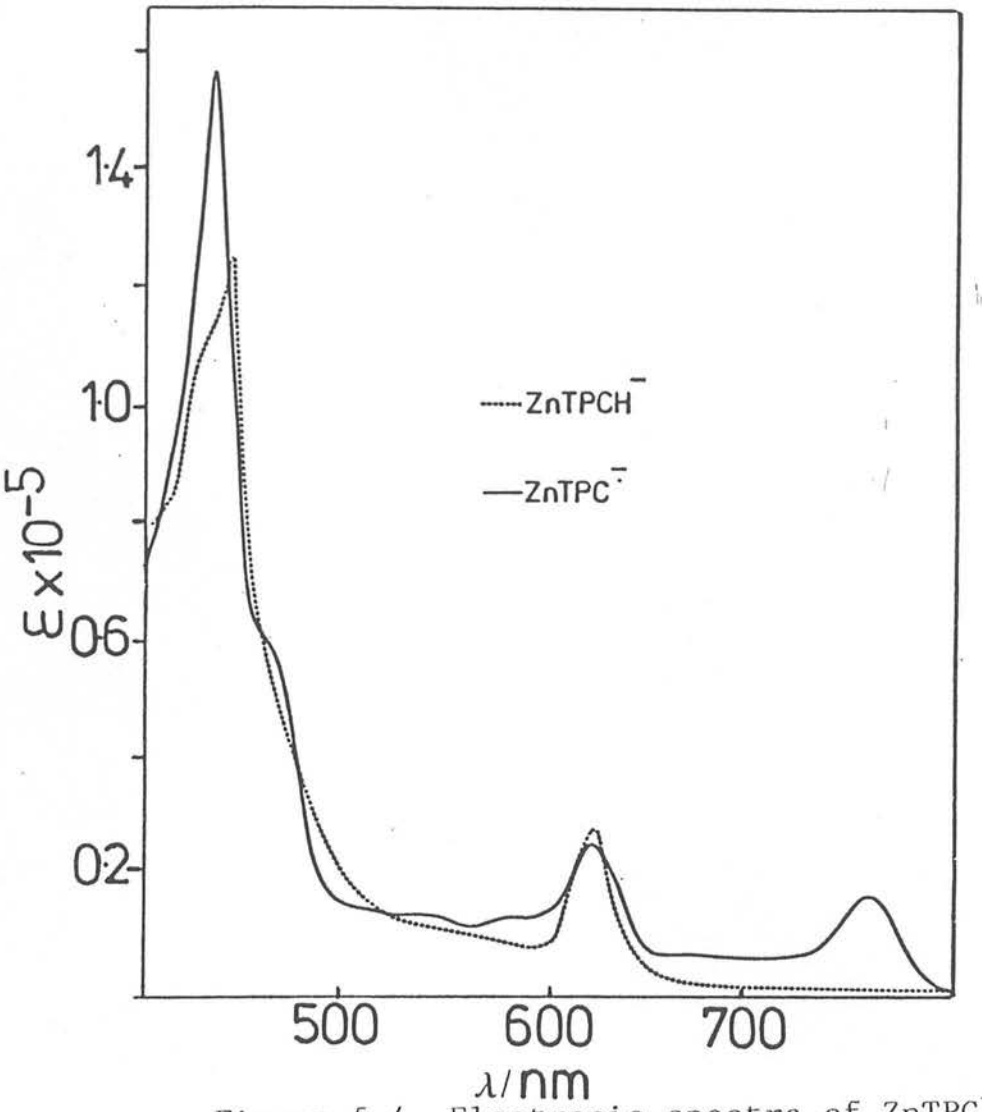

Figure 5.4 Electronic spectra of $ZnTPC^{\cdot-}$ and $ZnTPCH^-$ at 20°C (DMSO/0.1M $TBABF_4$)

$ZnOEC^-$ and $ZnTPC^-$ and are assigned as metallochlorin π -anion radicals. $NiOEC^-$, $ZnOEC^-$ and $ZnTPC^-$ all displayed isotropic ESR signals. No hyperfine was observed. The ESR data are listed below

	g value*	ΔH/G
$ZnOEC^-$	2.0016	16.0
$NiOEC^-$	2.0020	18.0
$ZnTPC^-$	2.0018	16.5

* 293K data in DMSO/0.1M $TBABF_4$

The true metallochlorin π-anion radical species has thus been characterised for the first time in this work. The second reduction products of the zinc, copper and nickel chlorins were not sufficiently stable for spectral characterisation to be achieved. Protonation of the π-dianion proved to be extremely rapid in DMSO. The resulting species displayed similar electrochemical behaviour to the metallophlorins (see Chapter 3), namely a semi-reversible one-electron reduction and an irreversible two-electron oxidation back to the parent metallochlorin. The $E_{\frac{1}{2}}$ values for these redox steps were comparable with those observed for the corresponding metallophlorins. The electronic spectrum of the ultimate product from the second reduction of ZnTPC is shown in Figure 4, and is assigned as $ZnTPCH^-$. The optical absorption

properties of $ZnTPCH^-$ are similar to those previously reported for the chlorin-phlorins[13,14](3).

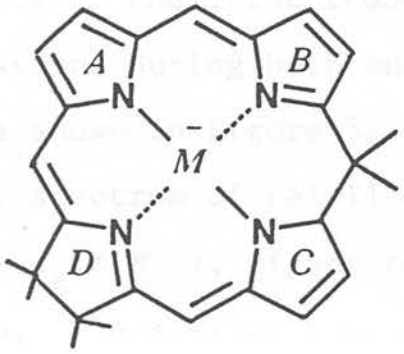

(3)

These tetrahydroporphyrins are isoelectronic with the bacteriochlorin macrocycle. However no rearrangement of the chlorin-phlorin to the bacteriochlorin was observed.

As predicted from the voltammetric results the reduction pathway of the iron and cobalt chlorins proceeds as in the corresponding porphyrin complexes. The first two reduction products of Fe(III)OECCl and Fe(III)TPCCl were stable at room temperature in CH_2Cl_2. Voltammetric and spectroelectrochemical data are consistent with the following reduction sequence-

1. $Fe(III)CCl \xrightarrow{+e^-} Fe(II)C + Cl^-$

2. $Fe(II)C \xrightarrow{+e^-} (Fe(I)C)^-$

where C = TPC, OEC

Free chloride ion was detected voltammetrically after bulk electrosynthesis of the first reduction product. The optical progressions during both one-electron reductions of Fe(III)OECCl are shown in Figure 5. The band at 754nm in the parent spectrum of Fe(III)OECCl is assigned as an $a_{1u}(\pi) \longrightarrow e_g(d\pi)$, ligand to metal, charge transfer transition. A similar band in the spectrum of Fe(III)OEPCl, which has been assigned as an $a_{1u}a_{2u} \longrightarrow e_g(d\pi)$[15], occurs at 634nm. The difference in energy between the CT band of the chlorin and the porphyrin is approximately 0.3eV. This agrees closely with the voltammetric results which measured the HOMO level (a_{1u}) to occur at 290mV to higher energy in the chlorin. During reduction the CT band and the Q_y band are noted to collapse and two new transitions appear between 700 and 500nm. The Soret band shifts to lower energy and decreases in intensity. The full spectrum of Fe(II)OEC is shown in Figure 6. The spectrum is unlike that of any other divalent metallochlorins studied. Although assignment of these bands is outwith the scope of this work it is interesting to note in passing the atypical electronic properties of the ferrous chlorin. The second reduction (Figure 5) results in a 'normal' neutral metallochlorin spectrum. Isosbestic points were maintained throughout reduction and Fe(II)OEC was recovered in full upon reoxidation of the product at the appropriate potential.

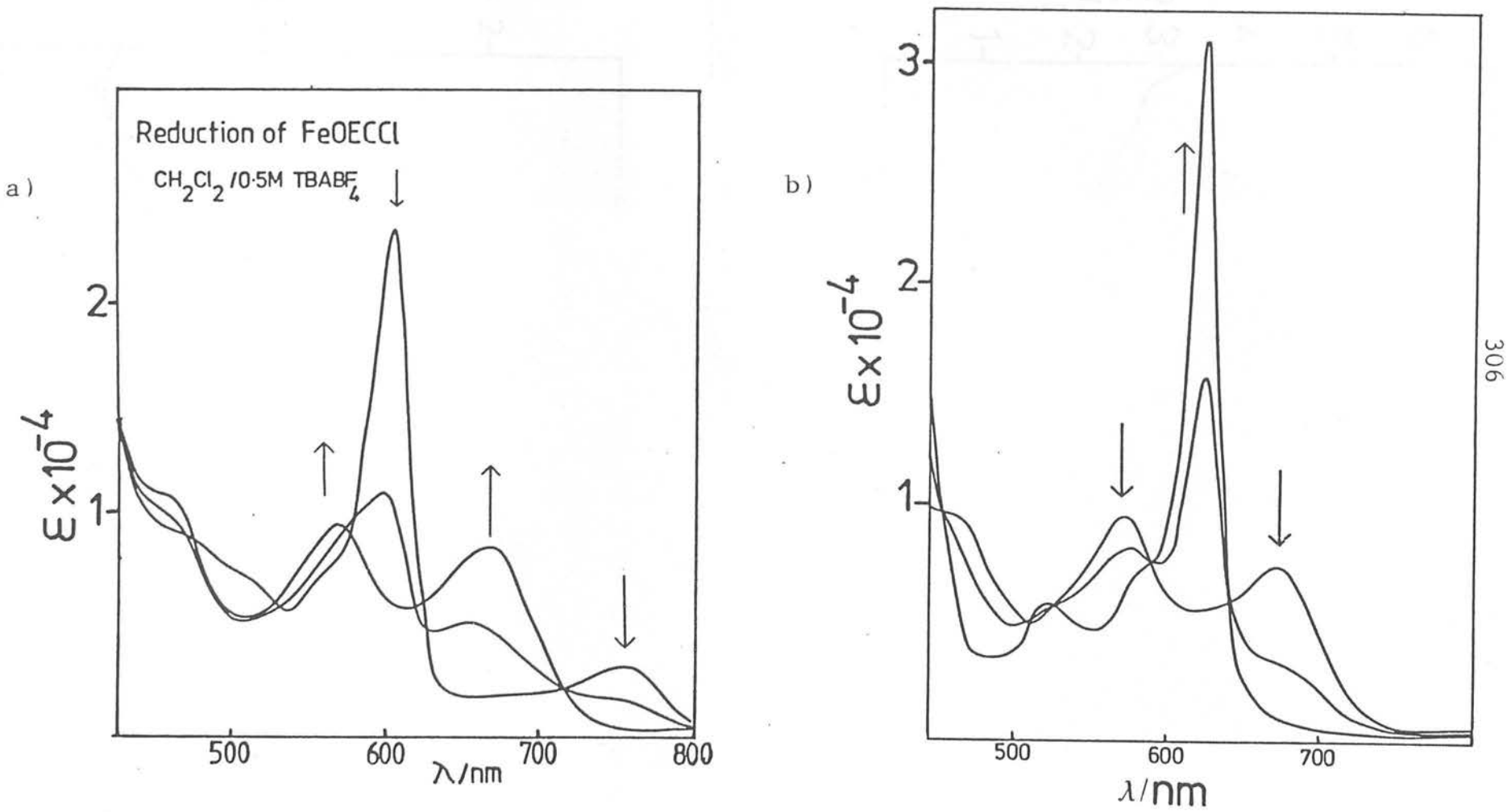

Figure 5.5 a) Spectral progression during the first reduction of Fe(III)OECCl
b) Spectral progression during the second reduction of Fe(III)OECCl.
(Room temperature, CH_2Cl_2/0.5M $TBABF_4$)

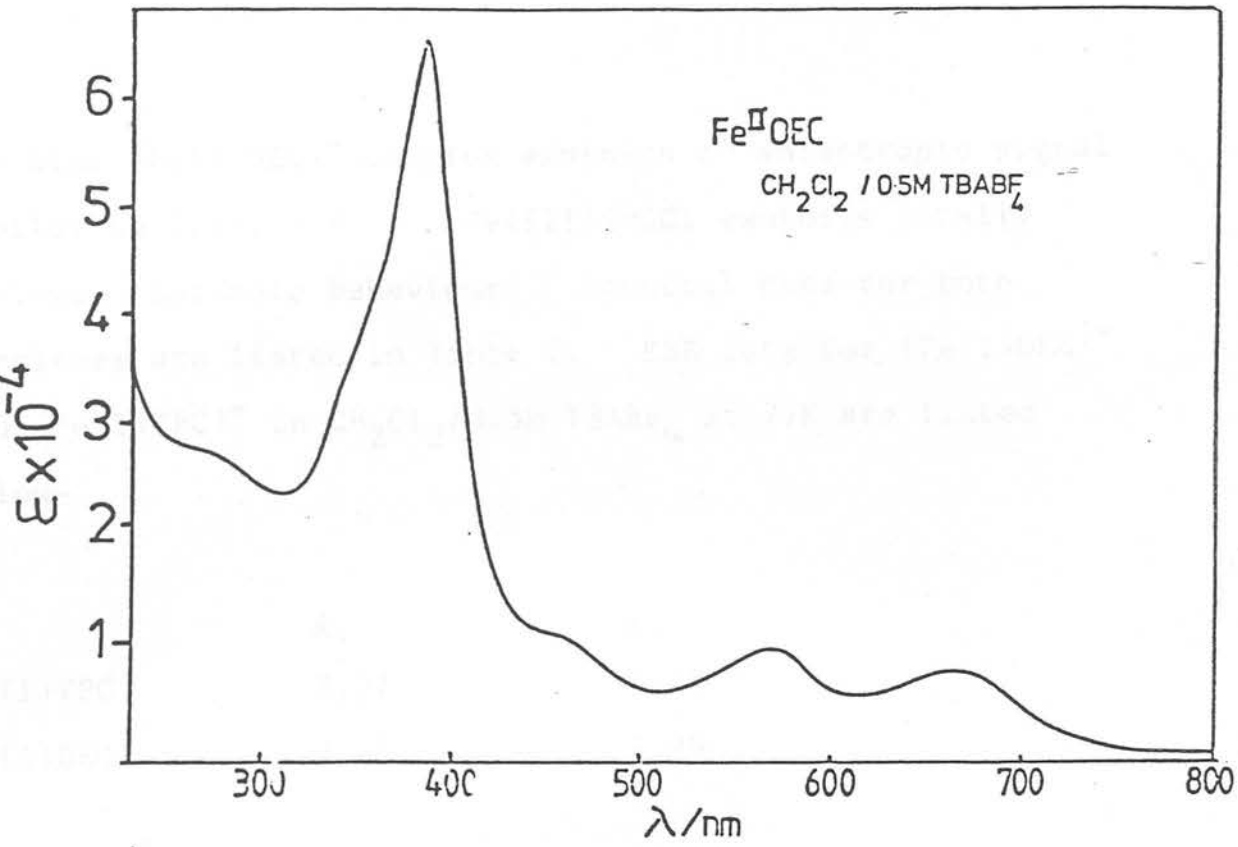

Figure 5.6 Electronic spectrum of Fe(II)OEC at 20°C

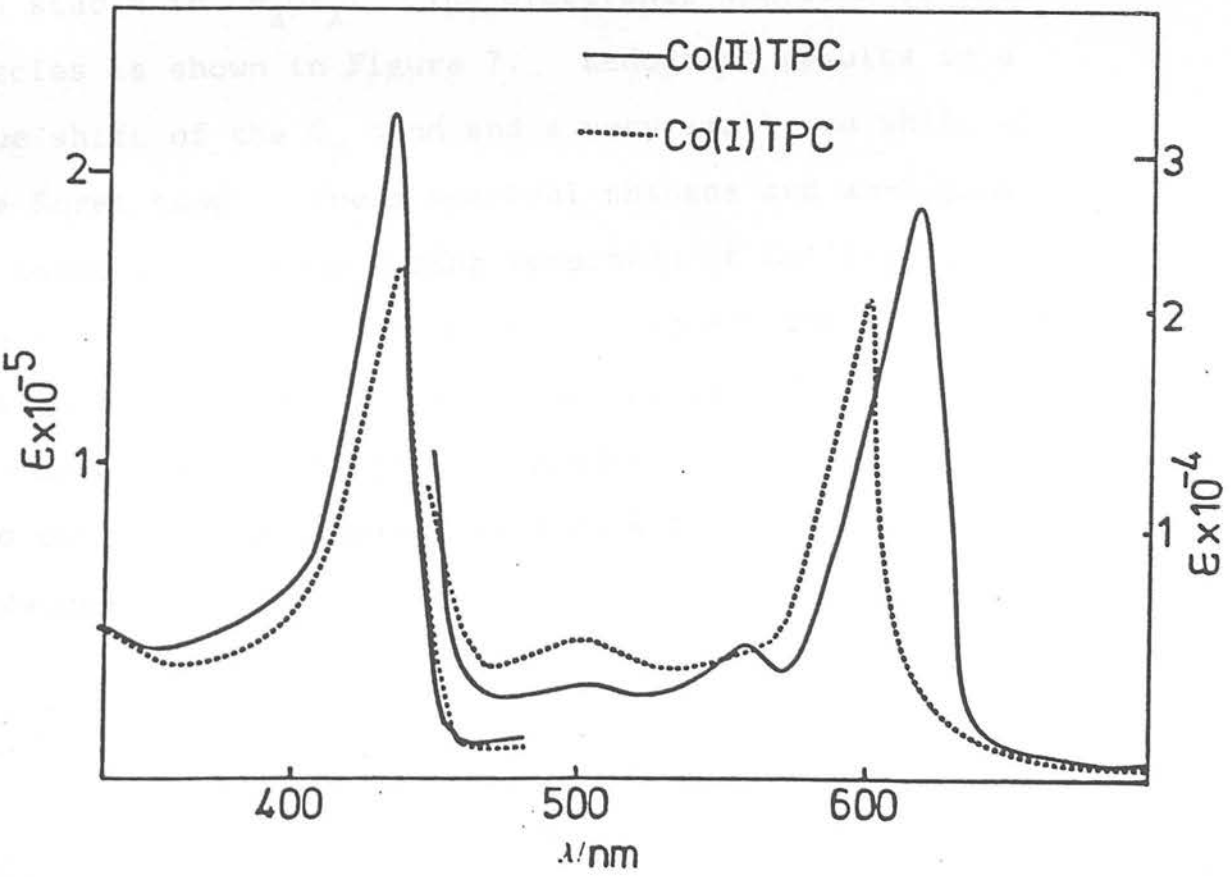

Figure 5.7 Electronic spectrum of Co(I) TPC at 20°C (CH_2Cl_2/0.5M $TBABF_4$)

The blue $(Fe(I)OEC)^-$ complex exhibits an anisotropic signal similar to $(Fe(I)OEP)^-$. Fe(III)TPCCl exhibits totally analogous cathodic behaviour. Spectral data for both complexes are listed in Table 2. ESR data for $(Fe(I)OEC)^-$ and $(Fe(I)TPC)^-$ in CH_2Cl_2/0.5M $TBABF_4$ at 77K are listed below-

	$g_\perp$	$g_{\parallel}$
Fe(I)TPC	2.37	1.97
Fe(I)OEC	2.40	1.99

The third and fourth reduction products of Fe(III)OECCl and Fe(III)TPCCl were unstable in both CH_2Cl_2 and DMSO. The first one-electron reduction product of Co(II) TPC was stable in CH_2Cl_2. The electronic spectrum of this species is shown in Figure 7. Reduction results in a blue shift of the Q_y band and a very small red shift of the Soret band. These spectral changes are analogous to those which occur during reduction of Co(II)TPP. The first reduction product of the cobalt chlorin is thus assigned as Co(I)TPC. This species was ESR silent. The second reduction product proved to be extremely unstable and could not be obtained in a pure form even at low temperature.

5.3 BIOACTIVE CHLORINS

The marine worm Bonellia viridis has, for almost a century, aroused interest in both the biochemical and biological fields, not least because of the marked sexual dimorphism it displays[16,17]. The female of the species (Figure 8) has a plumpish green body with a long, slender, terminally bifurcated, ciliated proboscis which, when extended for feeding, can reach a length of up to 1.5m. The male, however, is a microscopic dwarf (~ 1mm) whose internal organs, save those concerned with reproduction, are degenerate. For each female there are several males which live parasitically within the female. The females eggs are thus fertilised within her body and hatch out as free-swimming, sexually undifferentiated larvae. When these have reached a certain stage of growth they settle down on the sea bed. Should a larvae settle upon the proboscis of a female then all growth stops and it passes from a sexually indifferent phase into a male phase. If the larvae come to rest a significant distance away from the female, it will continue to grow and pass into a female phase[18,19]. Therefore sex differentiation is not determined at fertilisation by some genetic component, but by environmental factors related to either association or to lack of association with other members of the species. The chlorin-based macrocycle, bonellin has been identified as the physiologically active pigment involved in

Figure 5.8

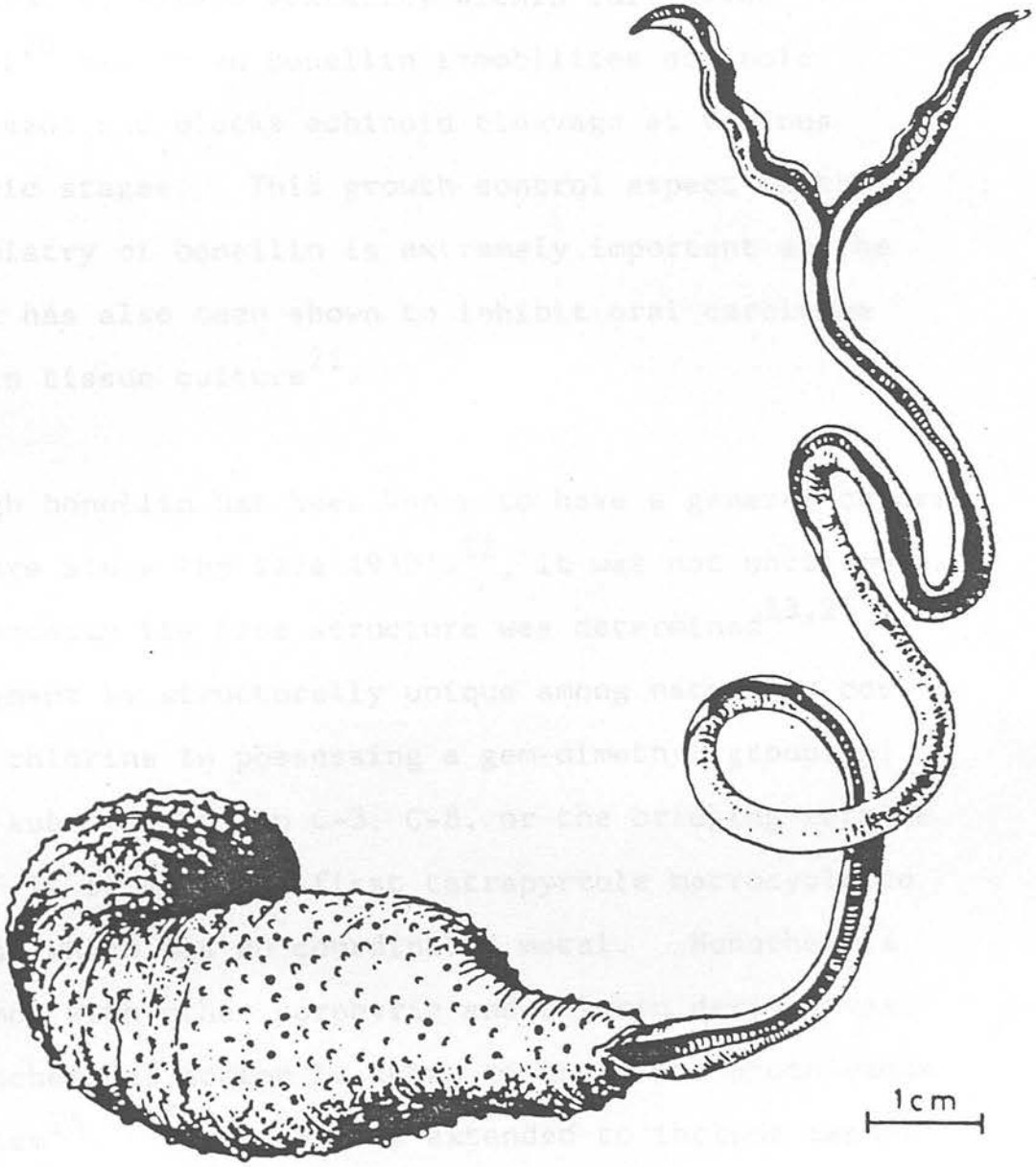

Bonellia viridis Rol. (female)

repression of female sexuality within the larvae[18]. Nigrelli[20] has shown bonellin immobilises echinoid spermatazoa and blocks echinoid cleavage at various embryonic stages. This growth control aspect of the biochemistry of bonellin is extremely important as the pigment has also been shown to inhibit oral carcinoma cells in tissue culture[21].

Although bonellin has been known to have a general chlorin structure since the late 1930's[22], it was not until much more recently its true structure was determined[23,24]. The pigment is structurally unique among naturally occurring chlorins in possessing a gem-dimethyl grouping, and no substituents on C-3, C-8, or the bridging methine C-15. It is also the first tetrapyrrole macrocycle to be found which has no coordinated metal. Nonetheless, in common with other porphyrin and chlorin derivatives, its biochemical action is known to involve a photo-redox mechanism[25]. The study was extended to include methyl pheophorbide a (MePheo a.), a product of chlorophyll degradation[26], in order to evaluate the effect, if any, the isocyclic ring has on the π core of the chlorinato moiety.

Bonellin was studied as the dimethyl ester (1; R = Me), henceforth referred to as H_2Bn. A preliminary study of the electrochemistry of H_2Bn in CH_3CN and methyl-

naphthalene had been undertaken previous to this work by McQueen[27]. Two one-electron reductions and a one-electron oxidation were observed. A cyclic voltammogram of H_2Bn in CH_3CN is shown in Figure 9. A reexamination of the voltammetry in CH_2Cl_2 showed H_2Bn to undergo two fully reversible oxidations and two fully reversible reductions. Coulometric measurements during bulk-electrogeneration of the first reduction product and comparative d.c. voltammetry showed all the waves to involve one-electron. $E_{\frac{1}{2}}$ values for all the electron-transfer steps are listed in Table 4. The energy difference between the first one-electron oxidation and first one-electron reduction of 2.00V agrees closely with the measured ΔE(1st ox - 1st red) value exhibited by the model metallochlorins. Moreover, this value closely matches the energy of the Q_y band in the absorption spectrum of H_2Bn (1.94eV)[28], indicating both techniques are again mapping the same levels of the energy manifold. MePheo a. exhibits very similar voltammetric behaviour. Figure 10 shows an a.c. voltammogram of the chlorophyll derivative in CH_2Cl_2. Two one-electron reductions and three oxidation waves were observed. Temperature-dependent voltammetric studies and bulk electrogeneration at the plateau of the second oxidation wave showed the third anodic wave was in fact due to a daughter product arising from the second oxidation. This daughter product was not identified.

Table 5.4 Voltammetric and spectral data for H_2Bn and MePheo a.

a) Redox potentials for H_2Bn and Me Pheo a. in CH_2Cl_2/0.5M $TBABF_4$ (Volts vs Ag/AgCl) at 20°C

	$E_{\frac{1}{2}}$(2nd ox)	$E_{\frac{1}{2}}$(1st ox)	$E_{\frac{1}{2}}$(1st red)	$E_{\frac{1}{2}}$(2nd red)
H_2Bn	1.09	0.60	-1.40	-1.85
Me Pheo a.	1.12	0.73	-1.18	-1.51
(H_2OEC	0.76	0.36	-1.55	-2.00)

b) Spectral data for the oxidation products (CH_2Cl_2) and reduction products (CH_3CN) of H_2Bn and Me Pheo a.

Wavelength maxima, nm (extinction coefficient x 10^{-3})

H_2Bn	641(15.9), 620(2.7), 590(2.5), 542(1.3), 523(1.9), 494(8.3), 488(8.0), 394(149)
H_2Bn^+	700(3.6), 600-500 broad absorption, 392(82.4)
H_2Bn^-	725, 564, 452
$(H_2Bn^-)_2$	680(12.2), 524(12.6), 486(8.8)
Me Pheo a	664(53.2), 610(4.1), 559(2.0), 529(5.4), 500(13.2), 416(146)
Me Pheo a^+	684(2.4), 637(3.0), broad absorption 600-500, 410(77)
Me Pheo a^-	699(3.6), 664(12.2), 526(60.2), 410(62.6) 380(67.6)

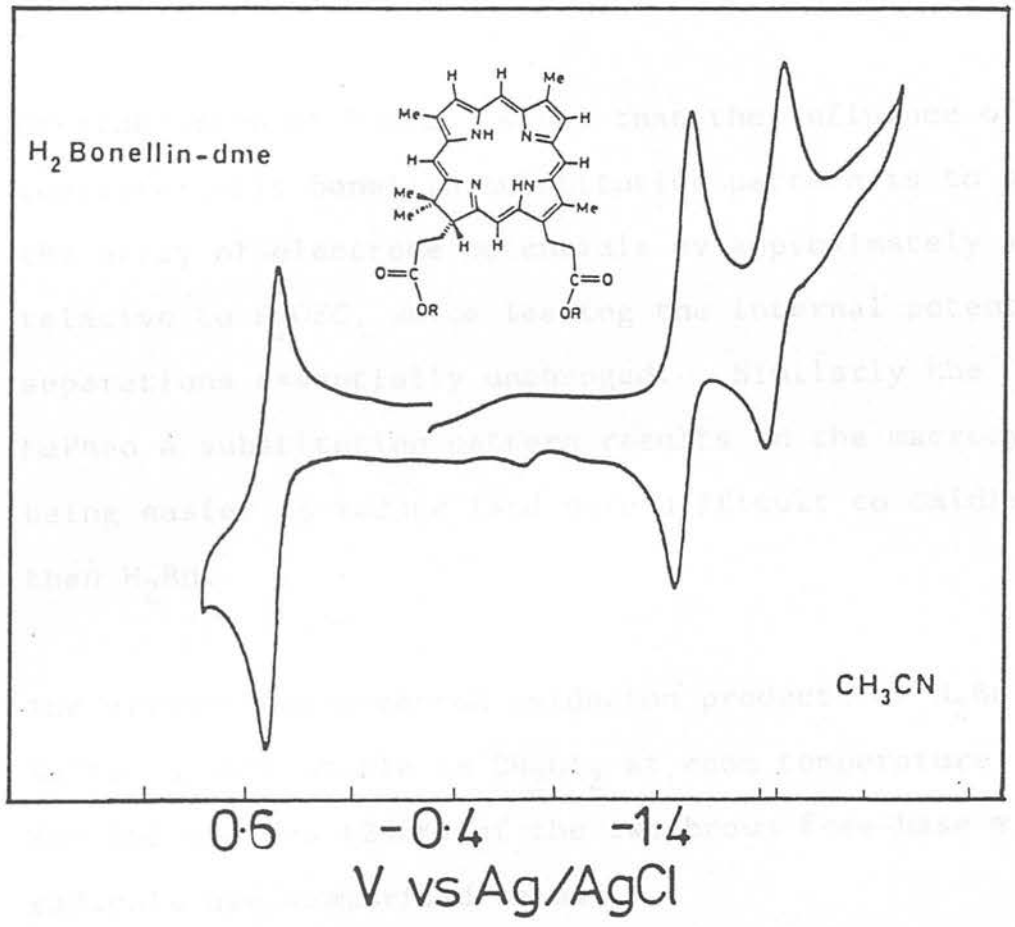

Figure 5.9 Room temperature cyclic voltammogram of Bonellin-dme in CH_3CN/0.1M $TBABF_4$

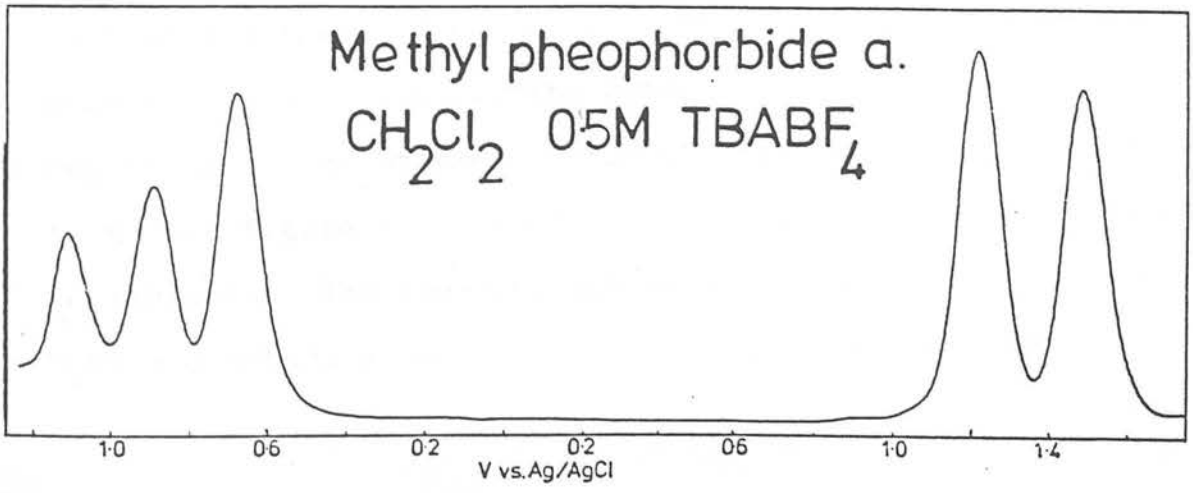

Figure 5.10 A.c. voltammogram of methyl pheophorbide a at 20°C

Consideration of Table 3 shows that the influence of the characteristic bonellin substitution pattern is to shift the array of electrode potentials by approximately +0.15V relative to H_2OEC, while leaving the internal potential separations essentially unchanged. Similarly the MePheo a. substitution pattern results in the macrocycle being easier to reduce (and more difficult to oxidise) than H_2Bn.

The primary one-electron oxidation products of H_2Bn and MePheo a. were stable in CH_2Cl_2 at room temperature. The ESR spectra (250K) of the two brown free-base π - cation radicals are summarised below-

	g value	a_H
$(H_2Bn)^{+}$	2.0018	6.0
(MePheo a.)$^{+}$	2.0019	6.0

These values are very similar to the ESR signals observed for the metallochlorin π -cation radicals. Also, the optical absorption spectra of $(H_2Bn)^{+}$ and (MePheo a.)$^{+}$ display the same overlapping broad bands in the visible region as do the oxidation products of the metallochlorins (e.g. see Figure 1). Electronic spectral data are listed in Table 4. The two-electron oxidation products of both H_2Bn and MePheo a. were unstable on the required time-

scale to enable spectral characterisation to be carried out, even at low temperature.

Although the one-electron oxidation products of H_2Bn and MePheo a. display similar electronic properties to the metallochlorin π-cation radicals, the cathodic electrochemistry of the two naturally occurring macrocycles differs significantly from that of the model metallocomplexes. The reduction products of MePheo a. and H_2Bn were unstable in CH_2Cl_2. However spectral monitoring of the first one-electron reduction step of both complexes was sucessfully achieved in CH_3CO and DMSO. The second reduction products, though, were unstable in non-coordinating and coordinating media.

Although the classic cyclic voltammetric behaviour observed for H_2Bn suggests a straightforward one-electron redox step for the first reduction, this proved not to be the case. On the extended time-scale of the in situ bulk electrogeneration there was definite evidence of it being a two-stage, one-electron process. On reduction of H_2Bn in CH_3CN at the plateau of the first reduction the Q_y band at 639nm is noted to progressively collapse. This decrease in intensity is accompanied by the simultaneous growth of new bands at 725, 564 and 452nm. These new transitions closely resemble the characteristic bands

of the metallochlorin π-anion radical (see Figure 3). However as the reduction proceeds these bands unexpectedly collapse (Figure 11). After electrolysis is complete the final spectrum is dominated by a relatively intense broad band centred at 680nm and two sharper bands to higher energy (524 and 486nm). Unfortunately the Soret region of the spectrum could not be monitored as this resulted in decomposition of the reduction product. The two-stage nature of the process was confirmed by the existence of two independent sets of isosbestic points. In the early stages of reduction isosbestic points were noted at 645, 620, 585, 505 and 478nm. In the latter stages isosbestic points were maintained at 730, 712, 628 and 545nm (Figure 11). It is stressed that all these spectral changes take place at the potential appropriate for the first H_2Bn reduction. Protonation of the π-anion radical can be ruled out. The ultimate product does not display either the spectral characteristics or the electrochemical properties of a chlorin-phlorin. The stirred voltammogram of the electrogenerated product coincides with that of the starting material, apart from inversion of current, and coulometry confirmed only one electron is involved in the redox step. Any involvement of the substituents at the periphery of H_2Bn can be discounted as the same sequence of spectroscopic changes occur upon reduction of H_2OEC. The course of the electrolysis of this complex was independent of both temperature (+20° to -35°C) and solvent (CH_3CN, DMSO, $HCONMe_2$). H_2TPC does not, however, exhibit this type of behaviour.[29]

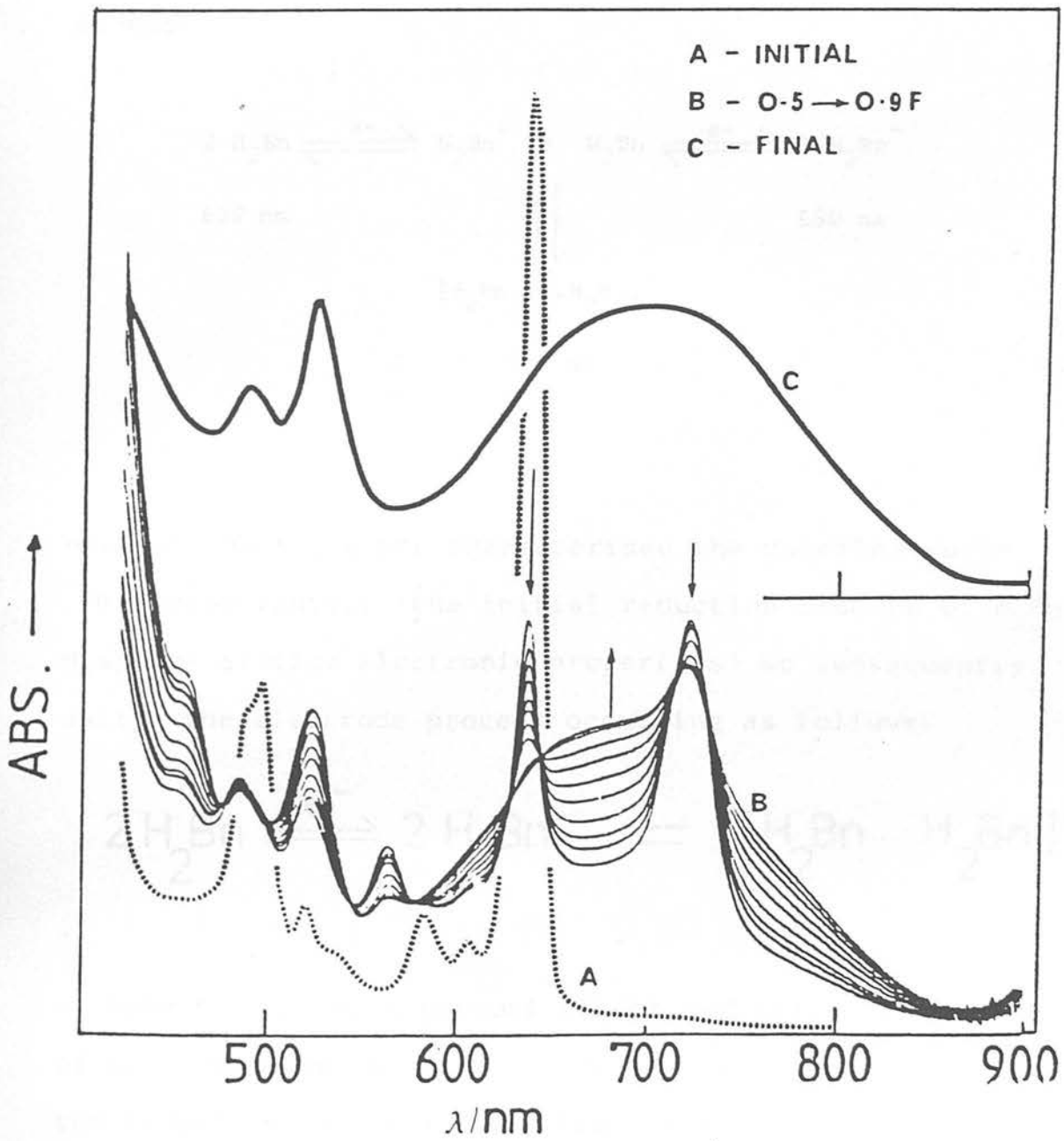

Figure 5.11 Electronic spectrum of electrogenerated $(\text{Bonellin-dme})^-$ in CH_3CN
F = inferred value of the charge accepted in Faraday mol^{-1}

In an earlier publication[30] we interpreted these results as being consistent with the following electrode reaction scheme-

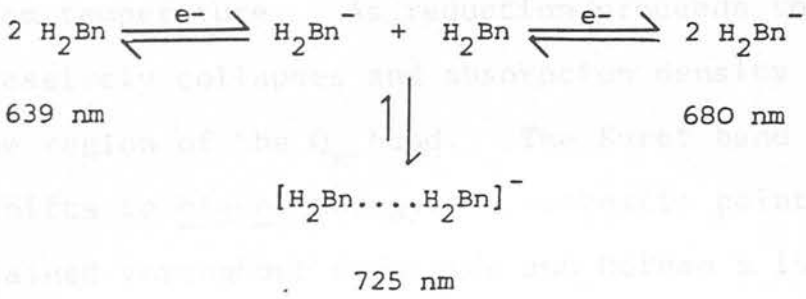

However, having since characterised the metallochlorin π -anion radical (the initial reduction product of H_2Bn displays similar electronic properties) we subsequently assign the electrode process occurring as follows-

$$2\,H_2Bn \overset{e^-}{\rightleftharpoons} 2\,H_2Bn^{\cdot-} \rightleftharpoons [H_2Bn\cdots\cdots H_2Bn]^{2-}$$

- where the ultimate product of the reduction is a dimer of two π-anion radicals. ESR in situ monitoring of the reduction supports the latter interpretation. During the initial stages of the cathodic process an isotropic signal appears ($g = 2.0010$, $\Delta H = 18G$ at 250K). This signal decays in the latter stages of the reduction and the final product is ESR silent.

The first reduction of MePheo a. is contrastingly a straightforward one-electron, one-step process. Figure 12 shows the optical progression during reduction in DMSO at room temperature. As reduction proceeds the Q_y band progressively collapses and absorption density increases in the region of the Q_x band. The Soret band splits and shifts to higher energy. Isosbestic points are maintained throughout reduction and MePheo a. is recovered fully at the appropriate potential. The final spectrum (Figure 12) is similar to the initial spectrum in that three main regions of absorption are noted. Similar to the metallochlorin π-anion radical case, a band in the spectrum of $(\text{MePheo a.})^-$ coincides with the Q_y band of the starting material. The spectral changes in the region of the Q_x band though, are strikingly different and must be due, in part at least, to the isocyclic ring present in the structure of the chlorophyll derivative. The yellow reduction product displays an isotropic ESR signal ($g = 2.0001$, $\Delta H = 20G$ at 292K). Spectral data for the reduction products of both H_2Bn and MePheo a. are listed in Table 4.

5.4 CONCLUSION

Although bonellin possesses a unique substitution pattern the present spectroelectrochemical studies suggest that its electronic structure does not differ materially from

a)

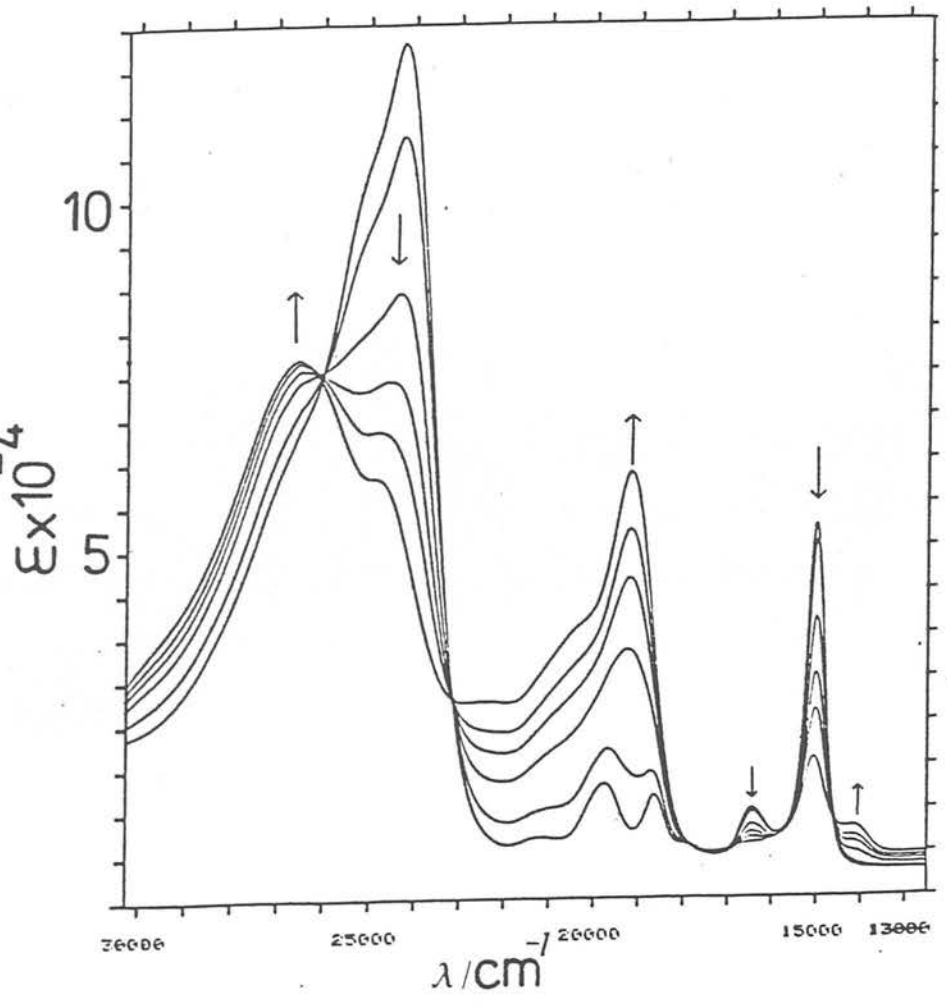

b)

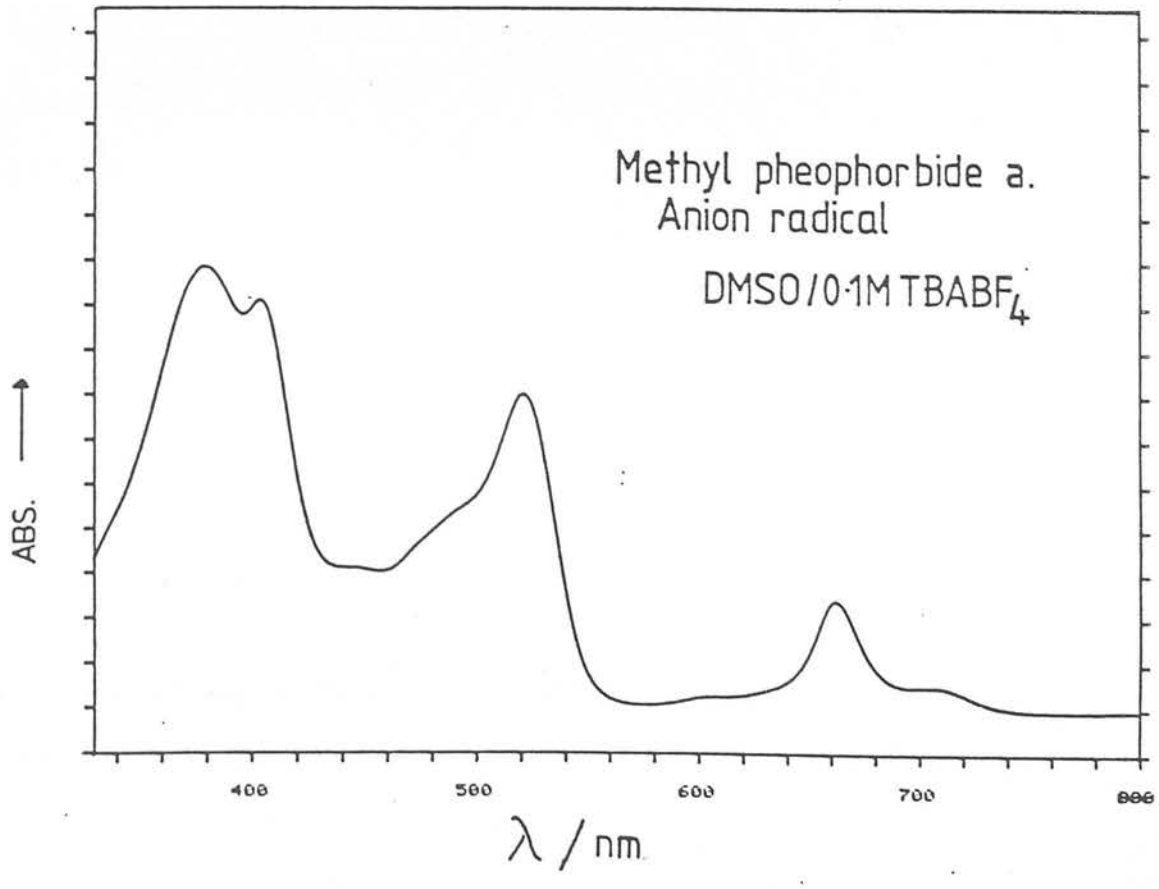

Figure 5.12 a) Optical progression during the one-electron reduction of methyl pheophorbide a (20°C)
b) Final spectrum

that of the symmetrically alkylated chlorins. The structural oddity of bonellin occurring as a free-base in vivo may however be relevant as dimerisation of the metallochlorin π-anion radicals was not observed. As bonellin acts via a photo-redox mechanism[21], the observed dimerisation of the π-anion radicals of H_2Bn could well be involved in reductive quenching of photo-activated H_2Bn[28]. The ability of porphyrin-type complexes to form aggregates determines many of their physical and biological properties such as optical absorption, quantum yield of fluorescence and magnetic resonances[31]. Much work has been done on chlorophyll aggregates and the role they play in photosynthesis[32], and the role of the bonellin π-anion radical dimer could well have some similar bioactive role. The reduction behaviour of the chlorophyll derivative, methyl pheophorbide a. was unique and more work is obviously required to determine the electronic effect of the isocyclic ring on the core of the chlorinato moiety.

5.5 EXPERIMENTAL

Metallochlorins are unstable with respect to light-induced oxidations by molecular oxygen[6] and it was necessary to perform all critical manipulations and physical measurements under a pure dinitrogen or argon atmosphere and with minimal exposure to light. H_2OEC, H_2TPBC

and H_2TPC were prepared by the method of Whitlock et al[33]. The metallated chlorins were prepared by standard literature procedures[33-37]. Cross contamination of chlorin and porphyrin complexes and chlorin and bacteriochlorin complexes was common. Purification was achieved by dry column chromatography[38] on alumina. Acetonitrile was purified by the method of Walter and Ramaley[39]. Methyl pheophorbide a and bonellin were kindly supplied by Professor Andrew Pelter (University College of Swansea). Electrochemical and spectroelectrochemical techniques have been described previously in Chapters 2 and 3, respectively.

REFERENCES : CHAPTER 5

1. R.H. Felton, G.M. Sherman and H. Linschitz, Nature, 1964, 203, 637.
2. A. Stanienda, Z. Naturforsch., Teil B, 1968, 23, 147.
3. J. Fajer, D.C. Brune, M.S. Davis, A. Forman and L.D. Spaulding, Proc. Natl. Acad. Sci. U.S.A., 1975, 72, 4956.
4. H. Berg and K. Kramarczyk, Biochim. Biophys. Acta., 1967, 131, 141.
5. J. Fajer, M.S. Davis, D.C. Brune, L.D. Spaulding, D.C. Borg and A. Forman, Brookhaven Symp. Biol., 1976, 28, 74.
6. J.-H. Fuhrhop, Z. Naturforsch., Teil B, 1970, 25, 255.
7. A.M. Stolzenberg, L.O. Spreer and R.H. Holm, J. Am. Chem. Soc., 1980, 102, 364.
8. D. Chang, T. Malinski, A. Ulman and K.M. Kadish, Inorg. Chem., 1984, 23, 817.
9. D. Feng, Y. Ting and M.D. Ryan, Inorg. Chem., 1985, 24, 612.
10. M. Gouterman, J. Mol. Spectrosc., 1961, 6, 138.
11. C.K. Chang, L.K. Hanson, P.F. Richardson, R. Young and J. Fajer, Proc. Natl. Acad. Sci., U.S.A., 1981, 78, 2652.

12. J. Fajer, D.C. Borg, A. Forman, R.H. Felton, D. Dolphin and L. Vegh, Proc. Nat. Acad. Sci. U.S.A., 1974, 71, 994.

13. H.H. Inhoffen, J. Pure Appl. Chem., 1968, 17, 443.

14. H.H. Inhoffen and P. Jager, Tetrahedron Lett., 1964, 21, 1317.

15. H. Kobayashi, T. Higuchi and K. Eguchi, Bull. Chem. Soc. Jpn., 1975, 48, 3137.

16. F. Baltzer, Revue. Suisse. Zool., 1937, 16, 89.

17. G. Bacci, 'Sex Determination', Pergamon Press, 1965.

18. P.J. Schembri, M.Sc. Thesis, University of Malta, 1977.

19. F.B.D. de Silva, Varkbl. Biol., 1934, 15, 221.

20. F.R. Nigrelli, M.S. Stempien, G.D. Ruggieri, V.R. Liguori and J.T. Cecil, Fed. Proc., 1967, 26, 1197.

21. A. Pelter, private communication.

22. E. Lederer, Compt. rend. Acad Sci. Paris, 1939, 209, 528.

23. A. Pelter, J.A. Ballantine, V. Ferrito, V. Jaccarini, A.F. Psaila and P.J. Schembri, J. Chem. Soc., Chem. Commun., 1976, 999.

24. A. Pelter, J.A. Ballantine, A.F. Psaila, P. Murray-Rust, V. Ferrito, P. Schembri and V. Jaccarini, J. Chem. Soc., Perkin Trans. I., 1980, 1080.

25. L. Agius, V. Jaccarini, J.A. Ballantine, V. Ferrito,

A. Pelter, A.F. Psaila and V.A. Zammit, Comp. Biochem. Physiol. B., 1979, 63, 109.

26. R.C. Dougherty, H.H. Strain, W.A. Svec, R.A. Uphaus and J.J. Katz, J. Am. Chem. Soc., 1970, 92, 2826.

27. R.C.S. McQueen, Ph.D. Thesis, Edinburgh University, 1983.

28. J.I. Mathews, S. Braslavsky and P. Camilleri, Photochem. Photobiol., 1980, 32, 733.

29. G. Peychal-Heiling and G.S. Wilson, Anal. Chem., 1971, 43, 550.

30. G.A. Heath, M.R. Low, R.C.S. McQueen and A. Pelter, J. Chem. Soc., Perkin Trans. II, 1984, 305.

31. K.M. Smith "Porphyrins and Metalloporphyrins", Elsevier, Amsterdam, 1975 and references therein.

32. J.J. Katz, L.J. Shipman, T.M. Cotton and T.R. Janson, "The Porphyrins" Ed. D. Dolphin, Academic Press, 1980, Vol. V, Chapter 9.

33. H.W. Whitlock Jr., R. Hanaver, M.Y. Oester and B.K. Bower, J. Am. Chem. Soc., 1969, 91, 7485.

34. G.D. Dorough and F.M. Huennekens, J. Am. Chem. Soc., 1952, 74, 3974.

35. J.A.S. Cavaleiro and K.M. smith, J. Chem. Soc., Perkin Trans. I., 1973, 2149.

36. U. Eisner, J. Chem. Soc., 1957, 3461.

37. A.H. Corwin and P.E. Weis, J. Org. Chem., 1957, 27, 4285.

38. B. Loev and M.M. Goodman, Chem. Indus., 1967, 2026.

39. M. Walter and L. Ramaley, Anal. Chem., 1973, 45, 165.

CHAPTER 6 : SPECTROELECTROCHEMICAL STUDIES ON METALLOPHTHALOCYANINES

6.1 INTRODUCTION

Spectroelectrochemical studies on metallophthalocyanines (MPc) are desirable in view of their potential as electrocatalysts[1-3], where an understanding of the redox processes of the phthalocyanine molecule is essential for the design of more efficient catalysts, and with regard to their possible use as electrochromic materials[4,5]. The related metallobenzoporphyrin (MTBP) macrocyclic systems have recently been shown to possess highly conducting 'molecular metal' properties upon treatment with iodine[6]. Again, understanding of the electron transfer processes occurring at the TBP macrocycle is fundamental in any attempt to explain this phenomenon. However, in contrast to the numerous studies on metalloporphyrins, relatively little spectroelectrochemistry has been carried out on MPc and MTBP complexes[7-16]. This is mainly due to their low solubilities in suitable solvents for electrochemistry which limits the use of optically transparent thin-layer electrodes. Rollman and Iwamoto[8] overcame the insolubility problem by studying the cathodic redox properties of a series of tetrasulphonato-phthalocyanines. The ionic substituents allowed electrochemical measurements

to be made in DMSO. Two or three one-electron reductions were observed for the Co(II), Ni(II) and Cu(II) derivatives. A later study by Clack et al[17] reported a polarographic investigation of the unsubstituted complexes in DMF. These were examined as the soluble $Li^{+}(MPc)^{-}$ salts (M = Mn, Fe, Co, Ni, Cu, Zn, Mg) obtained by generating the monoanion by lithium reduction. Three one-electron reductions were noted for the complexes with a redox-inert metal centre. (Thus as for the porphyrin moiety the Pc ring is capable of accepting up to four electrons). The different experimental environments employed by the two sets of workers has however resulted in serious inconsistencies in the electrochemical data presented. The relative order of first reduction potentials observed by Clack for instance was quite different from that observed by Rollman and Iwamoto, as was the gap between the first and second reductions. Lever and Wilshire have demonstrated[7] the strong influence of the coordinating medium on the cathodic behaviour of MPc complexes and thus the above inconsistencies are not entirely unexpected. Lever has also reported the cathodic and anodic data for Mn, Fe, and Co phthalocyanines in pyridine.[18] The primary redox events of all these complexes were noted as metal-based electron-transfer events. The differing central ion coordination number and spin states exhibited by the metal ions in this medium however precluded syst-

ematic comparison with other data.

In previous studies in our laboratory McQueen has reported on the cathodic electrochemistry of the unsubstituted complexes in the non-coordinating medium of methylnaphthalene at 150°C[19]. Two one-electron reductions were noted for the Fe(II), Co(II), Ni(II), Cu(II) and Zn(II) phthalocyanine complexes. From the observed trend in the $E_{\frac{1}{2}}$ values all waves were assigned as macrocycle-based redox steps except the first reduction of Co(II)Pc and the second reduction of Fe(II)Pc, which were ascribed as Co(II)Pc/Co(I)Pc and $Fe(II)Pc^{-}/Fe(I)Pc^{-}$ couples respectively. Spectroscopic characterisation of the electrode products proved impracticable due to the nature of the experimental medium.

The anodic behaviour of phthalocyanines is even less well documented. It has generally been reported that the electrochemical oxidation of the Pc ring results in degradation of the complex[8,20]. Gavrilov et al[13] have also recently reported the anomalous oxidative voltammetric response of metallo-tetraalkylphthalocyanines, despite potentiometric evidence for discrete one-electron oxidations[21]. Electronic spectra of $ZnPc^{+\cdot}$ species have been obtained either from transient species with lifetimes in the order of microseconds[22] or as thin films in the

solid state, where chemical[23] or electrochemical[24] oxidation was used. Due to extensive intermolecular coupling effects however these solid state spectra are quite different when compared with respective solution spectra[25]. This makes the assignment of transitions in the absorption spectrum very difficult. Electronic spectra of the parent MPc species have been rationalised by Gouterman and co-workers[26-28]. The highest occupied molecular π orbitals are calculated to have a_{1u} and a_{2u} symmetry and the lowest empty ring orbitals are an e_g degenerate pair. Again the metal valence orbitals may be buried inside the filled Pc levels or filled and/or empty valence orbitals may occur in the HOMO/LUMO gap. In addition empty metal orbitals may lie at energies comparable to, or above, the LUMO Pc level. The optical absorption spectrum however is dominated by the same π / π * transitions as were present in the porphyrin spectra. Figure 1 shows a calculated molecular orbital scheme for phthalocyanine and the electronic transitions which can occur. The visible/near uv region is dominated by the Q band ($1a_{1u} \longrightarrow 1e_g$) and the B(Soret) band ($1a_{2u} \longrightarrow 1e_g$). Other π / π * transitions occur at higher energy to the B band. An important difference between metalloporphyrins and metallophthalocyanines however is the predicted energies of the two highest occupied molecular orbitals. In the porphyrin energy

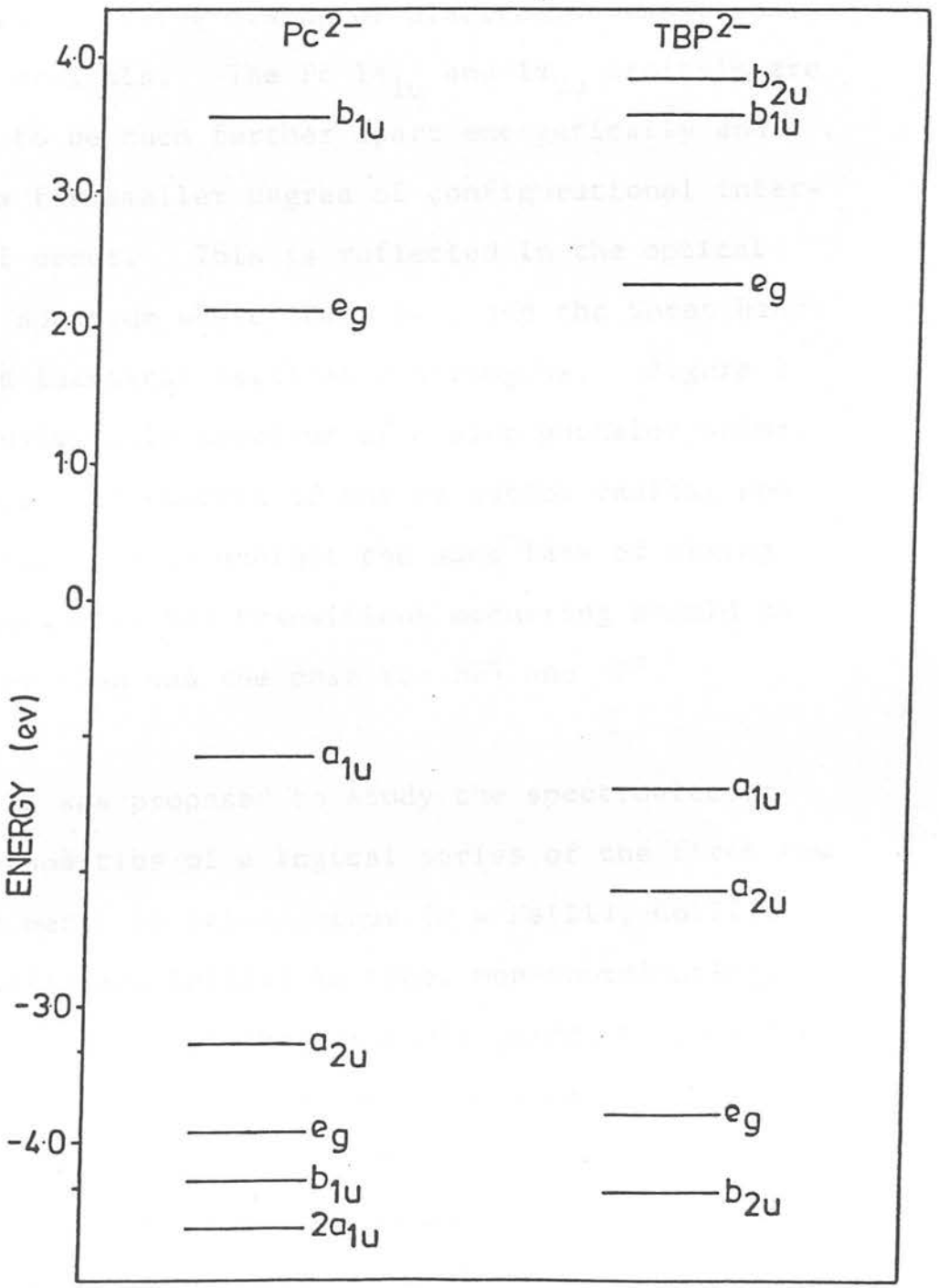

Figure 6.1 M.O. scheme for the phthalocyanine and tetrabenzoporphyrin dianion ligands (from ref 35).

manifold the $3a_{2u}$ and $1a_{1u}$ levels are very close in energy resulting in extensive mixing of electronic transitions from these orbitals. The Pc $1a_{1u}$ and $1a_{2u}$ orbitals are calculated to be much further apart energetically and therefore a far smaller degree of configurational interaction will occur. This is reflected in the optical absorption spectrum where the Q band and the Soret band have almost identical oscillator strengths. Figure 2 shows the uv/visible spectrum of a zinc phthalocyanine. If the electronic spectra of the Pc cation radical and anion radical were to exhibit the same lack of mixing then assignment of the transitions occurring should be much simpler than was the case for MP^{+} and MP^{-}.

Therefore it was proposed to study the spectroelectrochemical properties of a logical series of the first row transition metal phthalocyanines (M = Fe(II), Co(II), Ni(II), Cu(II) and Zn(II)) in true, non-coordinating, solution. Instead of the insoluble parent pigment the macrocycle employed was the alkylated tetra (tert iarybutyl)-phthalocyanine moiety (1). The ^{t}butyl substituent greatly improved the solubility of these species in organic media and redox measurements were routinely achieved in CH_2Cl_2/0.5M $TBABF_4$ at 20°C. The study was extended to the related tetrabenzoporphyrin macrocycle (2) in order to quantify the electronic effect of the nitrogen aza-

Figure 6.2 Uv/visible spectrum of $ZnBu_4Pc$

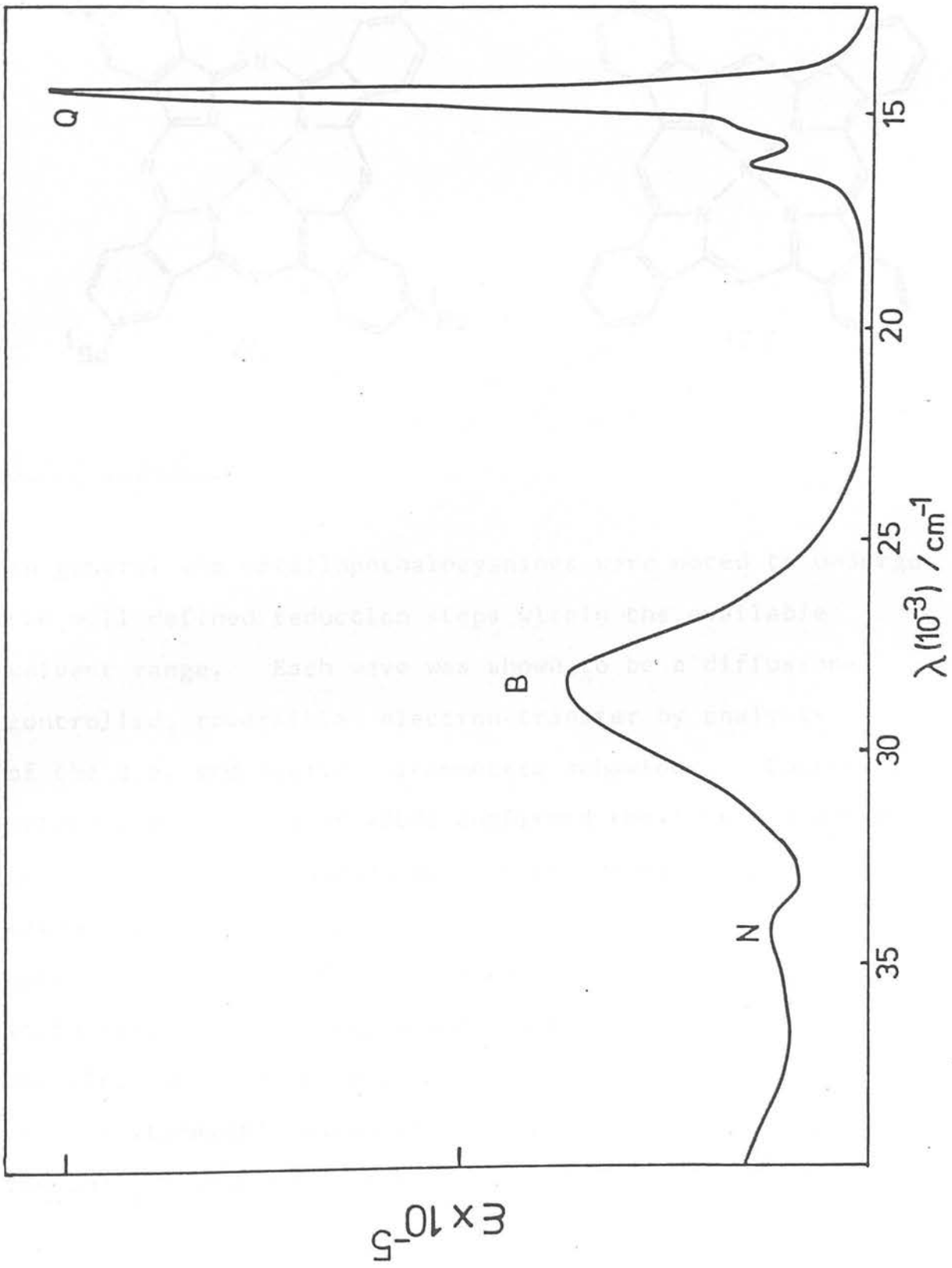

bridge at the meso-position of the Pc macrocycle.

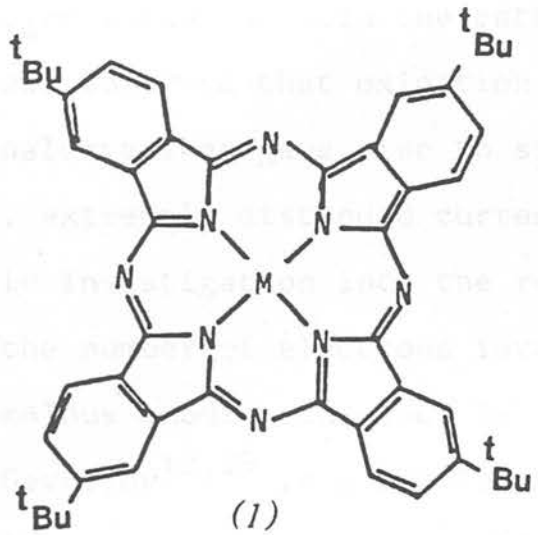

(1)

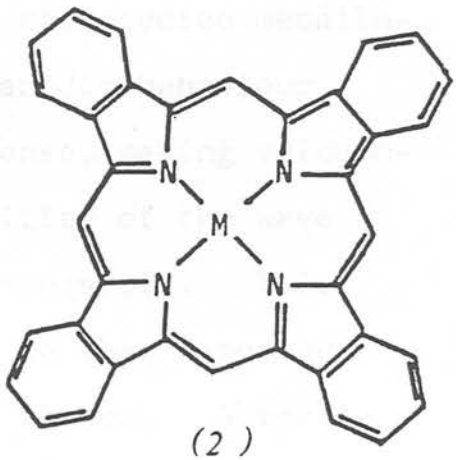

(2)

6.2 RESULTS

In general the metallophthalocyanines were noted to undergo two well defined reduction steps within the available solvent range. Each wave was shown to be a diffusion-controlled, reversible, electron-transfer by analysis of the a.c. and cyclic voltammetric behaviour. Coulometric measurements at -20°C confirmed the first reduction step of all the complexes to involve one electron. The second reduction product was not stable on the required extended time-scale for coulometry, but comparative d.c. voltammetry conclusively showed this wave also to involve one electron. In direct contrast to the observed discrete voltammetric waves observed in the cathodic region, the anodic electrochemistry was extremely ill-defined.

Figure 3 shows a cyclic voltammogram of the free base H_2Bu_4Pc including both the cathodic and anodic regions. It was observed that oxidation of all the studied metallophthalocyanines gave rise to similar anodic behaviour i.e. extremely distended current response, making voltammetric investigation into the reversibility of the wave or the number of electrons involved impossible. This anomalous anodic behaviour is similar to that reported by Gavrilov[13,29] in a dichlorobenzene medium. Surprisingly, coulometric investigation at room temperature on the first oxidation (at a potential positive of the complete 'wave') showed only one electron to be involved in the primary oxidation step of all the metallophthalocyanines and the free-base. Therefore although voltammetric monitoring of the electron-transfer appeared anomalous, bulk electrogeneration showed that the overall redox couple involves only one-electron. Moreover the parent neutral phthalocyanine could be regenerated fully when the potential was reversed to a value negative of the distended wave. This suggested the anodic voltammetric response was merely an experimental artefact occurring at the surface of the working electrode (e.g. absorption of the pigment onto the Pt button electrode). Indeed if one employed very dilute solutions of the phthalocyanine under investigation ($\sim 5 \times 10^{-7}$M) and a very sensitive excitation technique, namely differential pulse voltammetry[30], normal anodic

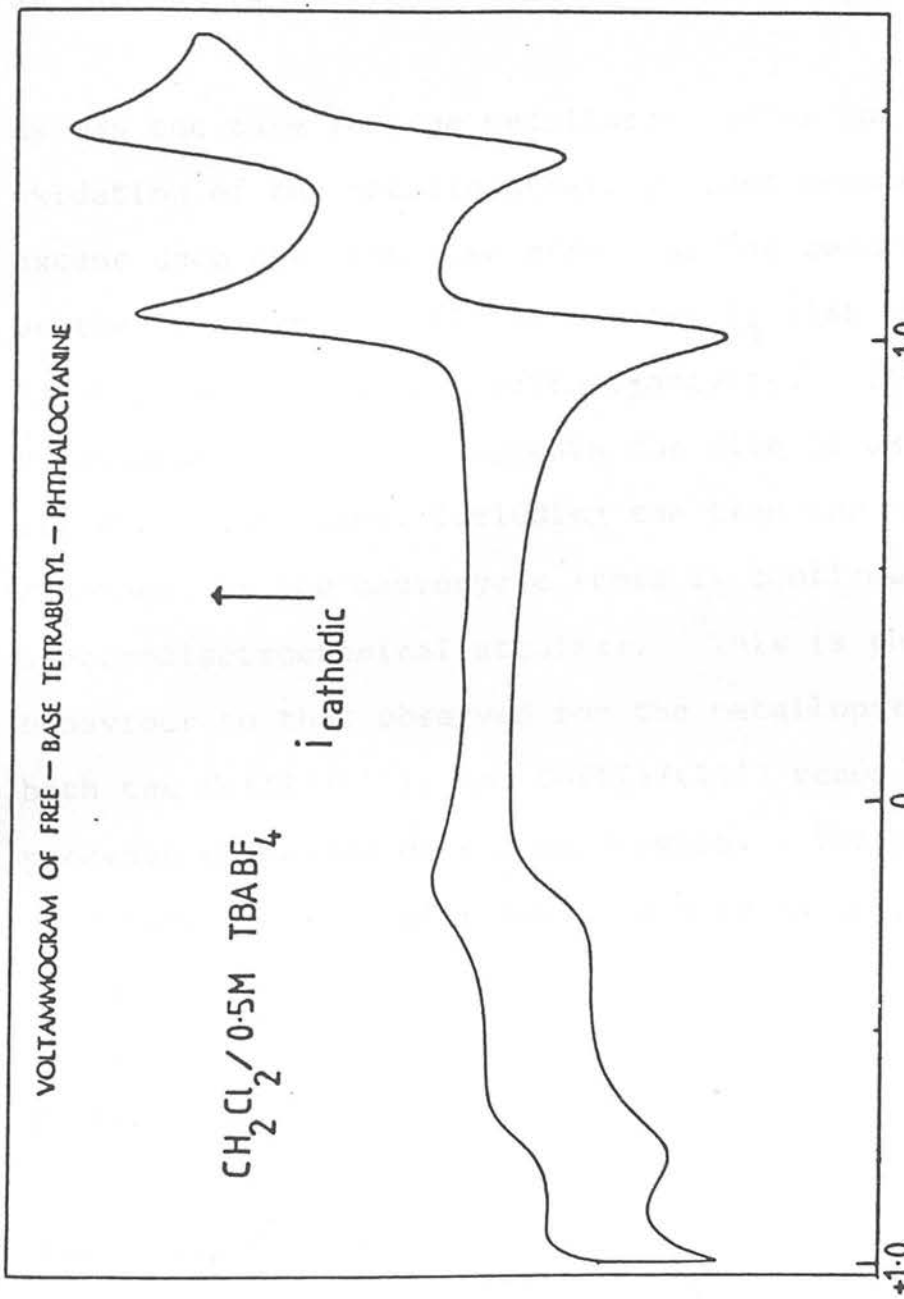

Figure 6.3 Cyclic voltammogram of H_2Bu_4Pc at 20°C

voltammetric response for the first oxidation of the MBu_4Pc species was achieved and accurate $E_{\frac{1}{2}}$ values obtained. The second oxidation was found to be almost completely irreversible. The cathodic and anodic $E_{\frac{1}{2}}$ values displayed by the MBu_4Pc series are listed in Table 1.

As was the case for the metalloporphyrins the ease of oxidation of the metallophthalocyanines depends to a great extent upon the inductive effect of the central metal on the macrocycle. Figure 4 shows $E_{\frac{1}{2}}$ (1st ox) plotted against central metal electronegativity. The linear relationship obtained suggests the site of oxidation in all these complexes, including the iron and cobalt phthalocyanines, is the macrocycle (this is confirmed later by spectroelectrochemical studies). This is then different behaviour to that observed for the metalloporphyrins where both the Fe(II)/(III) and Co(II)/(III) redox couples preceded oxidation of the macrocycle. The phthalocyanine macrocycle is generally noted to oxidise at potentials

- 150mV more negative than the TPP macrocycle and
- 100mV more negative than the OEP macrocycle (see Table 2.1).

The reason for the easier ring oxidation of phthalocyanines must either be due to the substitution of -N- for -CH- at the meso position or to the extended conjugative

Table 6.1 Redox potentials of MBu_4Pc in CH_2Cl_2/0.5M $TBABF_4$ at 20°C (Volts vs. Ag/AgCl)

	$E_{\frac{1}{2}}$(2nd ox)	$E_{\frac{1}{2}}$(1st ox)	$E_{\frac{1}{2}}$(1st red)	$E_{\frac{1}{2}}$(2nd red)
H_2	0.92	0.40	-1.12	-1.52
Zn(II)	0.84	0.33	-1.27	-1.65
Cu(II)	0.95	0.42	-1.18	-1.62
Ni(II)	0.95	0.43	-1.12	-1.69
Co(II)	0.94	0.41	-1.08	-2.01
Fe(II)	0.90	0.39	-1.29	-1.69
ZnTBP	0.63	0.23	-1.68	-2.09

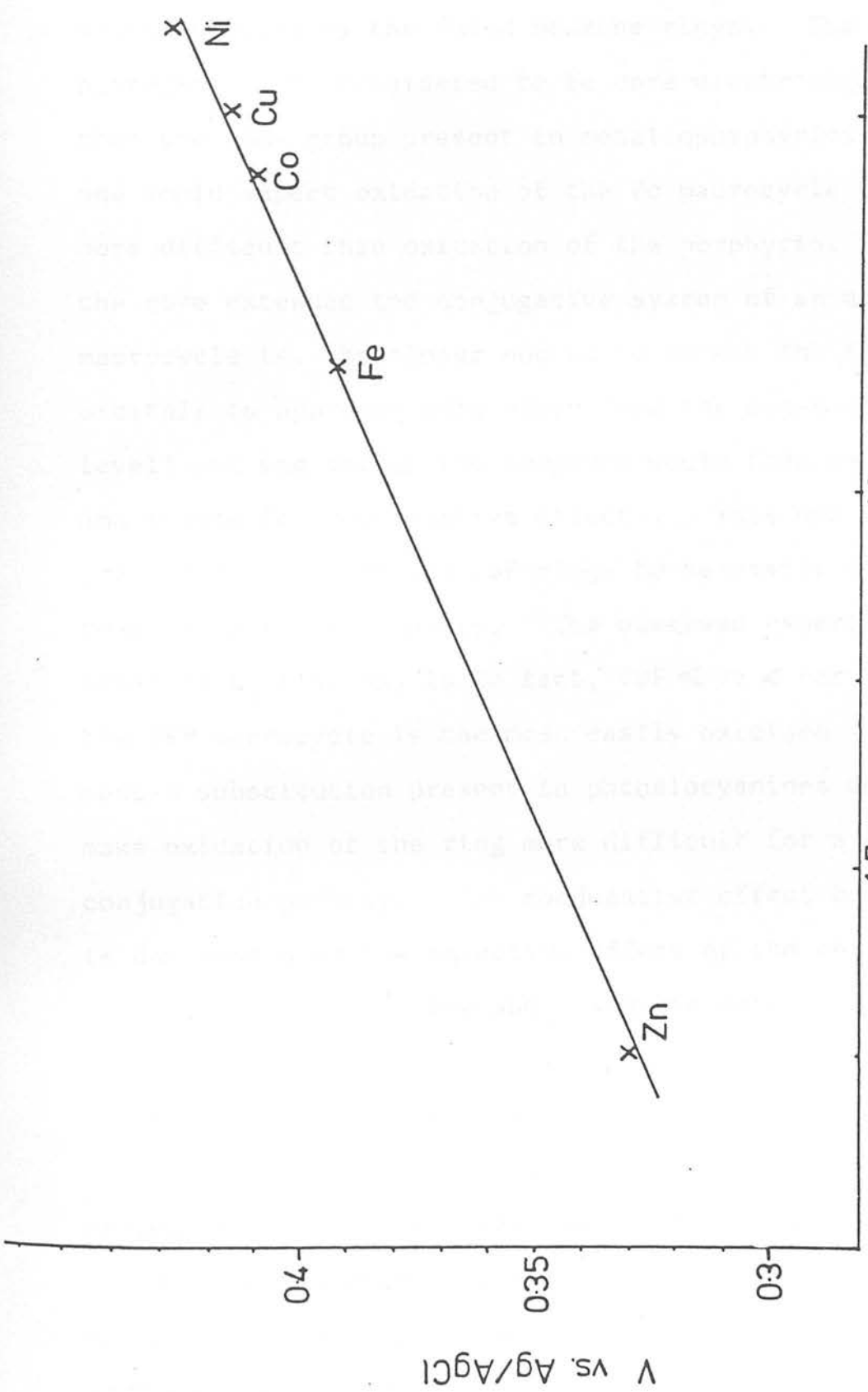

Figure 6.4 First oxidation of the M(II)Bu_4Pc series plotted against central-metal electronegativity (X)

system offered by the fused benzene rings. The meso-nitrogen can be considered to be more electronegative than the -CH- group present in metalloporphyrins and thus one would expect oxidation of the Pc macrocycle to be more difficult than oxidation of the porphyrin. However the more extended the conjugative system of an aromatic macrocycle is, the closer one would expect the frontier orbitals to approach each other (and the non-bonding level) and the easier the compound would then be to oxidise and reduce (the conjugative effect). Thus one would predict both the Pc and TBP rings to be easier to oxidise than the porphyrin moiety. The observed experimental order of $E_{\frac{1}{2}}$ (1st ox) is in fact, TBP < Pc < Por, where the TBP macrocycle is the most easily oxidised. The meso-N substitution present in phthalocyanines does then make oxidation of the ring more difficult for a given conjugation pathway. The conjugative effect however is dominant over the inductive effect of the meso-N when comparing phthalocyanine and porphyrin data.

Another striking difference between the anodic chemistry of porphyrins and phthalocyanines is the value of ΔE(1st ox/2nd ox). We have discussed in Chapter 2 how this figure can be viewed as a measure of the 'fit' of the metal in the macrocycle cavity (the larger ΔE(1st ox/2nd ox), the better the fit). The phthalocyanine macro-

cycle has a much smaller cavity size than the porphyrin ring (the distance between the N atoms of the pyrrole rings and the centre of the molecule is at least 0.05A smaller than that in porphyrin)[28], and thus the geometric overlap of the first row transition metal d-orbitals and the pyrrolic N orbitals will be greater for the MPc species as compared to the corresponding MPor complex. The main cause of cavity contraction in phthalocyanines would appear to be the replacement of the bridging meso -CH- group in porphyrin by nitrogen atoms in Pc. The most direct and important stereochemical consequence of this substitution is to be seen in the bonding angle at the bridging meso-position. For NiOEP, for instance, the meso-bridging angle is 125.1° as compared to 117° in NiPc[31]. The contraction of the bond angle is presumably attributable to the larger spatial demands of the lone pair of electrons on the meso-N atom. This evaluation of the anodic redox data receives support in the measured ΔE(1st ox/2nd ox) value of the tetrabenzoporphyrin (Table 1), which is much smaller than for the phthalocyanine ring.

The cathodic redox trends of the phthalocyanines also show significant differences from those displayed by the metalloporphyrins. For the MBu_4Pc series we find, as was the case in the previous methylnaphthalene study on

the parent phthalocyanines by McQueen[19,32], that $NiBu_4Pc$ is more difficult to reduce than $CuBu_4Pc$. This is the reverse of the order of ease of reduction observed for the copper and nickel porphyrins, where the copper porphyrin was harder to reduce. McQueen[19] attributed this inversion to the anomqlously easy one-electron reduction of nickel porphyrins suggesting the energy of the LUMO was lowered by ruffling of the macrocycle[31] (ruffling of the ring being induced by the small Ni(II) ion). The voltammetric data presented in this work however has shown that the nickel porphyrins are in fact harder to reduce than is predicted by the inductive model. (This is reflected in the observed trend of ΔE(1st ox/1st red) values presented in Chapter 2). We would like to propose instead that the reason for the inversion of the copper and nickel cathodic data for the two different macrocycles is caused by the relatively greater degree of $d\pi \longrightarrow \pi^*$ back-bonding present in the phthalocyanine complexes. This again arises from the smaller cavity size of Pc, allowing greater mixing of the metal $d\pi$ orbitals and the e_g π^* degenerate pair of the ring. The energy match between the metal $d\pi$ orbitals and the e_g (π^*) orbital will also be better for the metallophthalocyanines as the LUMO of the ring must be at lower energy than in the porphyrins i.e. the phthalocyanine ring is more easily reduced by -200mV than TPP and - 400mV than OEP. The extent of

π back-bonding in the MBu_4Pc complexes is also reflected spectroscopically, where the energy of the Q band ($1a_{1u} \longrightarrow 1e_g$) is again dependent upon the central metal as shown below in Table 2.

Table 2: Energy of Q(0,0) band for M(II) Bu_4Pc

	Zn	Cu	Ni	Co	Fe
λ max/nm	678	677	670	669	664
λ max/cm^{-1}	14750	14770	14930	14950	15060

Thus the inversion of $E_{\frac{1}{2}}$(1st red) values is caused by the larger cathodic shift of the Ni(II)Pc/Ni(II)Pc^- couple compared to the Ni(II)Por/Ni(II)Por^- couple due to more electron density being donated back to the Pc ring from the metal d π orbitals than is the case in nickel porphyrins. As for the metalloporphyrins then there is no linear relationship between central metal electronegativity and $E_{\frac{1}{2}}$(1st red) and indeed π back-bonding is sufficiently significant in the bonding of metallophthalocyanines as to affect the order of ease of reduction for the first row transition metal complexes. (Spectroscopic characterisation of the primary cathodic electrode products show the first reduction of the cobalt and iron phthalocyanines to be metal-based).

The relative order of ease of reduction for the three types of macrocycle studied is Pc < Por < TBP with the tetrabenzoporphyrin most difficult to reduce. The fact that the TBP macrocycle is harder to reduce than the porphyrin moiety is surprising considering what has previously been mentioned concerning the conjugative-effect. However it has been noted that π^* antibonding levels can be destabilised by the fusion of benzene rings onto the aromatic core[33], which would render reduction more difficult. The experimental observations are in good agreement with extended Huckel calculations by Gouterman et al[28] which predict shifts of the macrocyclic LUMO of -0.2eV upon fusion of benzene rings onto the pyrrole units. The ease of reduction of phthalocyanines must therefore be entirely due to the aza-substitution at the meso-position. Unlike the $1a_{1u}$ HOMO which is calculated to have little electron density at the meso position the $1e_g$ LUMO is predicted to have considerable electron density at the bridging positions[34]. Thus the greater electronegativity of the nitrogen atom will have a considerable inductive effect on the energy of the lowest acceptor orbital. This would appear to be far more important than the destabilising effect of the fused benzene rings, resulting in the greater electron affinity of the Pc ring. It is interesting to note that our voltammetric results are not in agreement with a recent semi-empirical CNDO-CI

study[35] which predicts the energy of the LUMO to rise through the series Pc < TBP < Por. It is clear from our data that for the extended macrocycles a very sensitive balance of inductive and conjugative effects exists, affecting the energies of the HOMO and the LUMO quite differently. The trend in the electrochemical value

ΔE(1st ox/1st red) does however agree with the CNDO-CI calculations[35] of the size of the frontier orbital gap for all three macrocycles. It is noted that ΔE(1st ox/1st red) increases through the series Pc < TBP < Por as does the energy of the Q band-

	Q(0,0)/eV	ΔE(1st ox/1st red)
$ZnBu_4Pc$	1.83	1.60
ZnTBP	2.06	1.91
ZnTPP	2.10	2.17

McQueen has commented[19] that the lower value obtained electrochemically for the frontier orbital gap of phthalocyanines (as compared to the spectroscopic measurement) suggests the two techniques are in fact mapping different orbitals within the macrocycle. Huckel calculations[28] have indeed predicted the HOMO of the Pc ring is a $N_{p\sigma}$ orbital, not the a_{1u} orbital (the symmetry allowed donor orbital for the Q band). However uv/visible spectral characterisation of the one-electron oxidation product

of the MBu_4Pc series in this work shows electrochemical oxidation does in fact involve removal of an electron from the a_{1u} orbital. Instead, as will be discussed later, we propose the difference in the two experimental values of the HOMO/LUMO energy gap arises primarily from a splitting of the e_g degenerate level upon reduction.

Spectral characterisation of the electrode products of the MBu_4Pc series was only possible for the first oxidation product and the first reduction product. Both the doubly-reduced and doubly-oxidised species were unstable on the required time-scale. Importantly both the cation radical and anion radical of H_2Bu_4Pc were stable at room temperature and thus reference spectra for the electrode products of the metallated species were available. Figure 5 shows the optical spectral changes which occur during the one-electron oxidation of H_2Bu_4Pc in CH_2Cl_2/0.5M $TBABF_4$ at 20°C. As in the case of the free-base porphyrins the parent spectrum of H_2Bu_4Pc has a split Q band due to the lower symmetry of the metal-free species. As oxidation proceeds the parent Q bands are noted to collapse and three less intense bands are seen to grow in the visible/near ir region. Very little change occurs at the uv end of the electronic spectrum where the Soret band shifts only slightly to the blue. Isosbestic points are maintained at 740, 584, 388 and 324nm throughout oxidation

Figure 6.5

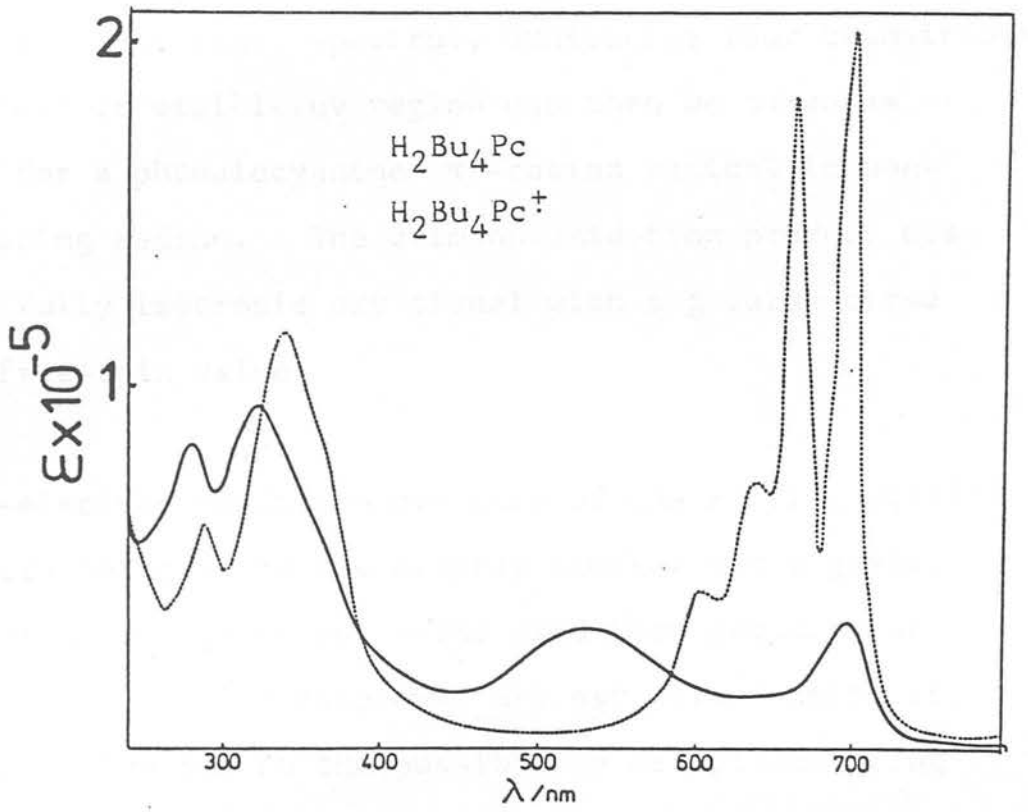

a) Optical absorption spectrum of $H_2Bu_4Pc^+$ in CH_2Cl_2/0.5M $TBABF_4$ at 20°C

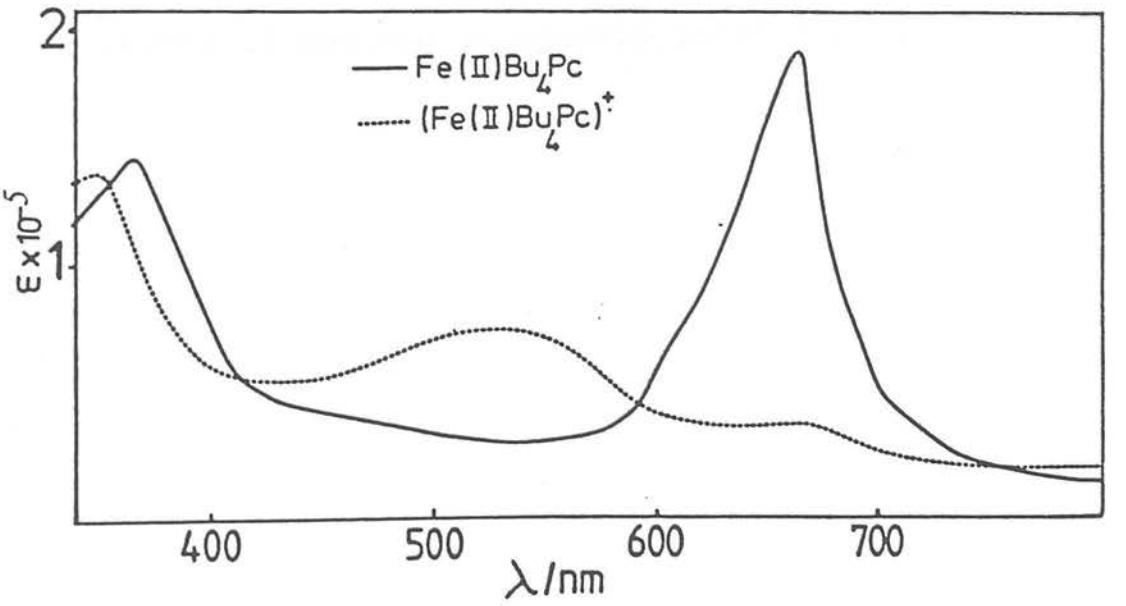

b) Optical absorption spectrum of Fe(II) Bu_4Pc^+ in CH_2Cl_2/0.5M $TBABF_4$ at 20°C

and full recovery of H_2Bu_4Pc was obtained at an appropriate potential. The final spectrum, exhibiting four transitions in the near ir/visible/uv region can then be taken as typical for a phthalocyanine π -cation radical in non-coordinating medium. The crimson oxidation product displays a fully isotropic esr signal with a g value close to the free-spin value.

The one-electron oxidation products of the Fe(II), Ni(II) and Zn(II) phthalocyanines display similar esr signals. No hyperfine was observed. The oxidation products of the Co(II) and Cu(II) complexes are esr silent which is non-informative due to the possibility of spin-coupling in the oxidised species. The available esr data for the MBu_4Pc π cation radicals are listed in Table 3.

Table 3: 290K ESR data for the one-electron oxidation products of the MBu_4Pc species in CH_2Cl_2/0.5 $TBABF_4$

	g	ΔH/G
$H_2Bu_4Pc^+$	2.0054	4.5
$NiBu_4Pc^+$	2.0062	6.0
$ZnBu_4Pc^+$	2.0055	5.0
$FeBu_4Pc^+$	2.0064	6.5

Figure 6.6 Optical progression during the one-electron oxidation of $Co(II)Bu_4Pc$

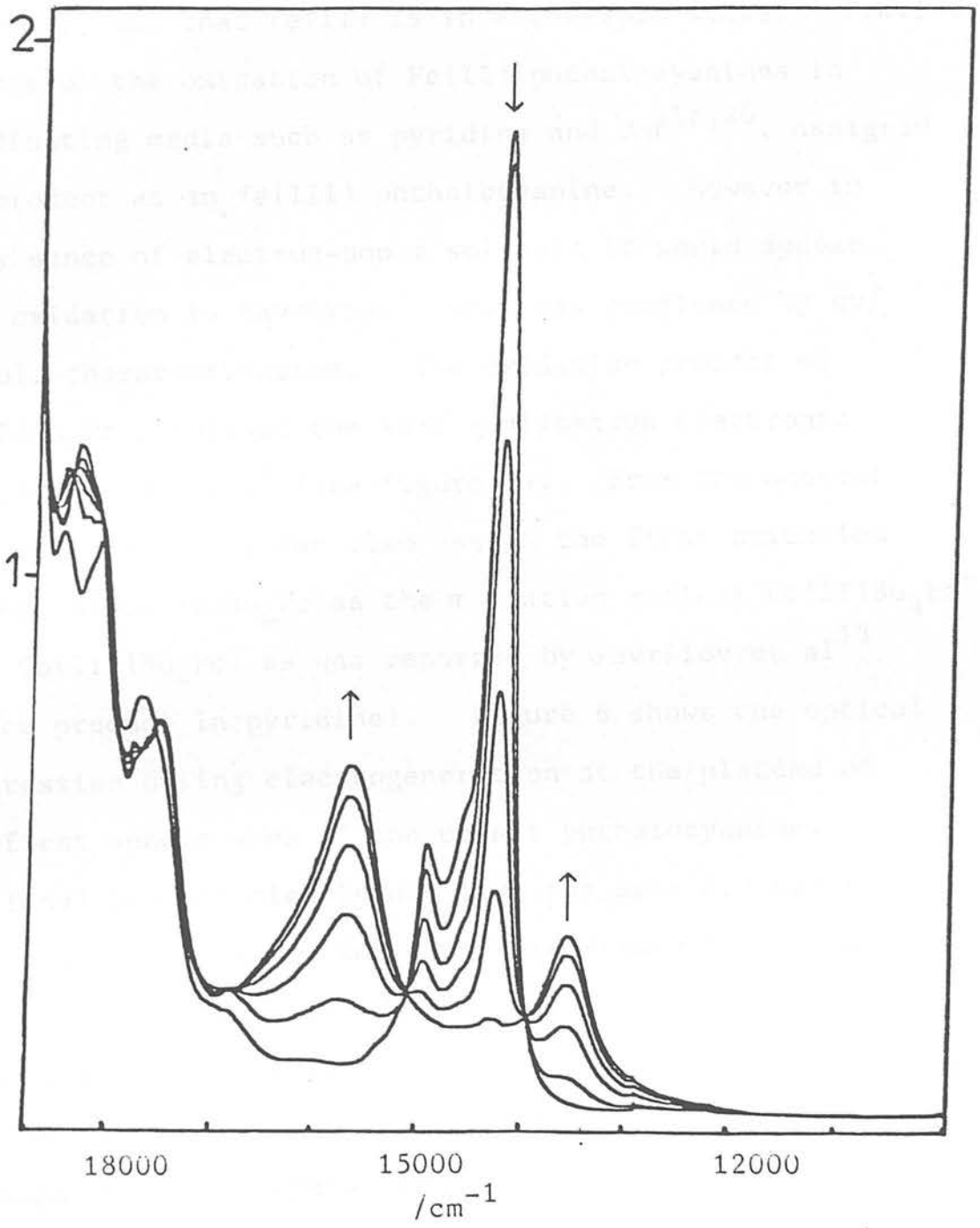

The isotropic g value for the iron complex suggests that oxidation has taken place at the macrocycle rather than the metal, and that Fe(II) is in a low-spin state. Previous reports on the oxidation of Fe(II) phthalocyanines in coordinating media such as pyridine and DMF[18,20], assigned the product as an Fe(III) phthalocyanine. However in the absence of electron-donor solvents it would appear ring oxidation is favoured. This was confirmed by uv/visible characterisation. The oxidation product of $Fe(II)Bu_4Pc$ displayed the same qualitative electronic spectrum as $H_2Bu_4Pc^+$ (see figure 5). From the optical spectral results we can also assign the first oxidation product of $Co(II)Bu_4Pc$ as the π - cation radical $Co(II)Bu_4Pc^+$ (not $Co(III)Bu_4Pc$) as was reported by Gavrilov et al.[13] as the product in pyridine). Figure 6 shows the optical progression during electrogeneration at the plateau of the first anodic wave of the cobalt phthalocyanine. The final product clearly displays the same electronic spectral properties as $ZnBu_4Pc^+$ (see figure 7). The one-electron oxidation products of $NiBu_4Pc$ and $CuBu_4Pc$ give rise to similar spectra. All uv/visible data for the MBu_4Pc^+ species are listed in Table 4. Therefore although the metallophthalocyanines display very attenuated anodic voltammetric waves the spectroelectrochemical results indicate a simple one-electron transfer at the macrocycle is occurring in all cases.

Table 6.4 Spectral data for the oxidation products of MBu_4Pc

	Wavelength maxima, nm (extinction coefficient x 10^{-3})
H_2Bu_4Pc	698(202), 662(176), 638(64.2), 600(36.7), 338(104), 282(53.2)
$H_2Bu_4Pc^+$	838(1.2), 700(35.4), 526(34.6), 326(96)
$ZnBu_4Pc$	678(204), 646(48.7), 611(38.2), 340(86.9), 286(34.7)
$ZnBu_4Pc^+$	840(8.4), 722(22.1), 510(30.2), 459(31.4), 328(80.4)
$CuBu_4Pc$	677(269), 635(69.3), 600(61.0), 388(122.1), 286(54.4)
$CuBu_4Pc^+$	840(2.6), 722(20.6), 509(24.5), 460(28.2), 317(90.2)
$NiBu_4Pc$	670(144), 640(42.7), 603(32.1), 362(28.8), 331(46.9), 293(55.1)
$NiBu_4Pc^+$	839(2.4), 721(36.5), 502(52.3), 460(29.2), 314(35.6)
$CoBu_4Pc$	669(178), 641(58.5), 605(42.6), 325(89.4), 285(97.7)
$CoBu_4Pc^+$	840(1.8), 720(34.6), 500(62.2), 313(110.6)
$FeBu_4Pc$	664(180), 616(39.2), 325(140)
$FeBu_4Pc^+$	720(4.2), 495(52.2), 370(138)

Table 6.5 Spectral data for the reduction products of MBu_4Pc

	Wavelength maxima, nm (extinction coefficient x 10^{-3})
$H_2Bu_4Pc^-$	676(26.2), 620(76.2), 582(139), 388(100) 326(114)
$ZnBu_4Pc^-$	680(22.4), 646(74.6), 574(69.2), 382(74.6), 326(84.2)
$CuBu_4Pc^-$	679(20.1), 642(69.2), 572(70.4), 381(80.0), 324(40.2)
$NiBu_4Pc^-$	670(14.6), 637(72.2), 562(82.4), 370(92.1), 320(40.7)
$(CoBu_4Pc)^-$	660(142), 610(40.1), 315(90.2)
$(FeBu_4Pc)^-$	654(110), 325(204)

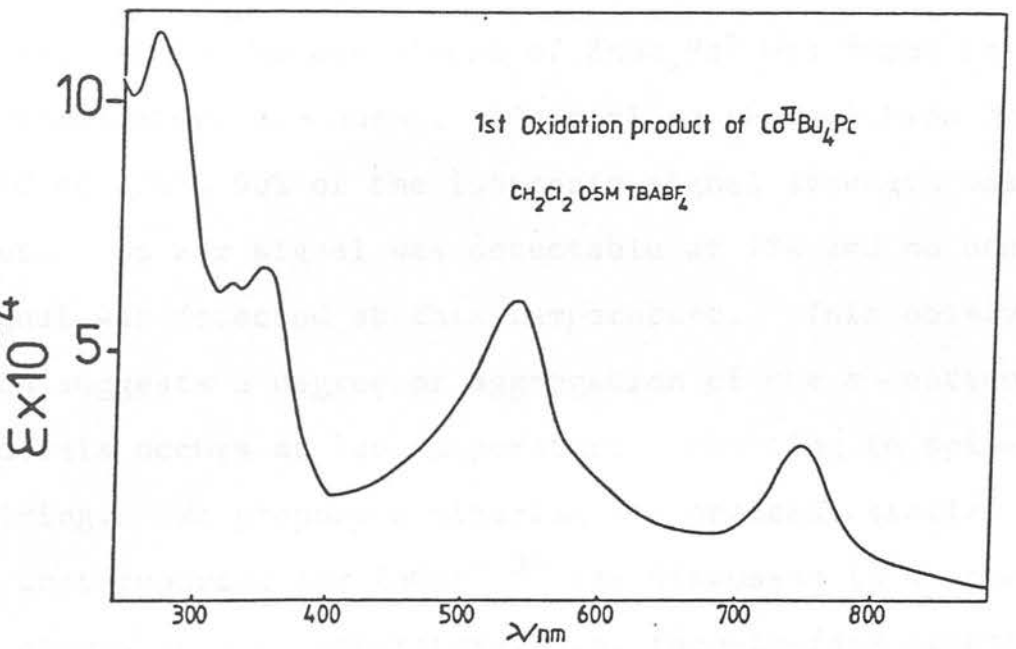

a) Optical absorption spectrum of the one-electron oxidation product of $CoBu_4Pc$ (20°C)

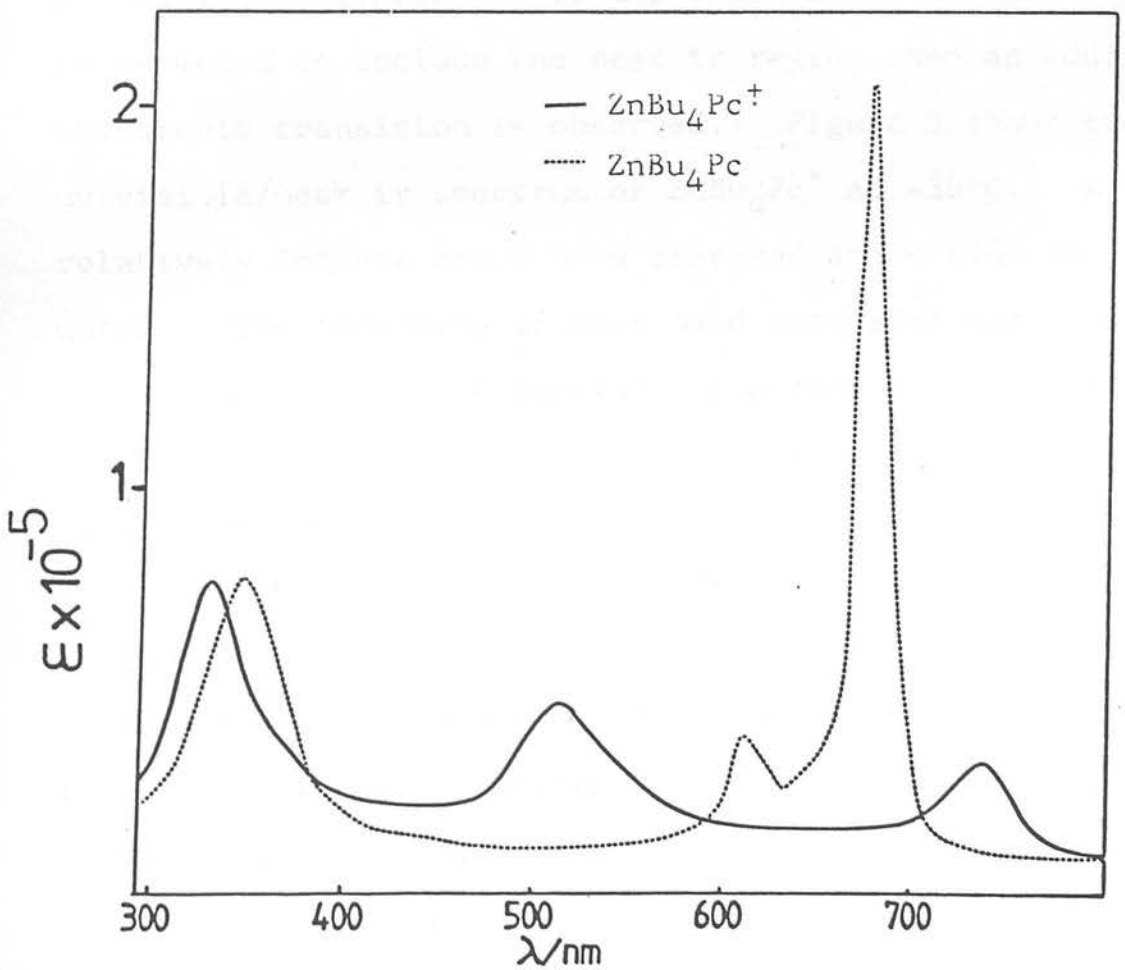

b) Optical absorption spectrum of the one-electron oxidation product of $ZnBu_4Pc$ (20°C)

Interestingly the esr signal of $ZnBu_4Pc^+$ was found to be temperature dependent. On cooling the solution from 20°C to -70°C 90% of the isotropic signal strength was lost. No esr signal was detectable at 77K and no other signal was detected at this temperature. This observation suggests a degree of aggregation of the π - cation radicals occurs at low temperature, resulting in spin-pairing. We propose a dimerisation process, similar to that reported for $ZnOEP^+$ [36] (as discussed in Chapter 3) occurs at low temperature, i.e. face-to-face dimerisation of two macrocyclic rings resulting in a π — π' bond. Uv/visible evidence is also available for this proposed dimerisation. If the spectral wavelength range is extended to include the near ir region then an additional electronic transition is observed. Figure 8 shows the uv/visible/near ir spectrum of $ZnBu_4Pc^+$ at -30°C. A relatively intense broad band centered at ~ 1000 nm is noted. The intensity of this band increases upon cooling the solution from 20°C to -70°C, the same temperature range where the esr signal was noted to decay considerably. This transition is similar to a band reported[36] in the spectrum of the dimer $(ZnOEP^+)_2(Br)_2$ but is slightly red-shifted. The shape and intensity of this band suggests it arises from a charge-transfer transition (most likely from the dimer ground state to a dication-neutral phthalocyanine pair). Similar temperature-dependent optical

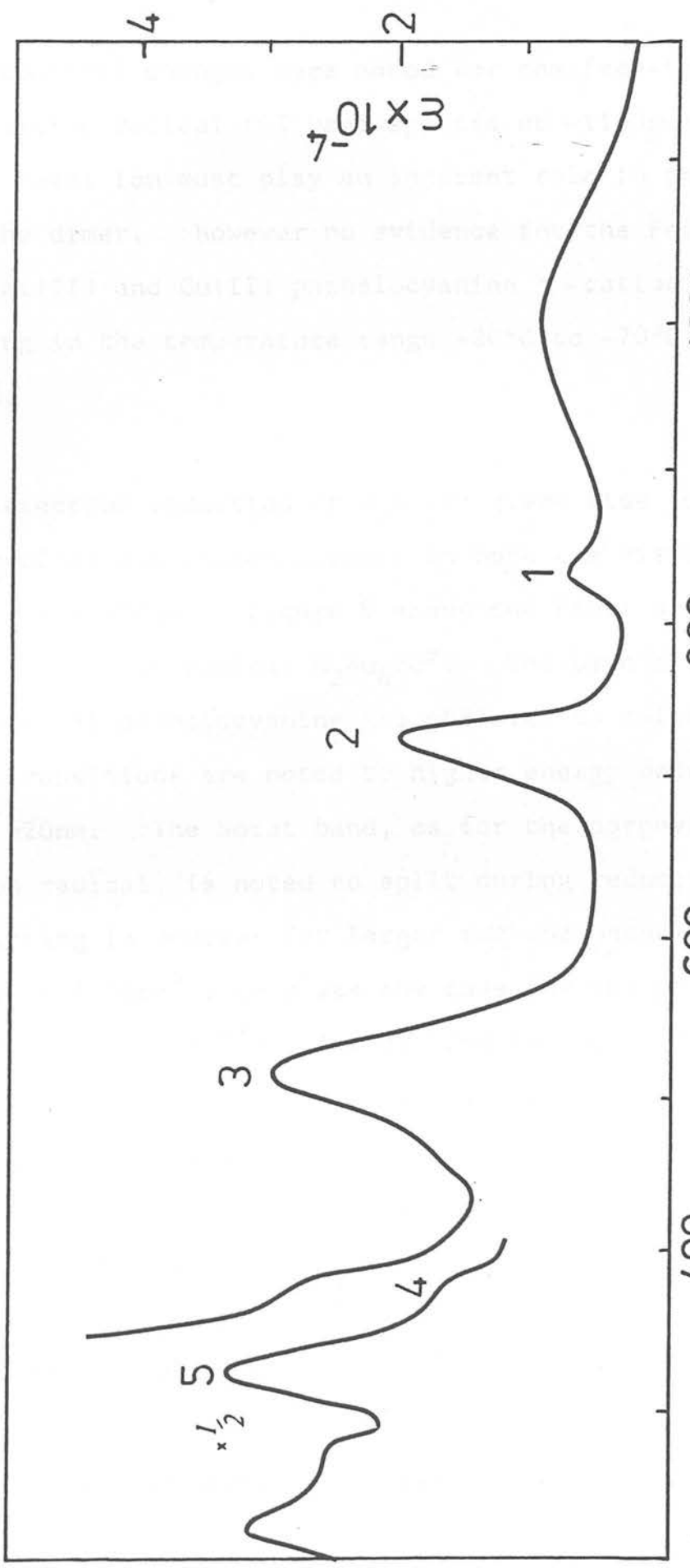

Figure 6.8 Near ir/visible of $(ZnBu_4Pc^{+\cdot})_2$ at -35°C in CH_2Cl_2/0.5M $TBABF_4$

and esr spectral changes were noted for the free-base H_2Bu_4Pc cation radical (CT band appears at ~ 1100nm) and thus the metal ion must play an innocent role in the bonding of the dimer. However no evidence for the Fe(II), Co(II), Ni(II) and Cu(II) phthalocyanine π - cation radicals dimerising in the temperature range +20°C to -70°C was observed.

The one-electron reduction of H_2Bu_4Pc gives rise to significant optical absorption changes in both the visible and near uv regions. Figure 9 snows the final spectrum of the green anion radical $H_2Bu_4Pc^{-}$. The parent Q bands of the neutral phthalocyanine are observed to collapse and new transitions are noted to higher energy between 700 and 520nm. The Soret band, as for the porphyrin π - anion radical, is noted to split during reduction. The splitting is however far larger for the phthalocyanine moiety (~ $4000cm^{-1}$) than was the case for the porphyrin macrocycle (~ $1100cm^{-1}$) A weak band in the near ir is also noted to grow upon reduction. Isosbestic points are maintained at 740, 630, 380, 316, 296 and 280nm throughout reduction and H_2Bu_4Pc is regenerated in full at the appropriate potential.

Similar spectral changes occur on reduction of the Zn(II), Cu(II), and Ni(II) phthalocyanines with the growth of a weak band in the near ir, two new transitions appearing

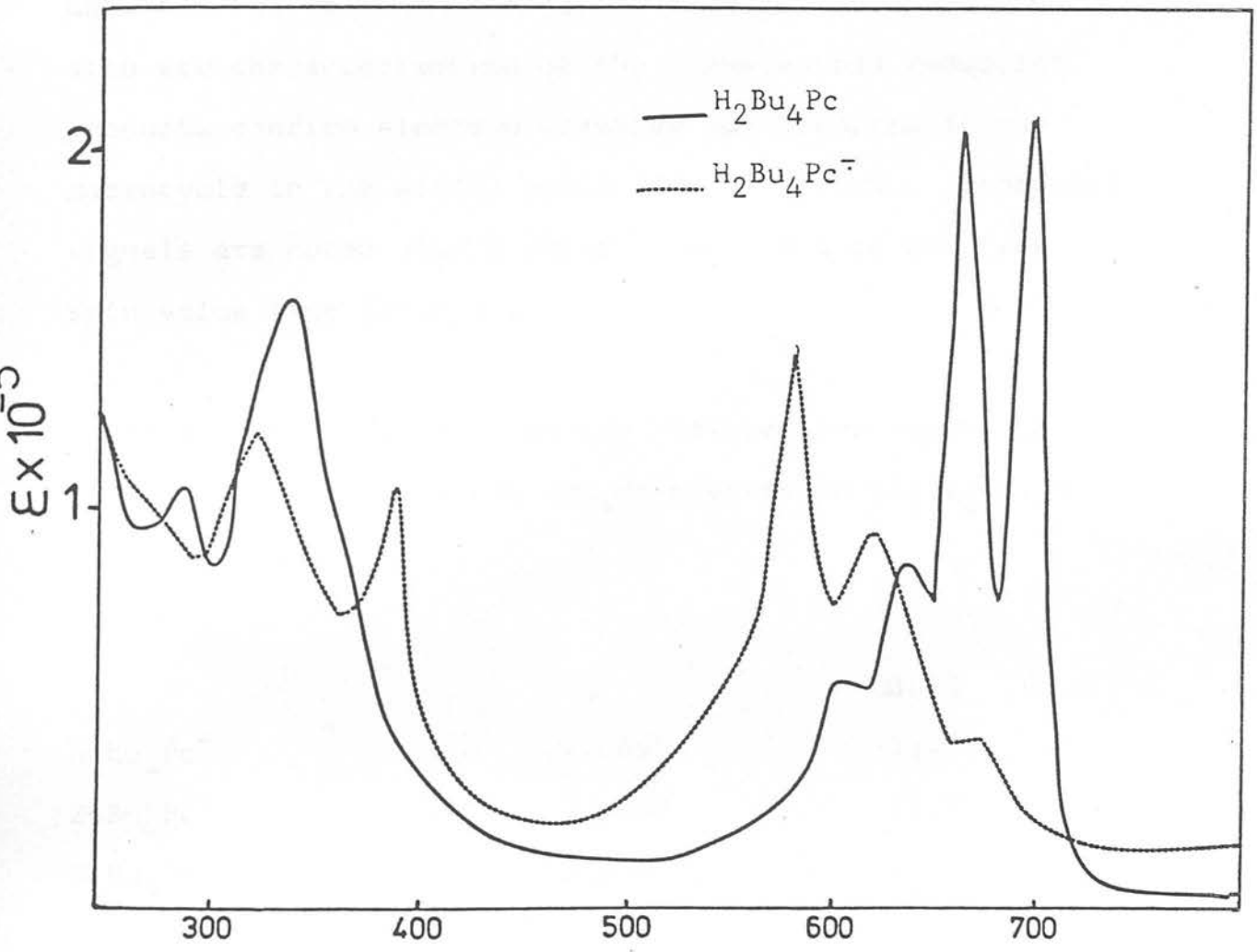

Figure 6.9 Optical absorption spectrum of the one-electron reduction product of H_2Bu_4Pc

at higher energy than the parent Q band, and a splitting of the Soret band in the near uv region. The optical spectrum of Zn(II)Bu_4Pc^- is shown in Figure 10 and spectral data for the π-anion radicals listed in Table 5. In situ esr characterisation of the one-electron reduction products confirm electron transfer has occurred at the macrocycle in the Ni(II) and Zn(II) complexes. Isotropic signals are noted with g values very close to the free-spin value (see Table 6).

Table 6: 290K ESR data for the one-electron reduction products of the MBu_4Pc species in CH_2Cl_2/0.5M $TBABF_4$

	g	ΔH/G
$H_2Bu_4Pc^-$	2.0051	12.0
$ZnBu_4Pc^-$	2.0053	12.0
$NiBu_4Pc^-$	2.0069	14.5

The one-electron reduction product of Co(II)Bu_4Pc is esr silent. However the optical spectral changes during reduction indicate electron-transfer occurs at the metal as has been reported previously for other cobalt phthalocyanines[37-39]. A small red shift of the Q band occurs and the Soret band shifts to the blue by $-1000cm^{-1}$. No splitting of the Soret band is observed. Another

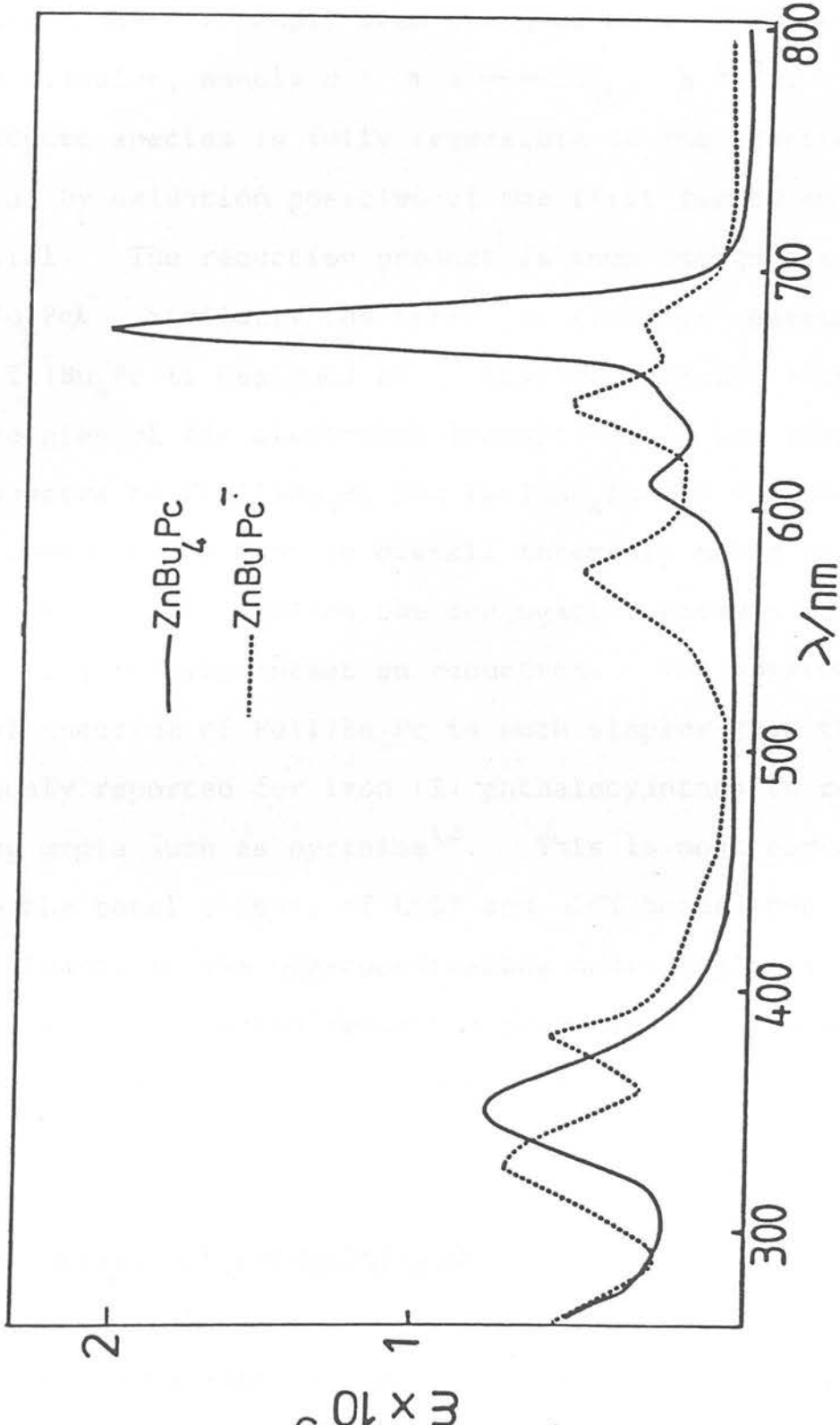

Figure 6.10 Optical absorption spectrum of the one-electron reduction product of $ZnBu_4Pc$

intense band appears at 504nm upon reduction. This transition has previously been assigned as a metal $\longrightarrow$ ligand charge transfer, namely d (π) $\longrightarrow$ $1b_{1u}$(π^*)[40]. The reduced species is fully reversible to the starting material by oxidation positive of the first reduction potential. The reduction product is thus assigned as $(Co(I)Bu_4Pc)^-$. Similarly the first one-electron reduction of $Fe(II)Bu_4Pc$ is assigned as a metal-based redox step. The energies of the electronic transitions in the absorption spectra of $Fe(II)Bu_4Pc$ and $Fe(I)Bu_4Pc$ are virtually coincident with no loss in overall intensity noted (see Figure 11). This implies the conjugative pathway of the Pc ring remains intact on reduction. The observed optical spectrum of $Fe(I)Bu_4Pc$ is much simpler than that previously reported for iron (I) phthalocyanines in coordinating media such as pyridine[18]. This is most certainly due to the total absence of LMCT and MLCT bands involving axial ligands in the non-coordinating media employed in this work. The second reduction products of the cobalt and iron phthalocyanines were not sufficiently stable in CH_2Cl_2 for spectral characterisation to be achieved.

6.3 MOLYBDENUM PHTHALOCYANINES

Molybdenum phthalocyanines have been known for several years[41] but full characterisation of these species has yet to be achieved. McQueen[19] has suggested from ir

Figure 6.11 ESR and uv/visible spectra of the one-electron reduction product of $Fe(II)Bu_4Pc$

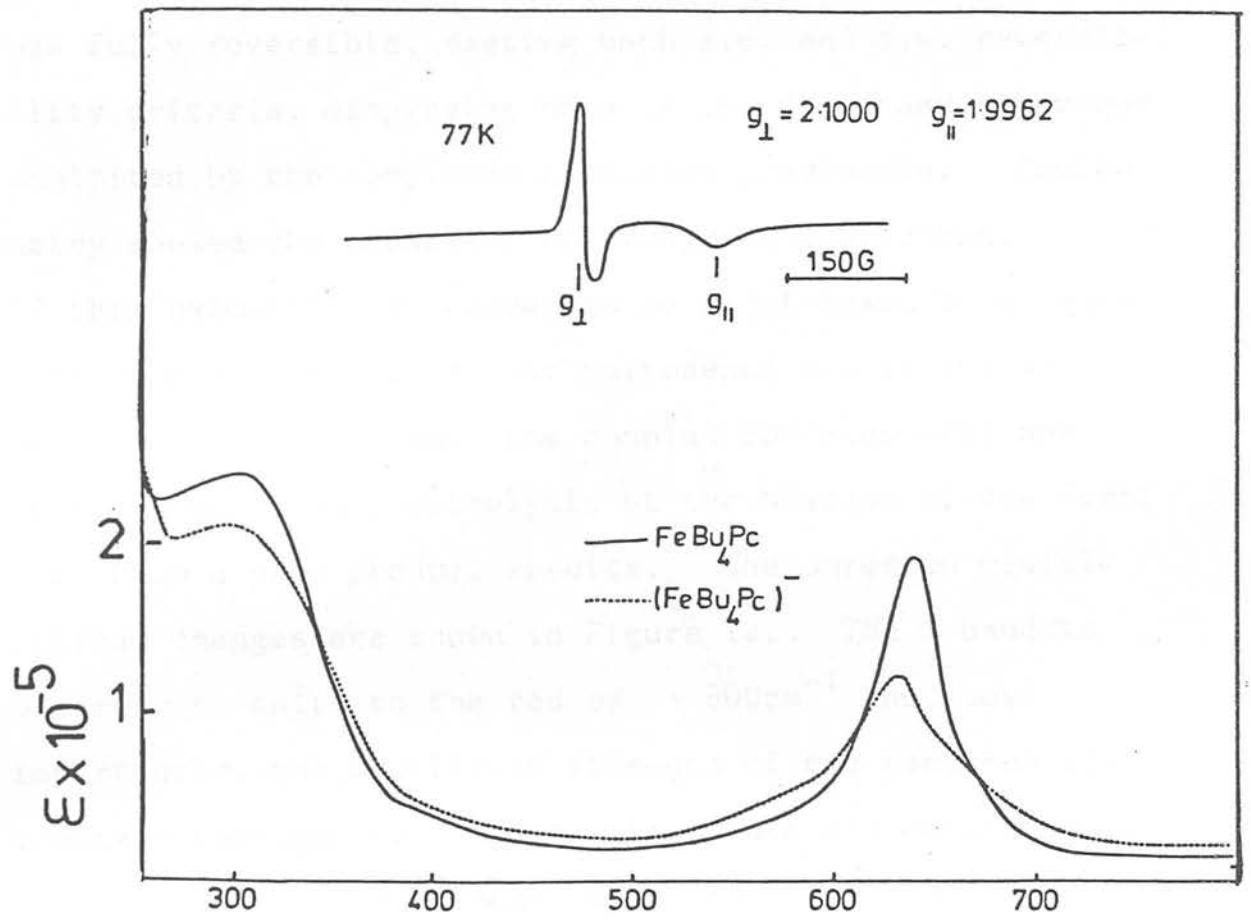

studies that the structure contains an Mo = O linkage. However this does not distinguish between Mo(IV)(O)Pc and $Mo(VI)(O)_2Pc$. In a brief study of the electrochemistry of this species we observed that the complex displays a one electron oxidation at +0.22V. This anodic wave was fully reversible, meeting both a.c. and c.v. reversibility criteria, displaying none of the distended behaviour exhibited by the complexes discussed previously. Coulometry showed the oxidation to involve one electron. If this oxidation was proven to be metal-based this would then be strong evidence that molybdenum was in the 4+ oxidation state and that the complex contains only one Mo = O bond. On electrolysis at the plateau of the first oxidation a blue product results. The observed visible optical changes are shown in Figure 12. The Q band is observed to shift to the red by ~ $600cm^{-1}$ and, most importantly, the oscillator strength of the band remains constant throughout. Isosbestic points are maintained at 752 and 708nm throughout oxidation and the parent complex is fully recovered on reverse electrolysis. None of the characteristic Pc cation radical peaks are noted. The oxidation is thus assigned as a metal-based $Mo^{IV/V}$ couple and the parent complex must therefore be Mo(IV)(O)Pc.

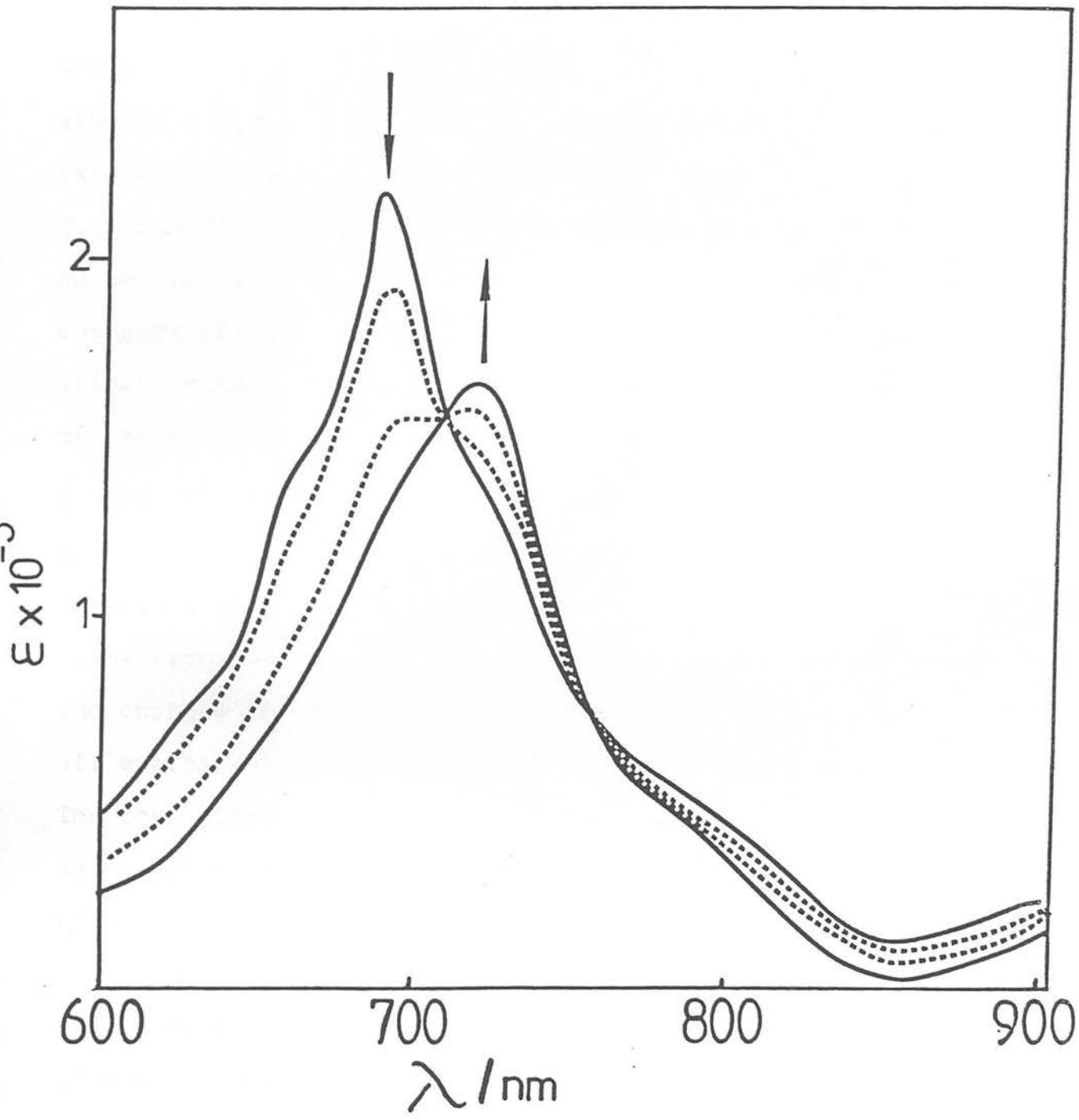

Figure 6.12 Optical progression during the one-electron oxidation of "Molybdenum phthalocyanine"

6.4 DISCUSSION

All the first-row transition-metal phthalocyanine complexes studied are noted to undergo a macrocycle-based one-electron oxidation. The removal of an electron from the π conjugation pathway can be assumed, as was the case for the porphyrin ring, not to greatly affect the one-electron energies of the π orbital array and hence have little affect on the bond order. The ground state configuration of the phthalocyanine cation radical will then be $(a_{2u})^2 a_{1u}$ giving rise to a $^2A_{1u}$ state. The spectral changes observed upon oxidation will therefore be expected to reflect the existence of a hole in the $1a_{1u}$ orbital (i.e. additional transitions of the type $e_g(\pi) \longrightarrow 1a_{1u}(\pi)$ are expected) and changes in spin-pairing energy. The MBu_4Pc^+ species all exhibited similar optical absorption properties. The characteristic electronic spectrum of the phthalocyanine cation radical presented in this work is however quite different from a previous report on the oxidation products of ZnPc by Luk'yanets et al[21]. In a potentiometric study they treated ZnPc with ferric perchlorate, in a 4 : 1 mixture of nitrobenzene and acetophenone, and observed only a small blue shift of the Q band with no loss in intensity occurring. No other transitions were noted, and no mention of the reversibility of the process

discussed. They assigned the oxidation product as $ZnPc^{+}$. It is likely however, in the experimental medium employed, the π -cation radical had a very limited lifetime and the observed product was in fact a neutral zinc phthalocyanine complex (nucleophilic addition having occurred at the macrocycle). A much more recent study by Stillman et al.[42], which appeared at the time of writing, reported the electrochemical generation of the π -cation radical of ZnPc in CH_2Cl_2, in the presence of pyridine, imidazole or cyanide. The absorption spectrum observed for the π -cation radical was very similar to that presented in this work. Stillman observed five well-defined transitions in the uv/visible region, the energies of which were largely independent of the axial ligand. A subsequent complementary MCD study[43], incorporating band deconvolution, assigned the $ZnPc^{+}$ transitions as follows-

	Energy	Assignment
Band 1 :	$12,200cm^{-1}$	$1e_g \longrightarrow 1a_{1u}$
Band 2 :	$14,000cm^{-1}$	$1a_{1u} \longrightarrow 1e_g$ (Q band)
Band 3 :	$19,500cm^{-1}$	unassigned
Band 4 :	$23,600cm^{-1}$	$2e_g \longrightarrow 1a_{1u}$
Band 5 :	$27,000cm^{-1}$	$1a_{2u} \longrightarrow 1e_g$ (B band)

Although we have only optical absorption data available, we disagree to a significant extent with the above assign-

ments. Firstly, if there is no configurational interaction between the electronic transitions of both the parent neutral metallophthalocyanine and the π-cation radical then one would expect the energy of the Q band to shift to higher energy upon oxidation (as the energy of the $1a_{1u}$ level will decrease on removal of an electron). This intuitive approach is supported by a recent theoretical treatment of the electronic spectra of MPc and MPc^{+} which predicts a blue-shift of the Q band upon oxidation[44]. Band 2, which Stillman has assigned as the $1a_{1u} \longrightarrow 1e_g$ transition is in fact red-shifted from the Q band of the parent complex. A second discrepancy in the above assignment is that the lowest-energy allowed electronic transition of the π-cation radical (D_{4h} symmetry) is predicted to be $1a_{2u} \longrightarrow 1a_{1u}$. The optical absorption spectrum of $ZnBu_4Pc^{+}$, measured from $2500cm^{-1}$ in this work, shows the first electronic transition occurs at $11,900cm^{-1}$ which corresponds closely with band 1 in the spectrum of $ZnPc^{+}$. No other transition to lower energy (excepting the $\pi - \pi'$ band of the $(ZnBu_4Pc^{+})_2$ dimer) is observed.

The electronic spectral properties of the parent metallophthalocyanines, with regard to the dependence on the central metal, are very similar to those of the metalloporphyrins. The energies of both the Q band and the B band of the MBu_4Pc series reflect the degree of

$d\pi \longrightarrow \pi^*$ back-bonding present in each complex (as does the energy of the Q band of the hypso-metalloporphyrins). Thus the energy of the Q transition increases through the series Zn < Cu < Ni < Co < Fe, as does the energy of the B band, reflecting the amount of mixing of the metal d(π) orbitals and the $1e_g$(π *) level in each complex. Transitions in the electronic spectrum of the phthalocyanine π -cation radical which show a similar dependence on the metal centre must therefore have some metal-character and obviously involve promotion of an electron to the $1e_g$ level. Transitions involving promotion of an electron to the singly-occupied $1a_{1u}$ level should be largely independent of the central metal ion.

The first five electronic transitions observed for $ZnPu_4Pc^+$ (see Figure 8) in this work occur at the following energies-

	Energy	Assignment
Band 1	$11,900cm^{-1}$	$1a_{2u} \longrightarrow 1a_{1u}$
Band 2	$13,850cm^{-1}$	$1e_g \longrightarrow 1a_{1u}$
Band 3	$19,600cm^{-1}$	$1a_{1u} \longrightarrow 1e_g$
Band 4	$21,770cm^{-1}$	$2e_g \longrightarrow 1a_{1u}$
Band 5	$30,500cm^{-1}$	$1a_{2u} \longrightarrow 1e_g$

All the MBu_4Pc^+ species exhibit analogous spectra.

Table 2 shows the energies of bands 1, 2 and 4 to occur at similar energies for all the π -cation radicals. The energies of bands 3 and 5 though, exhibit the same hypso-behaviour as the neutral metallophthalocyanine Q and B transitions. Band 5 is very close in energy and band shape to the Soret band of the parent complex. Indeed, very little change is expected in the Soret region of the spectrum as the energies of the $1a_{2u}(\pi)$ and $1e_g(\pi^*)$ levels will be largely unaffected by removal of an electron from the $1a_{1u}$ orbital. The small shift in this transition upon oxidation indicates little or no configurational interaction between the transitions of either the parent complex or the π -cation radical exists. Band 5 is thus assigned as the $1a_{2u} \longrightarrow 1e_g$ Soret transition. This agrees with Stillman's assignment of this band. By the same reasoning we assign band 3 as the $1a_{1u} \longrightarrow 1e_g$ transition. Also, the oscillator strength of band 3 is approximately half (0.46) that of the Q band of $ZnBu_4Pc$. This is as would be predicted by simple statistical reasoning. The assignment of bands 3 and 5 as the Q and B band, respectively, of the π -cation radical receives support from further analysis of the electronic spectrum. As bands 3 and 5 involve promotion of an electron to the same orbital, the energy difference between the two transitions will be a direct measure of the energy gap between the $1a_{2u}$ and $1a_{1u}$ orbitals in the phthalocyanine π -cation radical. Moreover, this gap can be mapped directly, as the $1a_{2u} \longrightarrow 1a_{1u}$ transition is symmetry allowed.

This transition, as already mentioned, should be the lowest energy band observed in the electronic spectrum. If we then assign band 1 as the $1a_{2u} \longrightarrow 1a_{1u}$ transition then the energy of band 1 plus the energy of band 3 should equal the energy of band 5. Table 4 shows this is indeed the case, the energy match being exact, emphasising again the lack of configurational interaction in the π-cation radical. Bands 2 and 4, as they are independent of the metal centre are assigned as $1e_g \longrightarrow 1a_{1u}$ and $2e_g \longrightarrow 1a_{1u}$ respectively.

The order of the electronic transitions assigned in this work disagrees with the contemporary MCD analysis[43]. We are confident, however, our internal comparison of spectral data, in a non-coordinating medium, for a logical series of metallophthalocyanine π-cation radicals, is worthwhile and in better agreement with theoretical prediction[44].

The lack of configurational interaction exhibited by both the neutral and oxidised Pc macrocycle is not repeated in the spectrum of either zinc tetrabenzoporphyrin (ZnTBP) or $ZnTBP^+$. Figure 13 shows the electronic spectra of ZnTBP and $ZnTBP^+$. Overlapping visible absorptions are noted in the π-cation radical spectrum, which are far weaker than the Soret transition. A small blue shift of both the Soret band and the Q band occurs on oxidation.

Figure 6.13 Electronic spectra of ZnTBP and the one-electron oxidation product. (CH_2Cl_2/0.5M $TBABF_4$/0.3mM pyridine)

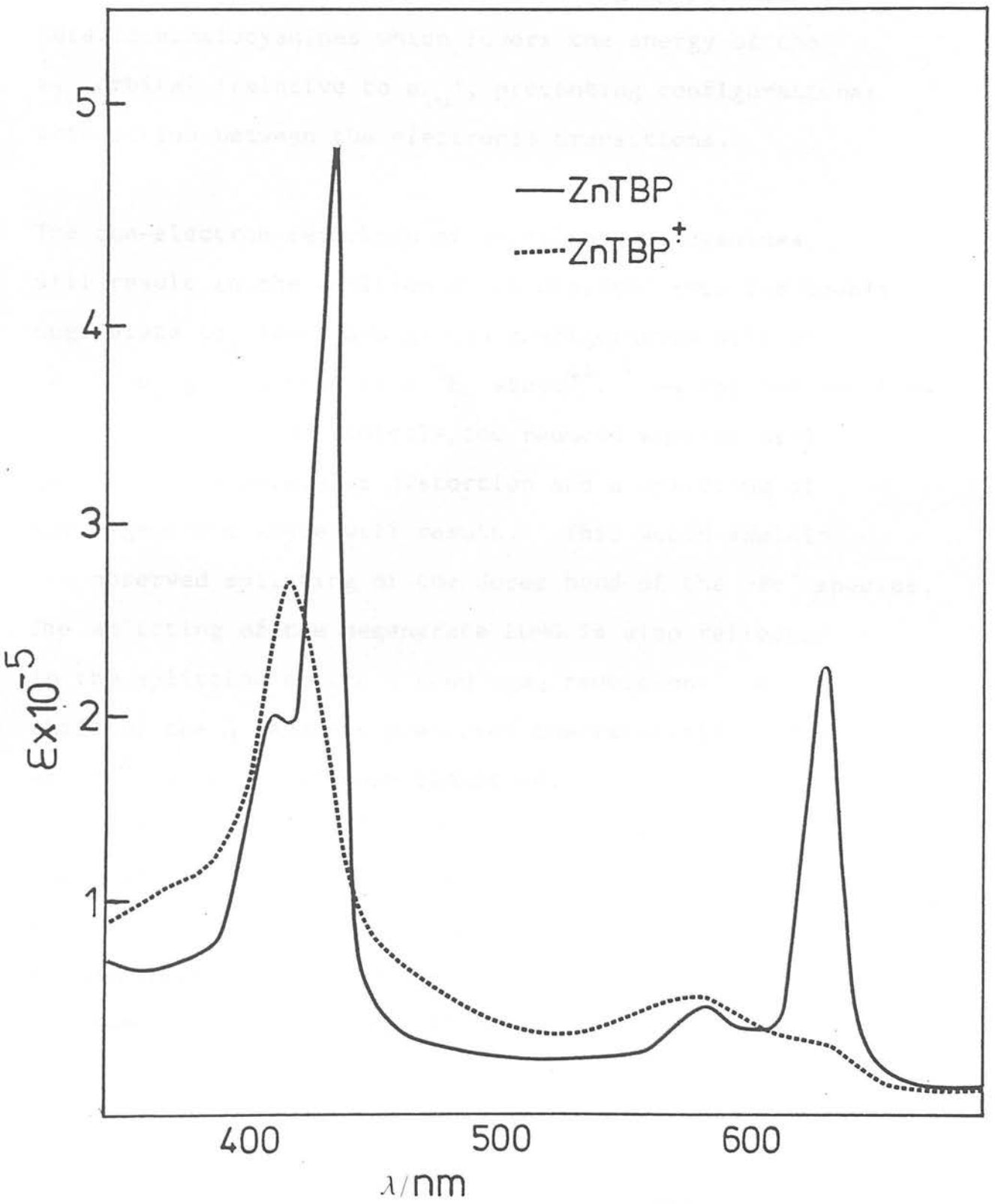

Generally the spectrum of $ZnTBP^{+}$ is more like the spectrum of MP^{+} rather than MPc^{+}. It can be deduced then, it is the presence of -N- at the meso-bridging position in metallophthalocyanines which lowers the energy of the a_{2u} orbital (relative to a_{1u}), preventing configurational interaction between the electronic transitions.

The one-electron reduction of metallophthalocyanines will result in the addition of an electron into the doubly degenerate $1e_g$ level and ground configuration will be $(a_{1u})^2 e_g$ giving rise to a ^2E_g state[44]. As for the metalloporphyrin π -anion radicals, the reduced species will be subject to molecular distortion and a splitting of the degenerate state will result. This would explain the observed splitting of the Soret band of the MPc^{-} species. The splitting of the degenerate LUMO is also reflected in the splitting of the Q band upon reduction. A blue shift of the Q band, as predicted theoretically by Gouterman et al.[44], is observed upon reduction. The splitting of the Q band is however far smaller in energy terms than the splitting of the Soret band and it is probable the $1a_{1u}(\pi) \longrightarrow e_g(\pi^*)$ transition mixes with the near ir transitions which have previously been assigned[44] as $\pi^* \longrightarrow \pi^*$ bands originating from the $1e_g(\pi^*)$ level.

6.5 EXPERIMENTAL

The electrochemical and spectroelectrochemical techniques used in this chapter have been adequately described previously. Molybdenum phthalocyanine was obtained from Pfaltz and Bauer Inc., U.S.A. and used without further purification. H_2Bu_4Pc was prepared by the method of Luk'yanets et al.[45] and metallated as described by McQueen.[19] ZnTBP was prepared by the method of Edwards et al..[46]

REFERENCES : CHAPTER 6

1. C.M. Leiber and N.S. Lewis, J. Am. Chem. Soc., 1984, 106, 553.
2. T. Hirai and J. Yamaki, J. Electrochem. Soc., 1985, 132, 2125.
3. B. Simic-Glavaski, S. Zecevic and E. Yeager, J. Phys. Chem., 1983, 87, 4555.
4. M.M. Nicholson and F.A. Pizzarello, J. Electrochem. Soc., 1981, 128, 1740.
5. G.C.S. Collins and D.J. Schiffrin, J. Electroanal. Chem., Interfacial Electrochem. 1982, 139, 335.
6. J. Martinsen, L.J. Pace, T.E. Phillips, B.M. Hoffman and J.A. Ibers, J. Am. Chem. Soc., 1982, 104, 83.
7. A.B.P. Lever and J.P. Wilshire, Inorg. Chem., 1978, 17, 1145.
8. L.D. Rollman and R.T. Iwamoto, J. Am. Chem. Soc., 1968, 90, 1455.
9. D.W. Clack and J.R. Yandle, Inorg. Chem., 1972, 11, 1738.
10. D. Dolphin, B.R. James, A.J. Murray and J.R. Thornback, Can. J. Chem., 1980, 58, 1125.
11. J. Ferraudi, S. Oishi, S. Muraldiharan, J. Phys. Chem., 1984, 88, 5261.
12. L.A. Bottomley, J.N. Gorce, V.L. Goedken and C. Ercolani, Inorg. Chem., 1985, 24, 3733.

13. V.I. Gavrilov, L.G. Tomilova, I.V. Shelepin and E.A. Luk'yanets, Electrokhimiya, 1979, 15, 1058.

14. N. Kobayashi, H. Shirai and N. Hojo, J. Chem. Soc., Dalton Trans., 1984, 2107.

15. N. Kobayashi and Y. Nishiyama, J. Phys. Chem., 1985, 89, 1167.

16. A. Vogler, B. Rethwisch, H. Kunkely, J. Huttermann and J.O. Besenhard, Angew. Chem., Int. Ed. Engl., 1978, 17, 951.

17. D.W. Clack, N.S. Hush and I.S. Woolsey, Inorg. Chim Acta., 1976, 19, 129.

18. A.B.P. Lever and J.P. Wilshire, Can. J. Chem., 1976, 54, 2514.

19. R.C.S. McQueen, PhD Thesis, Edinburgh University, 1983.

20. A.B.P. Lever, S. Licoccia, K. Magnell, P.C. Minor and B.C. Ramaswamy, "Electrochemical and Spectro-electrochemical Studies of Biological Redox Components", Advances in Chemistry 201; American Chemical Society : Washington, D.C., 1982, p. 237.

21. S.F. Vul'fson, O.L. Kaliya, O.L. Lebedeo and E.A. Luk'yanets, Zh. Organ. Khim., 1976, 12, 123.

22. H. Ohtani, T. Kobayashi, T. Ohno, S. Kato, T. Tanno and A. Yamada, J. Phys. Chem., 1984, 88, 4431.

23. J.F. Myers, G.W. Rayner-Canham and A.B.P. Lever, Inorg. Chem., 1975, 14, 461.

24. J.M. Green and L.R. Faulkner, J. Am. Chem. Soc., 1983, 105, 2950.

25. B.R. Hollebone and M.J. Stillman, J. Chem. Soc., Faraday Trans. 2, 1977, 74, 2107.

26. A.J. McHugh, M. Gouterman and C. Weiss, Jr., Theor. Chim. Acta., 1972, 24, 346.

27. A.M. Edwards and M. Gouterman, J. Mol. Spectrosc., 1970, 33, 292.

28. A.M. Schaffer and M. Gouterman, Theor. Chim. Acta., 1972, 25, 62; 1973, 30, 9.

29. V.I. Gavrilov, E.A. Luk'yanets and I.V. Shelepin, Electrokhimiya, 1981, 17, 1183.

30. D.T. Sawyers and J.L. Roberts, "Experimental Electrochemistry for Chemists", Wiley, New York, 1974.

31. J.L. Hoard "Porphyrins and Metalloporphyrins", Ed. K.M. Smith, Elsevier, Amsterdam, 1975, Chapter 8.

32. R.H. Campbell, G.A. Heath, G.T. Hefter and R.C.S. McQueen, J. Chem. Soc., Chem. Commun., 1983, 1123.

33. I. Flemming, "Frontier orbitals and organic Chemical Reactions", Wiley Interscience, 1976, Chapter 2.

34. M. Gouterman, J. Mol. Spectrosc., 1961, 6, 138.

35. L.K. Lee, N.H. Sabelli and P.B. LeBreton, J. Phys. Chem., 1982, 86, 3926.

36. J.-H. Fuhrhop, P. Wasser, D. Reisner and D. Mauzerall, J. Am. Chem. Soc., 1972, 94, 7996.

37. W.A. Nevin, W. Liu, M. Melnik and A.B.P. Lever,

J. Electroanal. Chem. Interfacial Electrochem., 1986, 213, 217.

38. J. LeMoigne and R.J. Even, J. Chem. Phys., 1985, 82, 6472.

39. W.A. Nevin, M.R. Hempstead, W. Liu, C.C. Leznoff and A.B.P. Lever, Inorg. Chem., 1987, 26, 570.

40. M.J. Stillman and A.J. Thompson, J. Chem. Soc., Faraday Trans. 2, 1974, 70, 790.

41. A.B.P. Lever, Adv. Inorg. Radiochem., 1965, 7, 51 and references therein.

42. T. Nyokong, Z. Gasyna and M.J. Stillman, Inorg. Chem., 1987, 26, 548.

43. T. Nyokong, Z. Gasyna and M.J. Stillman, Inorg. Chem., 1987, 26, 1087.

44. P.C. Minor, M. Gouterman and A.B.P. Lever, Inorg. Chem., 1985, 24, 1894.

45. S.A. Mikhalenko, S.V. Barkanoon, O.L. Lebedev and E.A. Luk'yanets, Zh. Obschi. Chim., 1971, 41, 2735.

46. L. Edwards, M. Gouterman and C.B. Rose, J. Am. Chem. Soc., 1976, 98, 7638.

POSTGRADUATE COURSES ATTENDED

"History of the Chemistry Department"

Dr. W.P. Doyle, 1983.

"Electrochemistry in and out of Mothballs"

Dr. G.A. Heath, 1983.

"Homogeneous Catalysis"

Dr. T.A. Stephenson, 1983.

"The Chemistry of Photographic Processes"

Dr. L.A. Williams, 1984.

University of Strathclyde Inorganic Club

Conference 1983, 84, 85.

"Inorganic Cluster Chemistry"

Dr. A.J. Welch, 1984.

"Chemical Technology and Industrial Chemistry"

Dr. A.J.S. Nicol and Dr. R.S. Sinclair

"Recent Developments in Electrochemistry"

Dr. H.H. Girault, 1985.

"Inorganic Biochemistry Discussion Group"

1984 (Imperial College, London).

"Applications of ESR Spectroscopy"

Dr. T. Lindsell (Heriot Watt Univ.) 1986.

"Organic Electrochemistry"

Dr. A. Bellamy (1984).

"Organom etallic Chemistry of the Transition Elements"

Dr. G.A. Heath, (1984).